THE UNIVERSITY OF MICHIGAN

INDUSTRY PROGRAM OF THE COLLEGE OF ENGINEERING

QUANTITATIVE METALLOGRAPHY OF CYLINDERS, CUBES, AND OTHER POLYHEDRONS

Edward J. Myers

A dissertation submitted in partial fulfillment
of the requirements for the degree of
Doctor of Philosophy in the
University of Michigan
Department of Metallurgical Engineering
1961

February, 1962

IP-552

ACKNOWLEDGMENTS

The author wishes to express his sincere gratitude to Professor M. J. Sinnott, Chairman of his Doctoral Committee. Without his encouragement, advice, and patience, this work would not have been done. Appreciation is also expressed to the other members of the Committee, Professors J. R. Frederick, E. E. Hucke, D. V. Ragone, and C. A. Siebert for their interest and contributions.

The author also wishes to thank Doctor D. W. Breuer, Head, Mechanics Department, Air Force Institute of Technology, under whom he served while performing this work, for fullhearted support and consideration. Sincere thanks also go to Doctor (formerly Lieutenant) Lee McCullough, for invaluable discussions of the mathematical techniques, and to Mr. Larry Odell and Mr. Wayne Kimmel, for obtaining the IBM 7090 results, and to Mr. W. O. Campbell, Mr. J. A. Simpson, and S/Sgt. David A. Medina for the line drawings.

Finally, I am grateful to my wife for typing the rough draft of this dissertation and to her and our children for their sacrifices and understanding.

TABLE OF CONTENTS

TABLE OF CONTENTS CONT'D

TABLE OF CONTENTS CONT'D

LIST OF TABLES

LIST OF TABLE CONT'D

LIST OF FIGURES

LIST OF FIGURES CONT'D

LIST OF FIGURES CONT'D

LIST OF FIGURES CONT'D

ABSTRACT

The purpose of this work was to develop and extend quantitative relationships connecting the shape, size, and number of dispersed phase particles which may be observed on a plane section of a multiphase system with the three-dimensional values of these parameters for the particles or phases present in the solid.

By the solution of trigonometric integral equations, relations have been derived which connect the number of particles observed in a plane section with the number and size of particles actually present in the solid for uniformly sized but randomly dispersed and oriented particles of nine different polyhedral shapes.

Relations have also been derived which determine the relative frequencies of the possible section shapes obtained on random plane sections cutting through a dispersion of randomly oriented particles having the shapes of cylinders, cubes, octahedrons, tetrahedrons, rhombic dodecahedrons, and tetrakaidecahedrons.

The relations have been derived by double integration and summation of equations of the form

$$P = A \int_{\Theta_a}^{\Theta_b} \int_{\phi_a(\Theta)}^{\phi_b(\Theta)} [(B \sin\Theta + C \cos\Theta) \sin^2\phi + D \cos\phi \sin\phi] \, d\phi d\Theta$$

For some of the integral equations developed, exact analytical solutions by the methods of integral calculus were found. Many of the equations,

however, were of sufficient complexity that solutions were obtained with an IBM 7090 digital computer.

Experimental verification of the theoretical relations developed for cubes and cylinders was obtained by preparing synthetic samples containing randomly dispersed cubes and cylinders. Measurements made by sectioning and microscopic examination of synthetic samples of cubes and four different cylindrical shapes support the theoretical predictions.

The relations derived which connect the number of particles observed per unit section, N_S, with the number of particles present per unit volume, N_V, are given in the following table.

TABLE I

Shape	Relation
Cubes	$N_S = N_V \cdot 1\frac{1}{2}\, a$
Rectangular Parallelepipeds	$N_S = N_V \cdot \frac{1}{2}(a+b+c)$
Thin Rectangular Plates	$N_S = N_V \cdot \frac{1}{2}(a+b)$
Long Square Rods	$N_S = N_V \cdot \frac{1}{2}\, c$
Octahedrons	$N_S = N_V \cdot a \cdot \frac{3\sqrt{2}}{\pi}\ \operatorname{arccot}\sqrt{2}$
Tetrahedrons	$N_S = N_V \cdot a \cdot \frac{3\sqrt{2}}{\pi}\ \arctan\sqrt{2}$
Rhombic Dodecahedrons	$N_S = N_V \cdot \frac{\sqrt{3}}{2}\, a$
Tetrakaidecahedrons	$N_S = N_V \cdot \frac{3}{2\sqrt{2}}\, a$
Hexagonal Prisms	$N_S = N_V \cdot (\frac{3}{4}\, a + \frac{1}{2}\, c)$

In the above table, for octahedrons, tetrahedrons, rhombic dodecahedrons, and tetrakaidecahedrons, "a" is the edge length of the circumscribed cube. For the hexagonal prism, "a" is the length of the base diagonal and "c" is the altitude of the prism.

The relative frequencies of various shaped sections of cylinders depend upon the length to diameter ratio of the cylinders and are proportional to the terms given in the following table.

TABLE II

Cylinder Section	Frequency Relation
Ellipses	$\frac{1}{2}$ (ℓ-d arctan ℓ/d)
Singly Truncated Ellipses	d arctan ℓ/d
Doubly Truncated Ellipses	$\frac{1}{2}$ ($\frac{\pi d}{2}$ - d arctan ℓ/d)

The relative frequencies with which sections of polyhedrons having various numbers of sides on a section are observed are presented in the following table.

TABLE III

RELATIVE FREQUENCIES OF SECTIONS (%)

Sides on	Polyhedron				
Section	Cube	Octahed.	Tetrahed.	Rh. Dod.	Tetrakai.
3	28.0	--	71.2	4.0	7.3
4	48.7	44.8	28.8	13.4	13.4
5	18.7	--	--	16.2	11.8
6	4.6	55.2	--	29.9	31.2
7	--	--	--	19.1	18.3
8	--	--	--	16.3	13.1
9	--	--	--	1.1	3.8
10	--	--	--	--	1.1

The above results are exact for dispersed particles having uniform size and shape and random orientations. If particle shape is

known, the relations permit analysis of degree of non-randomness of orientation. The relations also permit analysis of non-uniformly sized particles in a more accurate manner than previously possible.

I. INTRODUCTION

While metallography has long been the metallurgist's most important tool, it is now obvious that quantitative metallographic methods are essential in order to change this art into the science needed for the design of alloys meeting the ever-increasing demands of modern technology. The principal difficulty arises from the fact that metals are opaque and that observations made on a plane of polish are not readily converted into the three-dimensional parameters which determine the properties of the solid. This fact has been recognized by many, and, although much work has been performed to put metallography on a quantitative basis, it can be fairly stated that the subject is still in its infancy.

Since virtually all metals used for their structural strength and integrity are polyphase alloys, quantitative methods of determining and describing the state of dispersion of the phases present are necessary for adequately studying the effects of these variables on alloy properties.

This dissertation describes the results of a study of the quantitative correlation between the numbers and sizes of various shaped particles in a three-dimensional solid, corresponding to phases in an alloy, and the numbers and shapes of the two-dimensional sections of these particles observed on a plane of polish.

A brief literature survey is included to describe other work in the field of quantitative metallography and to list previously developed quantitative relations connecting particle shape, size, and number in opaque bodies with their plane sections.

The following portions are arranged in a more or less chronological order, proceeding from the simpler developments to the more complicated. Section III, Analysis of Problem, presents the basic trigonometric integral calculus approach used in this dissertation and uses the method to re-solve earlier known relations. Section IV develops the relative frequencies of various section shapes of cylinders as a function of cylinder shape. Section V extends the technique to cubes, developing the probability of sectioning a cube or rectangular parallelepiped and the relative frequencies of cube sections of various numbers of sides.

Section VI, General Approach to Polyhedron Problem, discusses and summarizes the analytical methods used for solving the cube problem and prepares the groundwork for the developments to follow. Sections VII to X present quantitative relations for numbers of particles and shapes of sections for other polyhedrons of cubic symmetry. Section XI presents the probability of sectioning a hexagonal prism, the only non-cubic polyhedron considered.

The final sections describe the preparation of synthetic samples of dispersed cylinders of four different shapes and dispersed cubes. Experimental measurements made upon these dispersed particles are compared with theoretical results, using statistical techniques wherever possible.

Appendix A contains detailed evaluations of several definite integrals that occur many times during the solutions of the various polyhedrons. Appendix B describes the digital computer solution of the trigonometric integral equations arising from this work. Appendix C lists the symbols used in the text.

II. REVIEW OF LITERATURE

The field of quantitative metallography is a large one and can be considered a branch of the mathematical discipline, topology. The questions of surfaces, volumes, shapes, sizes, numbers, and orientations of poly-phasic, poly-crystalline, or poly-cellular bodies are of importance to physicists, chemists, biologists, botanists, mineralogists, geologists, and ceramists, as well as to civil engineers, crystallographers, and metallographers.

Countless numbers of papers, several excellent reviews, and even a few complete books have covered this area, so no attempt at completeness will be made in this literature survey. It will suffice to mention briefly the most important applications of quantitative methods to metallography and to describe in somewhat more detail previous studies concerned with measurements of dispersed particles.

It seems appropriate at this point to mention the two most complete and most recent treatments of this topic: "Stereometric Metallography" (in Russian), by S. A. Saltykov[1], and the Symposium on Quantitative Metallography at the University of Florida.[2] Also a current review article has been presented by Underwood.[17]

Application of Topology

Many early studies of shapes of cells, invoking topological principles, have been made by botanists and mathematicians. The most notable application of topology to metallography was by Smith.[34] He points out that the atomic and macroscopic structure of matter

depends upon physical forces and the mathematical requirement of space filling.

The classification of shapes is nearly always an essential prerequisite to an understanding of the physical forces involved. The nature of these requirements leads to be remarkably close analogy between biological cells, soap froths, and metal grains. For irregular polygons on a plane surface, the following form of Euler's Law is always applicable:

$$P - E + C = 1 \qquad (1)$$

where P, E, and C are the number of polygons, edges, and corners, respectively. For the faces, edges, and corners of polyhedrons, Euler's Law is

$$F - E + C = 2 \qquad (2)$$

For a three-dimensional network of cells we have

$$C - E + P - B = 1 \qquad (3)$$

where B stands for cells (bodies) and the other letters are as above.

Surface Area

Extending the work to measurement of surface or grain boundary area in a polycrystalline metal, Smith and Guttman[3,5] showed in 1952 that the specific grain boundary area in a solid, S_V, could be determined by the number of intersections of the boundaries by a random line across a plane section of the microstructure, N_L, where

$$S_V = 2 N_L \qquad (4)$$

Saltykov[1] reports that this equation is identical to one developed and published by him in 1945.[6] This relation is of such fundamental importance that it was developed again independently, by Duffin, Meussner, and Rhines[7] in 1953 and by Horikawa in 1954.[16]

The measurement of surface or intergranular area, along with measurement of volume fraction of phases, the determination of grain size, and the determination of numbers, sizes, and shapes of dispersed microparticles, constitute the four most important metallographic properties to be measured quantitatively in order to correlate the spatial microstructure of an alloy with its physical and mechanical properties.

Volume Fraction

The measurement of volume fraction of phases may be accomplished by the classical methods of areal, lineal, or point analyses. This is based upon the fact that for random sampling

$$f_V = f_A = f_L = f_P \qquad (5)$$

The volume fraction of a phase is equal to its areal fraction on a random cross section, which is equal to the fractional length of random linear intercepts which cross that phase on a random section, which is equal to the fraction of randomly distributed points which lie on a section of the phase. It may be seen that each term in Equation (5) represents a reliable, random statistical sample of the term preceding it, even if the phase distribution is not random. If the phase distribution is random, which is often a reasonable approximation, a systematic, rather than

random, sampling of a specimen by cuts, lines, or points is a more convenient way to perform the areal, lineal, or point analyses, and Equation (5) is still applicable.

The first measurement of volume fraction was apparently by Delesse in 1848[8], who showed mathematically the equality of areal fraction and volume fraction. The areas of grains of phases may be measured by planimeter, visual estimation, or by photographing or sketching the plane section and cutting out and weighing the portions corresponding to each phase. It can readily be seen that, if the microstructure is at all finely dispersed, any of these methods will be very tedious and subject to considerable error. Nevertheless, the method of areal analysis may occasionally be convenient, particularly for phases present in very small amounts, as with non-metallic inclusions in steel.[1]

In 1898 Rosiwal[9] presented his mathematical derivation for volume fraction by lineal analysis, a much more convenient technique and one which is widely used today. As previously indicated, one measures the fraction of length of a randomly or systematically applied line that crosses the phase of interest. Mechanical and automated techniques using this method, the Hurlbut counter described by Howard and Cohen[10], the Wentworth integrating stage[11], and the "flying-spot" photoelectric cell[12], have greatly simplified its application. Glagolev also developed a number of designs of devices for lineal analysis.[1] Discussions concerning the accuracy and convenience of lineal analysis have been presented by several people: notably, Howard and Cohen[10], Saltykov[1], and Hilliard and Cahn[13].

In 1930, the method of point counting for determining volume fraction was introduced by Thompson[15] and, shortly thereafter, independently, by Glagolev[1,14]. In the American literature, the first application of point counting to quantitative metallography was by Howard and Cohen[10]. Point counting directly at the microscope is easy and rapid with the simplest of devices, grids or points. Devices for further speeding up the analysis have been developed by Glagolev[1]. Point counting is considered by many investigators, Hilliard and Cahn[13], Chayes[18], and Saltykov[1], to be the most generally useful method for determining volume fraction.

Grain Size

The grain size of a single phase metal is, of course, a fundamental factor strongly influencing nearly all physical and mechanical properties. More particularly, the term, "grain size," means average grain size, because in any real system there would always be a range of grain sizes, and more commonly it refers to average cross sectional areas of grains revealed in the plane of polish. Some of the more common ways of reporting grain size are[19]:

a) Grains per sq. mm.

b) Average area of grain (sq. mm.)

c) Mean diameter of grain (mm.)

d) Arbitrary numbers (the Timken, ASTM, exponential scale based on number of grains in a given area.)

In addition to the above, grain size may be reported as the average linear intercept on a random plane section (Heyn's Intercept Method)[20].

It will be noted that all the above are expressed directly in terms of dimensions observed from a cross section of the grains. This may be more or less descriptive of the true spatial grain size, depending primarily upon grain shape. Saltykov[1] particularly criticizes the use of a single parameter to describe grain size and suggests the inclusion of other measurements showing grain boundary area, departures from the equiaxed condition, and others. He says that to completely describe geometric grains we need their size, their surface area, their number per unit volume, and their shape. However, as a minimum, the total volume of particles and their total surface per unit volume should be evaluated.

Johnson[22] described a technique for obtaining spatial grain sizes, which was based, in part, on earlier work by Scheil.[23,24,25] Others have attempted to compute grain size of a metal from grain areas on a plane section by assuming certain fixed grain shapes.[26,27]

Grain Shape, Single Phase

The actual shapes of metal grains as revealed by fracture surfaces or grains isolated from a solid have intrigued investigators for a long time. In 1775 Grignon[21] described grains revealed in an aggregate of iron. Since then, numerous others have separated out individual grains by fracture in the hot-short range or by intergranular chemical attack. An ingenious stereoscopic micro-radiographic technique by Williams and Smith[29] revaled grain shapes and boundaries in an aluminum-tin alloy.

Considering the requirements for space filling as well as minimizing surface tension forces, Lord Kelvin[28] in 1894 showed that an assemblage of uniformly sized tetrakaidecahedrons (cuboctahedrons or truncated octahedrons) (Figure 1) would fill space with a minimum of surface area. This fourteen faced polyhedron meets the surface tension requirements of no more than three grains at an edge and no more than four edges at a corner, but it does not completely satisfy the requirement for 120° dihedral angles between grain boundaries where three adjacent grains meet at an edge, as discussed by Smith.[3,4] However, with the introduction of a slight double curvature of the faces, changing the surface area very slightly, the 120° dihedral angles can be obtained. This very behavior has been demonstrated in experiments using soap froths (Figure 2).[3]

The rhombic dodecahedron (Figure 3) and its hexagonal variant (Figure 4) are space filling bodies and were considered by Harker and Parker[31] to be ideal grain shapes because the surface tension requirement of 120° dihedral angles where three grains meet at an edge is satisfied. The rhombic dodecahedron fills space on a face centered cubic lattice, in contrast to the tetrakaidecahedron, which stacks on a body centered cubic lattice. Per unit volume, the rhombic dodecahedron has a slightly greater surface to volume ratio than the tetrakaidecahedron (5.34539 to 5.31474),[32] but a greater difficulty is that a rhombic dodecahedron array has eight edges meeting at some corners (as does its hexagonal variant), and this is an unstable condition with regard to surface tension.

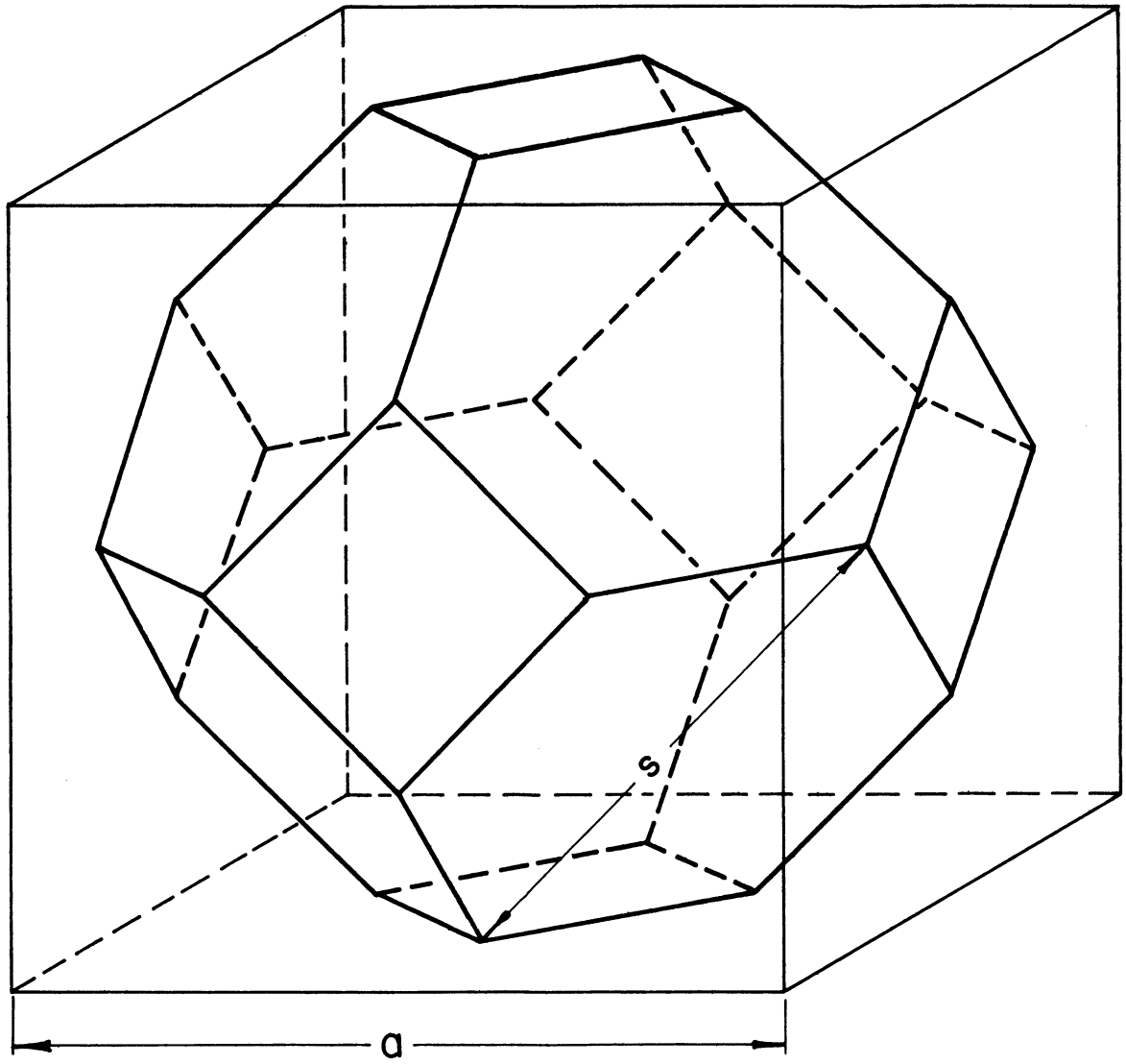

Figure 1. Tetrakaidecahedron.

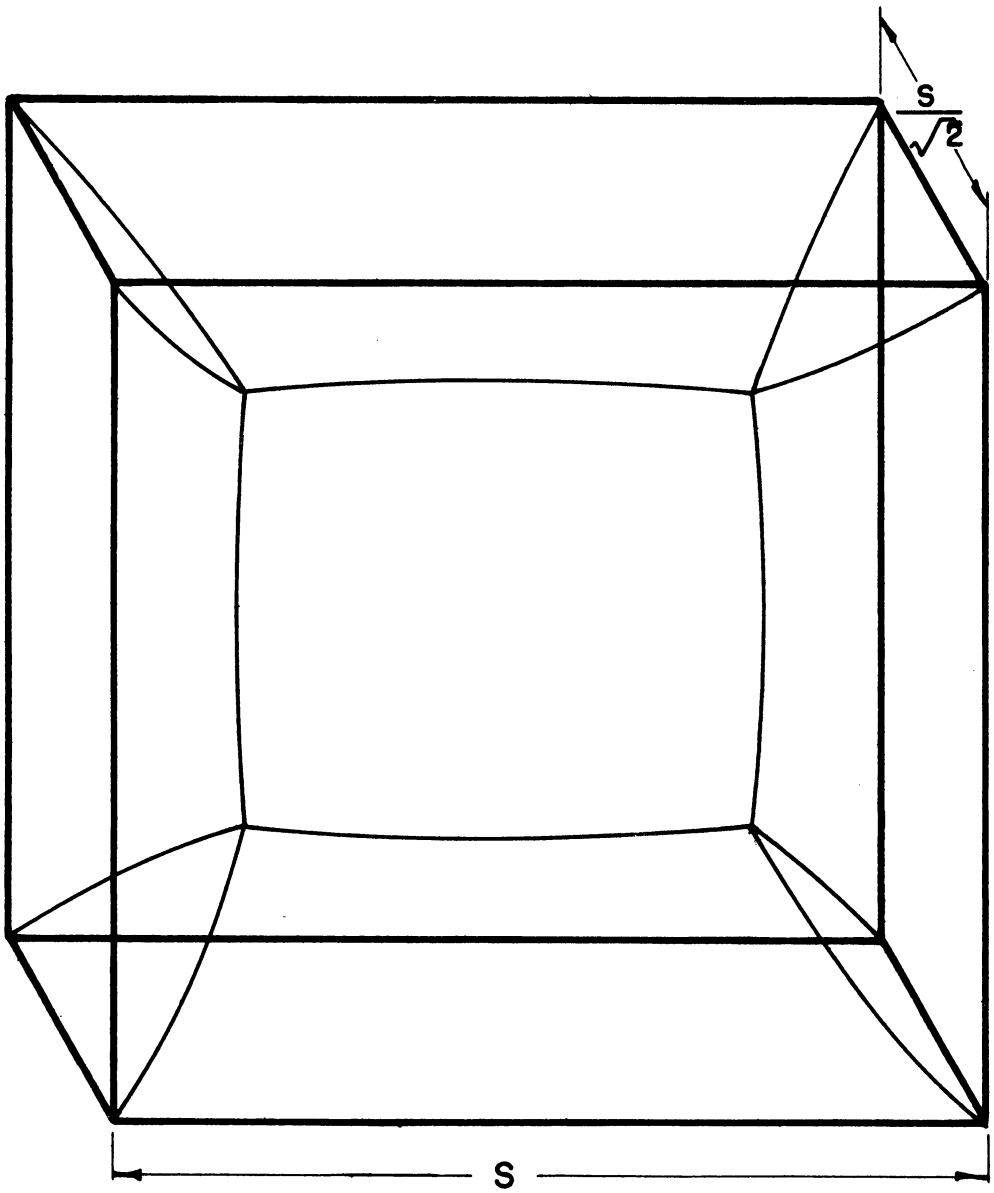

Figure 2. Soap Film in Wire Frame Showing Faces of Tetrakaidecahedron Modified by Surface Tension.

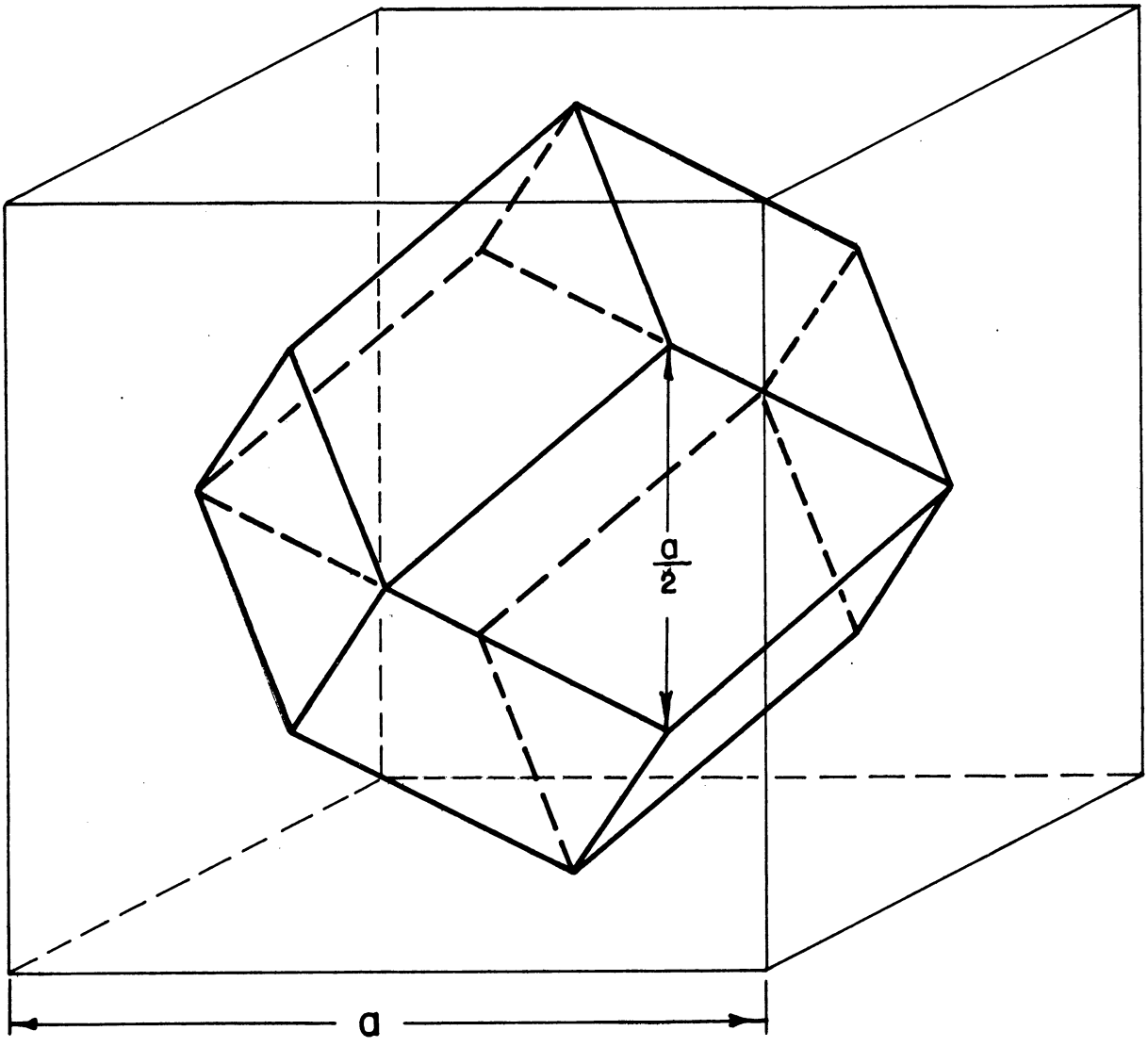

Figure 3. Rhombic Dodecahedron.

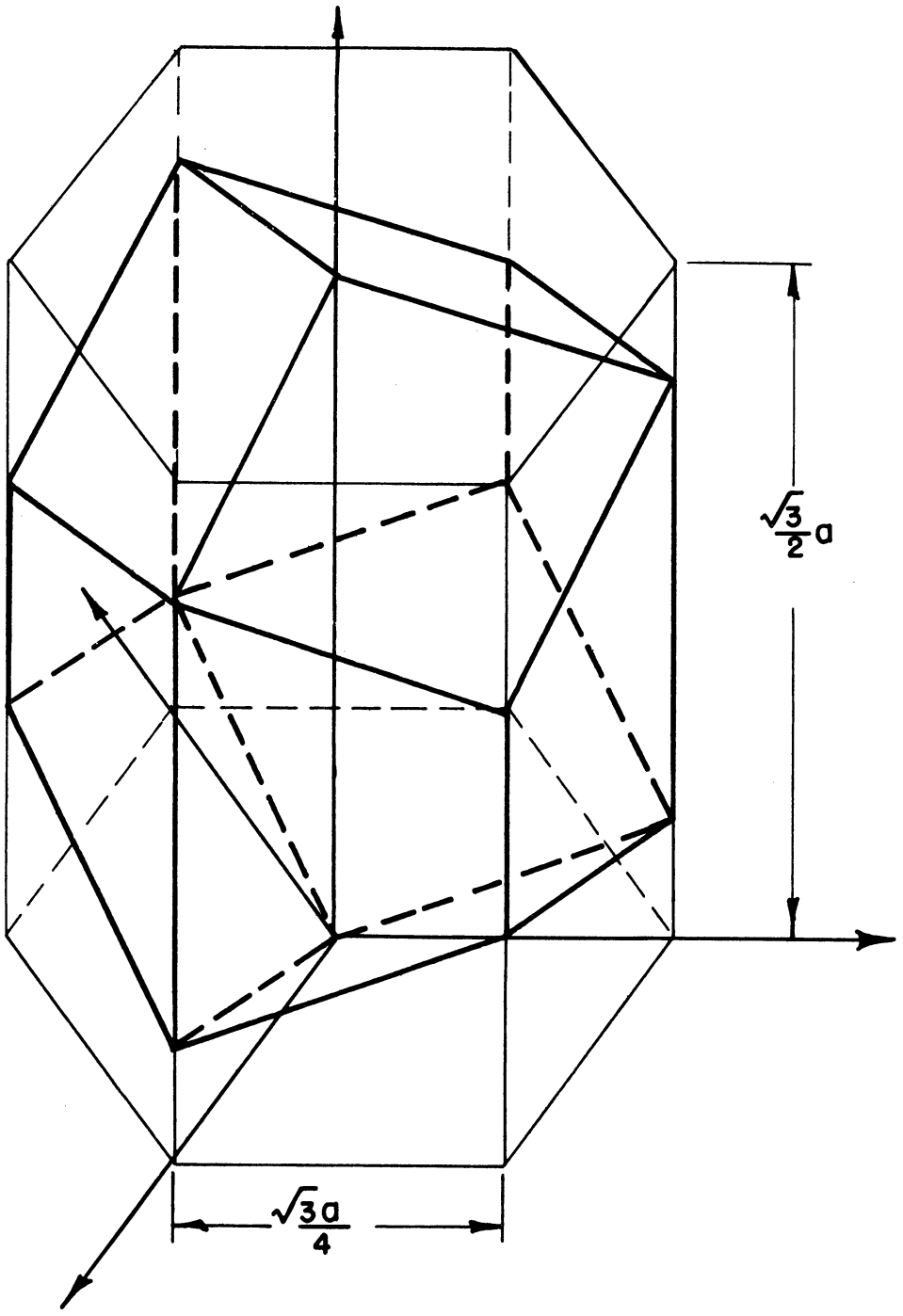

Figure 4. Hexagonal Equivalent of Rhombic Dodecahedron.

The result of such an unstable situation would be the immediate formation of a new, small square face at each such corner, or two new faces per polyhedron, forming a fourteen-faced modification of the rhombic dodecahedron, which still fills space on a face centered cubic lattice and better satisfies surface tension requirements (Figure 5). This has also been shown on experiments with soap froths (Figure 6).[33] This modified, fourteen faced, nearly rhombic polyhedron has a slightly smaller surface to unit volume ratio (5.34525) and is the minimum surface figure filling space on a face centered cubic lattice.

However, it can be shown[32] that, by compressing this modified polyhedron perpendicularly to the newly created faces, a continuous series of uniform, space filling bodies are obtained. As their faces maintain minimum total area, the two new faces will gradually expand and the surface to unit volume ratio will decrease still further. This proceeds in a monotonic manner until the dimension in the compression direction is $1/\sqrt{2}$ times the original dimensions. A minimum is reached at this point in surface to unit volume ratio, and the shape of this body is the tetrakaidecahedron with body centered cubic symmetry. This may be seen if one imagines the wire frame and soap froth of Figure 6 gradually shortened in the direction perpendicular to the central face until the frame and froth of Figure 2 are achieved, at the thickness to edge length ratio of $1/\sqrt{2}$.

It might be added that other distortions of these figures, maintaining fourteen faces, would still fill space and closely approach minimum surface energy. It may thus be seen why the calculation of

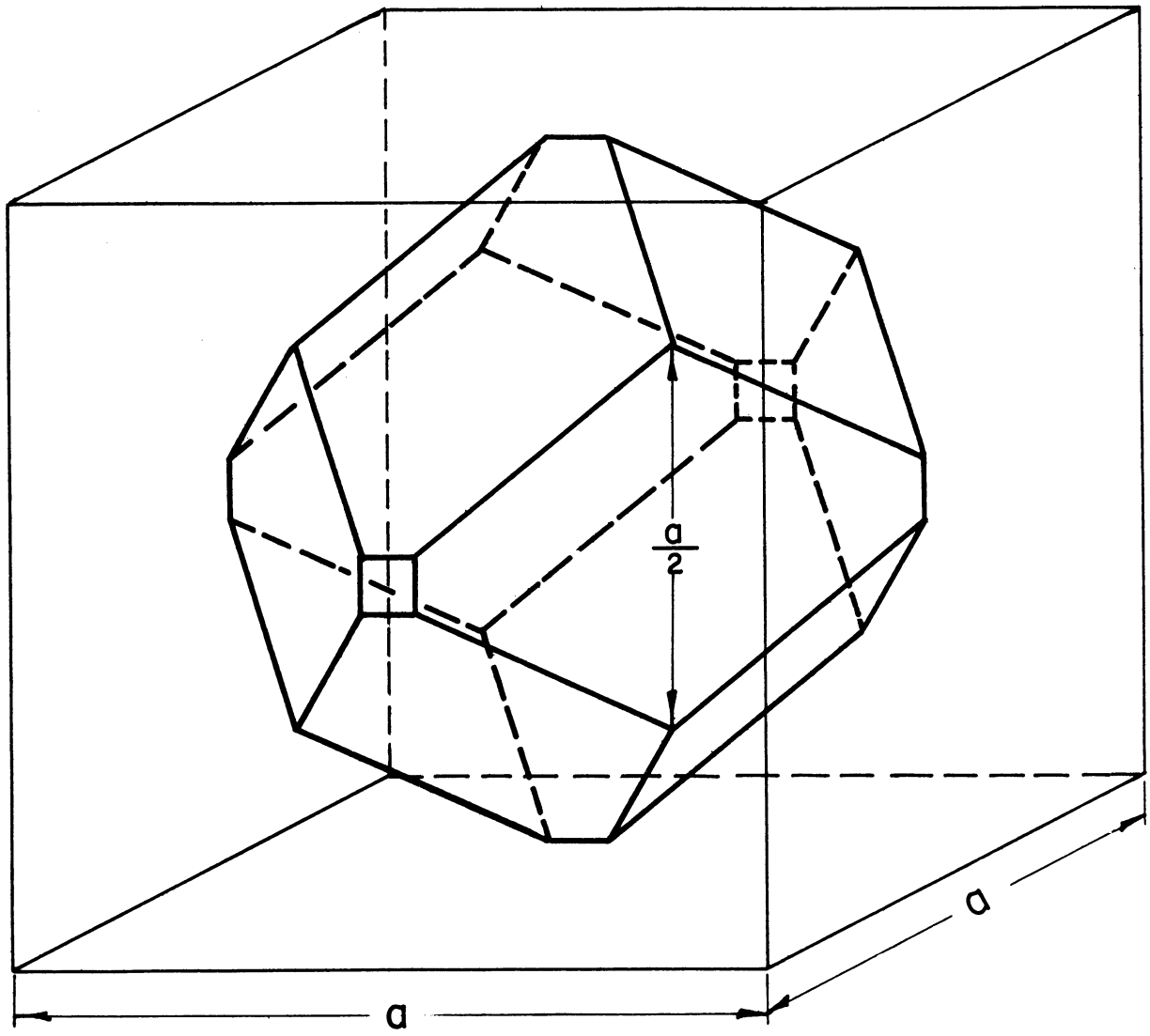

Figure 5. Modified Rhombic Dodecahedron of Minimum Surface.

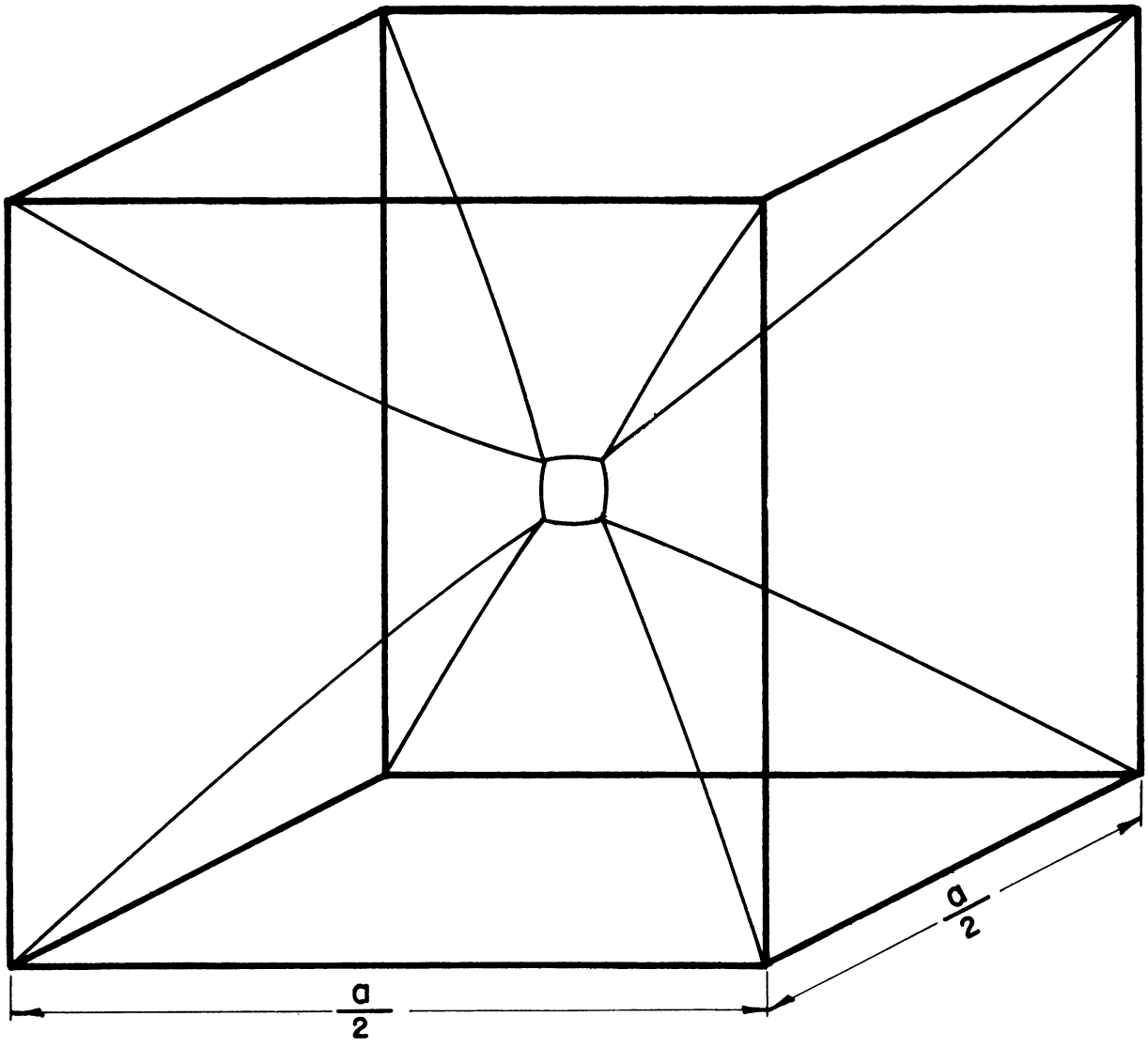

Figure 6. Soap Film in Wire Frame Showing Faces of Modified Rhombic Dodecahedron.

total surface area of polycrystalline metals, assuming the shapes of grains to be tetrakaidecahedrons, often gives good checks with independent measures of surface area using Equation (5).[17,26] Kaiser[27] proposed an empirical formula for surface area which assumes average grain specific surface somewhere between that of rhombic dodecahedrons and tetrakaidecahedrons.

Grain Shape, Dispersed Phases

The grain shapes of polyphase alloys present a variety an order of magnitude greater than for single phase alloys. Dispersed second phase grains may range from intergranular films, platelets, needles, regular or irregular polyhedrons, and volumes of revolution to nearly spherical particles. The parameters needed to describe the state of dispersion usually include particle numbers, shapes, sizes, size distributions, surface, and spacing. The difficulties involved in deriving exact relationships connecting particle size and number for any but the simplest of shapes have discouraged much effort in this direction. As a result, analyses of most particle distributions still require approximate methods. Only in the case of spheres and lamellae can anything like a thorough treatment be claimed.

Investigations on the interlamellar spacing of pearlite in steel have been reported many times. Some of the contributors in this area have been Belyayev[34], Pelissier, Hawks, Johnson, and Mehl[35,37], Gensamer, Pearsall, and Smith[36,38], Saltykov[1], and Gregory, Hall, and Bullock[39].

Probably the most completely studied case of dispersed particles regarding total number per unit volume and their size distributions is that of spheres. The relation connecting the number of spheres of uniform size per unit volume with the number of their sections observed per unit cross-sectional area is

$$N_S = N_V \cdot 2r \qquad (6)$$

This relation has been derived by Fullman[40], Scheil[23], Schwartz[41], Mirkin[42], and appears to have been recognized earlier by Scheil[43] and Hagerman[44]. Saltykov[1], apparently mistakenly, credits Mirkin with priority for this equation.

The validity of Equation (6) is almost intuitively obvious, as, if in a unit cube a sphere of radius r is placed, then a cross-sectional plane of unit area will intersect the sphere if it passes anywhere within a range of $2r$. Therefore, $2r$ is the probability of intersecting one sphere ($r \ll 1$). If there are N_V spheres of radius r in the unit cube, N_S will be the expected number observed on a unit cross-section as in Equation (6). The sections of the spheres observed will all be circles, of course, varying in radius from r to 0.

If the spheres present are not of a single size, their sections observed will still be circles, but the determination of number present per unit volume becomes more difficult. Scheil[43] did this first by a method requiring measurements of section diameters, grouping into size intervals, and then successive subtraction, going

from larger size to smaller, of the smaller sections which are due to previously computed larger spheres. A table was presented by Scheil for this successive subtraction. Schwartz[41] described the same method in a more convenient form, and Saltykov[1] and Underwood[17] have presented additional tables for use of the Scheil Method.

A more straightforward method for determination of sphere size distribution from random secant measurements was presented by Lord and Willis[45]. The length of intersections of circles (secants) in a random linear traverse (Rosiwal traverse) may readily be converted into sphere size distribution. Lord and Willis used this method for air bubbles in concrete, and Brophy and Sinnott[46] have used it for nodular graphite in cast iron. Cahn and Fullman[47] have presented an alternate mathematical approach based upon random secants, similar in principle to that of Lord and Willis.

The relations for numbers of circular plates and circular rods per unit volume were derived by Fullman[40] and later extended by him to cylindrical particles[48]. The relations reported by Fullman are:

Circular Platelet	$N_S = N_V \cdot \frac{\pi r}{2} \quad (r \gg t)$	(7)
Round Needle	$N_S = N_V \cdot \frac{\ell}{2} \quad (\ell \gg r)$	(8)
Cylinder	$N_S = N_V \cdot \frac{1}{2} (\pi r + \ell)$	(9)

Relations for size and number of ellipsoids of revolution have been developed by DeHoff and Rhines.[49]

For polyhedral particles, exact relations connecting size and number have been more difficult to derive than for bodies of revolution. Saltykov[1] reports approximate formulas for determining numbers of uniformly sized particles shaped as cubes and tetrakaidecahedrons. For cubes, Saltykov gives

$$N_V = \frac{16\,(N_S)^2}{6\Sigma\, S} \tag{10}$$

where S is total intergranular area, and for tetrakaidecahedrons he reports

$$N_V = \frac{6(1+2\sqrt{3})\cdot 36(N_S)^2}{(18)^2\ \Sigma\, S}$$

$$N_V = 2.98\,\frac{(N_S)^2}{\Sigma\, S} \tag{11}$$

The shapes of plane sections of polyhedrons were considered briefly by Rutherford, Aborn, and Bain[26], who showed that plane sections of a cube may have 3, 4, 5, or 6 sides (Figure 7). Hull and Houk[50] further investigated the shapes and areas of sections of several polyhedrons. This was done by making a wire model of the polyhedron, mounting it on a tilting bench vise on an elevating table, and measuring the sections obtained at various elevations. To represent all possible orientations of the polyhedrons, they selected from 26 to 35 orientations, by means of a polar stereographic plot, which they felt to be as complete and representative sampling as possible with the given number of positions. For the cube, their selected orientations,

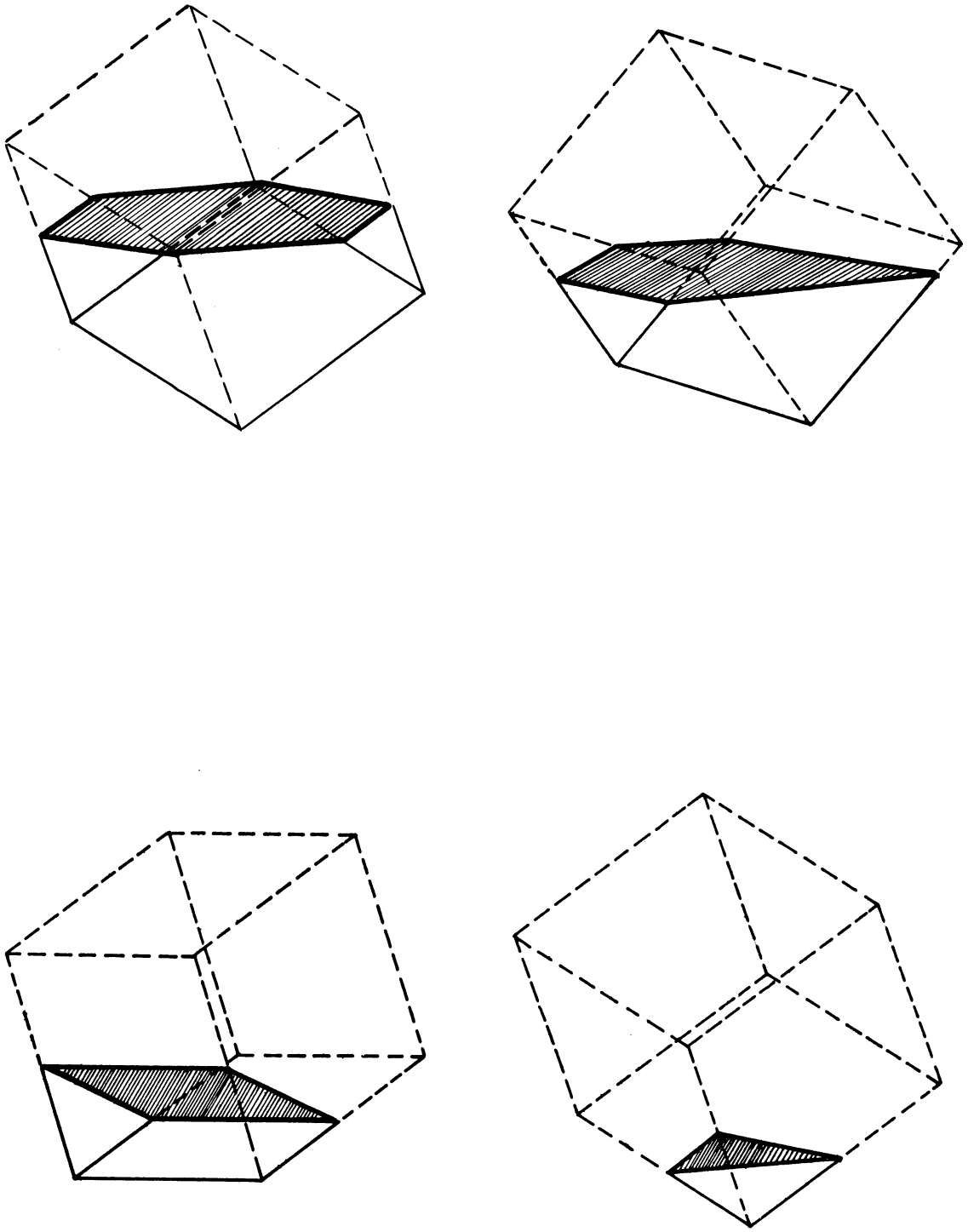

Figure 7. 3, 4, 5 and 6 Sided Plane Sections of a Cube.

shown as 5° solid angles, are given in Figure 8. The relative frequencies of the various shaped intersections of cubes and tetrakaidecahedrons obtained by Hull and Houk[50] are given in Table I.

TABLE I

FREQUENCY OF SECTIONS OF POLYHEDRONS
(DERIVED FROM DATA BY HULL AND HOUK[50])

Number of Sides	Relative Frequency (%)	
	Cube	Tetrakaidecahedron
3	28.9	7.9
4	42.0	14.5
5	18.1	12.9
6	10.0	29.5
7	--	17.9
8	--	12.8
9	--	4.0
10	--	0.5

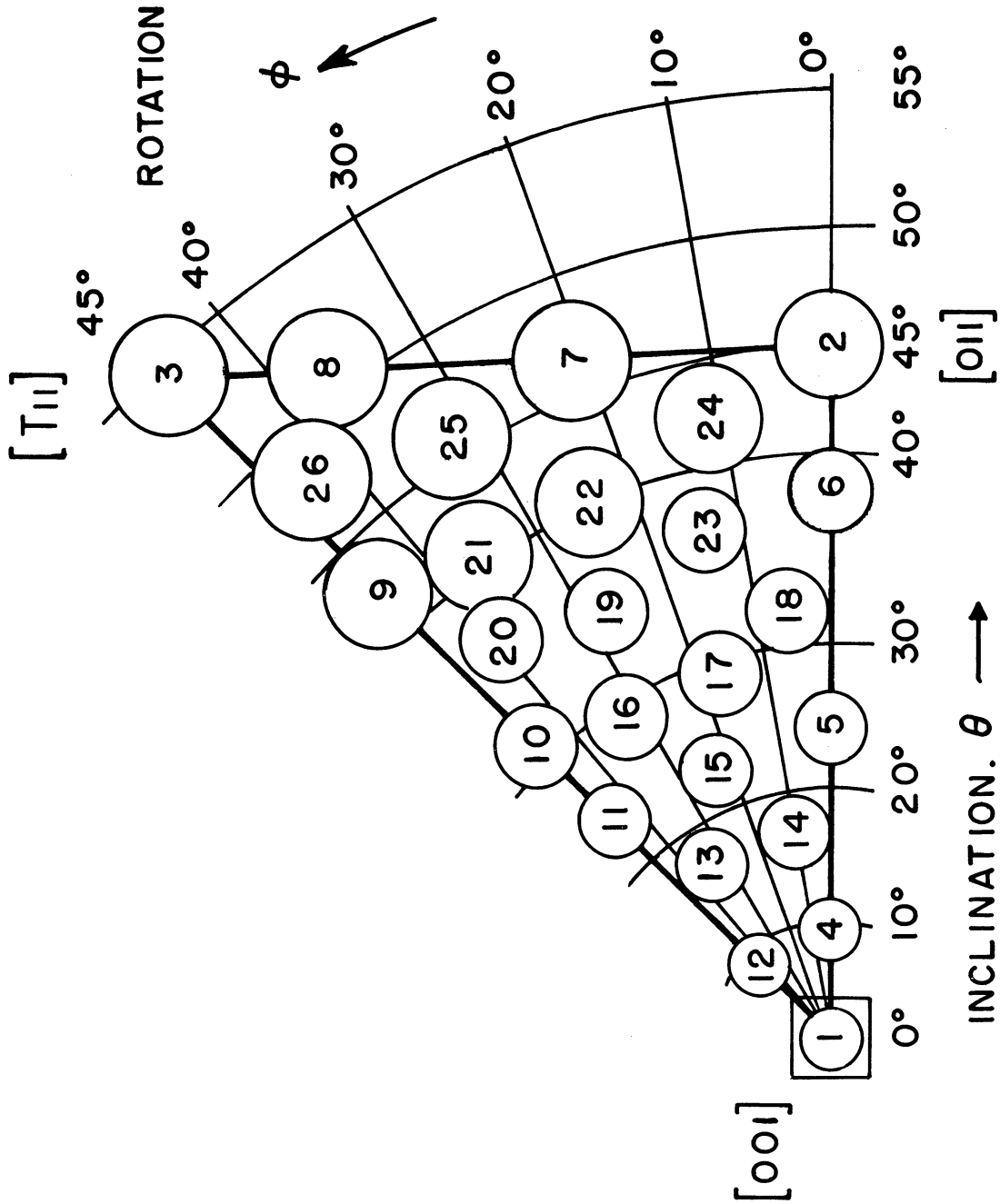

Figure 8. Polar Stereographic Orientation Plot by Hull and Houk[50]. Circles are 5° Solid Angles.

III. ANALYSIS OF PROBLEM

All conventional metallographic observations, whether by means of the optical microscope or by electron microscope, are observations made upon a plane section of a specimen, usually polished and etched. Since metals are opaque to electromagnetic radiation, except in the very thinnest of films, the spatial microstructure cannot be observed directly and inferences about its form must be made from what we see on the sectioning plane. If a structure exists within the solid that is not revealed by a sectioning plane, then we either remain ignorant of that structure or we discover it at a later time, possibly by means of subsequent sectioning planes or, less fortunately, by unanticipated behavior of the material. Hence, representative sampling by careful consideration of choice of sectioning plane or planes is essential.

Probability of Sectioning a Particle in a Solid

Along these same lines, the likelihood that a given feature of the spatial structure will be revealed by a sectioning plane depends upon the size or extent of the feature; if it is very small or occurs in very small amounts, we are less likely to see it. A small particle imbedded within a given volume is less likely to be revealed by a sectioning plane than a larger particle would. For particles of equal volume but having different shapes, the probabilities of their being intersected by a given plane will also depend upon their shapes. Thus the probability of observing a dispersed particle in a solid on a

random sectioning plane through the solid depends upon the size of the particle and its shape.

For a given shape we may be able to express the effect of shape upon this probability by a suitable coefficient or term, known as the shape factor, and then for particles having this shape the probability of intersection will be the shape factor times the size. Thus we can say, in general, for a given shape

$$P_i = (\text{shape constant})(\text{size variable}) \qquad (12)$$

where P_i is the probability of intersection. Only a few of these expressions, for simple shapes, are known exactly and reported in the literature. These are listed in Table II.

TABLE II

PROBABILITY OF SECTIONING A PARTICLE IN A SOLID

Shape	Probability
Sphere	$P_i = 2r$
Circular Platelet	$P_i = \frac{\pi}{2} r$
Rod	$P_i = \frac{\ell}{2}$
Cylinder	$P_i = \frac{\pi r}{2} + \frac{\ell}{2}$

In Table II, r and ℓ are radius and length, the size factors, and the other portions of each expression are the various shape constants. The techniques for performing the computations to arrive at the relations of Table II have varied slightly among investigators, but the derivations presented by Fullman[40,48] provide a good description of the usual approach.

The importance of these expressions stems from their necessity in determining the numbers of particles in an opaque body since the number of particles observed on a plane section is proportional to the total number of particles in the solid and the probability of intersecting such a particle.

$$N_S = N_V \cdot P_i \qquad (13)$$

If we know P_i, we can measure N_S and compute N_V. Thus, the more P_i's we know for various shaped particles, the more quantitative and powerful will be our investigative tools. For irregular shapes or for shapes not exactly solved, it is necessary to use approximation methods, generally based upon some assumption as to shape.

Probability Not Dependent Upon Orientation

To consider the general approach required for all problems of this type, consider the probability of an event as the proportion of successful events out of the total number of possible events. Consider first a sphere of radius r in a larger solid which we shall take as a cube of unit volume. If we pass a series of cross-sectioning planes through the cube parallel to one of its faces, then, of all sectioning planes, those that pass within a distance r of the center of the sphere will cut the sphere. This means that if we uniformly pass parallel planes from top to bottom of the unit cube (a distance, one), then the proportion of planes cutting the cube will be 2r/1 or 2r. Thus, 2r/1 will be equal to the proportion of successful events out of total events, and 2r will be the probability of intersection of the sphere. 2r is, of course, the diameter of the sphere and is

the distance between top and bottom tangent planes that will cut the sphere.

This can be said for any particle: for parallel sectioning planes, the planes that cut the particle will be those between the top and bottom parallel tangent planes to the particle. Thus, the distance between top and bottom tangent planes, which can be considered as the maximum projected height of the particle in a direction normal to the sectioning planes, will be proportional to the probability of intersecting the particle. For a sphere, this distance is always the same, its diameter, but for particles having any other shape the distance between top and bottom tangent planes will vary, depending upon the orientation of the particle with respect to the sectioning plane.

If the orientation of a non-spherical particle is fixed with respect to the sectioning plane, its projected height or probability of intersection is usually easily calculated. However, for a dispersed particle in an opaque solid, such orientation is rarely known in advance and the initial choice of sectioning plane is usually a random one with respect to the particle.

If all possible orientations of particles are considered equally likely, it makes no difference whether we consider the sectioning planes to be oriented at random also or whether we consider the sectioning planes to be fixed, usually parallel cuts, and the particles oriented at random. For calculations as well as for experimental convenience, the latter procedure is much preferred.

However, such calculations will not be valid for dispersed particles having preferred orientations unless the sectioning planes are randomized. Since the mere collection of statistical data is rarely the purpose of our investigations, the experimentally difficult process of randomizing section planes is rarely necessary.

In spherical coordinates, all possible directions originating from a point can be expressed by two angles: ϕ, the angle between any given direction and the normal to the reference plane, and θ, the angle between the perpendicular projection of the given direction into the reference plane and a given reference direction, also lying in the reference plane. This may be seen in Figure 9a. ϕ may be called the angle of tilt and θ the angle of rotation.

Since any given orientation can be expressed by these two angles, and the distance, D, between top and bottom parallel tangent planes of a particle is a function of ϕ and θ, then for a fixed ϕ and θ

$$P_i(\phi,\theta) = D(\phi,\theta) \qquad (14)$$

Since what we usually want is P_i (all ϕ, θ), this is $\overline{D}$ (all ϕ,θ), or the average distance between top and bottom tangent planes for all orientations. Then the average distance between tangent planes for a large number of random orientations, or the experimentally observed P_i, should very nearly equal the average for all orientations, or the theoretical value.

In order to determine $\overline{D}$ (all ϕ, θ) it is necessary to consider the effect of ϕ and θ on D and then integrate over all orientations. The total of all possible orientations can be expressed by a

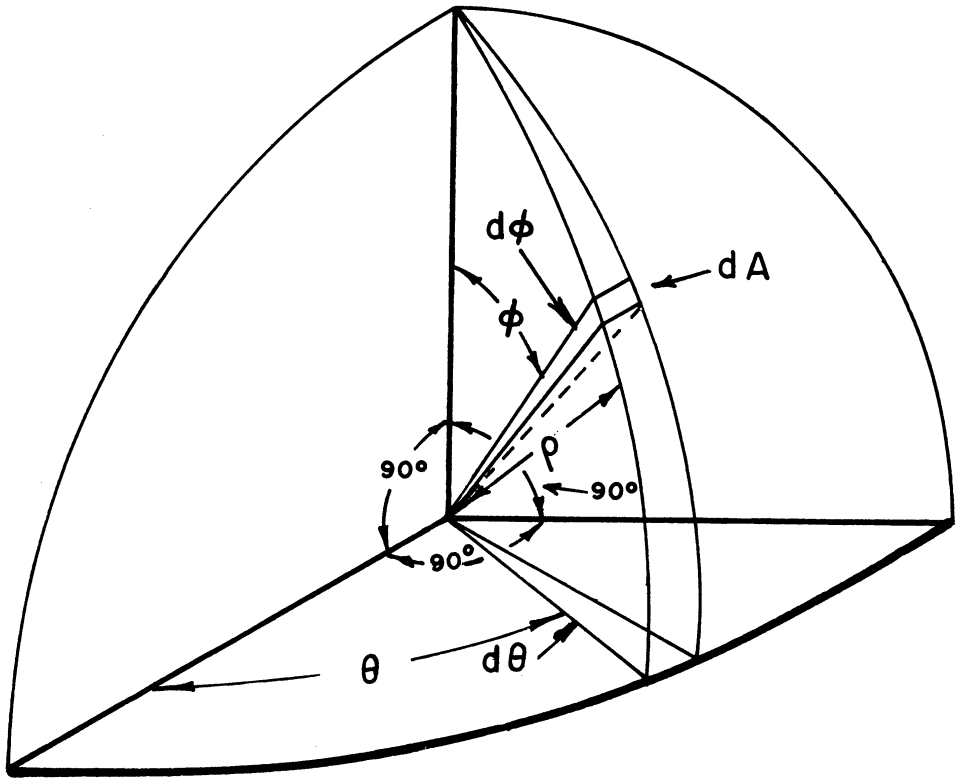

a.

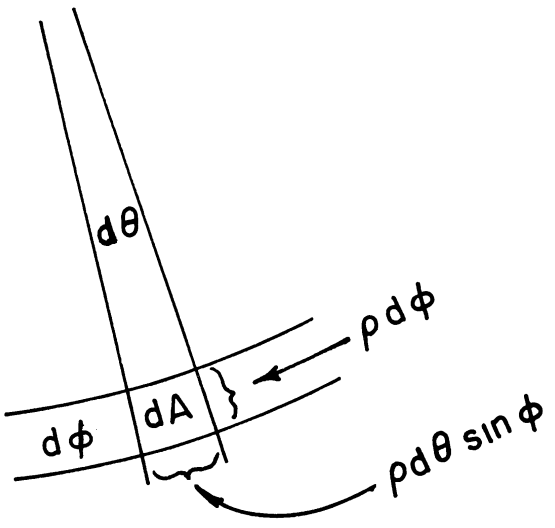

b.

Figure 9. Spherical Coordinates.

vector, ρ, which over all ϕ and θ would form a sphere, the surface of which would represent all orientations. The probability of a single, fixed orientation would be infinitesimally small, but the probability of an incremental range of orientations would be the incremental area of the sphere surface expressing that range, divided by the total surface area of the sphere, as shown in Figure 9.

$$dA = \rho d\phi \cdot \rho \sin \phi d\theta = \rho^2 \sin \phi d\phi d\theta \tag{15}$$

But the total surface of the sphere is $4\pi\rho^2$. Therefore, the probability of a given incremental orientation range is

$$P_\rho(d\phi, d\theta) = \frac{\rho^2 \sin \phi d\phi d\theta}{4\pi\rho^2} = \frac{\sin \phi d\phi d\theta}{4\pi} \tag{16}$$

Summing over all ϕ and θ, the probability that the vector ρ is included in all possible orientations is given by

$$\begin{aligned} P_\rho(\text{all } \phi, \theta) &= \int_0^{2\pi} \int_0^{\pi} \frac{\sin\phi \, d\phi d\theta}{4\pi} \\ &= \frac{1}{4\pi} \int_0^{2\pi} -\cos\phi \Big|_0^{\pi} d\theta = \frac{1}{4\pi} \int_0^{2\pi} 2 d\theta \\ &= \frac{1}{2\pi} \theta \Big|_0^{2\pi} = 1 \end{aligned} \tag{17}$$

Probability Dependent Upon Orientation

Now consider $D(\phi, \theta)$, the distance between tangent planes of a particle which, in general, depends on ϕ and θ. The probability of intersecting a given particle in a given position is equal to the distance between tangent planes in that position times the probability of

obtaining that position.

$$P_i \, d\phi d\theta = D(\phi,\theta) \cdot P_\rho(d\phi, d\theta)$$
$$= D(\phi,\theta) \cdot \frac{\sin \phi d\phi d\theta}{4\pi} \qquad (18)$$

Integrating,

$$P_i(\text{all } \phi,\theta) = \bar{D} \text{ (all } \phi,\theta) = \int_0^{2\pi} \int_0^{\pi} D(\phi,\theta) \frac{\sin \phi d\phi d\theta}{4\pi} \qquad (19)$$

This expression has been presented by DeHoff.[51] D depends upon shape, size, and orientation, and must be expressed in general terms in these parameters. Then, by integrating Equation (19) over all possible orientations, $\bar{D}$, or P_i, can be determined, which will be in terms of shape and size.

For example, take a sphere of radius r, the case previously considered. D will equal 2r for all ϕ and θ.

$$P_i(\text{sphere}) = \int_0^{2\pi} \int_0^{\pi} 2r \frac{\sin \phi d\phi d\theta}{4\pi} = 2r, \qquad (20)$$

as previously obtained.

For a circular platelet of radius r and negligible thickness, it is shown in Figure 10 that $D = 2r \sin \phi$. ϕ is the angle that the platelet normal makes with the vertical. It therefore follows that

$$P_i \text{ (circular platelet)} = \bar{D} \text{ (circular platelet)}$$
$$= \int_0^{2\pi} \int_0^{\pi} 2r \sin\phi \cdot \frac{\sin \phi d\phi d\theta}{4\pi} \qquad (21)$$

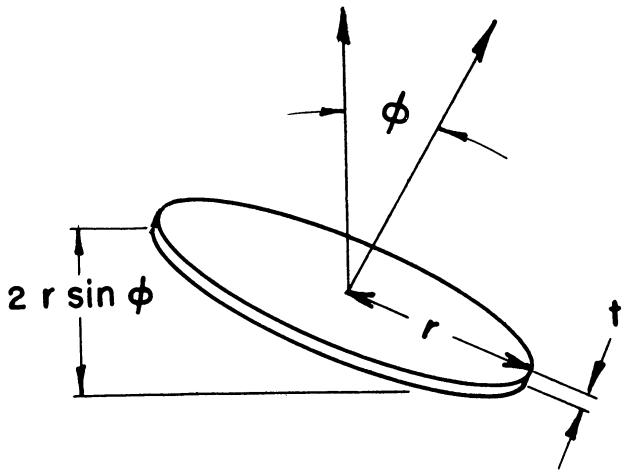

Figure 10. Circular Platelet.

$$= \frac{r}{2\pi} \int_0^{2\pi} \int_0^{\pi} \sin^2\phi d\phi d\theta = \frac{r}{2\pi} \int_0^{2\pi} \frac{1}{2} (\phi - \sin\phi\cos\phi) \Big|_0^{\pi} d\theta$$

$$= \frac{r}{2\pi} \int_0^{2\pi} \frac{\pi d\theta}{2} = \frac{\pi r}{2} \qquad (22)$$

Thus result agrees with that previously given by Fullman[40], which was obtained by a slightly different approach.

For a long needle of length ℓ and negligible radius, it is shown in Figure 11 that $D = \ell \cos \phi$. Therefore, it follows that

$$P_i \text{ (needle)} = \frac{1}{4\pi} \int_0^{2\pi} \int_0^{\pi} \ell \cos\phi \cdot \sin\phi d\phi d\theta \qquad (23)$$

$$= \frac{\ell}{4\pi} \int_0^{2\pi} \frac{1}{2} \sin^2\phi \Big|_0^{\pi} d\theta \qquad (24)$$

However, since $\sin \phi$ equals zero at both limits, it is necessary to change the limits of integration, as follows:

$$P_i \text{ (needle)} = \frac{\ell}{4\pi} \int_0^{2\pi} \sin^2\phi \Big|_0^{\pi/2} d\theta = \frac{\ell}{4\pi} \int_0^{2\pi} d\theta$$

$$= \frac{\ell}{2} \, . \qquad (25)$$

This result also was obtained by Fullman[40] by a different method.

For a cylinder of radius r and length ℓ, we see from Figure 12 that $D = 2r \sin \phi + \ell \cos \phi$. Therefore,

$$P_i(\text{cylinder}) = \frac{1}{4\pi} \int_0^{2\pi} \int_0^{\pi} (2r \sin\phi + \ell\cos\phi) \cdot \sin \phi d\phi d\theta \qquad (26)$$

Equation (26) is simply an addition of Equations (21) and (23), for platelets and needles, and results in

$$P_i(\text{cylinder}) = \frac{1}{2} (\pi r + \ell) \qquad (27)$$

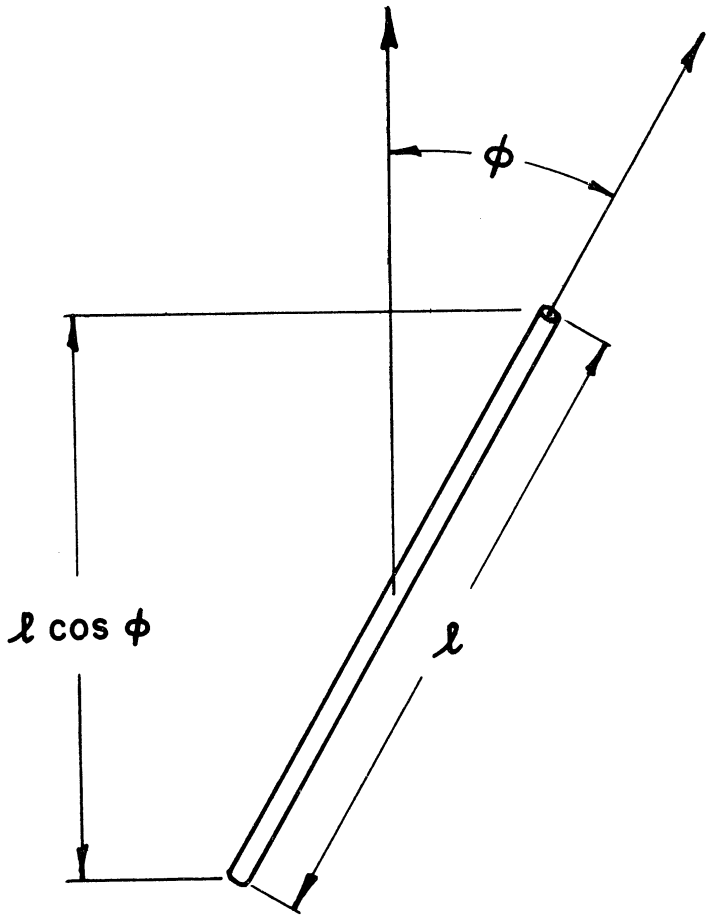

Figure 11. Needle or Rod.

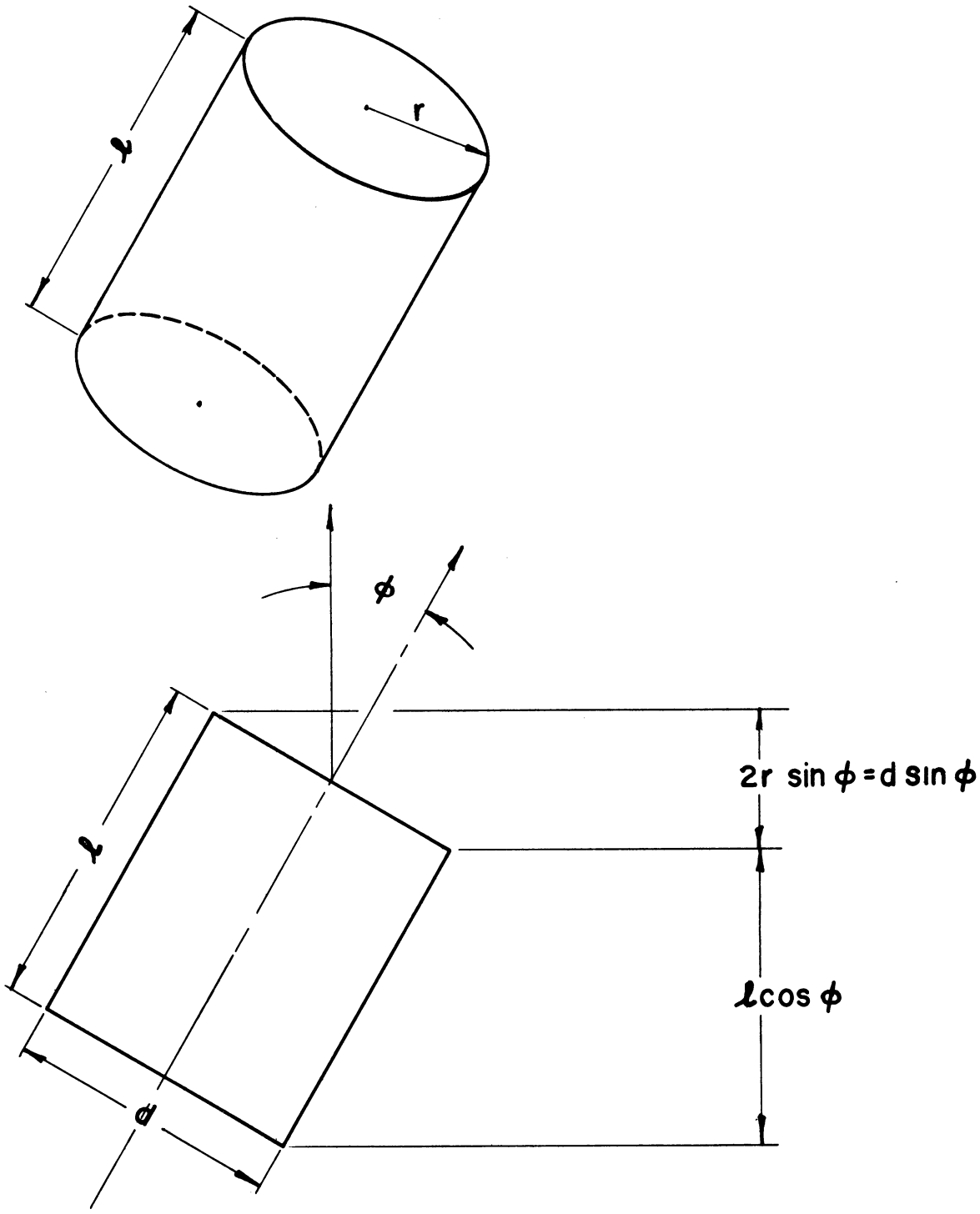

Figure 12. Cylinder.

Again, this agrees with a result previously obtained by Fullman[48].

It may be noted that in none of these cases, sphere, circular platelet, round needle, or cylinder, is Θ involved in expressing D, the distance between tangent planes. In fact, all cases could have been solved without considering Θ. Take the cylinder, for example.

$$P_i \text{ (cylinder)} = \int_0^{\pi/2} (2r \sin\phi + \ell \cos\phi)\sin\phi d\phi$$
$$= \frac{1}{2}(\pi r + \ell) \qquad (27)$$

This is still the same result as before, and was obtained by considering only angles of tilt, ϕ, from 0° to 90°. The probability function for ϕ is the term, $\sin\phi$. Θ is not considered because the cylinder is a solid of revolution and rotating it has no effect on D. Therefore, D is the same as before and so is the final result. In the simplest case, the sphere, D does not even involve ϕ, and integration is not even necessary.

As was shown for a needle, it is not always necessary, or, in some cases, even desireable, to integrate over the whole sphere of orientations. One may integrate over any convenient fraction of the sphere and multiply by the reciprocal of that fraction. Computing P_i (platelet) by integrating over one octant and multiplying by eight, we get

$$P_i \text{ (platelet)} = 8 \int_0^{\pi/2}\int_0^{\pi/2} 2r \sin\phi \cdot \frac{\sin\phi d\phi d\Theta}{4\pi}$$
$$= \frac{\pi r}{2} \qquad (22)$$

This result is the same as before.

In general terms, for one octant,

$$\overline{D} = \frac{2}{\pi} \int_0^{\pi/2} \int_0^{\pi/2} D(\phi,\theta) \cdot \sin \phi d\phi d\theta \qquad (28)$$

If the object is a volume of revolution,

$$\overline{D} = \int_0^{\pi/2} D(\phi) \cdot \sin \phi d\phi \qquad (29)$$

The most convenient choice of integration limits will, in general, be dictated by the symmetry of the solid object or particle that we are considering.

This general method will now be extended to obtain various new results that can be used to describe:

a) relative frequencies of various section shapes of cylinders

b) the probability of intersection by cross-sectioning plane for several polyhedrons

c) relative frequencies of various section shapes for these polyhedrons.

The general method is as described; the main problem will be in determining the $D(\phi,\theta)$ and the ϕ and θ values over which to integrate.

IV. SECTIONS OF CYLINDERS

Types of Sections

If a cylinder is cut by a random sectioning plane, then there are three general possibilities for classifying the shapes of sections obtained: the plane may cut neither end of the cylinder, it may cut one end, or it may cut both ends. Similarly, for cylindrical particles randomly distributed and oriented in a solid, if a sectioning plane is passed through the solid, then the shapes of sections which are cut from the cylindrical particles may be elliptical, may show one straight edge, or may show two straight edges. These section shapes may be referred to as ellipses, singly-truncated ellipses or cups, and doubly-truncated ellipses or barrels. Typical cuts of cylinders and their section shapes are shown in Figures 13, 14, and 15.

The variables affecting the types of sections obtained will be the shape of the cylinder or its ℓ/d ratio, the orientation of the cylinder or its ϕ, tilt angle, and the relative position of the sectioning plane. A wide variety of different appearing section shapes may be obtained, depending upon these variables just mentioned, but all can be classed into one of three groups: barrel, B, ellipse, E, or cup, C.

From the dimensions of the sections obtained from uniform size cylinders, one can deduce quite a bit about the dimensions of the cylinder. Since all sections are basically elliptical, even though truncated, let us refer to section width in the direction

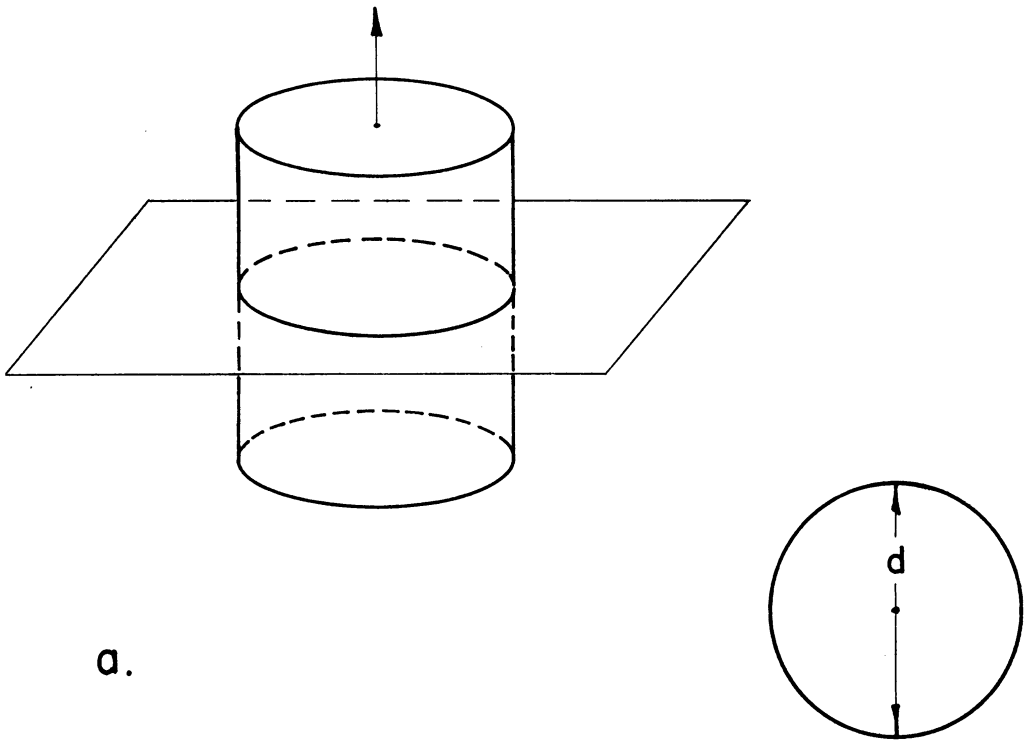

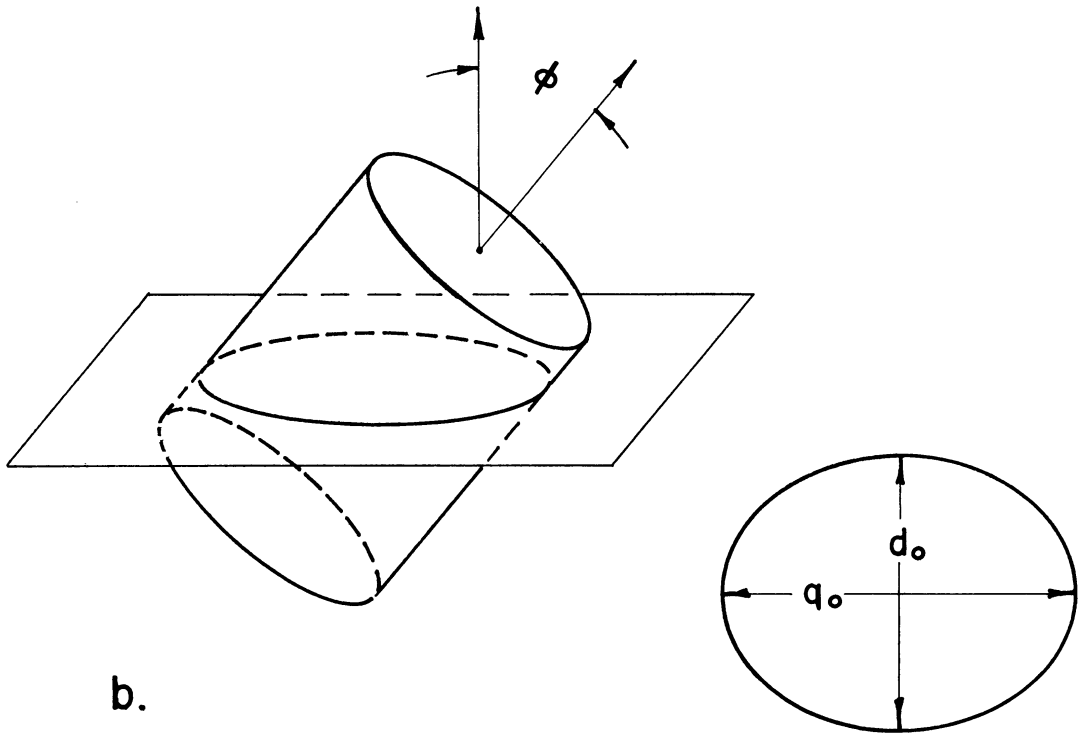

Figure 13. Elliptical Sections of Cylinders.

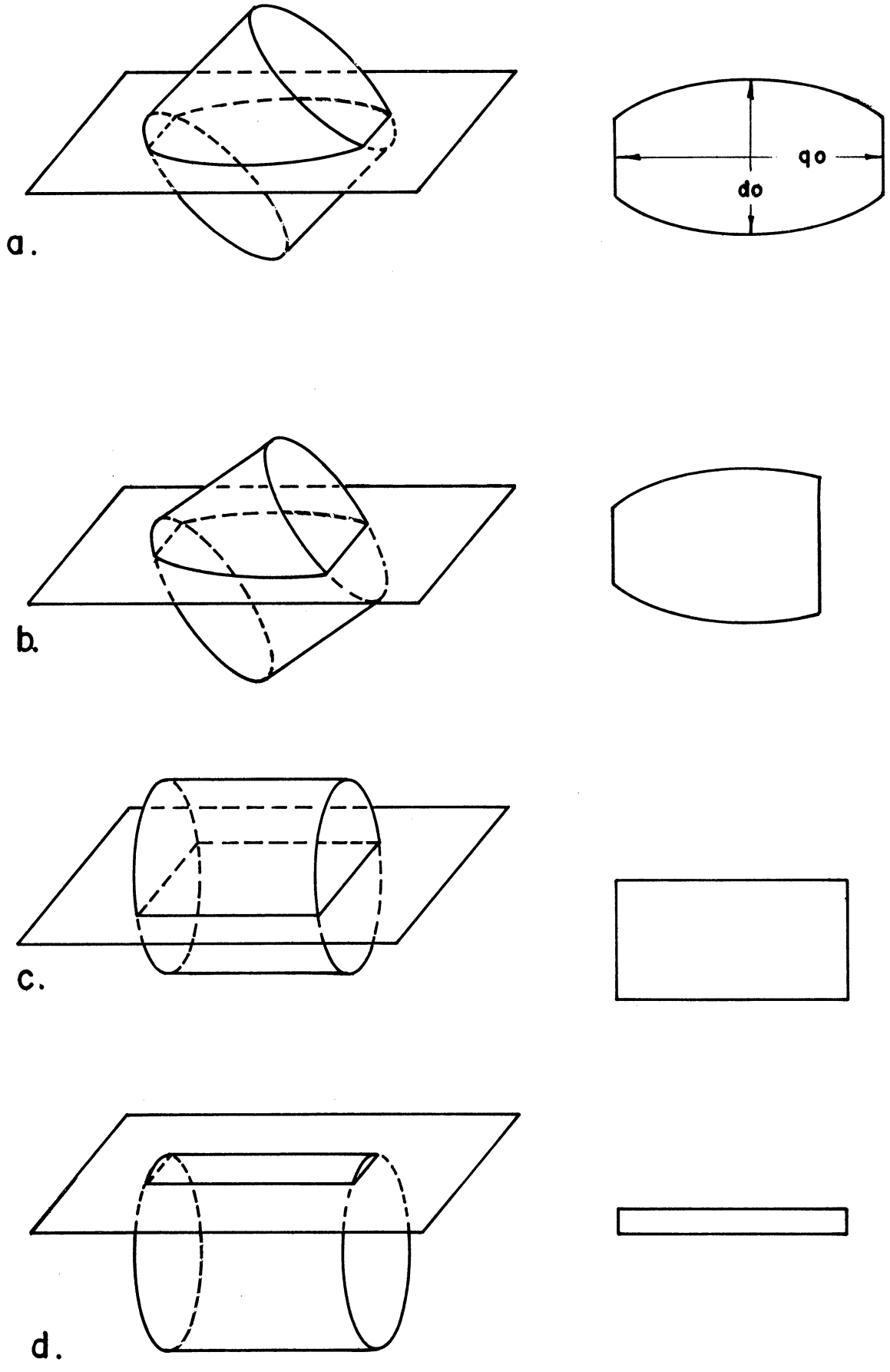

Figure 14. Barrel Sections of Cylinders.

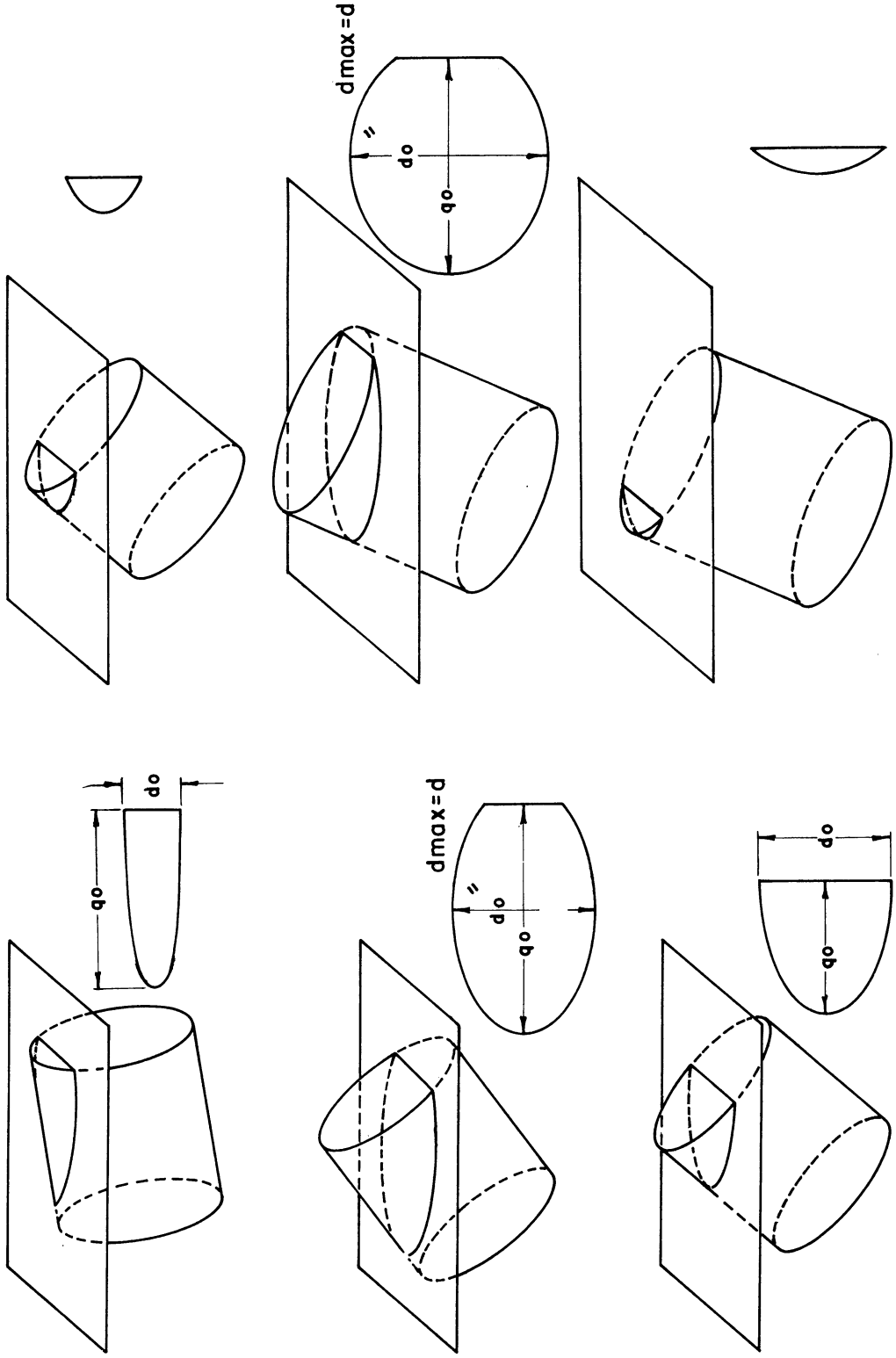

Figure 15. Cup Sections of Cylinder.

of the minor axis of the ellipse or parallel to a straight side as "d_o" and to the section length in the direction of the major axis of the ellipse perpendicular to a straight edge as "q_o". Then, for elliptical sections d_o always equals d, the true diameter of the cylinder. For barrel and cup sections, d_o will equal d in a certain fraction of cases and will vary between zero and d in the rest of the cases. Thus, for uniform cylinders the diameter should be deduced quite readily by inspection.

To obtain ℓ, the cylinder length, consider q_o. For ellipses, q_o will vary from d_o or d to $\sqrt{\ell^2 + d_o^2}$. If we take $q_{max.}$ as an estimate of $\sqrt{\ell^2 + d_o^2}$, then for ellipses

$$\ell = \sqrt{q_{max.}^2 - d_o^2} \qquad (30)$$

As a check against barrels and cups, in both of these cases $d_{max.}$ equals d and q_o will vary from ℓ in the case of barrels and zero in the case of cups to $\sqrt{\ell^2 + d_{max.}^2}$. Again, saying $q_{max.} = \sqrt{\ell^2 + d_{max.}^2}$, then for barrels and cups

$$\ell = \sqrt{q_{max.}^2 - d_{max.}^2} \qquad (31)$$

It may be noted that in the case of barrels an easier way to get ℓ may be using $\ell = q_{min.}$ Reference to Figures 13, 14, and 15 will clarify this discussion.

Fullman[48] gives equations for calculating d and ℓ directly from sections of cylinders, but these are fairly complicated and require determination of average particle section area and average particle

traverse length, both of which may require a considerable amount of effort to obtain. Thus, the above indirect method for estimating ℓ and d may often prove useful.

Consider the possibility of directly measuring $q_{max.}$ It may be seen from Figure 16 that $q_{max.}$, although it is the maximum limiting length measured in all three cases, ellipses, barrels, and cups, is still only a limiting, singular case. $q_{max.}$ is actually only obtained when ϕ, the tilt angle, equals arctan ℓ/d and when the sectioning plane cuts exactly through the center of the cylinder. Thus, for orientation ϕ = arctan ℓ/d, $q_{max.}$ is the transition section between upper cups and lower cups. In this orientation, it may be observed, no barrels or ellipses are obtained as sections, and $q_{max.}$ is the maximum length of cups. However, $q_{max.}$ is approached closely as the maximum length of barrels and of ellipses for values of ϕ very close to arctan ℓ/d, again, for central cuts.

It is obvious that the ratio, ℓ/d, expresses the shape of the cylinder. The angle that expresses the limiting orientations for certain shaped sections or cuts of the cylinder is

$$\phi_1 = \arctan \ell/d \qquad (32)$$

For $\phi <$ arctan ℓ/d, it is impossible to get barrel sections, and only ellipses and cups are obtained. For $90° > \phi >$ arctan ℓ/d, it is impossible to get elliptical sections, and only barrels and cups are obtained. We shall use ϕ_1, as expressed by Equation (32), in determining the relative frequencies of the various shaped sections of randomly oriented cylinders.

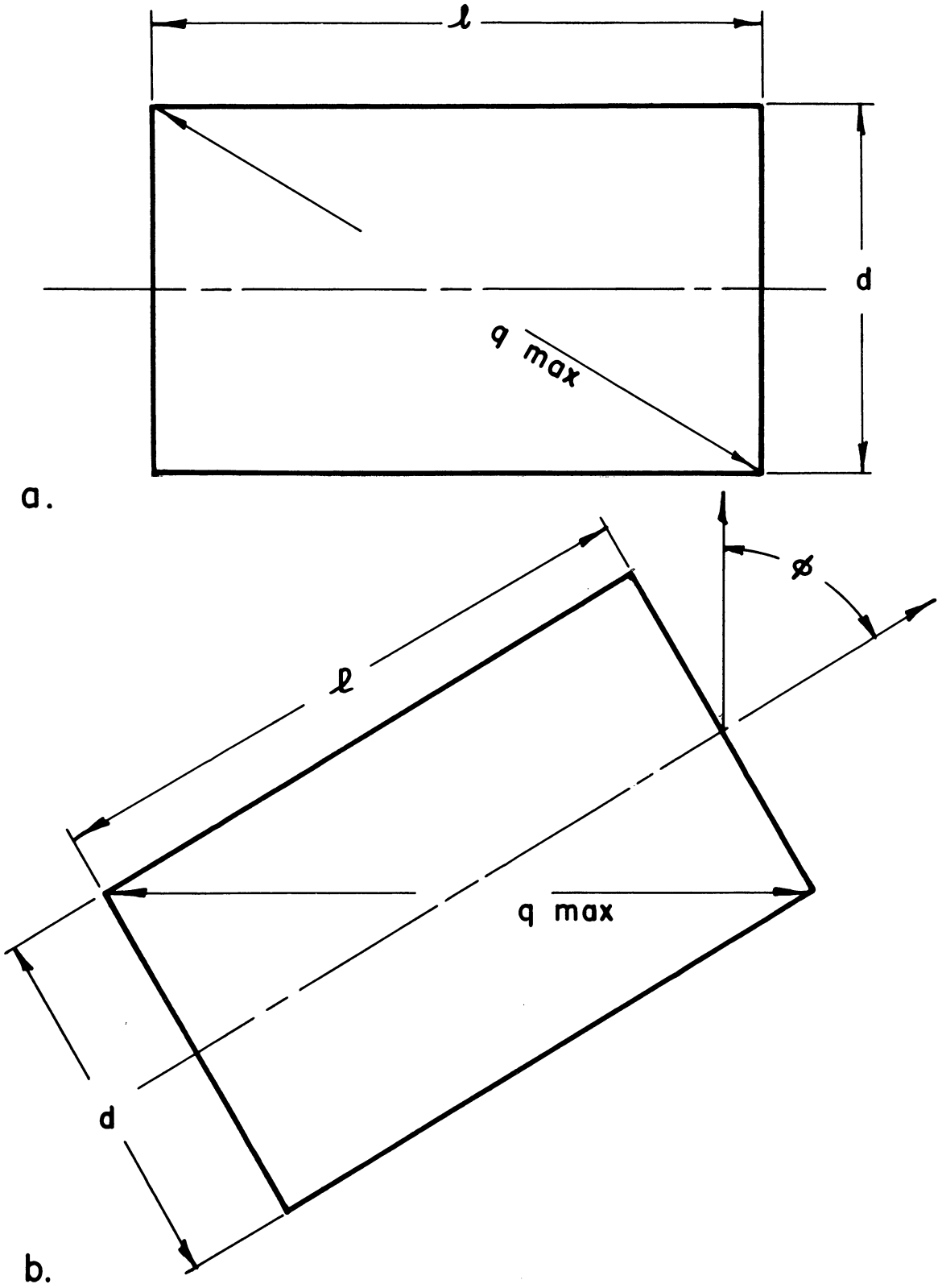

Figure 16. Major Parameters of a Cylinder.

Relative Frequencies of Sections

Heretofore we have considered qualitatively the possible shapes of sections obtained from cylinders. Now we shall consider this matter quantitatively. As before, ϕ will be the angle between axis of cylinder and the normal to the sectioning plane, and ℓ and d will be the length and diameter, respectively, of the cylinder. A cup will be a singly-truncated elliptical section, symbol C; a barrel will be a doubly-truncated elliptical section, symbol B; and an untruncated or plain elliptical section will have the symbol E.

First we shall obtain the D functions for these three type sections, or the distance normal to the sectioning planes over which each of these sections may be obtained. This will be related to the probability of obtaining the particular sections in an exactly analogous manner to that previously described for certain whole particles.

For the cylinder, to obtain the D functions of sections, it will be necessary to consider two cases:

Case I $\quad 0 \leq \phi \leq \arctan \ell/d$

Case II $\quad \arctan \ell/d \leq \phi \leq 90°$

Then we can collect the different D's for the various cases, ellipse, barrel, or cup, and integrate over the proper range to obtain $\overline{D}$, the average height over which each section is obtained, or its probability. Comparing the $\overline{D}$'s for the sections with the $\overline{D}$'s for the whole cylinder, we obtain the relative frequencies of the section shapes for any given cylinder shape.

Consider Case I, $0 \leq \phi \leq \arctan \ell/d$, as shown in Figure 17a.

$$D = h_1 + h_2 + h_3 \tag{33}$$

For plane sections passing through elevation ranges h_1 and h_3, we observe cups as the sections of the cylinder. For cuts over the range h_2 we observe ellipses. But $h_1 = h_3 = d \sin \phi$ and $h_2 = \ell \cos \phi - h_1 = \ell \cos \phi - d \sin \phi$. Therefore, for cup shaped sections we find that

$$D_C = h_1 + h_3 = 2 d \sin \phi \quad (0 \leq \phi \leq \arctan \ell/d) \tag{34}$$

We also see that, for Case I, elliptical sections are given by

$$D_E = h_2 = \ell \cos \phi - d \sin \phi \ (0 \leq \phi \leq \arctan \ell/d) \tag{35}$$

Next, for Case II, we have $\arctan \ell/d \leq \phi \leq 90°$, as shown in Figure 17b, and

$$D = h_4 + h_5 + h_6 \tag{36}$$

For cuts through h_4 and h_6 we get cups. For h_5 cuts we get barrels. But $h_4 = h_6 = \ell \cos \phi$ and $h_5 = d \sin \phi - \ell \cos \phi$. Therefore, for cups we have, in Case II

$$D_C = h_4 + h_6 = 2 \ell \cos \phi \quad (\arctan \ell/d \leq \phi \leq 90°) \tag{37}$$

For barrels in Case II, we have

$$D_B = h_5 = d \sin \phi - \ell \cos \phi \ (\arctan \ell/d \leq \phi \leq 90°) \tag{38}$$

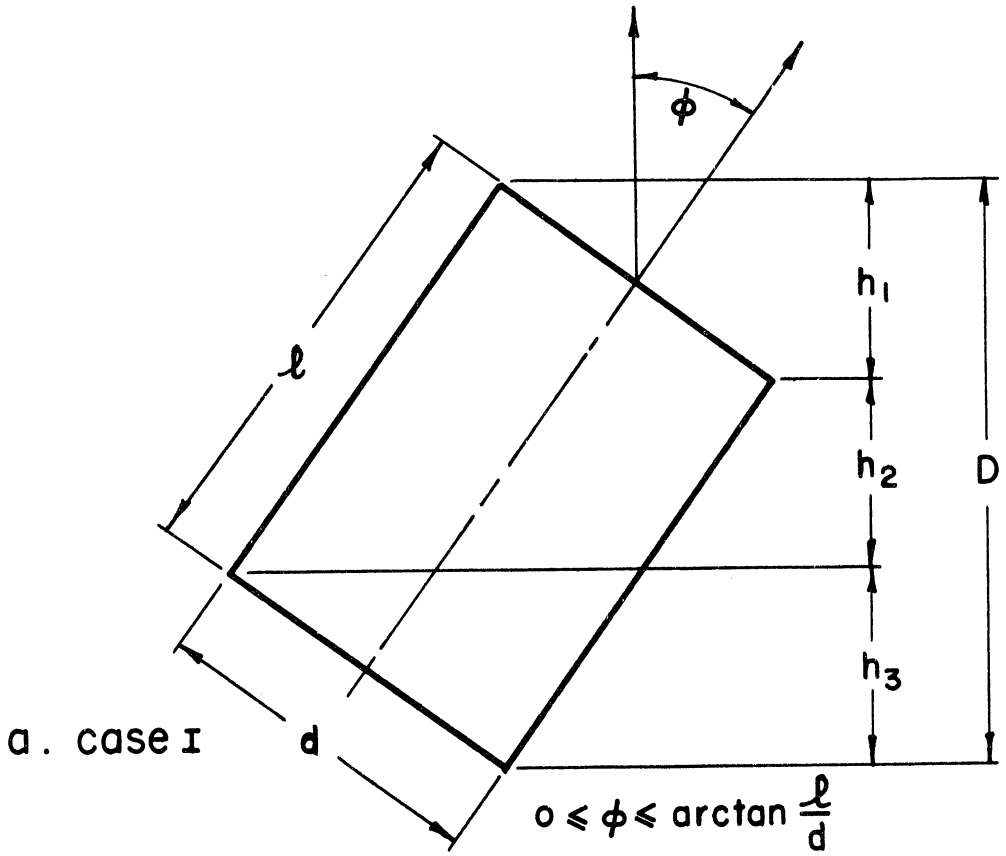

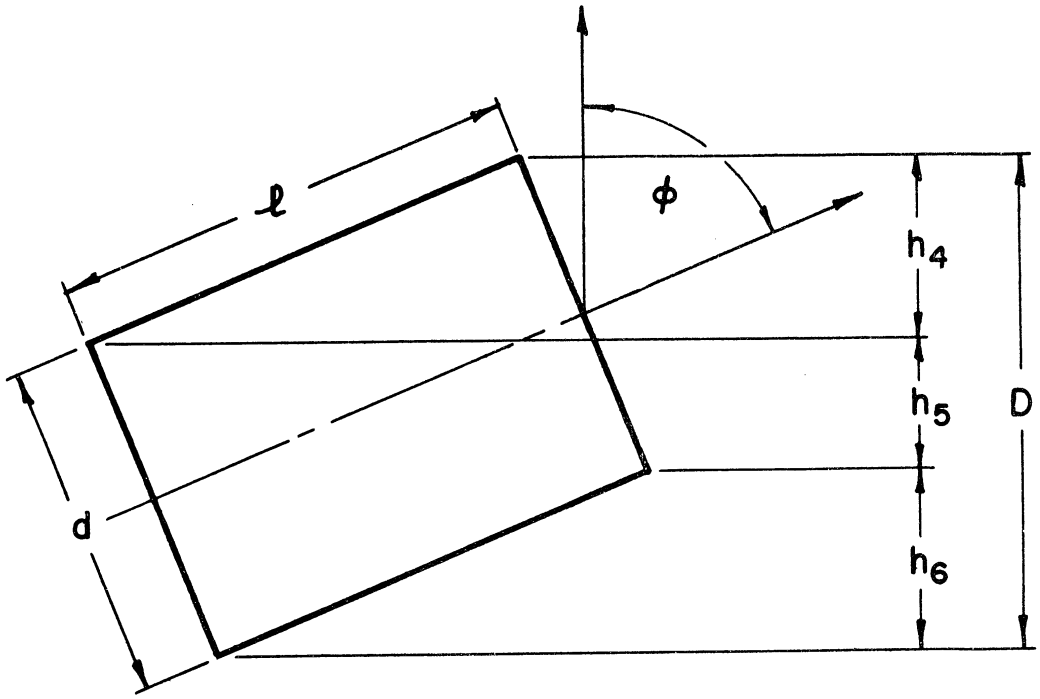

Figure 17. Two Orientations of Cylinders.

Since ellipses are observed only for $0 \leq \phi \leq \arctan \ell/d$, $\bar{D}_E$ is obtained by integrating over these limits in one octant of the orientation sphere, using the D_E from Equation (35).

$$\begin{aligned} \bar{D}_E &= \frac{2}{\pi} \int_0^{\pi/2} \int_0^{\arctan \ell/d} (\ell \cos \phi - d \sin \phi) \sin \phi \, d\phi \, d\theta \\ &= \frac{2}{\pi} \int_0^{\pi/2} \left[\frac{\ell}{2} \sin^2 \phi - \frac{d}{2} (\phi - \sin \phi \cos \phi) \right]_0^{\arctan \ell/d} d\theta \end{aligned} \tag{39}$$

But $\sin(\arctan \ell/d) = \ell / \sqrt{\ell^2 + d^2}$

and $\cos(\arctan \ell/d) = d / \sqrt{\ell^2 + d^2}$

Therefore, for ellipses

$$\begin{aligned} \bar{D}_E &= \frac{1}{\pi} \int_0^{\pi/2} \left[\ell \cdot \frac{\ell^2}{\ell^2 + d^2} - d\left(\arctan \frac{\ell}{d} - \frac{\ell d}{\ell^2 + d^2}\right) \right] d\theta \\ &= \frac{1}{\pi} \int_0^{\pi/2} \left[\ell \cdot \frac{\ell^2}{\ell^2 + d^2} + \ell \cdot \frac{d^2}{\ell^2 + d^2} - d \arctan \frac{\ell}{d} \right] d\theta \\ &= \frac{1}{\pi} \left(\ell - d \arctan \frac{\ell}{d}\right) \int_0^{\pi/2} d\theta \\ \bar{D}_E &= \frac{1}{2} \left(\ell - d \arctan \frac{\ell}{d}\right) \end{aligned} \tag{40}$$

The above result from integration of Equation (39) may also be obtained by integration of

$$\bar{D}_E = \int_0^{\arctan \ell/d} (\ell \cos \phi - d \sin \phi) \sin \phi \, d\phi \tag{41}$$

For barrels, we use the D_B from Equation (38) and integrate over limits $\arctan \ell/d \leq \phi \leq 90°$ to obtain $\bar{D}_B$.

$$\bar{D}_B = \int_{\arctan \ell/d}^{\pi/2} (d \sin \phi - \ell \cos \phi) \sin \phi d\phi$$

$$= \frac{1}{2} [d(\phi - \sin \phi \cos \phi) - \ell \sin^2 \phi]_{\arctan \ell/d}^{\pi/2}$$

$$= \frac{1}{2} [\frac{\pi d}{2} - d \arctan \frac{\ell}{d} + d \cdot \frac{\ell d}{\ell^2 + d^2} - \ell + \ell \cdot \frac{\ell^2}{\ell^2 + d^2}]$$

$$= \frac{1}{2} [\frac{\pi d}{2} - d \arctan \frac{\ell}{d} + \ell \cdot \frac{d^2 + \ell^2}{\ell^2 + d^2} - \ell]$$

$$= \frac{\pi d}{4} - \frac{d}{2} \arctan \frac{\ell}{d} \qquad (42)$$

To obtain $\bar{D}_C$ for cups we have two D_C's over two angular intervals, Equations (34) and (37), which must be integrated and added.

$$\bar{D}_C = \int_0^{\arctan \ell/d} 2d \sin \phi \cdot \sin \phi d\phi$$

$$+ \int_{\arctan \ell/d}^{\pi/2} 2\ell \cos \phi \cdot \sin \phi d\phi$$

$$= d(\phi - \sin \phi \cos \phi)\Big|_0^{\arctan \ell/d} + \ell(\sin^2 \phi)\Big|_{\arctan \ell/d}^{\pi/2}$$

$$= d(\arctan \frac{\ell}{d} - \frac{\ell d}{\ell^2 + d^2}) + \ell(1 - \frac{\ell^2}{\ell^2 + d^2}$$

$$\bar{D}_C = d \arctan \ell/d \qquad (43)$$

Now, as a check, $\bar{D}_{TOTAL}$ for cylinders should equal the sum of the $\bar{D}$'s for their sections.

$$\bar{D}_{TOTAL} = \bar{D}_C + \bar{D}_E + \bar{D}_B$$

$$= (d \arctan \frac{\ell}{d}) + (\frac{\ell}{2} - \frac{d}{2} \cdot \arctan \frac{\ell}{d}) + (\frac{\pi d}{4} - \frac{d}{2} \cdot \arctan \frac{\ell}{d})$$

$$P_i(\text{cylinder}) = \frac{\pi d}{4} + \frac{\ell}{2} \qquad (27)$$

This agrees with the result obtained in Section III.

We now obtain the relative frequencies, f, for each shape of section of a cylinder, as a function of the length and diameter of the cylinder. From $f(\text{section}) = \frac{\bar{D}\ (\text{section})}{\bar{D}\ (\text{total})}$, we list these relations in Table III.

TABLE III

FREQUENCY OF SECTIONS OF CYLINDERS

Shape of Section	Frequency Relations
Cup	$\frac{d \arctan \frac{\ell}{d}}{\frac{\pi d}{4} + \frac{\ell}{2}} = \frac{2 \arctan \frac{\ell}{d}}{\frac{\ell}{d} + \frac{\pi}{2}}$
Ellipse	$\frac{\frac{1}{2}(\ell - d \arctan \frac{\ell}{d})}{\frac{\pi d}{4} + \frac{\ell}{2}} = \frac{\frac{\ell}{d} - \arctan \frac{\ell}{d}}{\frac{\ell}{d} + \frac{\pi}{2}}$
Barrel	$\frac{\frac{\pi d}{4} - \frac{d}{2} \arctan \frac{\ell}{d}}{\frac{\pi d}{4} + \frac{\ell}{2}} = \frac{\frac{\pi}{2} - \arctan \frac{\ell}{d}}{\frac{\ell}{d} + \frac{\pi}{2}}$

The relations of Table III will be used to check the experimental data obtained for cylinders. A graph of these functions versus ℓ/d ratio is presented in Figure 18.

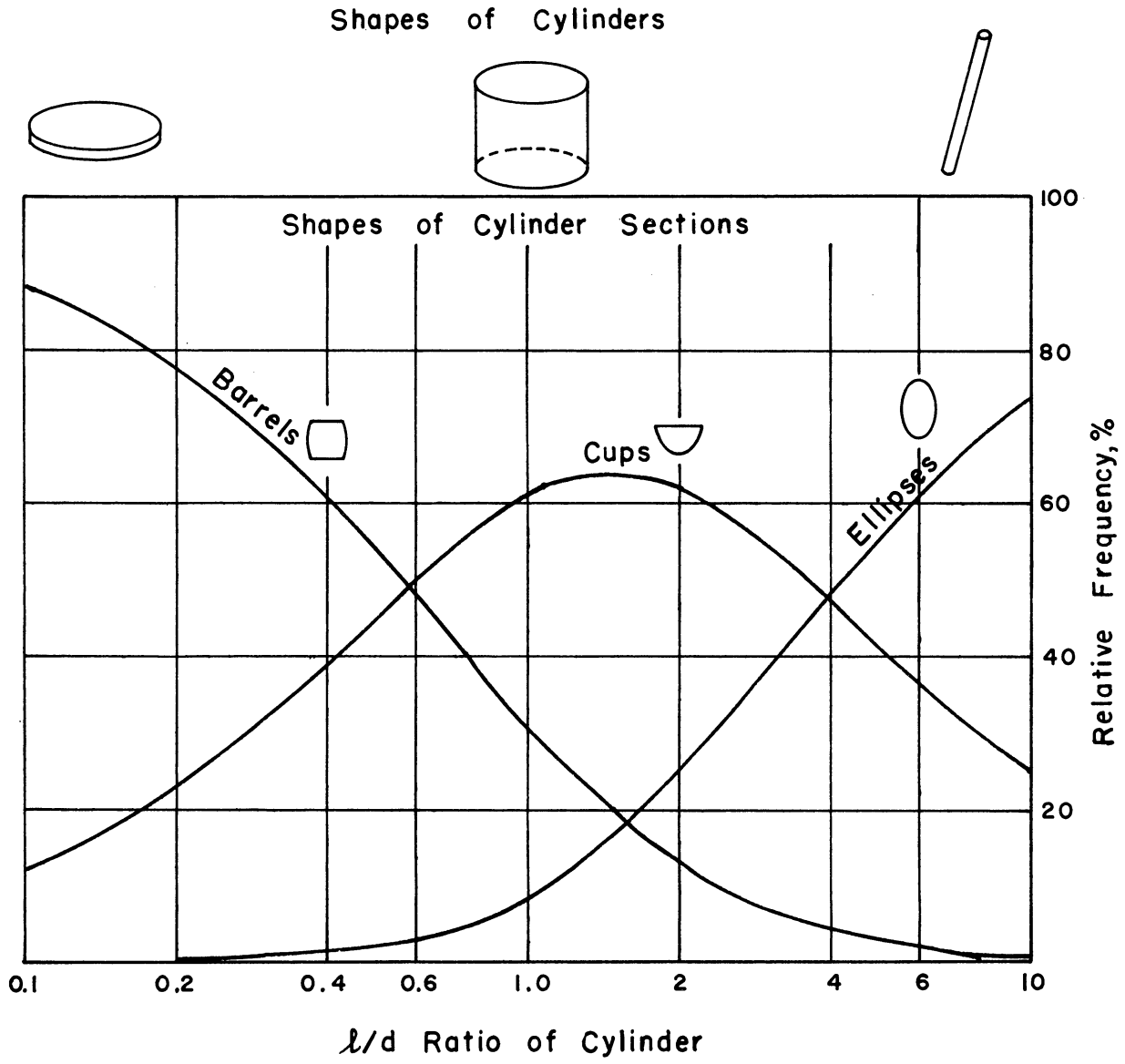

Figure 18. Relative Frequency of Cylinder Sections as Function of ℓ/d Ratio.

V. CUBES

Probability of Sectioning a Cube

Up until this point we have discussed and developed relations connecting particle shape, size, and number for solids of revolution. The methods of solution involved integrating over all orientations, expressed in terms of both ϕ and θ, tilt and rotation, although as a practical matter it was observed that only ϕ was needed as θ, rotation, had no effect on such bodies. A cube is not a solid of revolution, so it will be seen that θ must be included, as well as ϕ, in computing the probability of sectioning a cube.

Remembering that it is distance between parallel tangent planes, or projected height, that determines probability of intersection by a plane, reference to Figure 19a will show the limiting height values for the cube. If the cube has edge length "a", then with one face parallel to sectioning plane the projected height is "a". With the cube oriented as in Figure 19b, the projected height is "a" when $\phi = 0$, for any θ, as well as when $\theta = 0$ and $\phi = \pi/2$ and when $\theta = \pi/2$ and $\phi = \pi/2$.

We have projected height $= \sqrt{2}$ a when $\theta = 0$, $\phi = \pi/4$, when $\theta = \pi/2$, $\phi = \pi/4$, and when $\theta = \pi/4$, $\phi = \pi/2$. When $\theta = \pi/4$ and $\phi = \arctan \sqrt{2}$ (approximately $54^\circ\ 44'$) we have projected height $= \sqrt{3}$ a. This blankets the range of possibilities as $\sqrt{3}$ a is the maximum D and "a" is the minimum. We shall need $D(\phi,\theta)$, in terms of both ϕ and θ, to integrate over a suitable range of ϕ and θ for $\overline{D}$.

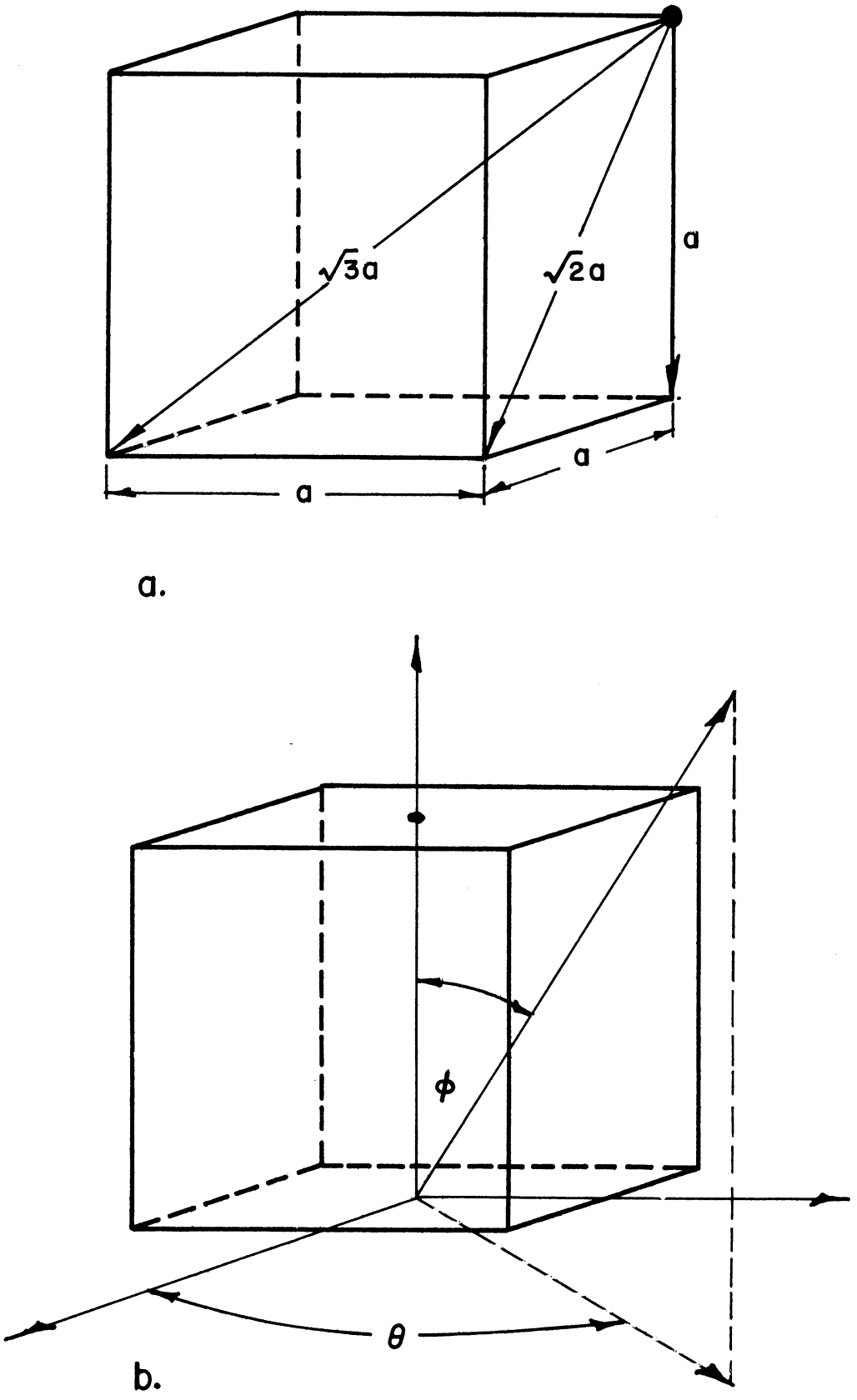

Figure 19. Major Parameters of a Cube.

First we shall number the corners of the cube, one through eight, as shown in Figure 20a. Now it will be seen that the distance between top and bottom parallel tangent planes, which will be the probability of intersection by a sectioning plane, will be represented by the vertical distance between top and bottom corners for a given orientation. So if the orientations of the cube are varied in the first octant, in the manner indicated by Figure 19b, then corner 1 will always be the top corner and corner 8 will always be the bottom corner, and we will want the projected height from corner 1 to corner 8. The easiest way to obtain this is to take another corner as reference corner, using corner 4 as indicated in Figure 20b, and consider this as a fixed point about which orientation changes are made. Then the resulting changes in elevations between corners 1 and 4 and corners 4 and 8 are computed separately; the total projected height is easily obtained from the sum of these two sub-heights.

Consider that we revolve or tilt the cube about corner 4 in a direction Θ, as shown in Figure 20b. The amount that the cube is tilted will be the angle ϕ, shown in Figure 20c. This is analogous to corner 1 following a circular path about the axis u-v which passes through corner 4. The radius of the circular path followed by corner 1 is the length m. These are shown in Figure 20b. As Θ is allowed to vary between 0° and 90°, the length of m may readily be seen to be

$$m = \sqrt{2}\, a \sin (\Theta + 45) \qquad (44)$$

From Figure 20c, it may be seen that

$$h_{1-4} = m \sin \phi$$

$$h_{1-4} = \sqrt{2}\, a \sin (\Theta + 45) \cdot \sin \phi \qquad (45)$$

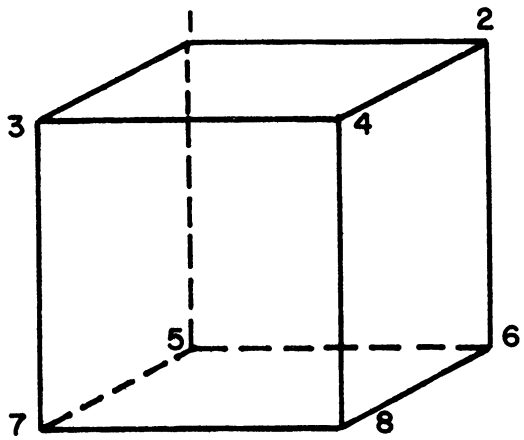

a.

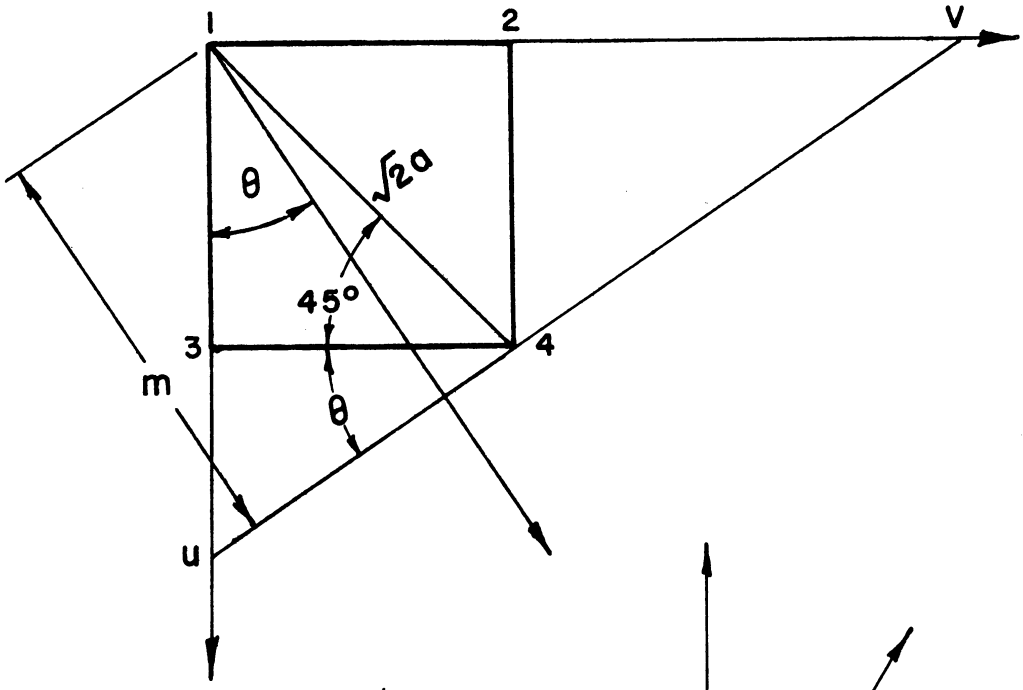

b.

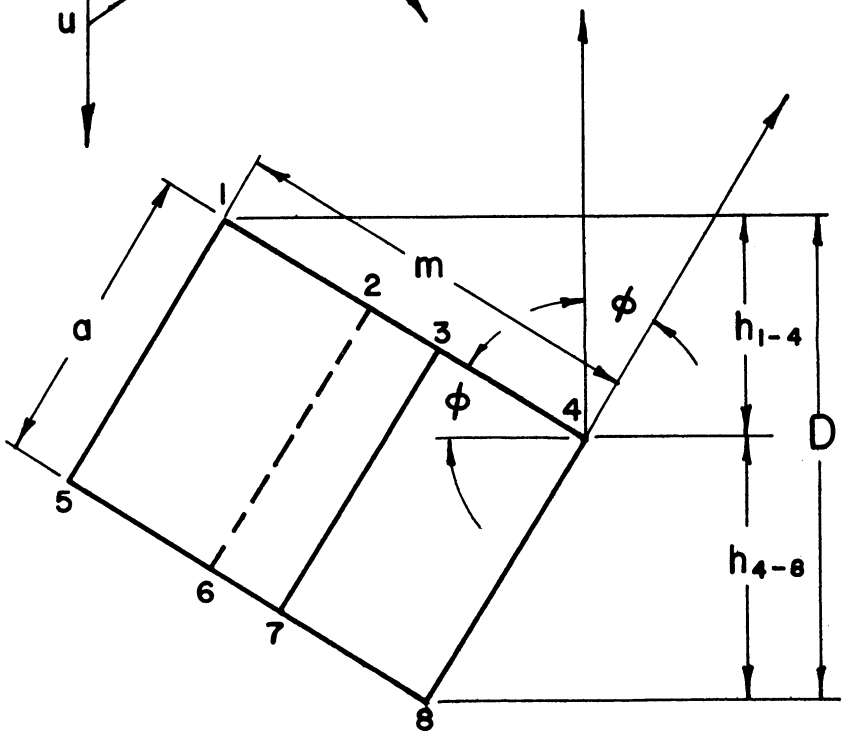

c.

Figure 20. Cube Corners and Radius of Revolution.

This is the projected height from corners 1 to 4.

From Figure 20c, the projected height from corners 4 to 8 will be

$$h_{4-8} = a \cos \phi \tag{46}$$

Therefore, the total projected height of the cube, D (cube), will be

$$\begin{aligned} D\ (\text{cube}) &= h_{1-4} + h_{4-8} \qquad (47) \\ &= \sqrt{2}\ a \sin\ (\theta + 45) \cdot \sin \phi + a \cos \phi \end{aligned}$$

But, from trigonometry

$$\sin(\theta + 45) = \frac{1}{\sqrt{2}} (\sin \theta + \cos \theta) \tag{48}$$

Therefore, the function giving projected height of a cube is

$$D\ (\text{cube}) = a\ (\sin \theta + \cos \theta) \sin \phi + a \cos \phi \tag{49}$$

It can be summarized that, for given θ, corner 1 rises above corner 4 with change in ϕ and this height is expressed as h_{1-4}, and corner 8 rises toward corner 4, the difference in elevation being h_{4-8}. The total elevation distance from corners 1 to 8, the difference between top and bottom tangent planes of the cube, is the sum expressed by Equation (49).

Now if we take Equation (49) for D (cube) and substitute it in Equation (28) and integrate over the first octant (permissible because of the cubic symmetry), we have

$$\bar{D}\ (\text{cube}) = \frac{2}{\pi} \int_0^{\pi/2} \int_0^{\pi/2} a[(\sin\theta + \cos\theta) \sin\phi + \cos\phi] \sin \phi d\phi d\theta \tag{50}$$

$$\bar{D}\ (\text{cube}) = \frac{2a}{\pi} \int_0^{\pi/2} \int_0^{\pi/2} (\sin\theta + \cos\theta) \sin^2\phi \, d\phi \, d\theta$$

$$+ \frac{2a}{\pi} \int_0^{\pi/2} \int_0^{\pi/2} \cos\phi \sin\phi \, d\phi \, d\theta$$

$$= \frac{2a}{\pi} \int_0^{\pi/2} (\sin\theta + \cos\theta) \frac{1}{2} (\phi - \sin\phi \cos\phi) \Big|_0^{\pi/2} d\theta$$

$$+ \frac{2a}{\pi} \int_0^{\pi/2} \frac{1}{2} \sin^2\phi \Big|_0^{\pi/2} d\theta$$

$$= \frac{a}{\pi} \int_0^{\pi/2} (\sin\theta + \cos\theta) \frac{\pi}{2} d\theta + \frac{a}{\pi} \int_0^{\pi/2} d\theta$$

$$= \frac{a}{2} \int_0^{\pi/2} (\sin\theta + \cos\theta) \, d\theta + \frac{a}{2}$$

$$\bar{D}\ (\text{cube}) = \frac{a}{2} (1 + 1) + \frac{a}{2} = \frac{3}{2} a \qquad (51)$$

Therefore, the probability of sectioning a cube is

$$P_i\ (\text{cube}) = \frac{3}{2} a \qquad (51)$$

This result leads directly to the relation for uniformily sized cubes

$$(\text{cube})\quad N_S = N_V \cdot \frac{3}{2} a \qquad (52)$$

Rectangular Parallelepipeds

The result just obtained for a cube can easily be extended to a rectangular parallelepiped of side lengths a, b, and c, Figure 21. For a given direction, θ, we again revolve the figure about a line, uv, which passes through corner 4 perpendicularly to direction θ. We can

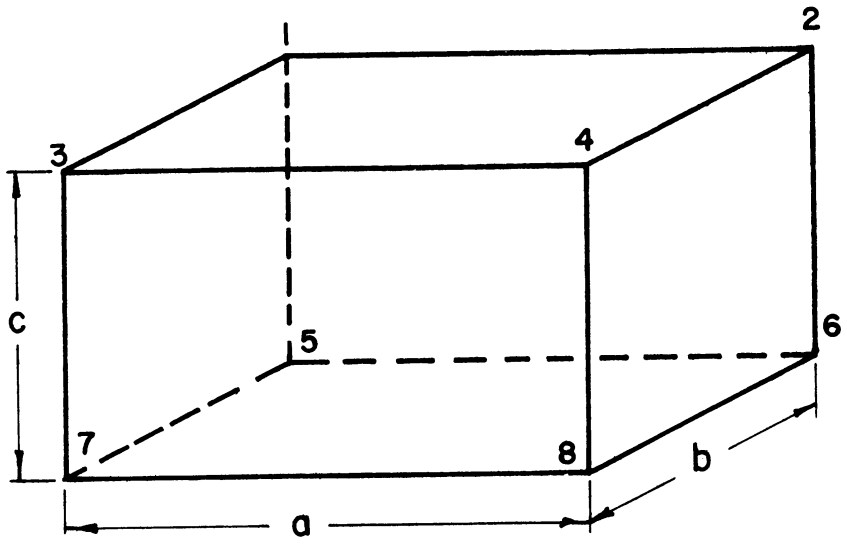

a.

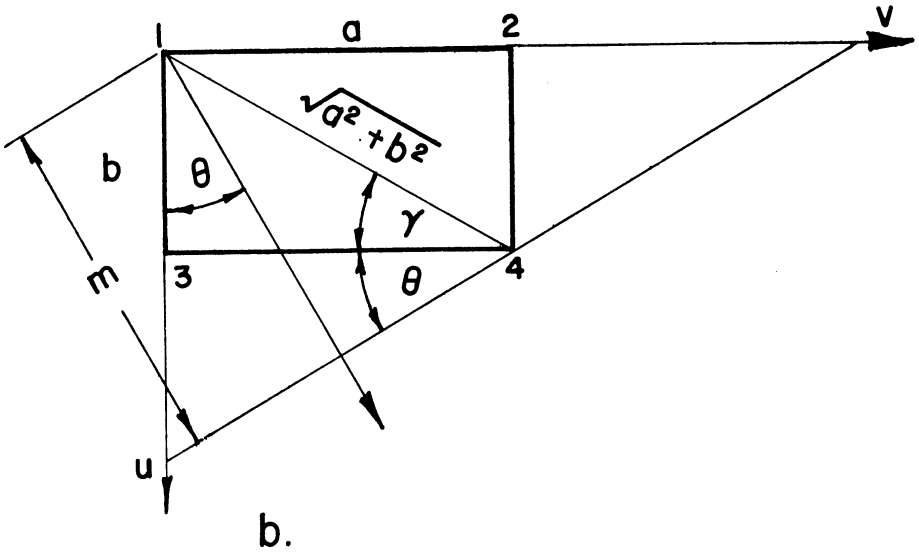

b.

Figure 21. Rectangular Parallelpiped.

see that the angle γ is given by

$$\gamma = \arcsin \frac{b}{\sqrt{a^2 + b^2}} \tag{53}$$

Therefore, m is equal to

$$m = \sqrt{a^2 + b^2} \sin (\theta + \gamma)$$

$$m = \sqrt{a^2 + b^2} \sin (\theta + \arcsin \frac{b}{\sqrt{a^2 + b^2}}) \tag{54}$$

The top tangent plane passing through corner 1 rises above corner 4 by

$$h_{1-4} = m \sin \phi = \sqrt{a^2 + b^2} \sin (\theta + \arcsin \frac{b}{\sqrt{a^2 + b^2}}) \cdot \sin \phi \tag{55}$$

Again, from trigonometry

$$\sin \left(\theta + \arcsin \frac{b}{\sqrt{a^2 + b^2}} \right) = (\sin \theta) \left(\frac{a}{\sqrt{a^2 + b^2}} \right) + (\cos \theta) \left(\frac{b}{\sqrt{a^2 + b^2}} \right)$$

$$= \frac{1}{\sqrt{a^2 + b^2}} (a \sin \theta + b \cos \theta) \tag{56}$$

Therefore, corner 1 rises above corner 4 by the amount

$$h_{1-4} = (a \sin \theta + b \cos \theta) \sin \phi \tag{57}$$

The lower tangent plane through corner 8 is distant from corner 4 by the amount

$$h_{4-8} = c \cos \phi \tag{58}$$

Therefore, the projected height of the rectangular paralelepiped is

$$D = h_{1-4} + h_{4-8} = (a \sin \theta + b \cos \theta) \sin \phi + c \cos \phi \tag{59}$$

This expression is used to find $\bar{D}$.

$$\bar{D} = \frac{2}{\pi} \int_0^{\pi/2} \int_0^{\pi/2} [(a \sin\theta + b \cos\theta) \sin^2\phi + c \cos\phi \sin\phi] \, d\phi d\theta$$

$$= \frac{2}{\pi} \int_0^{\pi/2} [(a \sin\theta + b \cos\theta) \frac{1}{2} (\phi - \sin\phi \cos\phi) + \frac{c}{2} \sin^2\phi]_0^{\pi/2} \, d\theta$$

$$= \frac{2}{\pi} \int_0^{\pi/2} [\frac{\pi}{4} (a \sin\theta + b \cos\theta) + \frac{c}{2}] \, d\theta$$

$$= \frac{1}{2} \int_0^{\pi/2} (a \sin\theta + b \cos\theta) \, d\theta + \frac{c}{\pi} \int_0^{\pi/2} d\theta$$

$$\bar{D} = \frac{1}{2} (a + b) + \frac{c}{2} = \frac{1}{2} (a + b + c) \qquad (60)$$

Therefore, the probability of sectioning a rectangular parallelepiped is

$$P_i \text{ (rectangular parallelepiped)} = \frac{1}{2} (a + b + c) \qquad (60)$$

From the above Equation (60), it may be seen that if the rectangular parallelepiped is cubic, we get

$$P_i \text{ (cube)} = \frac{1}{2} (a + a + a) = \frac{3}{2} a \qquad (51)$$

This is as before.

From Equation (60) it is also obvious that for a thin plate of width a, length b, and negligible thickness c, as in Figure 22a, we get

$$P_i \text{ (thin plate)} = \frac{1}{2} (a + b) \qquad (61)$$

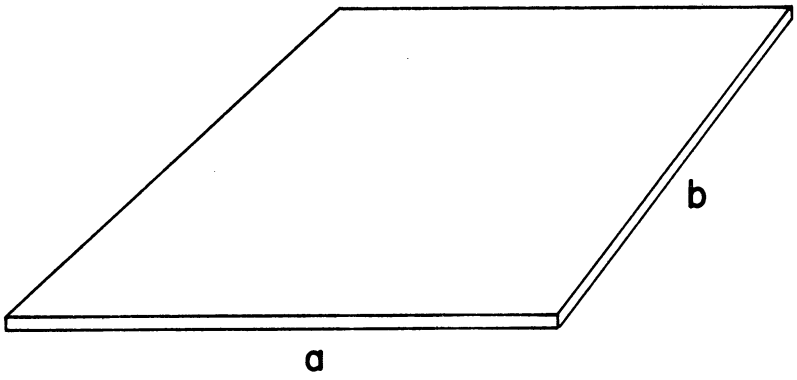

a-Plate

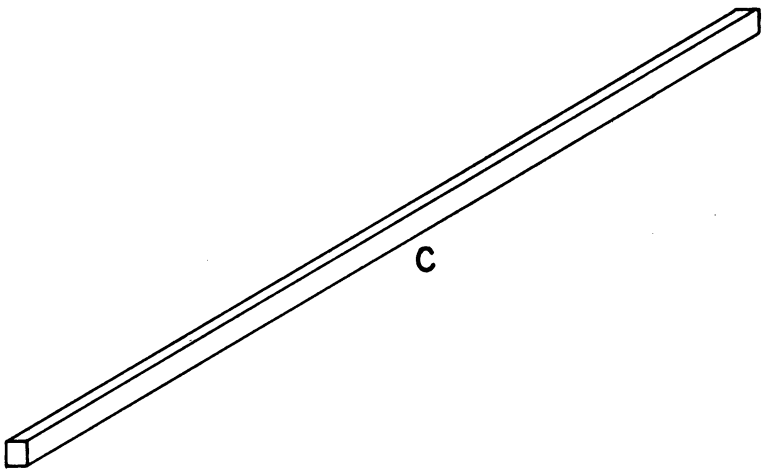

b-Rod

Figure 22. Thin Plate and Long Rod.

For a long rod of length c and negligible cross-section, as in Figure 22b, we get

$$P_i \text{ (long rod)} = \frac{1}{2} c \qquad (62)$$

The latter relation for a long rod of negligible cross-section can be seen to be identical to the previous expression, Equation (25), for a long round needle of negligible diameter, as may be expected, since in both cases the cross-section is considered negligible.

Before proceeding to develop similar relations for the probability of intersection of other polyhedrons, it will be more convenient to proceed to the consideration of the relative frequencies with which the various shaped sections cut from cubes are observed.

Shapes of Sections of a Cube

It has previously been shown by Rutherford, et al.[26] that sections from a cube may have three, four, five, or six edges, as in Figure 7. The various types of sections cut from a cube will depend upon θ, the rotation or direction of tilt, ϕ, the amount of tilt, and the elevation of the cut. If a cube is tilted directly over on one edge, for $\theta = 0$ in Figure 23a, then for any ϕ and any elevation of cut only four sided sections would be obtained. For an orientation involving a general θ and ϕ other types of sections would result. For instance, in Figures 23b and 23c we have a typical θ and two typical values of ϕ. It will be noted that for the orientation of Figure 23b we can obtain 3, 4, or 5 sided sections only, while for the orientation of Figure 23c we obtain these and 6 sided sections

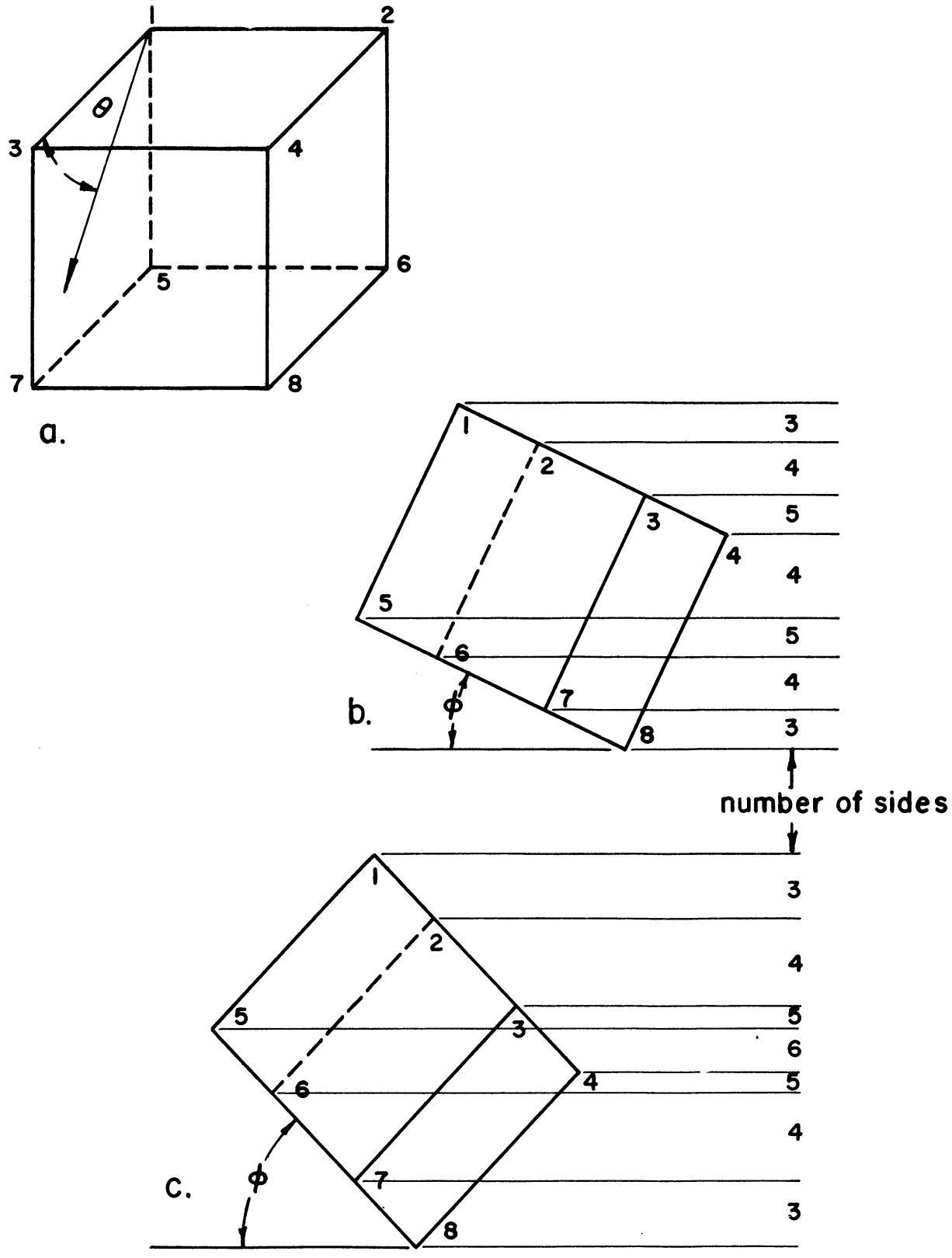

Figure 23. Cube. Number of Sides per Section.

as well. Thus, a careful consideration of the relationship between orientations and the types of sections obtained is necessary.

Since we have previously integrated the cube over one octant of orientations, let us examine the number of possible types of sections for all orientations in the octant. If a detailed analysis similar to that indicated by Figure 23 is carried out and the results tabulated on the map of an octant, the possible section shapes will be as shown in Figure 24. The various crystallographic poles are indicated on the octant for convenience. It will be noted that the octant is divided into 12 smaller spherical triangles, and that for the orientations represented by 6 of these triangles only 3, 4, or 5 sided sections of a cube are obtained, while in the other 6 triangles 3, 4, 5 and 6 sided sections are obtained.

The problem may be greatly simplified when it is realized that, because of the symmetry of the cube, only a portion of this octant need be considered in detail. The portion selected will be that spherical triangle with corners at the 001, 101, and 111 poles. This is exactly one sixth of the octant shown, one forty-eighth of the whole sphere, and represents a true sample of all orientations of a cube. Therefore, all further work on the cube and other shapes of cubic symmetry will be done considering only orientations in this 1/48th sphere bounded by 001, 101, and 111 poles. It may be noted, as discussed earlier, that in orientation 001 we have the minimum projected height of the cube, i.e., "a", while in orientation 101

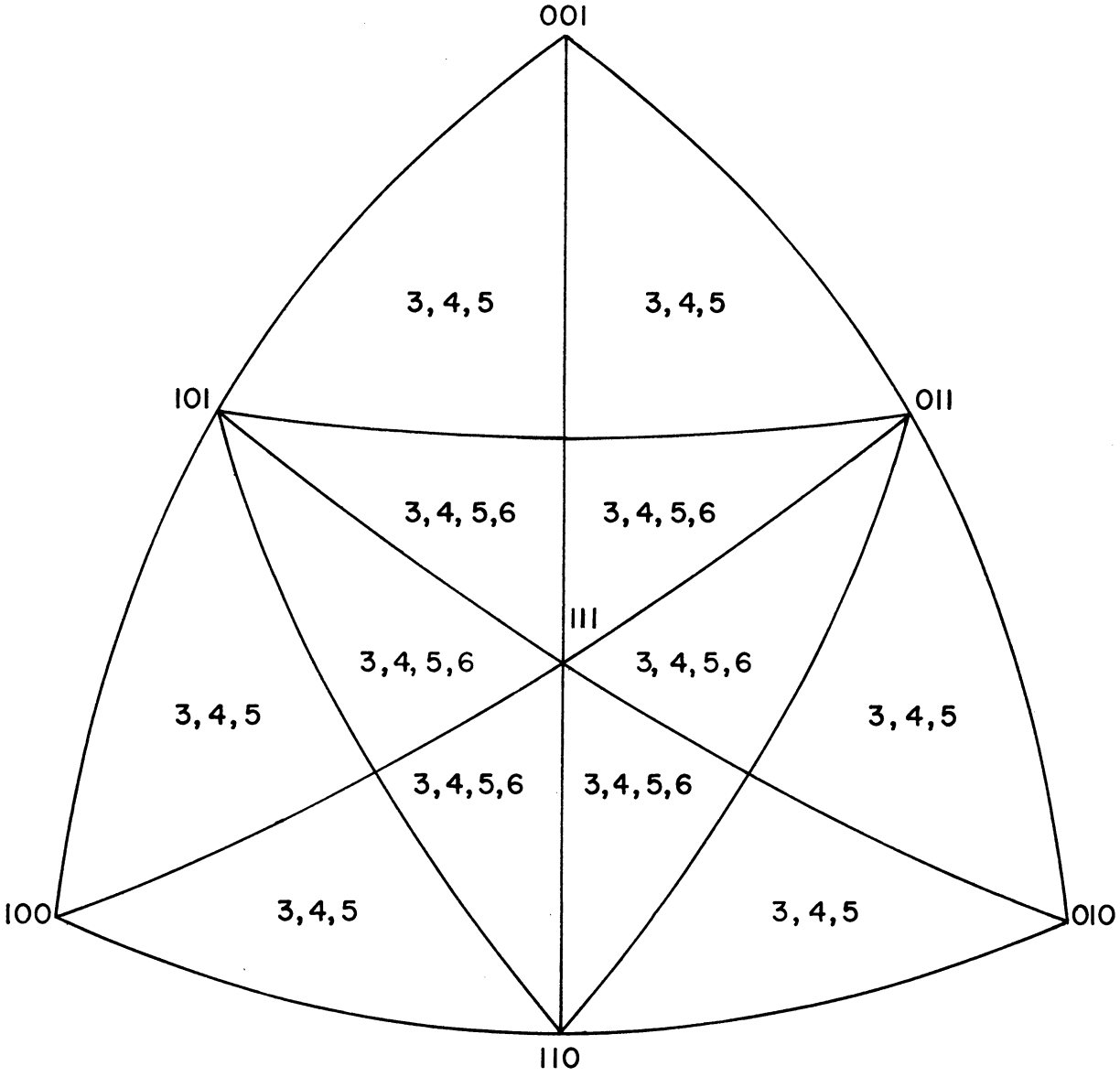

Figure 24. Spherical Octant. Sides on Cube Sections.

the projected height is $\sqrt{2}$ a and in orientation 111 the projected height is a maximum, $\sqrt{3}$ a.

Let us consider what the parameters of this triangle are in terms of ϕ and θ, as shown in Figure 25. The edges of the spherical triangle are $\theta = 0$, $\theta = 45°$, and an arc we shall call $\phi_2(\theta)$. There is also an inner arc that we shall need and will call $\phi_1(\theta)$. The corners of the triangle are $\phi = 0$; $\theta = 0$, $\phi = 45°$; and $\theta = 45°$, $\phi = \arctan\sqrt{2}$. Now we shall solve for $\phi_2(\theta)$ and $\phi_1(\theta)$.

Referring to Figures 25 and 26 and to a 001 standard stereographic projection by Barrett[53], we see that the direction of angle ϕ_2 is a series of poles from 101 to 111 or passing through line 3-4, Figure 26. In fact, as θ varies from 0 to 45° the line determining the value of ϕ_2 moves with θ in a manner to always pass through the edge 3-4. We call the length of this line g. If the cube is considered to have a side length of unity, then

$$g^2 = 1^2 + \tan^2\theta + 1^2 = 2 + \tan^2\theta$$

$$g = \sqrt{2 + \tan^2\theta}$$

But $\cos \phi_2 = \frac{1}{g}$

Therefore,

$$\phi_2 = \arccos \frac{1}{\sqrt{2 + \tan^2\theta}} \qquad (63)$$

However, this relation can be given in other forms.

$$\arccos \frac{1}{\sqrt{2 + \tan^2\theta}} = \arctan \sqrt{\tan^2\theta + 1}$$

$$\phi_2 = \arctan \sqrt{\sec^2\theta} = \arctan (\sec \theta)$$

$$\tan \phi_2 = \sec \theta$$

$$\cot \phi_2 = \cos \theta$$

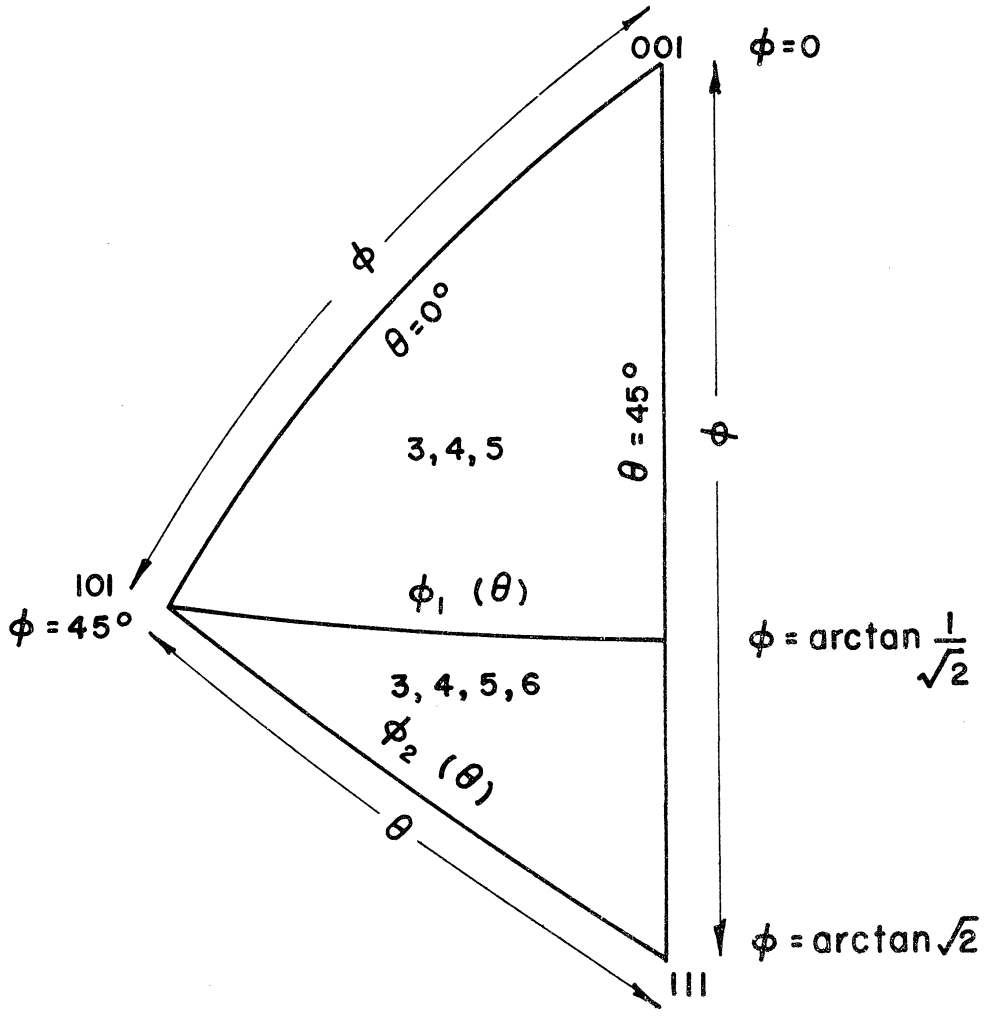

Figure 25. Spherical Triangle. Sides on Cube Sections.

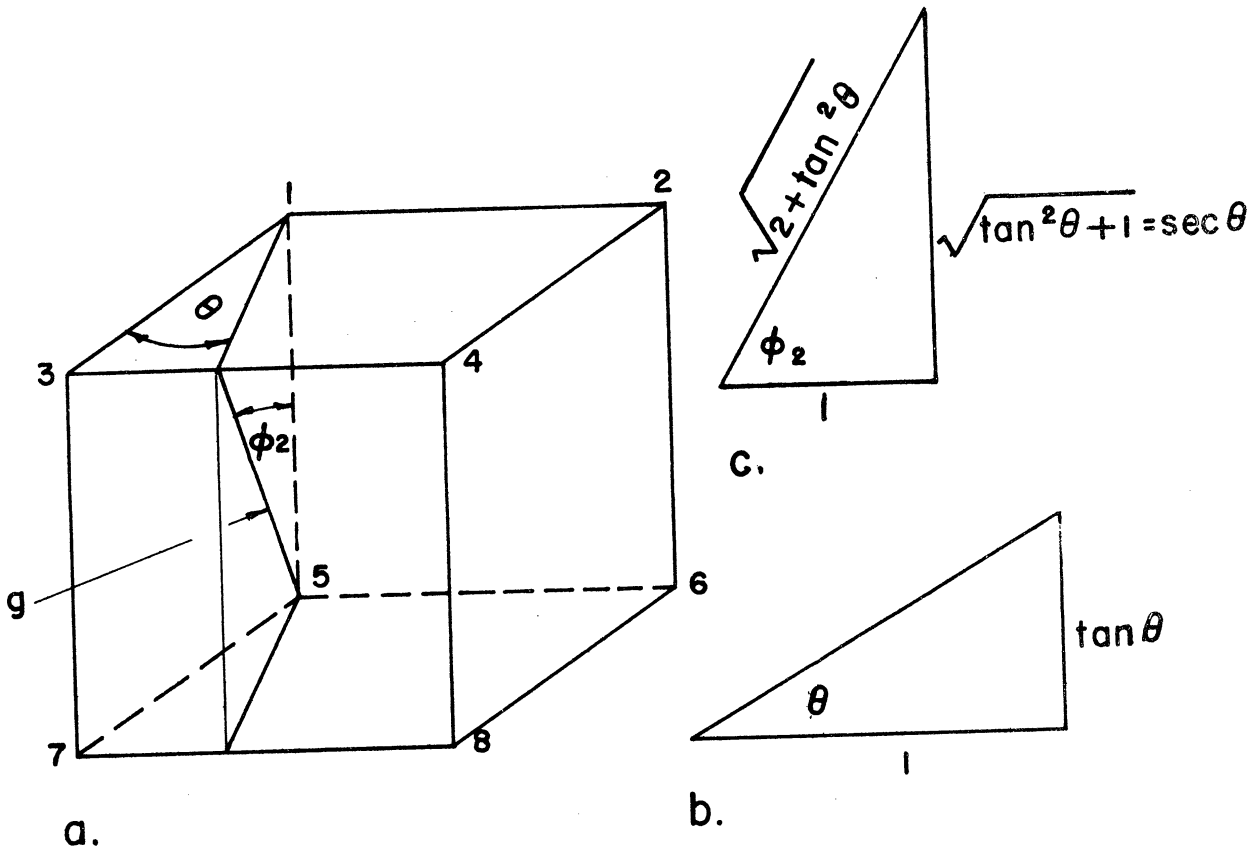

Figure 26. Cube. Solving for $\phi_2(\theta)$.

Finally,

$$\phi_2 = \text{arccot } (\cos \theta) \tag{64}$$

Although ϕ_2 can be expressed in many alternate forms, that given above in Equation (64) is one of the simplest and shall be used in all further computations.

As a check on the validity of this result, let us see if the area defined by this triangle is actually 1/48th of a sphere.

$$A = \int_0^{\pi/4} \int_0^{\text{arccot}(\cos\theta)} \rho^2 \sin \phi \, d\phi \, d\theta$$

$$= \rho^2 \int_0^{\pi/4} -\cos \phi \Big|_0^{\text{arccot}(\cos\theta)} d\theta$$

$$= \rho^2 \int_0^{\pi/4} \left(1 - \frac{\cos \theta}{\sqrt{1 + \cos^2\theta}}\right) d\theta$$

In Appendix A it is shown that

$$\int_0^{\pi/4} \frac{\cos \theta \, d\theta}{\sqrt{1 + \cos^2\theta}} = \frac{\pi}{6}$$

Thus we get

$$A = \rho^2 \left(\frac{\pi}{4} - \frac{\pi}{6}\right) = \frac{\pi\rho^2}{12} \tag{65}$$

This is exactly 1/48th of the surface of a sphere.

As additional verification of ϕ_2, we should be able to check our result for P_i (cube), by modifying Equation (50).

$$P_i \text{ (cube)} = 48 \cdot \frac{1}{4\pi} \int_0^{\pi/4} \int_0^{\text{arccot}(\cos\theta)} a[(\sin\theta + \cos\theta)\sin\phi + \cos\phi]\sin\phi \, d\phi \, d\theta$$

$$= \frac{12a}{\pi} \int_0^{\pi/4} [(\sin\theta + \cos\theta)\frac{1}{2}(\phi - \sin\phi\cos\phi) + \frac{1}{2}\sin^2\phi]_0^{\text{arccot}(\cos\theta)} d\theta$$

$$= \frac{6a}{\pi} \int_0^{\pi/4} \{(\sin\theta + \cos\theta)[\text{arccot}(\cos\theta) - \frac{\cos\theta}{1+\cos^2\theta}] + \frac{1}{1+\cos^2\theta}\} d\theta$$

$$= \frac{6a}{\pi} \int_0^{\pi/4} [\sin\theta \cdot \text{arccot}(\cos\theta) + \cos\theta \cdot \text{arccot}(\cos\theta)$$

$$- \frac{\sin\theta\cos\theta}{1+\cos^2\theta} - \frac{\cos^2\theta}{1+\cos^2\theta} + \frac{1}{1+\cos^2\theta}] \, d\theta$$

The solutions of these integrals are shown in Appendix A.

$$P_i \text{ (cube)} = \frac{6a}{\pi}[\frac{\pi}{4} - \frac{1}{\sqrt{2}}\arctan\sqrt{2} + \ell n\frac{2}{\sqrt{3}} + \frac{\pi}{4} + \frac{3}{\sqrt{2}}\arctan\sqrt{2}$$

$$- \frac{\pi}{\sqrt{2}} - \ell n\frac{2}{\sqrt{3}} - \frac{\pi}{4} - \frac{1}{\sqrt{2}}\arctan\sqrt{2} + \frac{\pi}{2\sqrt{2}}$$

$$- \frac{1}{\sqrt{2}}\arctan\sqrt{2} + \frac{\pi}{2\sqrt{2}}]$$

$$= \frac{6a}{\pi}[\frac{\pi}{4}] = \frac{3}{2}a \qquad (51)$$

Thus $\phi_2 = \text{arccot}(\cos\theta)$ is confirmed.

Since we shall need $\phi_1(\theta)$, we shall compute it at this time. Referring to Figures 25 and 27 we see that ϕ_1 is the angle at which, for any θ, corners 4 and 5 are at the same elevation. This will mean that the direction ϕ_1 will pass through corner 5 and the horizontal line uv which is perpendicular to θ and passes through corner 4. Reference to Figures 20b and 27 will help show this. If the length

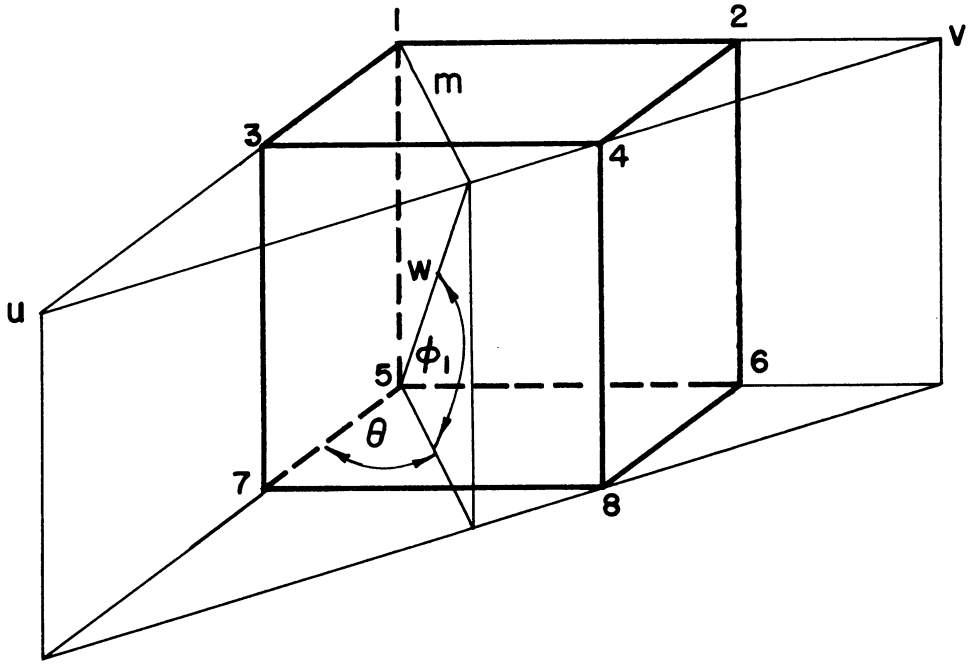

Figure 27. Cube. Solving for $\phi_1(\theta)$.

from corner 5 to line uv is called w, we find that $\cos \phi_1 = m/w$. The w we shall not use. The m has been found before.

$$m = \sqrt{2} \sin (\theta + 45) \tag{44}$$

$$m = (\sin \theta + \cos \theta) \tag{48}$$

If the cube edge is taken as unity, then we also see that

$$\tan \phi_1 = 1/m$$

$$\cot \phi_1 = m$$

$$\phi_1 = \operatorname{arccot} (\sin \theta + \cos \theta) \tag{66}$$

This is the form in which ϕ_1 will be used.

Having solved for $\phi_1(\theta)$ and $\phi_2(\theta)$, our presently required information about the orientation triangle is adequate, and we shall proceed to solve for the frequencies of the various shaped sections of cubes.

Probabilities of Sections of a Cube

Considering that we can get three, four, five, or six sided sections of a cube, we can refer to the probabilities of getting each of these sections as P_3, P_4, P_5, and P_6. From this,

$$P_3 + P_4 + P_5 + P_6 = P_1 \text{ (cube)} = 1.5a \tag{67}$$

We see from Figure 25 that for the spherical triangle, $\theta = 0$, $\theta = 45$, $\phi_2 = \operatorname{arccot} (\cos \theta)$, we get 3, 4, and 5 sided sections over the whole triangle and 6 sided sections only over the smaller triangle between $\phi_1 = \operatorname{arccot} (\sin \theta + \cos \theta)$ and ϕ_2. We need to find the appropriate expressions for distance between tangent planes for each type of section and then integrate over the corresponding ϕ and θ range.

The simplest procedure for doing this will be by numbering the corners of the cube and analyzing systematically for the various possible angular ranges to see which are the conditions for obtaining each of the types of sections. It must be remembered, of course, that our integration will be only over 1/48th of the total sphere of orientations so we multiply our integral by $12/\pi$ to get total probability. Thus the integral to be used will be

$$P_{SHAPE} = \frac{12}{\pi} \int_{0}^{\pi/4} \int_{\phi_a(\theta)}^{\phi_b(\theta)} D_{SHAPE}(\phi,\theta) \sin \phi \, d\phi \, d\theta \qquad (68)$$

ϕ_a and ϕ_b are the appropriate angular limits.

Consider first P_3. By reference to Figure 25 we see that parallel plane sections between corners 1 and 2 and also corners 7 and 8 give use three sided sections. Thus the vertical distance or projected height between corners 1 and 2 and between corners 7 and 8 will give us the probability of 3 sided sections. For the 1/48th spherical triangle we are working in, no other sets of corners give us 3 sided sections. Also, the vertical distance between corners 7 and 8 will always be the same as the vertical distance between corners 1 and 2, so we merely compute the latter and double it.

Referring to Figure 28, to find how high corner 1 rises above corner 2, consider that we rotate corner 1 in the direction θ about a horizontal line passing through corner 2. The effective radius of this rotation is m, where $m = a \sin \theta$. The vertical distance, then, from corner 1 to 2 will be

$$h_{1-2} = m \sin \phi$$

$$h_{1-2} = a \sin \theta \sin \phi \qquad (69)$$

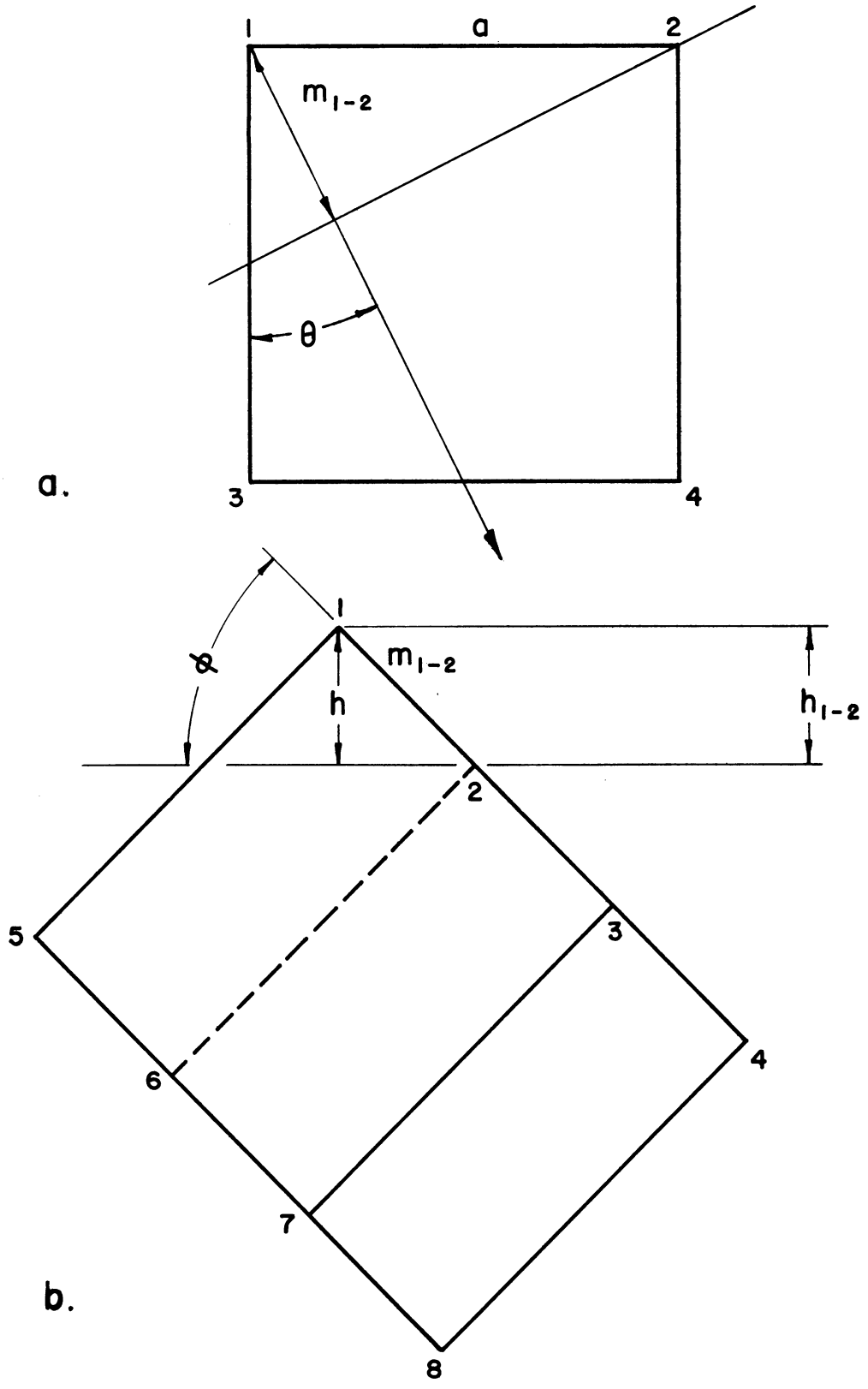

Figure 28. Cube. Computing P_3.

The total D for 3 sided sections then is $D_3 = 2h_{1\text{-}2}$.

$$D_3 = 2a \sin\theta \sin\phi \tag{70}$$

This applies over the whole angular range, θ from 0 to 45° and ϕ from 0 to $\phi_2 = \text{arccot}(\cos\theta)$.

We then integrate using the same basic Equation (68),

$$P_3 = \frac{12}{\pi} \int_0^{\pi/4} \int_0^{\text{arccot}(\cos\theta)} 2\,a \sin\theta \sin\phi \cdot \sin\phi \, d\phi \, d\theta$$

$$= \frac{12}{\pi} \cdot 2a \int_0^{\pi/4} \sin\theta \cdot \frac{1}{2} (\phi - \sin\phi \cos\phi) \Big|_0^{\text{arccot}(\cos\theta)} d\theta$$

$$= \frac{12a}{\pi} \int_0^{\pi/4} [\sin\theta \cdot \text{arccot}(\cos\theta) - \sin\theta \cdot \frac{\cos\theta}{1 + \cos^2\theta}] \, d\theta$$

Using integrals from Appendix A gives the desired result.

$$P_3 = \frac{12a}{\pi} [\frac{\pi}{4} - \frac{1}{\sqrt{2}} \arctan \sqrt{2} + \ell n \frac{2}{\sqrt{3}} - \ell n \frac{2}{\sqrt{3}}]$$

$$= \frac{12a}{\pi} [\frac{\pi}{4} - \frac{1}{\sqrt{2}} \arctan \sqrt{2}]$$

$$P_3 = a (3 - \frac{6\sqrt{2}}{\pi} \arctan \sqrt{2}) \tag{71}$$

Before proceeding at once to the balance of the calculations for sections of a cube, it will be well to pause and make a careful analysis of the types of sections expected on the basis of sectioning planes between various corners of the cube, as we did for three sided sections. We shall consider the two cases, for the angular regions shown in Figure 25:

Case I - 3, 4, and 5 sided sections: $\phi = 0$ to ϕ_1

Case II - 3, 4, 5, and 6 sided sections: $\phi = \phi_1$ to ϕ_2

The angle, $\phi_1 = \text{arccot}\ (\sin\theta + \cos\theta)$, is the angle at which corners 4 and 5 are at the same elevation. The angle, $\phi_2 = \text{arccot}\ (\cos\theta)$, is the angle at which corners 3 and 5 are at the same elevation and 4 and 6 are at the same elevation. Reference to Figure 23b shows that this position of the cube is representative of Case I, $\phi(0 \text{ to } \phi_1)$, while Figure 23c shows Case II, $\phi(\phi_1 \text{ to } \phi_2)$. Now if we tabulate the types of sections obtained for parallel cuts between consecutive corners, as in Figure 23, we obtain the data of Table IV.

TABLE IV

TYPES OF CUBE SECTIONS DEPENDING UPON ADJACENT CORNERS

Case I, $0 < \phi < \phi_1$		Case II, $\phi_1 < \phi < \phi_2$	
Corners	Sides on Section	Corners	Sides on Section
1-2	3	1-2	3
2-3	4	2-3	4
3-4	5	3-5	5
4-5	4	5-4	6
5-6	5	4-6	5
6-7	4	6-7	4
7-8	3	7-8	3

For 3 sided sections, we need h_{1-2} plus h_{7-8} for the entire range, $\phi(0 \text{ to } \phi_2)$, and, since $h_{1-2} = h_{7-8}$, $D_3 = 2h_{1-2}$, as we had. For 4 sided sections, we need h_{2-3} plus h_{6-7} for the entire range, $\phi(0 \text{ to } \phi_2)$,

and h_{4-5} for the range, $\phi(0 \text{ to } \phi_1)$. But $h_{2-3} = h_{6-7}$, so

$$D_4 = 2h_{2-3},\ \phi(0 \text{ to } \phi_2) + h_{4-5},\ \phi(0 \text{ to } \phi_1) \qquad (72)$$

For 5 sided sections we need h_{3-4} plus h_{5-6} for the range, $\phi(0 \text{ to } \phi_1)$, and h_{3-5} plus h_{4-6} for the range $\phi(\phi_1 \text{ to } \phi_2)$. But $h_{3-4} = h_{5-6}$, and $h_{3-5} = h_{4-6}$, and furthermore $h_{3-4} = h_{1-2}$. So for 5 sided sections,

$$D_5 = 2h_{1-2},\ \phi(0 \text{ to } \phi_1) + 2h_{3-5},\ \phi(\phi_1 \text{ to } \phi_2) \qquad (73)$$

For 6 sided sections we shall need

$$D_6 = h_{5-4},\ \phi(\phi_1 \text{ to } \phi_2) \qquad (74)$$

Thus, while we have h_{1-2}, we still need h_{2-3}, h_{4-5}, h_{3-5}, and h_{5-4}.

Referring to Figure 29a, we write down the following m's, effective radii of revolution:

$$m_{1-2} = a \sin \theta$$

$$m_{3-4} = a \sin \theta$$

$$m_{1-3} = a \cos \theta$$

$$m_{2-3} = a (\cos \theta - \sin \theta)$$

$$m_{1-4} = a (\sin \theta + \cos \theta)$$

From Figure 29b, we then list the projected heights:

$$h_{1-2} = m_{1-2} \sin \phi = a \sin \theta \sin \phi$$

$$h_{2-3} = m_{2-3} \sin \phi = a (\cos \theta - \sin \theta) \sin \phi$$

$$h_{4-5} = h_{4-8} - h_{5-8}$$

But $h_{5-8} = h_{1-4}$

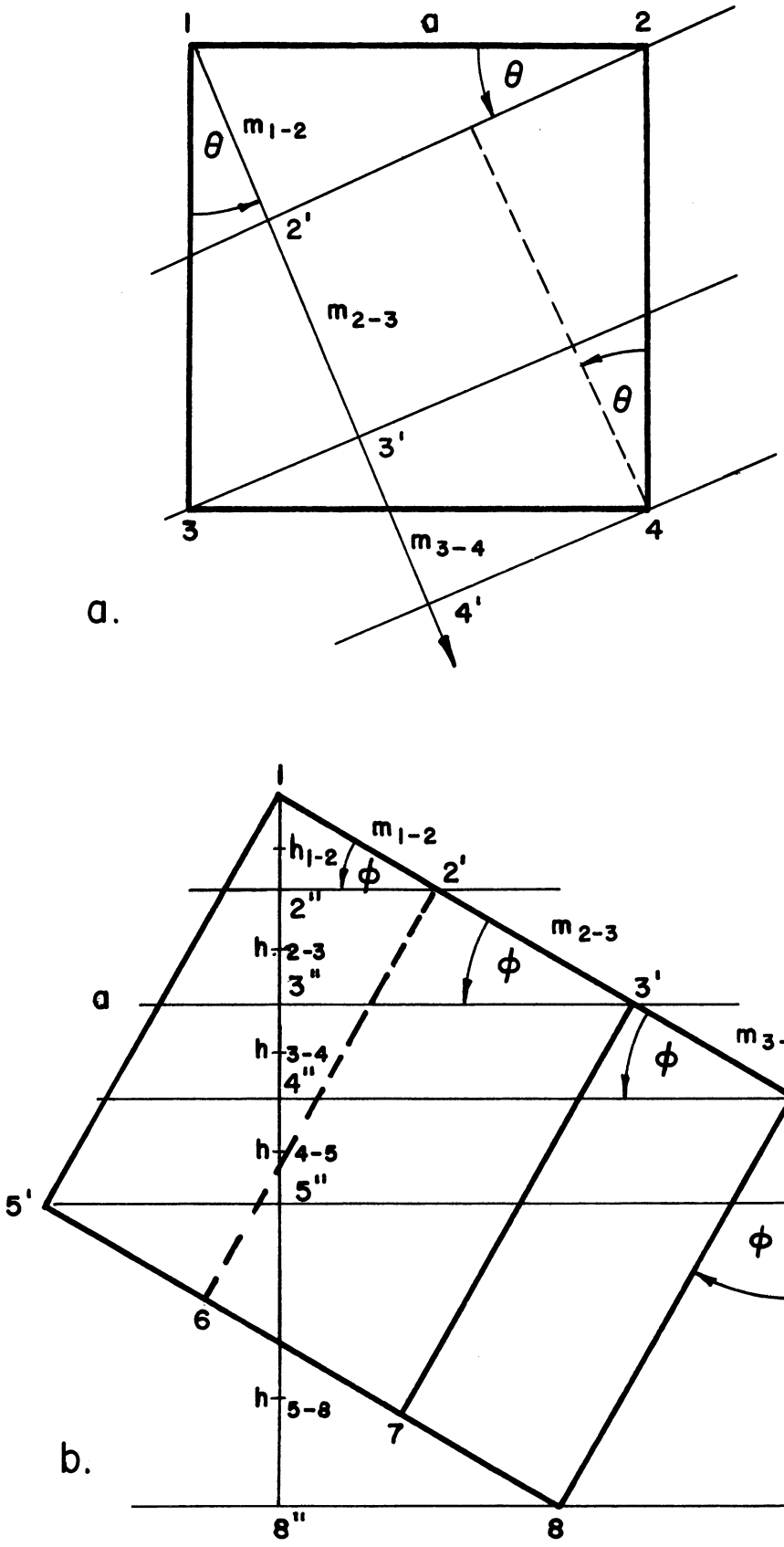

Figure 29. Cube. Computing D (shape).

Therefore, we have the following additional relations:

$$h_{4-5} = a\cos\phi - m_{1-4}\sin\phi$$

$$= a\cos\phi - a(\sin\theta + \cos\theta)\sin\phi$$

$$h_{5-4} = -h_{4-5}.$$

$$h_{3-5} = h_{3-4} + h_{4-5}$$

$$= a\sin\theta\sin\phi + a\cos\phi - a(\sin\theta + \cos\theta)\sin\phi$$

$$h_{3-5} = a\cos\phi - a\cos\theta\sin\phi$$

Summarizing, we now list relations to be used in solving for probabilities of obtaining various sided cube sections:

$$h_{1-2} = a\sin\theta\sin\phi \tag{75}$$

$$h_{2-3} = a(\cos\theta - \sin\theta)\sin\phi \tag{76}$$

$$h_{4-5} = a[\cos\phi - (\sin\theta + \cos\theta)\sin\phi] \tag{77}$$

$$h_{5-4} = a[(\sin\theta + \cos\theta)\sin\phi - \cos\phi] \tag{78}$$

$$h_{3-5} = a(\cos\phi - \cos\theta\sin\phi) \tag{79}$$

We shall now solve directly for P_4, using Equations (68) and (72):

$$P_4 = \frac{12}{\pi}\int_0^{\pi/4}\int_0^{\phi_2} 2h_{2-3}\cdot\sin\phi\,d\phi\,d\theta + \frac{12}{\pi}\int_0^{\pi/4}\int_0^{\phi_1} h_{4-5}\cdot\sin\phi\,d\phi\,d\theta$$

$$= \frac{12}{\pi}\cdot 2\int_0^{\pi/4}\int_0^{\operatorname{arccot}(\cos\theta)} a(\cos\theta - \sin\theta)\sin^2\phi\,d\phi\,d\theta$$

$$+ \frac{12}{\pi}\int_0^{\pi/4}\int_0^{\operatorname{arccot}(\sin\theta+\cos\theta)} a[\cos\phi - (\sin\theta + \cos\theta)\sin\phi]\sin\phi\,d\phi\,d\theta$$

$$= \frac{24a}{\pi}\int_0^{\pi/4}(\cos\theta - \sin\theta)\cdot\frac{1}{2}(\phi - \sin\phi\cos\phi)\Big|_0^{\operatorname{arccot}(\cos\theta)} d\theta$$

$$+ \frac{12a}{\pi} \int_0^{\pi/4} \left[\frac{1}{2}\sin^2\phi - (\sin\theta + \cos\theta)\cdot\frac{1}{2}(\phi - \sin\phi\cos\phi)\right]_0^{\operatorname{arccot}(\sin\theta+\cos\theta)} d\theta$$

$$P_4 = \frac{12a}{\pi} \int_0^{\pi/4} [\cos\theta \cdot \operatorname{arccot}(\cos\theta) - \sin\theta \cdot \operatorname{arccot}(\cos\theta) - \cos\theta \cdot \frac{\cos\theta}{1+\cos^2\theta}$$

$$+ \sin\theta \cdot \frac{\cos\theta}{1+\cos^2\theta}] \, d\theta$$

$$+ \frac{6a}{\pi} \int_0^{\pi/4} [\frac{1}{(\sin\theta+\cos\theta)^2+1} - \sin\theta \cdot \operatorname{arccot}(\sin\theta+\cos\theta)$$

$$- \cos\theta \cdot \operatorname{arccot}(\sin\theta+\cos\theta) + \sin\theta \cdot \frac{(\sin\theta+\cos\theta)}{(\sin\theta+\cos\theta)^2+1}$$

$$+ \cos\theta \cdot \frac{(\sin\theta+\cos\theta)}{(\sin\theta+\cos\theta)^2+1} \,] \, d\theta$$

For the first integral we use solutions from Appendix A, and the second integral we simplify further.

$$P_4 = \frac{12a}{\pi}\left[\frac{3}{\sqrt{2}}\arctan\sqrt{2} + (\frac{1-2\sqrt{2}}{4})\pi - \frac{\pi}{4} + \frac{1}{\sqrt{2}}\arctan\sqrt{2} - \ln\frac{2}{\sqrt{3}}\right.$$

$$\left. - \frac{1}{\sqrt{2}}\arctan\sqrt{2} - (\frac{1-\sqrt{2}}{4})\pi + \ln\frac{2}{\sqrt{3}}\right]$$

$$+ \frac{6a}{\pi} \int_0^{\pi/4} \left[\frac{1}{2+\sin 2\theta} - \sin\theta \cdot \operatorname{arccot}(\sin\theta+\cos\theta)\right.$$

$$- \cos\theta \cdot \operatorname{arccot}(\sin\theta+\cos\theta) + \frac{\sin^2\theta}{2+\sin 2\theta}$$

$$\left. + \frac{2\sin\theta\cos\theta}{2+\sin 2\theta} + \frac{\cos^2\theta}{2+\sin 2\theta}\right] d\theta$$

$$= \frac{12a}{\pi}\left[\frac{3}{\sqrt{2}}\arctan\sqrt{2} - \frac{\pi}{4} - \frac{\sqrt{2}\pi}{4}\right]$$

$$+ \frac{6a}{\pi} \int_0^{\pi/4} \left[\frac{2}{2+\sin 2\theta} - \sin\theta \cdot \operatorname{arccot}(\sin\theta+\cos\theta)\right.$$

$$\left. - \cos\theta \cdot \operatorname{arccot}(\sin\theta+\cos\theta) + \frac{2\sin\theta\cos\theta}{2+\sin 2\theta}\right] d\theta$$

The integrals listed above are solved in Appendix A.

$$P_4 = a\left(\frac{18\sqrt{2}}{\pi}\arctan\sqrt{2} - 3 - 3\sqrt{2}\right)$$

$$+ \frac{6a}{\pi}\left[\frac{\pi}{3\sqrt{3}} - \pi\left(\frac{3}{8} - \frac{1}{2\sqrt{2}} - \frac{1}{4\sqrt{3}}\right) - \frac{1}{\sqrt{2}}\arctan\sqrt{2} + \frac{1}{4}\ln\frac{3}{2}\right.$$

$$- \pi\left(\frac{1}{8} + \frac{1}{2\sqrt{2}} - \frac{1}{4\sqrt{3}}\right) + \frac{1}{\sqrt{2}}\arctan\sqrt{2} - \frac{1}{4}\ln\frac{3}{2}$$

$$\left. + \pi\left(\frac{1}{4} - \frac{1}{3\sqrt{3}}\right)\right]$$

$$= a\left(\frac{18\sqrt{2}}{\pi}\arctan\sqrt{2} - 3 - 3\sqrt{2}\right)$$

$$+ 6a\left(\frac{1}{3\sqrt{3}} - \frac{3}{8} + \frac{1}{2\sqrt{2}} + \frac{1}{4\sqrt{3}} - \frac{1}{8} - \frac{1}{2\sqrt{2}} + \frac{1}{4\sqrt{3}} + \frac{1}{4} - \frac{1}{3\sqrt{3}}\right)$$

$$= a\left(\frac{18\sqrt{2}}{\pi}\arctan\sqrt{2} - 3 - 3\sqrt{2}\right)$$

$$+ a\left(-\frac{3}{2} + \sqrt{3}\right)$$

$$P_4 = a\left(\frac{18\sqrt{2}}{\pi}\arctan\sqrt{2} - 4\frac{1}{2} + \sqrt{3} - 3\sqrt{2}\right) \qquad (80)$$

This is the desired result.

Next we solve for P_5 by using Equations (68) and (73) :

$$P_5 = \frac{12}{\pi}\int_0^{\pi/4}\int_0^{\phi_1} 2h_{1\text{-}2}\cdot\sin\phi\,d\phi\,d\theta + \frac{12}{\pi}\int_0^{\pi/4}\int_0^{\phi_2} 2h_{3\text{-}5}\cdot\sin\phi\,d\phi\,d\theta$$

$$= \frac{12}{\pi}\int_0^{\pi/4}\int_0^{\operatorname{arccot}(\sin\theta+\cos\theta)} 2a\sin\theta\sin^2\phi\,d\phi\,d\theta$$

$$+ \frac{12}{\pi}\int_0^{\pi/4}\int_{\operatorname{arccot}(\sin\theta+\cos\theta)}^{\operatorname{arccot}(\cos\theta)} 2a\,(\cos\phi - \cos\theta\sin\phi)\sin\phi\,d\phi\,d\theta$$

$$= \frac{24a}{\pi} \int_0^{\pi/4} \sin\theta \cdot \frac{1}{2} (\phi - \sin\phi \cos\phi) \Big|_0^{\operatorname{arccot}(\sin\theta + \cos\theta)} d\theta$$

$$+ \frac{24a}{\pi} \int_0^{\pi/4} \left[\frac{1}{2} \sin^2\phi - \cos\theta \cdot \frac{1}{2} (\phi - \sin\phi \cos\phi) \right]_{\operatorname{arccot}(\sin\theta + \cos\theta)}^{\operatorname{arccot}(\cos\theta)} d\theta$$

$$= \frac{12a}{\pi} \int_0^{\pi/4} \left[\sin\theta \cdot \operatorname{arccot}(\sin\theta + \cos\theta) - \sin\theta \left(\frac{\sin\theta + \cos\theta}{2 + \sin^2\theta} \right) \right] d\theta$$

$$+ \frac{12a}{\pi} \int_0^{\pi/4} \left[\frac{1}{1 + \cos^2\theta} - \frac{1}{2 + \sin 2\theta} - \cos\theta \cdot \operatorname{arccot}(\cos\theta) \right.$$

$$+ \cos\theta \cdot \operatorname{arccot}(\sin\theta + \cos\theta) + \cos\theta \left(\frac{\cos\theta}{1 + \cos^2\theta} \right)$$

$$\left. - \cos\theta \left(\frac{\sin\theta + \cos\theta}{2 + \sin 2\theta} \right) \right] d\theta$$

The above integrals are solved in Appendix A.

$$P_5 = \frac{12a}{\pi} \left[\pi \left(\frac{3}{8} - \frac{1}{2\sqrt{2}} - \frac{1}{4\sqrt{3}} \right) + \frac{1}{\sqrt{2}} \arctan\sqrt{2} - \frac{1}{4} \ln \frac{3}{2} \right.$$

$$- \frac{\pi}{12\sqrt{3}} + \frac{1}{4} \ln \frac{3}{2} - \frac{\pi}{8} + \frac{\pi}{6\sqrt{3}}$$

$$+ \frac{\pi}{2\sqrt{2}} - \frac{1}{\sqrt{2}} \arctan\sqrt{2} - \frac{\pi}{6\sqrt{3}}$$

$$- \frac{3}{\sqrt{2}} \arctan\sqrt{2} - \left(\frac{1 - 2\sqrt{2}}{4} \right) \pi$$

$$+ \frac{\pi}{8} + \frac{\pi}{2\sqrt{2}} - \frac{\pi}{4\sqrt{3}} - \frac{1}{\sqrt{2}} \arctan\sqrt{2} + \frac{1}{4} \ln \frac{3}{2}$$

$$\left. + \frac{1}{\sqrt{2}} \arctan\sqrt{2} + \left(\frac{1 - \sqrt{2}}{4} \right) \pi - \pi \left(\frac{1}{8} - \frac{1}{6\sqrt{3}} \right) - \frac{\pi}{12\sqrt{3}} - \frac{1}{4} \ln \frac{3}{2} \right]$$

$$P_5 = \frac{12a}{\pi}\left[(\arctan\sqrt{2})\left(\frac{1}{\sqrt{2}} - \frac{1}{\sqrt{2}} - \frac{3}{\sqrt{2}} - \frac{1}{\sqrt{2}} + \frac{1}{\sqrt{2}}\right) + (\ell n\ \frac{3}{2})\left(-\frac{1}{4} + \frac{1}{4} + \frac{1}{4} - \frac{1}{4}\right)\right.$$

$$+ \pi\left(\frac{3}{8} - \frac{1}{8} - \frac{1}{4} + \frac{1}{8} + \frac{1}{4} - \frac{1}{8}\right) + \pi\left(-\frac{1}{2\sqrt{2}} + \frac{1}{2\sqrt{2}} + \frac{1}{\sqrt{2}} + \frac{1}{2\sqrt{2}} - \frac{1}{2\sqrt{2}}\right)$$

$$\left. + \pi\left(-\frac{1}{4\sqrt{3}} - \frac{1}{12\sqrt{3}} + \frac{1}{6\sqrt{3}} - \frac{1}{6\sqrt{3}} - \frac{1}{4\sqrt{3}} + \frac{1}{6\sqrt{3}} - \frac{1}{12\sqrt{3}}\right)\right]$$

$$= \frac{12a}{\pi}\left[-\frac{3}{\sqrt{2}}\arctan\sqrt{2} + \frac{\pi}{4} + \frac{\pi}{\sqrt{2}} + \frac{\pi}{12\sqrt{3}}(-3 - 1 + 2 - 2 - 3 + 2 - 1)\right]$$

$$= \frac{12a}{\pi}\left[-\frac{3}{\sqrt{2}}\arctan\sqrt{2} + \frac{\pi}{4} + \frac{\pi}{\sqrt{2}} - \frac{\pi}{2\sqrt{3}}\right]$$

$$P_5 = a\left[-\frac{18\sqrt{2}}{\pi}\arctan\sqrt{2} + 3 + 6\sqrt{2} - 2\sqrt{3}\right] \qquad (81)$$

This is the desired result. Finally we solve for P_6, using Equations (68) and (74):

$$P_6 = \frac{12}{\pi}\int_0^{\pi/4}\int_{\phi_1}^{\phi_2} h_{5-4} \cdot \sin\phi\, d\phi\, d\theta$$

$$= \frac{12}{\pi}\int_{\operatorname{arccot}(\sin\theta+\cos\theta)}^{\pi/4}\int^{\operatorname{arccot}(\cos\theta)} a[(\sin\theta + \cos\theta)\sin\phi - \cos\phi]\sin\phi\, d\phi\, d\theta$$

$$= \frac{12a}{\pi}\int_0^{\pi/4}\left[(\sin\theta + \cos\theta)\frac{1}{2}(\phi - \sin\phi\cos\phi) - \frac{1}{2}\sin^2\phi\right]_{\operatorname{arccot}(\sin\theta+\cos\theta)}^{\operatorname{arccot}(\cos\theta)} d\theta$$

$$= \frac{6a}{\pi}\int_0^{\pi/4}\left\{(\sin\theta + \cos\theta)\left[\operatorname{arccot}(\cos\theta) - \frac{\cos\theta}{1+\cos^2\theta} - \operatorname{arccot}(\sin\theta+\cos\theta)\right.\right.$$

$$\left.\left. + \frac{\sin\theta + \cos\theta}{2 + \sin 2\theta}\right] - \frac{1}{1 + \cos^2\theta} + \frac{1}{2 + \sin 2\theta}\right\} d\theta$$

$$P_6 = \frac{6a}{\pi}\int_0^{\pi/4}\Big[\sin\theta\cdot\operatorname{arccot}(\cos\theta)+\cos\theta\cdot\operatorname{arccot}(\cos\theta)-\frac{\sin\theta\cos\theta}{1+\cos^2\theta}$$

$$-\frac{\cos^2\theta}{1+\cos^2\theta}-\frac{1}{1+\cos^2\theta}-\sin\theta\cdot\operatorname{arccot}(\sin\theta+\cos\theta)$$

$$-\cos\theta\cdot\operatorname{arccot}(\sin\theta+\cos\theta)+\frac{2\sin\theta\cos\theta}{2+\sin 2\theta}+\frac{2}{2+\sin 2\theta}\Big]\,d\theta$$

These integrals are solved in Appendix A.

$$P_6 = \frac{6a}{\pi}\Big[\frac{\pi}{4}-\frac{1}{\sqrt{2}}\arctan\sqrt{2}+\ell n\frac{2}{\sqrt{3}}+\frac{3}{\sqrt{2}}\arctan\sqrt{2}+\pi\Big(\frac{1-2\sqrt{2}}{4}\Big)$$

$$-\ell n\frac{2}{\sqrt{3}}-\frac{1}{\sqrt{2}}\arctan\sqrt{2}-\pi\Big(\frac{1-\sqrt{2}}{4}\Big)-\frac{\pi}{2\sqrt{2}}+\frac{1}{\sqrt{2}}\arctan\sqrt{2}$$

$$-\pi\Big(\frac{3}{8}-\frac{1}{2\sqrt{2}}-\frac{1}{4\sqrt{3}}\Big)-\frac{1}{\sqrt{2}}\arctan\sqrt{2}+\frac{1}{4}\ell n\frac{3}{2}$$

$$-\pi\Big(\frac{1}{8}+\frac{1}{2\sqrt{2}}-\frac{1}{4\sqrt{3}}\Big)+\frac{1}{\sqrt{2}}\arctan\sqrt{2}-\frac{1}{4}\ell n\frac{3}{2}$$

$$+\pi\Big(\frac{1}{4}-\frac{1}{3\sqrt{3}}\Big)+\frac{\pi}{3\sqrt{3}}\Big]$$

$$P_6 = \frac{6a}{\pi}\Big[(\arctan\sqrt{2})\Big(-\frac{1}{\sqrt{2}}+\frac{3}{\sqrt{2}}-\frac{1}{\sqrt{2}}+\frac{1}{\sqrt{2}}-\frac{1}{\sqrt{2}}+\frac{1}{\sqrt{2}}\Big)$$

$$+\pi\Big(\frac{1}{4}+\frac{1}{4}-\frac{1}{4}-\frac{3}{8}-\frac{1}{8}+\frac{1}{4}\Big)$$

$$+\pi\Big(-\frac{1}{\sqrt{2}}+\frac{1}{2\sqrt{2}}-\frac{1}{2\sqrt{2}}+\frac{1}{2\sqrt{2}}-\frac{1}{2\sqrt{2}}\Big)$$

$$+\pi\Big(+\frac{1}{4\sqrt{3}}+\frac{1}{4\sqrt{3}}-\frac{1}{3\sqrt{3}}+\frac{1}{3\sqrt{3}}\Big)\Big]$$

$$P_6 = \frac{6a}{\pi}\left[\sqrt{2}\arctan\sqrt{2} - \frac{\pi}{\sqrt{2}} + \frac{\pi}{2\sqrt{3}}\right]$$

$$= a\left(\frac{6\sqrt{2}}{\pi}\arctan\sqrt{2} - 3\sqrt{2} + \sqrt{3}\right) \qquad (82)$$

This is the desired result.

As a check, let us see if

$$P_3 + P_4 + P_5 + P_6 = P_i\,(\text{cube}) \qquad (67)$$

We add up the following equations:

$$P_3 = a\left[3 - \frac{6\sqrt{2}}{\pi}\arctan\sqrt{2}\right] \qquad (71)$$

$$P_4 = a\left[-4\frac{1}{2} + \frac{18\sqrt{2}}{\pi}\arctan\sqrt{2} + \sqrt{3} - 3\sqrt{2}\right] \qquad (80)$$

$$P_5 = a\left[3 - \frac{18\sqrt{2}}{\pi}\arctan\sqrt{2} - 2\sqrt{3} + 6\sqrt{2}\right] \qquad (81)$$

$$P_6 = a\left[\frac{6\sqrt{2}}{\pi}\arctan\sqrt{2} + \sqrt{3} - 3\sqrt{2}\right] \qquad (82)$$

Their sum is

$$P_{TOTAL} = a\left(\frac{3}{2}\right) = P_i(\text{cube}) \qquad (51)$$

This result is exactly as expected.

Relative Frequencies of Sections of a Cube

From the probabilities of intersection of each type of section of a cube, Equations (71), (80), (81), and (82), we can compute the relative frequency of each type section for randomly oriented cubes. We

determine relative frequency from $f_{shape} = \frac{P_{SHAPE}}{P_{TOTAL}}$. The results are given in Table V.

TABLE V

RELATIVE FREQUENCY OF SECTIONS OF CUBE

Number of Sides	Frequency
3	27.984%
4	48.677%
5	18.695%
6	4.644%
	100.000%

A direct comparison between the distribution computed theoretically by the foregoing analysis may now be made with the frequency distribution obtained by Hull and Houk[50] on their measurements of wire models. It should be noted that Hull and Houk presented their data in graphical form, and, with the uncertainties in reading of the graph plus the necessary conversion into percentages, the results attributed to them have been computed as closely as possible. The comparison is shown in Table VI.

TABLE VI

COMPARISON OF CUBE SECTION FREQUENCIES

Number of Sides on Cube Section	Hull and Houk[50] (statistical model)	This Work (mathematical)
3	29.0%	28.0%
4	42.9%	48.7%
5	18.2%	18.7%
6	10.0%	4.6%
	100.1%	100.0%

The above comparison shows, at first glance, a fair degree of correlation. Yet, when consideration is made of the care with which Hull and Houk made a suitable model, selected a representative sample of all possible orientations (over the same 1/48th spherical triangle used in the present mathematical analysis), and then took measurements at closely spaced elevations, the extent of the discrepancy between the results is noteworthy. For the 4 and 6 sided frequencies the agreement is particularly poor, differing by almost 6% in both cases. The agreement for 3 and 5 sided frequencies is much better, being within 1% or less. It is perhaps remarkable that Hull and Houk predict more than twice the frequency of 6 sided sections than is computed by the present work. To seek an explanation for these discrepancies, we shall look in more detail at the expected frequencies of the various sided sections as a function of cube orientation.

The computation of the probability of obtaining a given type of section of a cube at a fixed orientation involves using the basic $D_{(shape)}$ relation, the projected height which gives that given section, in general terms of ϕ and θ, and then computing the value of that D for the particular values of ϕ and θ desired. The $D_{(shape)}$ relations for the cube are derived from Equations (75), (76), (77), (78) and (79) and are listed in Table VII. These are the functions we integrated to get $P_{(shape)}$.

The general trend of the results, when mapped on the spherical triangle, may be somewhat anticipated as shown by Figure 30. There it is shown that 100% of the sections will be 4 sided when $\phi = 0$ for any θ

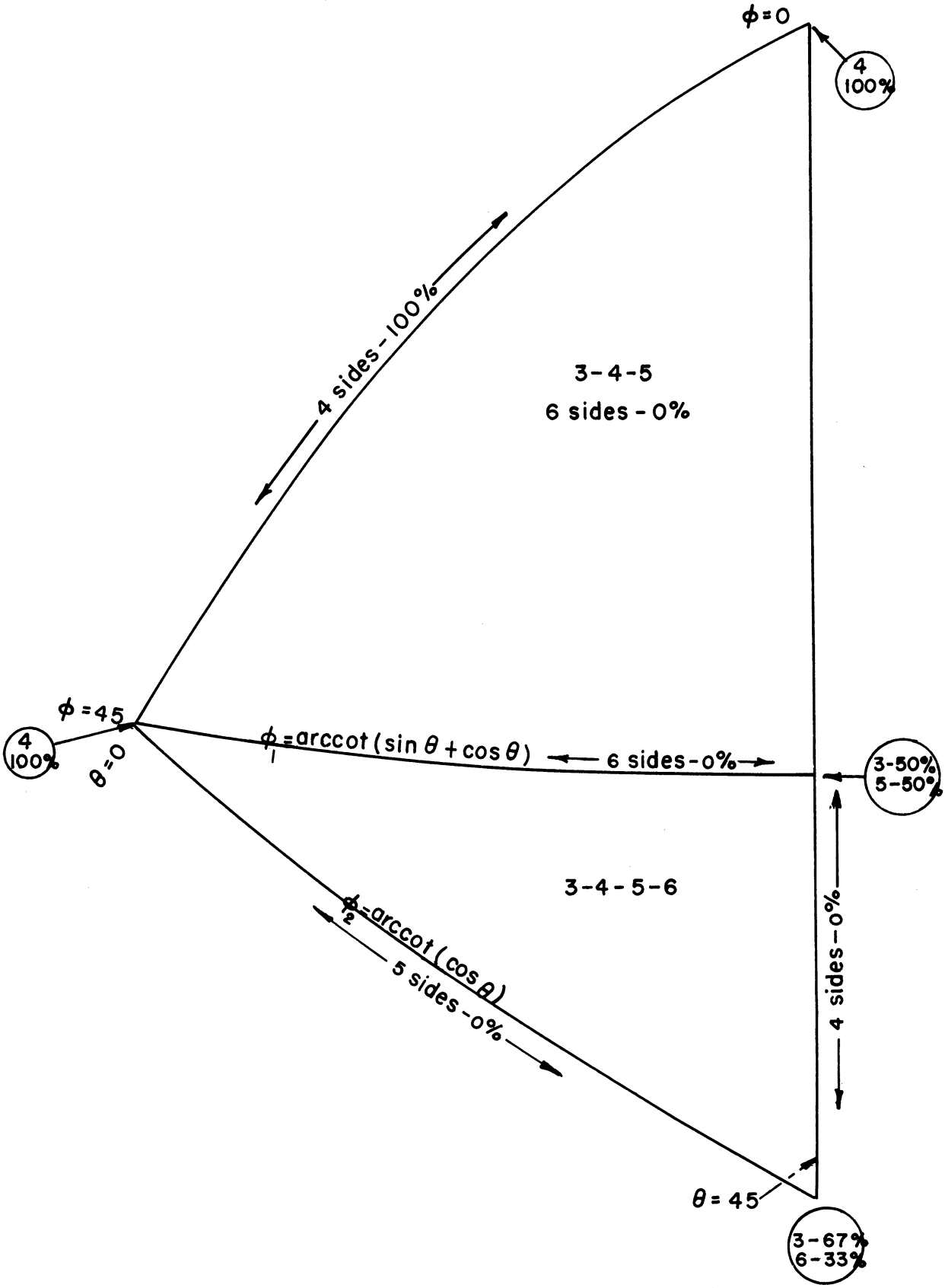

Figure 30. Spherical Triangle. Relative Frequencies of Cube Sections.

and also when $\theta = 0$ for any ϕ. This, of course, includes one entire side of our spherical triangle. When $\theta = 45°$ and $\phi = \phi_1 = \text{arccot}\,\sqrt{2}$, 50% of the sections will be 3 sided and the other 50% 5 sided. When $\theta = 45°$ and $\phi = \phi_2 = \text{arccot}\,1/\sqrt{2}$, 66 2/3% of the sections will be 3 sided and the other 33 1/3% 6 sided.

TABLE VII

D (SHAPE) RELATIONS FOR CUBE

Sides on Section	D (shape) Relation	Range
3	$2\,a\,\sin\theta\,\sin\phi$	0 to ϕ_2
4	$2\,a\,(\cos\theta - \sin\theta)\,\sin\phi$	0 to ϕ_2
	$a\,[\cos\phi - (\sin\theta + \cos\theta)\,\sin\phi]$	0 to ϕ_1
5	$2\,a\,\sin\theta\,\sin\phi$	0 to ϕ_1
	$2\,a\,(\cos\phi - \cos\theta\,\sin\phi)$	ϕ_1 to ϕ_2
6	$a\,[(\sin\theta + \cos\theta)\sin\phi - \cos\phi]$	ϕ_1 to ϕ_2

The relative probabilities of the sections will be somewhat different than the mere percentage frequencies indicate because at $\phi = 0$ the D(cube), projected height, is "a" while at $\theta = 45°$, $\phi = \phi_2 = \text{arccot}\,1/\sqrt{2}$ the D(cube) is $\sqrt{3}a$. These relative probabilities, the projected heights over which a certain type of section is observed as a function of orientation, are obtained by calculating D(shape) values from Table VII for (ϕ,θ). These are tabulated for each of the types of sections, 3, 4, 5, and 6 sided, in Tables VIII, IX, X, and XI. The tabular values are also graphed in Figures 31, 32, 33, 34, which show contours of relative probability density on the spherical triangle for each of the types of sections.

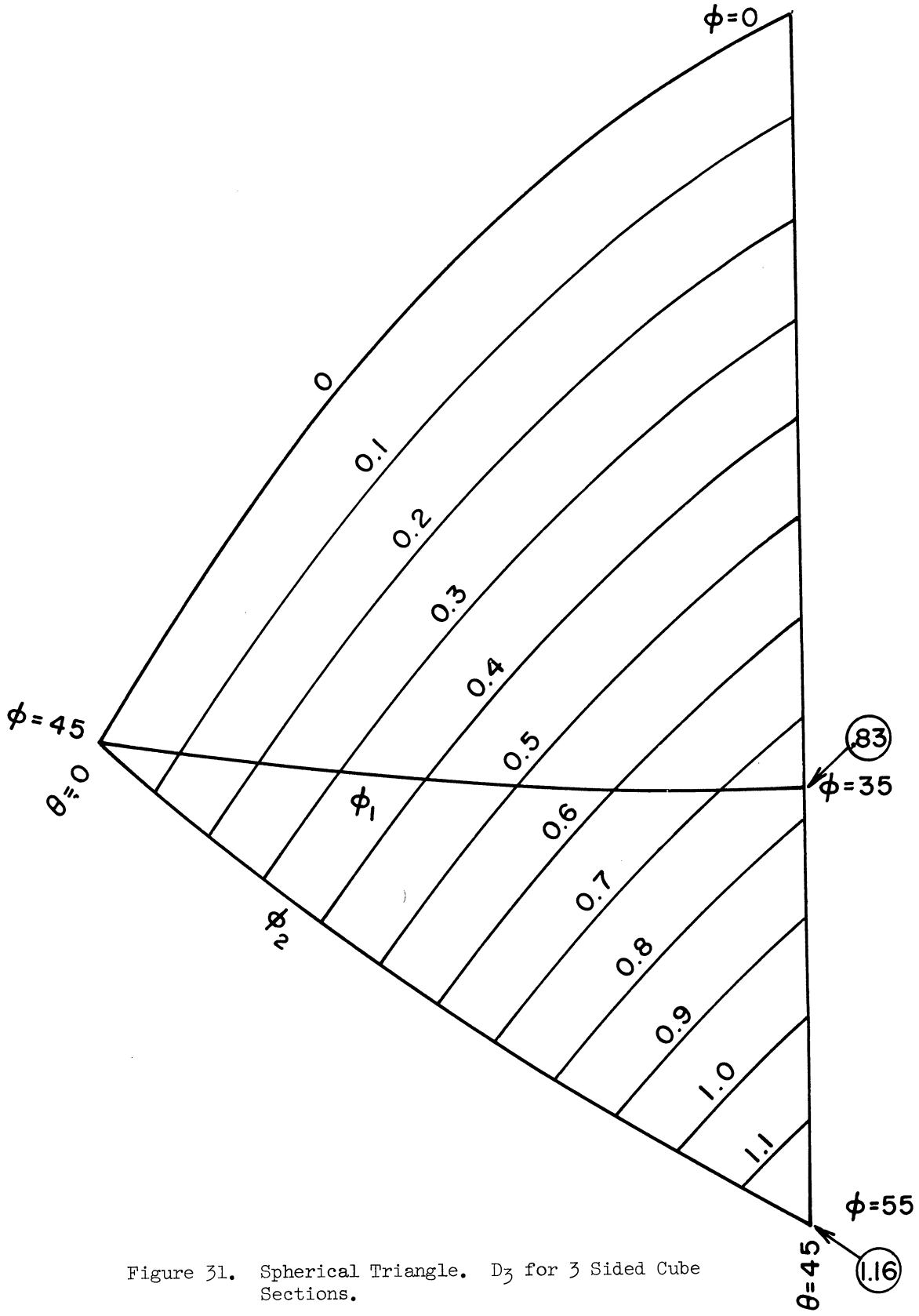

Figure 31. Spherical Triangle. D_3 for 3 Sided Cube Sections.

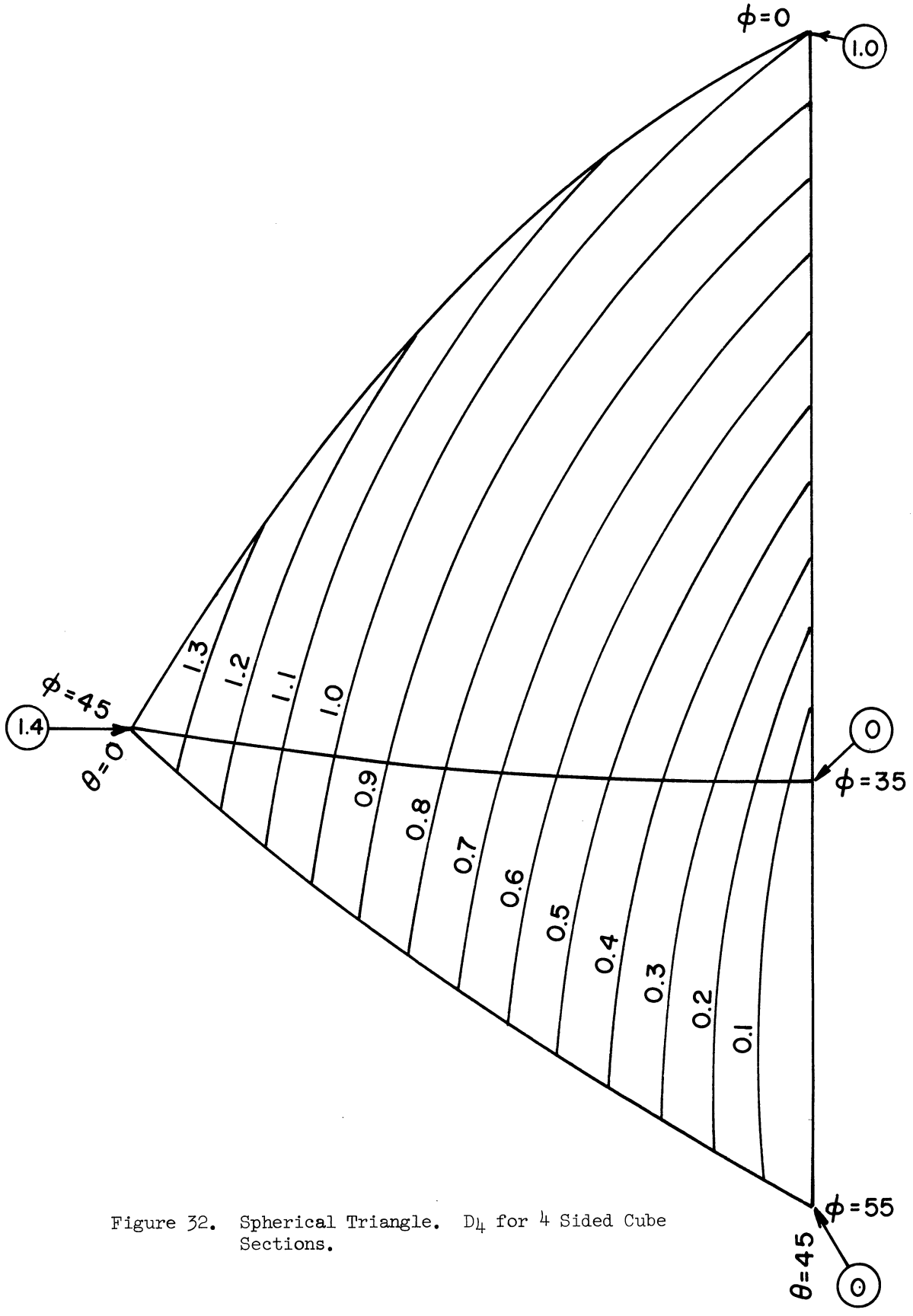

Figure 32. Spherical Triangle. D_4 for 4 Sided Cube Sections.

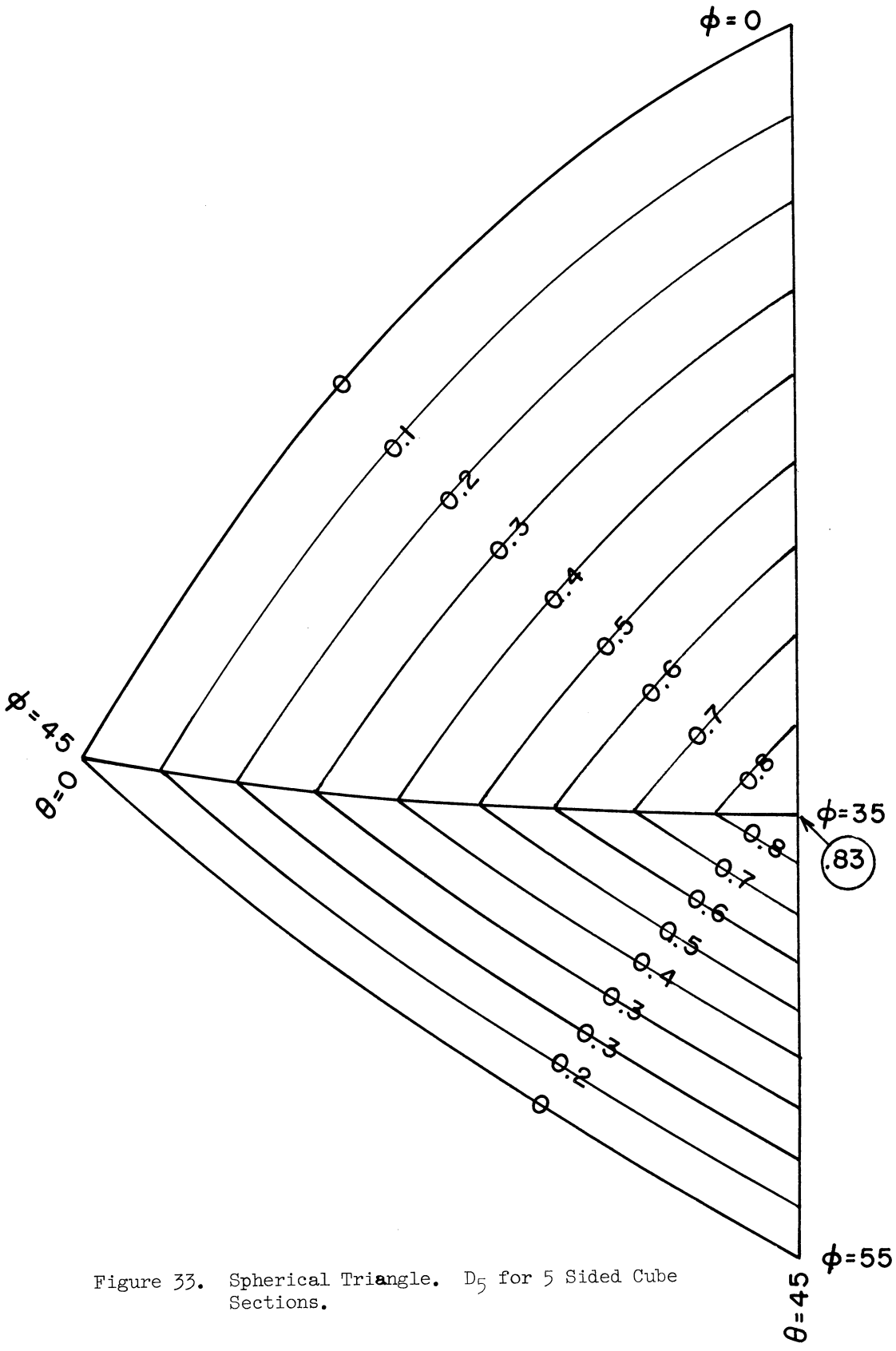

Figure 33. Spherical Triangle. D_5 for 5 Sided Cube Sections.

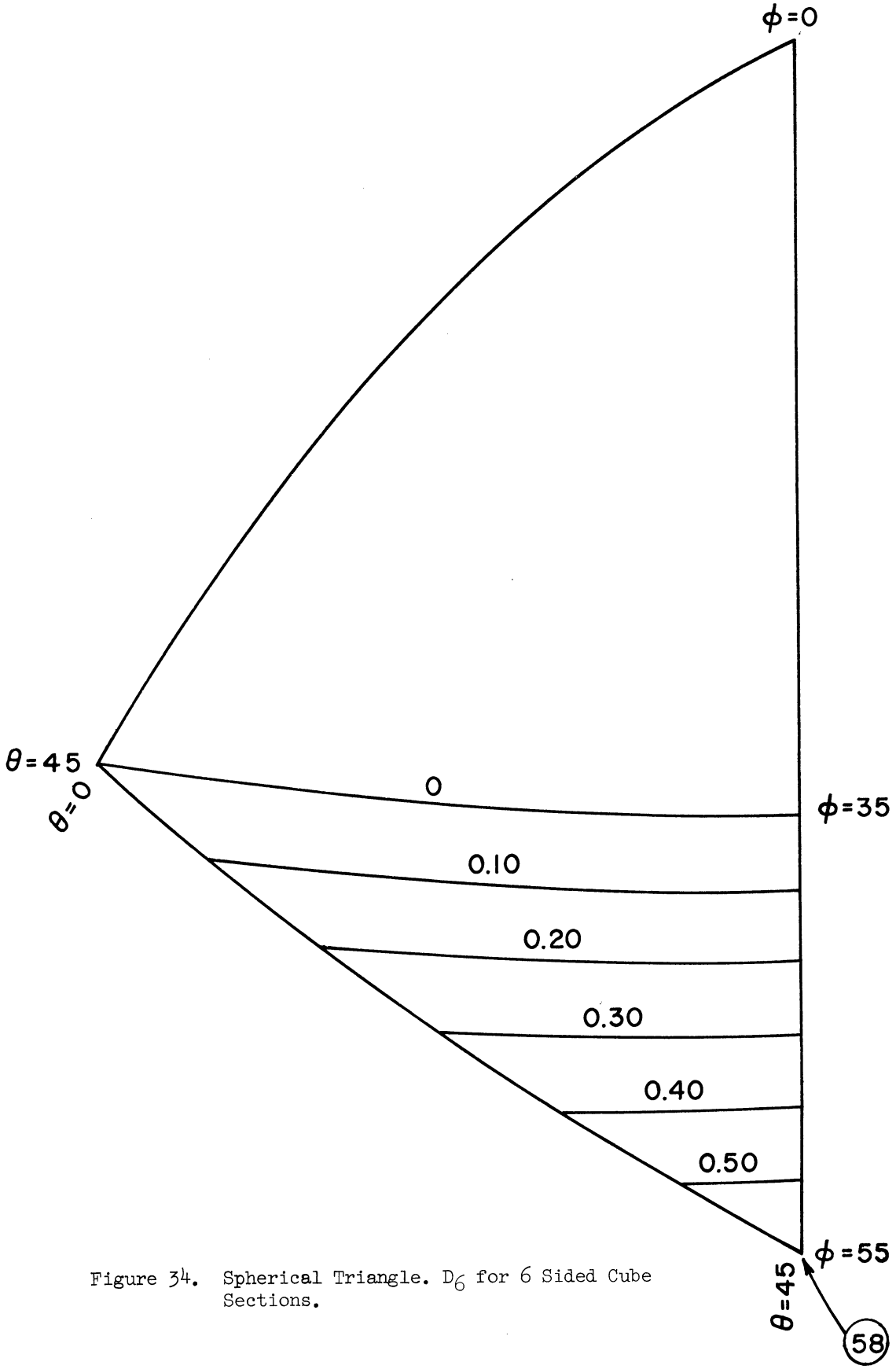

Figure 34. Spherical Triangle. D_6 for 6 Sided Cube Sections.

TABLE VIII

D_3 - PROJECTED HEIGHT FOR 3 SIDED CUBE SECTIONS
(UNITS OF CUBE EDGE LENGTH)

$\phi°/\theta°$	0	5	10	15	20	25	30	35	40	45
0	0	0	0	0	0	0	0	0	0	0
5	0	.02	.03	.05	.06	.07	.09	.10	.11	.12
10	0	.03	.06	.09	.12	.15	.17	.20	.22	.25
15	0	.05	.09	.13	.18	.22	.26	.30	.33	.37
20	0	.06	.12	.18	.23	.29	.34	.39	.44	.48
25	0	.07	.15	.22	.29	.36	.42	.48	.54	.60
30	0	.09	.17	.26	.34	.42	.50	.57	.64	.71
35	0	.10	.20	.30	.39	.48	.57	.66	.74	.81
40*	0	.11	.22	.33	.42	.51	.59	.67	.74	.82
ϕ_1*	0	.12	.23	.33	.44	.54	.64	.74	.83	.91
45	0	.12	.25	.37	.48	.60	.71	.81	.91	1.00
50	-	-	-	-	-	-	-	.88	.98	1.08
ϕ_2	0	.12	.25	.37	.50	.63	.76	.89	1.02	1.16

* The arrows indicate a change in the relative values of ϕ_1 and 40°. Beyond arrows ϕ_1 is less than 40°.

TABLE IX

D_4 - PROJECTED HEIGHT FOR 4 SIDED CUBE SECTIONS
(UNITS OF CUBE EDGE LENGTH)

$\phi°/\theta°$	0	5	10	15	20	25	30	35	40	45
0	1.00	1.00	1.00	1.00	1.00	1.00	1.00	1.00	1.00	1.00
5	1.08	1.06	1.04	1.01	.99	.96	.94	.92	.89	.87
10	1.16	1.11	1.07	1.02	.97	.92	.87	.83	.78	.74
15	1.22	1.16	1.09	1.02	.94	.87	.80	.73	.67	.60
20	1.28	1.19	1.10	1.00	.91	.82	.72	.63	.54	.46
25	1.33	1.22	1.10	.99	.87	.75	.64	.53	.42	.31
30	1.37	1.23	1.10	.96	.82	.69	.55	.42	.28	.16
35	1.39	1.24	1.09	.93	.77	.61	.46	.30	.15	.01
40	1.41	1.24	1.06	.89	.74	.58	.43	.29	.14	0
ϕ_1	1.41	1.23	1.06	.91	.77	.62	.47	.32	.16	0
45	1.41	1.29	1.15	1.00	.85	.68	.52	.35	.17	0
50	-	-	-	-	-	-	-	.38	.19	0
ϕ_2	1.41	1.29	1.16	1.02	.87	.72	.55	.38	.20	0

* The arrows indicate a change in the relative values of ϕ_1 and 40°. Beyond arrows ϕ_1 is less than 40°.

TABLE X

D_5 - PROJECTED HEIGHT FOR 5 SIDED CUBE SECTIONS
(UNITS OF CUBE EDGE LENGTH)

$\phi°/\theta°$	0	5	10	15	20	25	30	35	40	45
0	0	0	0	0	0	0	0	0	0	0
5	0	.02	.03	.05	.06	.07	.09	.10	.11	.12
10	0	.03	.06	.09	.12	.15	.17	.20	.22	.25
15	0	.05	.09	.13	.18	.22	.26	.30	.33	.37
20	0	.06	.12	.18	.23	.29	.34	.39	.44	.48
25	0	.07	.15	.22	.29	.36	.42	.48	.54	.60
30	0	.09	.17	.26	.34	.42	.50	.57	.64	.71
35	0	.10	.20	.30	.39	.48	.57	.66	.74	.81
40	0	.11	.22	.33	.42	.51	.59	.67	.74	.82
ϕ_1	0	.12	.23	.29	.32	.37	.42	.48	.55	.62
45	0	.01	.02	.05	.09	.13	.19	.26	.33	.41
50	-	-	-	-	-	-	-	.03	.11	.20
ϕ_2	0	0	0	0	0	0	0	0	0	0

* The arrows indicate a change in the relative values of ϕ_1 and 40°. Beyond arrows ϕ_1 is less than 40°.

TABLE XI

D_6 - PROJECTED HEIGHT FOR 6 SIDED CUBE SECTIONS
(UNITS OF CUBE LENGTH)

$\phi°/\theta°$	0	5	10	15	20	25	30	35	40	45
0	0	0	0	0	0	0	0	0	0	0
5	0	0	0	0	0	0	0	0	0	0
10	0	0	0	0	0	0	0	0	0	0
15	0	0	0	0	0	0	0	0	0	0
20	0	0	0	0	0	0	0	0	0	0
25	0	0	0	0	0	0	0	0	0	0
30	0	0	0	0	0	0	0	0	0	0
35	0	0	0	0	0	0	0	0	0	0
40	0	0	0	0	0	0	0	0	0	0
ϕ_1	0	0	0	.02	.06	.09	.11	.13	.14	.14
45	0	.06	.11	.16	.20	.23	.26	.28	.29	.29
50	-	-	-	-	-	-	-	.42	.44	.44
ϕ_2	0	.06	.13	.19	.25	.31	.38	.44	.51	.58

* The arrows indicate a change in the relative values of ϕ_1 and 40°. Beyond arrows ϕ_1 is less than 40°.

From the tabulated and graphed results certain observations may be made. Orientations in the lower portion of the spherical triangl between ϕ_1 and ϕ_2, particularly toward the 111 pole, will be weighted more heavily toward 3 sided sections and especially so toward 6 sided sections and will be weighted less than average for 4 sided sections. For 5 sided sections, the weighting is about equal above and below ϕ_1; these are weighted most heavily around $\theta = 45°$ and $\phi = \phi_1$. Thus the observed deviation between Hull and Houk's data and the present theoretical results, i.e., very high on frequency of 6 sides, a little high for 3 sides, and quite low on frequency for 4 sides, could readily be accounted for by a bias in their orientations tending to favor the lower triangle, especially toward the 111 pole. The factor of orientation is very sensitive regarding section distribution frequencies, so a small bias could affect results appreciably.

From a careful inspection of the orientations selected for testing by Hull and Houk, Figure 8, it is possible to imagine just such a bias as suggested above. The circles on their orientation plot indicate 5° solid angles, so equal coverage of the triangle by the circles would represent equal sampling. However, close scrutiny appears to strongly indicate a relatively greater coverage and overlap by the circles in the region favoring high 6 and low 4 sided frequencies, that is, in the direction of the 111 pole. Due to the previously mentioned sensitivity of this factor, it seems highly probable, in spite of the care and diligence exercised by Hull and Houk to select representative orientations, that a bias

of exactly the nature described was introduced, which accounts for the discrepancy in results. A further comparison of the results of this study with those of Hull and Houk will be made from the experimental data obtained from synthetic samples containing dispersed cubes, prepared as a part of this study.

VI. GENERAL APPROACH TO POLYHEDRON PROBLEM

As we have worked out the details for determining probability of intersection of a randomly orientation cube by a plane section as well as probabilities of obtaining different shaped sections of a cube, certain generalities about the methods required may have become apparent. First, it is essential to determine the upper and lower corners of the polyhedron which define the property to measure (such as 5 sided sections). Second, we must set up the expression which gives the vertical distance between these corners as a function of orientation. Third, we must find out what the angular limits are over which these same two corners define our desired property. Fourth, we must set up and integrate the required double integral that gives us the probability. Fifth, it will often be necessary to add up several such calculations to determine the desired result.

The first step, to determine the corners of interest which define the property to be measured, takes a little practice and usually some sketches will be necessary. In fact, unless the polyhedron is exceedingly simple, a few sketches will be essential. A step-by-step, graphical, descriptive geometry visualization is required and must be done carefully and with patience . Short cuts come with difficulty and depend upon the skill acquired in developing a three-dimensional visualization.

The second step, to set up the expression for the vertical distance between corners, has been derived rather laboriously for cubes on the basis of finding a horizontal effective radius, which we called m

and was in terms of θ, and then expressing the change in height in terms of ϕ, the angle by which the polyhedron was tilted in the direction θ. Actually, this process is exceedingly simple, so simple that it is merely necessary, in most cases, just to write down the expression. If we look at any cube for which we have numbered the corners, for example, Figures 20 and 29, for side length "a", we may see that the vertical distance from corner 1 to 2 will be $a\sin\theta\sin\phi$. The vertical distance from corner 1 to 3 (or 2 to 4) will be $a\cos\theta\sin\phi$. From 1 to 4 it will be $a(\sin\theta+\cos\theta)\sin\phi$. From 2 to 3 it will be $a(\cos\theta-\sin\theta)\sin\phi$. From 3 to 2 would be $a(\sin\theta-\cos\theta)\sin\phi$. A negative result means that the corner stated last is actually highest. From corner 4 to 8 the vertical distance is $a\cos\phi$. From corner 1 to 8 we have

$$D(\text{cube}) = a\,[(\sin\theta+\cos\theta)\sin\phi+\cos\phi] \qquad (49)$$

By now it should be apparent that we can consider the corners as located on a 3 dimensional rectangular coordinate system, travel from the upper corner (when tilted) to the lower corner along the coordinate axes, and write down the expression for their difference in height. For a cube, if we travel from left to right, as from 1 to 2, this gives us an $a\sin\theta$, which we also need to multiply by $\sin\phi$. Travelling from right to left would make it $-a\sin\theta$. Going from back to front, as from 1 to 3, would give $a\cos\theta\sin\phi$, and it would be negative for going backwards. From top to bottom, as from 4 to 8, would give $a\cos\phi$. Going fractional parts of the side length would merely require multiplying the expression by that fraction. Figure 35 illustrates the coordinate system described, showing the axes names and the directions taken as positive. Travelling in all 3 coordinate directions merely means adding up the 3 individual components along the coordinate

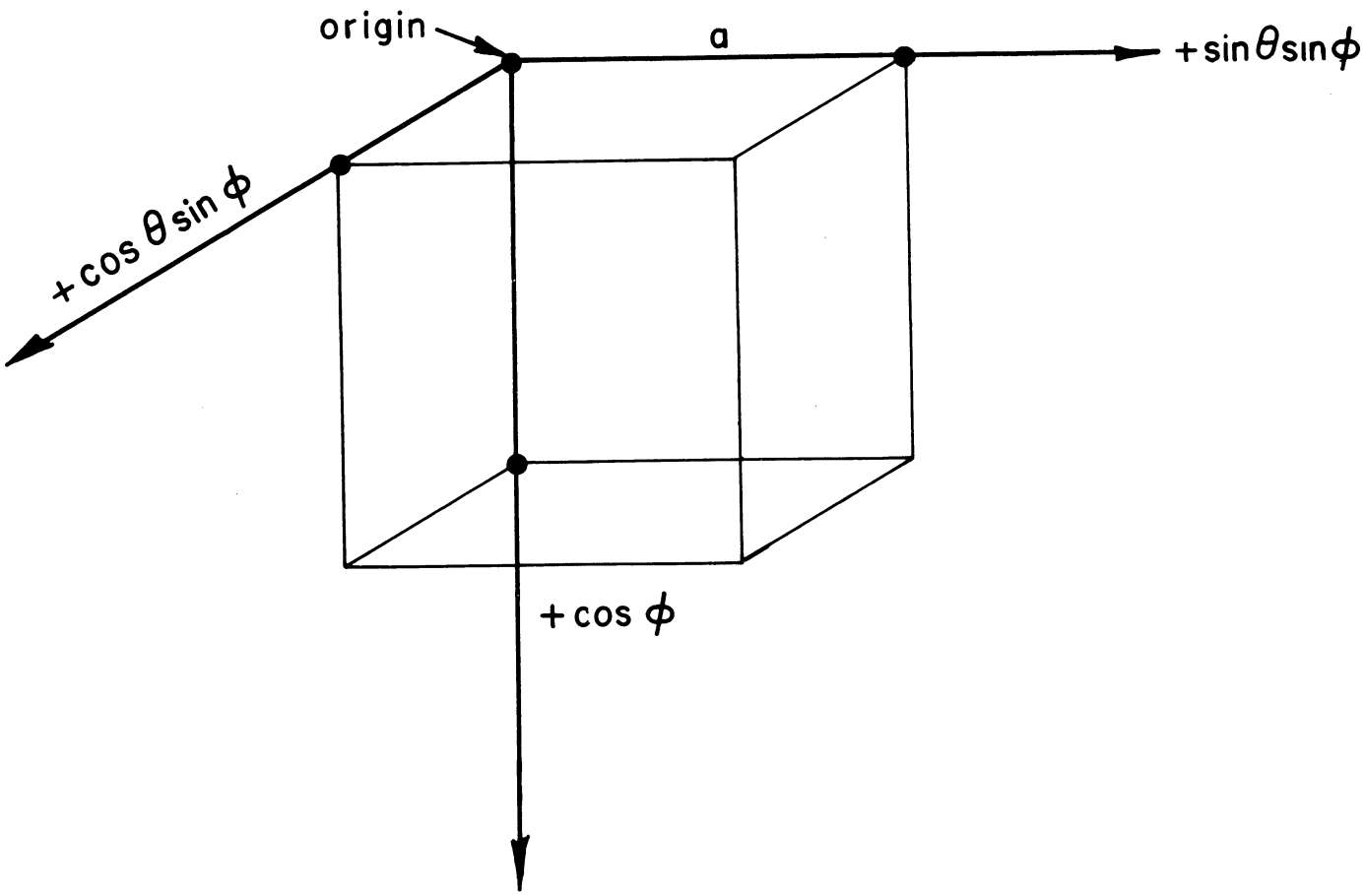

Figure 35. Coordinate Direction System.

axes. This procedure makes such analysis very simple, and is followed from here on.

The third step is to find out what the angular limits are over which the two corners in question are to be considered. This is relatively simple and is done in conjunction with the first step, determining the applicable corners, and using the information of the second step, finding the expression which specifies their height difference. It may be realized that a condition defined between two corners terminates when those corners become the same height. For instance, on the cube of Figure 23 we have 4 sided sections between corners 4 and 5 when 4 is on top and 6 sided sections between corners 5 and 4 with 5 on top. Thus the angle which gives $h_{4-5} = 0$ is a limiting angle for both cases. This is readily solved for in terms of ϕ, as will be shown:

$$h_{4-5} = a(-\sin\theta-\cos\theta)\sin\phi + a\cos\phi = 0$$

$$\frac{\cos\theta}{\sin\phi} = (\sin\theta + \cos\theta)$$

$$\phi = \phi_1 = \operatorname{arccot}(\sin\theta+\cos\theta) \qquad (66)$$

This is identical to the previously determined result. It may be noted, however, that this method of solving for ϕ_1 was much easier and more straightforward than the method described earlier.

Sometimes a θ other than 0° or 45° will be necessary as an integration limit. This occurs when two angles, $\phi(\theta)$'s, cross, and the θ of the intersection is obtained by setting the two $\phi(\theta)$'s equal to each other. For example, for the intersection of $\phi_1 = \operatorname{arccot}(\sin\theta+\cos\theta)$ and $\phi_2 = \operatorname{arccot}(\cos\theta)$ we have

$$\text{arccot}\,(\sin\theta + \cos\theta) = \text{arccot}\,(\cos\theta)$$

$$\sin\theta + \cos\theta = \cos\theta$$

$$\sin\theta = 0$$

Therefore, $\theta = 0°$ when $\phi_1 = \phi_2$ in our spherical triangle, which we also knew before. By this method we solve for the integration limits, $\phi(\theta)$, upper and lower, and θ, upper and lower, over any necessary orientation range.

The fourth step, integration, now follows. Setting up the integral is simple and straightforward, with all the previously determined information. Solving the integral in some cases may be easy, but in the general cases it is the most difficult step of all. The trouble arises from the inverse trigonometric functions needed to express the first integration limits, $\phi(\theta)$'s. Where our $\phi(\theta)$'s are no more complex than $\text{arccot}(\sin\theta+\cos\theta)$, we are able to solve the integrals exactly, as shown in Appendix A. As we proceed shortly to analyze more complicated polyhedrons, the rhombic dodecahedron and the tetrakaidecahedron, the $\phi(\theta)$'s do get more complex and exact integration is exceedingly difficult, if not impossible. As will be seen later, for this work such integrals were solved on a digital computer.

The computer solution, as will be seen, is simple, general, rapid, and accurate, so it makes integration no longer the operation of limiting difficulty in the solution of problems involving polyhedrons. When a computer is available for solving the integral equations, Step 1, determining the corners which give the desired property, usually is the most difficult and tedious operation. Step 5, adding appropriation portions

of previous calculations, of course, presents no difficulty.

In summary, then, we can say that all solutions for probability of sectioning polyhedral shaped particles dispersed in opaque bodies require one or more trigonometric expressions giving the distance between top and bottom corners or top and bottom tangent planes as a function of orientation, given by ϕ and θ. These are the $D(\phi,\theta)$ expressions which must be used in the integration over the appropriate ϕ and θ ranges. The total probability of sectioning is found by summing up or integrating over all orientations, usually by adding up several separate integration results. A general way of stating this is

$$P_i = \sum^{\text{all } \phi,\theta} \frac{A}{4\pi} \int_{\theta_a}^{\theta_b} \int_{\phi_a(\theta)}^{\phi_b(\theta)} D(\phi,\theta) \sin\phi \, d\phi \, d\theta \qquad (83)$$

$D(\phi,\theta)$ always has the form

$$D(\phi,\theta) = (D\sin\theta + E\cos\theta)\sin\phi + H\cos\phi \qquad (84)$$

In Equation (84) D, E, and H are constants on a rectangular coordinate system, being the x, y, and z components of the distances between top and bottom corners, as shown in Figure 35.

For bodies having cubic symmetry we need only consider orientations within the 001, 101, and 111 spherical triangle, and we have

$$P_i = \sum^{\text{all } \phi,\theta} \frac{12}{\pi} \cdot A \int_{\theta_a}^{\theta_b} \int_{\phi_a(\theta)}^{\phi_b(\theta)} D(\phi,\theta) \sin\phi \, d\phi \, d\theta \qquad (85)$$

An alternate form of this equation is

$$P_i = \sum^{\text{all } \phi,\theta} \frac{12}{\pi} \cdot A \int_{\theta_a}^{\theta_b} \int_{\phi_a(\theta)}^{\phi_b(\theta)} [(D \sin\theta + E \cos\theta)\sin^2\phi + H \cos\phi \sin\phi] \, d\phi d\theta \tag{86}$$

For probabilities of obtaining certain type sections of polyhedrons, the procedure is identical as above except that we need $D(\phi,\theta)$ for the corners of the polyhedron between which sectioning planes give us the section shape desired. The same general equations listed above are used to compute probabilities of certain sections.

We now proceed to the analysis of polyhedrons more complicated than the cube.

VII. OCTAHEDRON

Probability of Sectioning

The probability of intersecting an octahedron randomly oriented in space by a sectioning plane may readily be determined. Let us consider an octahedron inscribed in a cube of edge length "a", as shown in Figure 36. Since an octahedron has cubic symmetry, we will integrate over the same spherical traingle, 1/48th of a sphere, as we did for a cube. It may be seen that, over this range, distance between top and bottom tangent planes will always be that from the corner labelled 1 to corner 6 of Figure 36. This distance, in terms of the edge length of the circumscribed cube, will be

$$D = h_{1-6} = a \cos\phi \tag{87}$$

The probability of intersecting the octahedron will then be

$$P_i \text{ (octahedron)} = \frac{12a}{\pi} \int_0^{\pi/4} \int_0^{\operatorname{arccot}(\cos\theta)} \cos\phi \sin\phi \, d\phi \, d\theta$$

$$= \frac{12a}{\pi} \int_0^{\pi/4} \frac{1}{2} \sin^2\phi \Big|_0^{\operatorname{arccot}(\cos\theta)} d\theta$$

$$= \frac{6a}{\pi} \int_0^{\pi/4} \frac{d\theta}{1 + \cos^2\theta}$$

From Appendix A, this gives

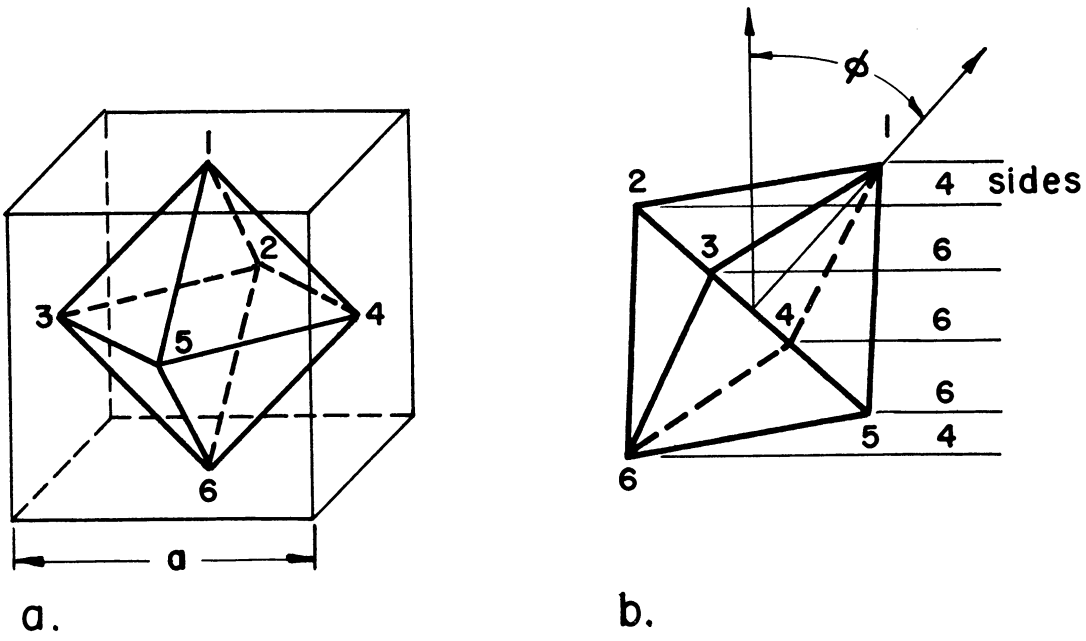

Figure 36. Octahedron.

$$P_i \text{ (octahedron)} = \frac{6a}{\pi}\left[\frac{\pi}{2\sqrt{2}} - \frac{1}{\sqrt{2}} \arctan\sqrt{2}\right]$$

$$P_i \text{ (octahedron)} = a\left(\frac{3}{\sqrt{2}} - \frac{3\sqrt{2}}{\pi} \arctan\sqrt{2}\right) \tag{88}$$

This is the desired result. An alternate form of this expression is

$$P_i \text{ (octahedron)} = a \cdot \frac{3\sqrt{2}}{\pi} \operatorname{arccot}\sqrt{2} \tag{89}$$

This numerically is

$$P_i \text{ (octahedron)} = 0.8312\ a \tag{90}$$

Frequency of Section Shapes

The frequencies with which various sections of randomly oriented octahedrons may be observed can also be readily calculated. From Figure 36b we see that we can only get 4 or 6 sided plane sections of octahedrons. The distances required for each of these cases will be $D_4 = 2h_{1\text{-}2}$ and $D_6 = h_{2\text{-}5}$. Setting up the necessary expressions to integrate, we have

$$P_4 = \frac{12}{\pi} \int_0^{\pi/4} \int_0^{\operatorname{arccot}(\cos\theta)} 2 \cdot \frac{a}{2} (-\cos\theta \sin\phi + \cos\phi) \sin\phi \, d\phi \, d\theta$$

$$= \frac{12a}{\pi} \int_0^{\pi/4} \left[-\cos\theta \cdot \frac{1}{2} (\phi - \sin\phi \cos\phi) + \frac{1}{2} \sin^2\phi\right]_0^{\operatorname{arccot}(\cos\theta)} d\theta$$

$$= \frac{6a}{\pi} \int_0^{\pi/4} \left(-\cos\theta \cdot \operatorname{arccot}(\cos\theta) + \frac{\cos^2\theta}{1+\cos^2\theta} + \frac{1}{1+\cos^2\theta}\right) d\theta$$

We use the results in Appendix A.

$$P_4 = \frac{6a}{\pi}\left[-\frac{3}{\sqrt{2}}\arctan\sqrt{2} + \left(\frac{2\sqrt{2}-1}{4}\right)\pi + \frac{1}{\sqrt{2}}\arctan\sqrt{2} + \left(\frac{1-\sqrt{2}}{4}\right)\pi\right.$$

$$\left. + \frac{\pi}{2\sqrt{2}} - \frac{1}{\sqrt{2}}\arctan\sqrt{2}\right]$$

$$P_4 = \frac{6a}{\pi}\left(-\frac{3}{\sqrt{2}}\arctan\sqrt{2} + \frac{\pi}{\sqrt{2}}\right)$$

$$P_4 = a\left(3\sqrt{2} - \frac{9\sqrt{2}}{\pi}\arctan\sqrt{2}\right) \qquad (91)$$

This is the desired result for 4 sided sections.

For 6 sided sections, we have

$$P_6 = \frac{12}{\pi}\int_0^{\pi/4}\int_0^{\operatorname{arccot}(\cos\theta)} a\cos\theta\sin^2\phi\,d\phi\,d\theta$$

$$= \frac{6a}{\pi}\int_0^{\pi/4}\cos\theta(\phi-\sin\phi\cos\phi)\Big|_0^{\operatorname{arccot}(\cos\theta)}d\theta$$

$$= \frac{6a}{\pi}\int_0^{\pi/4}\left[\cos\theta\cdot\operatorname{arccot}(\cos\theta) - \frac{\cos^2\theta}{1+\cos^2\theta}\right]d\theta$$

From Appendix A, we have

$$P_6 = \frac{6a}{\pi}\left[\frac{3}{\sqrt{2}}\arctan\sqrt{2} + \frac{\pi}{4} - \frac{\pi}{\sqrt{2}} - \frac{1}{\sqrt{2}}\arctan\sqrt{2} - \frac{\pi}{4} + \frac{\pi}{2\sqrt{2}}\right]$$

$$= \frac{6a}{\pi}\left[\sqrt{2}\arctan\sqrt{2} - \frac{\pi}{2\sqrt{2}}\right]$$

$$P_6 = a\left(\frac{6\sqrt{2}}{\pi}\arctan\sqrt{2} - \frac{3}{\sqrt{2}}\right) \qquad (92)$$

This is the other desired result.

From Equations (91) and (92), the relative frequencies of section shapes from randomly oriented octahedrons are given in Table XII.

TABLE XII

RELATIVE FREQUENCY OF SECTIONS OF OCTAHEDRON

Number of Sides	Frequency
4	44.8%
6	55.2%
	100.0%

VIII. TETRAHEDRON

Probability of Sectioning

For a tetrahedron, the development of the relationships for probability of intersecting the particle by a random plane and the expected frequencies of various plane sections proceeds as readily as for the octahedron. In Figure 37 we see a tetrahedron inscribed in a cube of edge length "a". Since a tetrahedron also has cubic symmetry, we find that our same spherical triangle between 001, 101, and 111 poles gives us a representative sample of all possible orientations.

Since corners 1 and 4, in Figure 37, will always be the top and bottom corners within our orientation range, we have

$$D(\text{tetrahedron}) = h_{1\text{-}4} = a(\cos\theta \sin\phi + \cos\phi) \qquad (93)$$

Therefore, our average distance between top and bottom tangent planes will be

$$\bar{D} = \frac{12a}{\pi} \int_0^{\pi/4} \int_0^{\operatorname{arccot}(\cos\theta)} (\cos\theta \sin^2\phi + \cos\phi \sin\phi)\, d\phi d\theta$$

$$= \frac{6a}{\pi} \int_0^{\pi/4} [\cos\theta(\phi - \sin\phi \cos\phi) + \sin^2\phi]_0^{\operatorname{arccot}(\cos\theta)} d\theta$$

$$= \frac{6a}{\pi} \int_0^{\pi/4} \left[\cos\theta \cdot \operatorname{arccot}(\cos\theta) - \frac{\cos^2\theta}{1 + \cos^2\theta} + \frac{1}{1 + \cos^2\theta}\right] d\theta$$

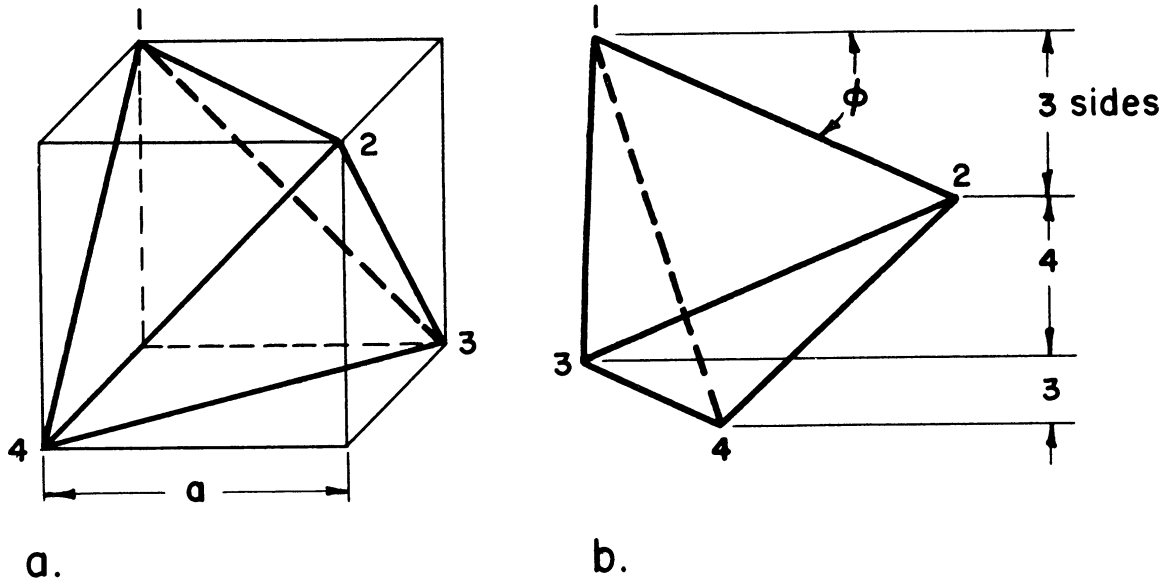

Figure 37. Tetrahedron.

Again, taking the solutions to these integrals from Appendix A, we have

$$P_i = \frac{6a}{\pi}\left[\frac{3}{\sqrt{2}}\arctan\sqrt{2} + \frac{\pi}{4} - \frac{\pi}{\sqrt{2}} - \frac{1}{\sqrt{2}}\arctan\sqrt{2} - \frac{\pi}{4} + \frac{\pi}{2\sqrt{2}} + \frac{\pi}{2\sqrt{2}} - \frac{1}{\sqrt{2}}\arctan\sqrt{2}\right]$$

$$= \frac{6a}{\pi}\left[\frac{1}{\sqrt{2}}\arctan\sqrt{2}\right]$$

$$P_i = a\left(\frac{3\sqrt{2}}{\pi}\arctan\sqrt{2}\right) \qquad (94)$$

This is the desired result. This may be given numerically as

$$P_i \text{ (tetrahedron)} = 1.2901\ a \qquad (95)$$

"a" is the edge length of the circumscribed cube.

Frequency of Section Shapes

To solve for the expected relative frequencies of sections having the various possible numbers of sides, we refer to Figure 37. There it is seen that only 3 and 4 sided sections are obtained from a tetrahedron.

For 3 sided sections we have

$$D_3 = h_{1\text{-}2} + h_{3\text{-}4}$$

$$= a(\sin\theta + \cos\theta)\sin\phi + a(\cos\theta - \sin\theta)\sin\phi$$

$$D_3 = 2a\cos\theta\sin\phi \qquad (96)$$

Setting up the necessary integral, we have

$$P_3 = \frac{12a}{\pi} \int_0^{\pi/4} \int_0^{\operatorname{arccot}(\cos\theta)} 2\cos\theta \sin^2\phi \, d\phi \, d\theta$$

$$= \frac{12a}{\pi} \int_0^{\pi/4} [\cos\theta (\phi - \sin\phi \cos\phi)]_0^{\operatorname{arccot}(\cos\theta)} d\theta$$

$$= \frac{12a}{\pi} \int_0^{\pi/4} [\cos\theta \cdot \operatorname{arccot}(\cos\theta) - \frac{\cos^2\theta}{1 + \cos^2\theta}] \, d\theta$$

Using results from Appendix A, we have

$$P_3 = \frac{12a}{\pi} [\frac{3}{\sqrt{2}} \arctan\sqrt{2} + \frac{\pi}{4} - \frac{\pi}{\sqrt{2}} - \frac{1}{\sqrt{2}} \arctan\sqrt{2} - \frac{\pi}{4} + \frac{\pi}{2\sqrt{2}}]$$

$$= \frac{12a}{\pi} [\sqrt{2} \arctan\sqrt{2} - \frac{\pi}{2\sqrt{2}}]$$

$$P_3 = a(\frac{12\sqrt{2}}{\pi} \arctan\sqrt{2} - 3\sqrt{2}) \qquad (97)$$

This is the desired result.

For 4 sided sections of a tetrahedron we have (referring to Figure 37)

$$D_4 = h_{2\text{-}3}$$

$$D_4 = a(-\cos\theta \sin\phi + \cos\phi) \qquad (98)$$

Again, the integral we need is

$$P_4 = \frac{12a}{\pi} \int_0^{\pi/4} \int_0^{\operatorname{arccot}(\cos\theta)} (-\cos\theta \sin^2\phi + \cos\phi \sin\phi) \, d\phi \, d\theta$$

$$P_4 = \frac{6a}{\pi} \int_0^{\pi/4} [-\cos\theta(\phi - \sin\phi\cos\phi) + \sin^2\phi]_0^{\operatorname{arccot}(\cos\theta)} d\theta$$

$$= \frac{6a}{\pi} \int_0^{\pi/4} [-\cos\theta \cdot \operatorname{arccot}(\cos\theta) + \frac{\cos^2\theta}{1 + \cos^2\theta} + \frac{1}{1 + \cos^2\theta}] \, d\theta$$

Using results from Appendix A,

$$P_4 = \frac{6a}{\pi} [-\frac{3}{\sqrt{2}} \arctan\sqrt{2} - \frac{\pi}{4} + \frac{\pi}{\sqrt{2}} + \frac{1}{2} \arctan\sqrt{2} + \frac{\pi}{4} - \frac{\pi}{2\sqrt{2}}$$

$$+ \frac{\pi}{2\sqrt{2}} - \frac{1}{\sqrt{2}} \arctan\sqrt{2}]$$

$$= \frac{6a}{\pi} [-\frac{3}{\sqrt{2}} \arctan\sqrt{2} + \frac{\pi}{\sqrt{2}}]$$

$$P_4 = a (-\frac{9\sqrt{2}}{\pi} \arctan\sqrt{2} + 3\sqrt{2}) \qquad (99)$$

This is the desired result.

As a check, the sum of the probabilities of 3 and 4 sided sections should equal the total probability for a tetrahedron.

$$P_3 = a (\frac{12\sqrt{2}}{\pi} \arctan\sqrt{2} - 3\sqrt{2}) \qquad (97)$$

$$P_4 = a (-\frac{9\sqrt{2}}{\pi} \arctan\sqrt{2} + 3\sqrt{2}) \qquad (99)$$

$$P_3 + P_4 = a (\frac{3\sqrt{2}}{\pi} \arctan\sqrt{2}) \qquad (94)$$

This is identical to the previous result.

We may now compute the relative frequencies of random plane sections of a tetrahedron, and list these in Table XIII.

TABLE XIII

RELATIVE FREQUENCY OF SECTIONS OF TETRAHEDRON

Number of Sides	Relative Frequency
3	71.15%
4	28.85%

IX. RHOMBIC DODECAHEDRON

Probability of Sectioning

We now consider the probability of intersecting a rhombic dodecahedron by a random sectioning plane, and then the relative frequencies with which the various sided sections may be expected. A rhombic dodecahedron was shown in Figure 3, and we redraw it in Figure 38 in order to number the corners, as required for our subsequent analysis. Again, we shall use the edge length "a" of the circumscribed cube in our calculations. A rhombic dodecahedron also has cubic symmetry, and our same spherical triangle between 001, 101, and 111 poles gives us all possible orientations to a representative degree.

To obtain the probability of intersecting a rhombic dodecahedron we consider again the corners through which top and bottom tangent planes pass. We find that corners 1 and 14 of Figure 38 are the top and bottom corners from $\phi = 0°$ until $\phi = \phi_1 = \text{arccot}\,(\sin\theta + \cos\theta)$, at which angle corner 2 is as high as corner 1 and corner 12 is as low as corner 14. From $\phi = \phi_1$ to $\phi = \phi_2 = \text{arccot}\,(\cos\theta)$, corners 2 and 12 are the top and bottom corners. To solve for $\overline{D}$ (rhombic dodecahedron) we then need $h_{1\text{-}14}$ from $0 \leq \phi \leq \phi_1$ and $h_{2\text{-}12}$ from $\phi_1 \leq \phi \leq \phi_2$.

$$h_{1\text{-}14} = a\cos\phi \tag{100}$$

$$h_{2\text{-}12} = \frac{a}{2}(\sin\theta + \cos\theta)\sin\phi + \frac{a}{2}\cos\phi \tag{101}$$

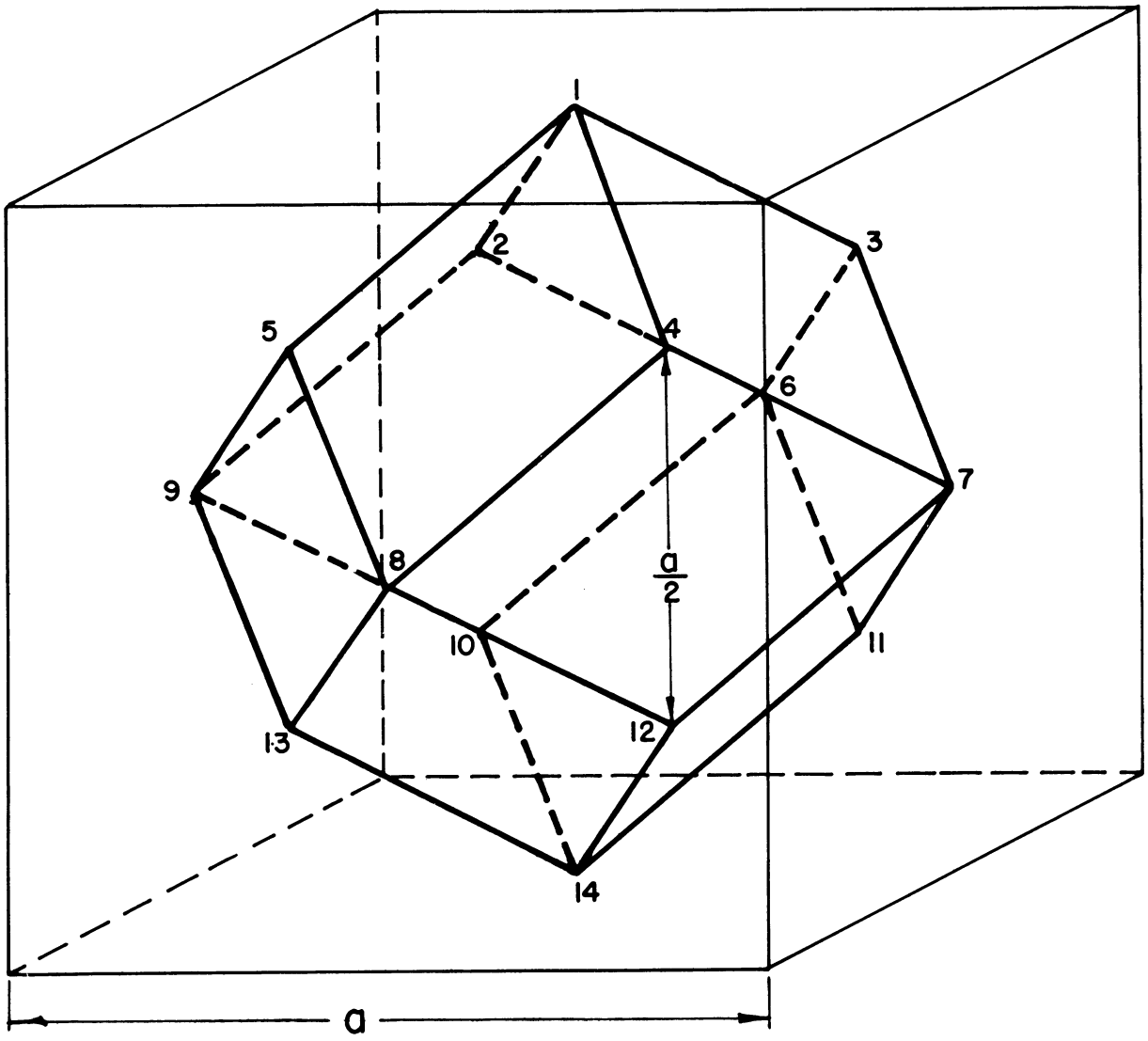

Figure 38. Rhombic Dodecahedron.

We then write down

$$\bar{D}_{R.D.} = \frac{12a}{\pi} \int_0^{\pi/4} \int_0^{\operatorname{arccot}(\sin\theta+\cos\theta)} \cos\phi \sin\phi \, d\phi d\theta$$

$$+ \frac{12a}{\pi} \int_0^{\pi/4} \int_{\operatorname{arccot}(\sin\theta+\cos\theta)}^{\operatorname{arccot}(\cos\theta)} [\tfrac{1}{2}(\sin\theta+\cos\theta)\sin^2\phi + \tfrac{1}{2}\cos\phi \sin\phi] \, d\phi d\theta$$

$$= \frac{6a}{\pi} \int_0^{\pi/4} [\sin^2\phi]_0^{\operatorname{arccot}(\sin\theta+\cos\theta)} \, d\theta$$

$$+ \frac{3a}{\pi} \int_0^{\pi/4} [(\sin\theta+\cos\theta)(\phi-\sin\phi\cos\phi)+\sin^2\phi]_{\operatorname{arccot}(\sin\theta+\cos\theta)}^{\operatorname{arccot}(\cos\theta)} d\theta$$

$$= \frac{6a}{\pi} \int_0^{\pi/4} \frac{d\theta}{2 + \sin 2\theta}$$

$$+ \frac{3a}{\pi} \int_0^{\pi/4} [\sin\theta \cdot \operatorname{arccot}(\cos\theta) + \cos\theta \cdot \operatorname{arccot}(\cos\theta)$$

$$- \frac{\sin\theta\cos\theta}{1+\cos^2\theta} - \frac{\cos^2\theta}{1+\cos^2\theta} + \frac{1}{1+\cos^2\theta}$$

$$- \sin\theta \cdot \operatorname{arccot}(\sin\theta+\cos\theta) - \cos\theta \cdot \operatorname{arccot}(\sin\theta+\cos\theta)$$

$$+ \frac{\sin^2\theta + 2\sin\theta\cos\theta + \cos^2\theta}{2+\sin 2\theta} - \frac{1}{2+\sin 2\theta}] \, d\theta$$

These integrals are solved in Appendix A.

$$\bar{D}_{R.D.} = \frac{6a}{\pi}\left[\frac{\pi}{6\sqrt{3}}\right] + \frac{3a}{\pi}\left[\frac{\pi}{4} - \frac{1}{\sqrt{2}}\arctan\sqrt{2} + \ln\frac{2}{\sqrt{3}}\right.$$

$$+ \frac{3}{\sqrt{2}}\arctan\sqrt{2} + \frac{\pi}{4} - \frac{\pi}{\sqrt{2}} - \ln\frac{2}{\sqrt{3}} - \frac{1}{\sqrt{2}}\arctan\sqrt{2}$$

$$- \frac{\pi}{4} + \frac{\pi}{2\sqrt{2}} + \frac{\pi}{2\sqrt{2}} - \frac{1}{\sqrt{2}}\arctan\sqrt{2} - \frac{3\pi}{8} + \frac{\pi}{2\sqrt{2}} + \frac{\pi}{4\sqrt{3}}$$

$$- \frac{1}{\sqrt{2}}\arctan\sqrt{2} + \frac{1}{4}\ln\frac{3}{2} - \frac{\pi}{8} - \frac{\pi}{2\sqrt{2}} + \frac{\pi}{4\sqrt{3}} - \frac{1}{4}\ln\frac{3}{2}$$

$$\left. + \frac{1}{\sqrt{2}}\arctan\sqrt{2} + \frac{\pi}{4} - \frac{\pi}{3\sqrt{3}}\right]$$

$$= \frac{a}{\sqrt{3}} + \frac{3a}{\pi}\left[\frac{\pi}{2} - \frac{\pi}{2} + (\arctan\sqrt{2})\left(-\frac{1}{\sqrt{2}} + \frac{3}{\sqrt{2}} - \frac{1}{\sqrt{2}} - \frac{1}{\sqrt{2}} - \frac{1}{\sqrt{2}} + \frac{1}{\sqrt{2}}\right)\right.$$

$$\left. + \frac{\pi}{\sqrt{2}}\left(-1 + \frac{1}{2} + \frac{1}{2} + \frac{1}{2} - \frac{1}{2}\right) + \frac{\pi}{\sqrt{3}}\left(\frac{1}{4} + \frac{1}{4} - \frac{1}{3}\right)\right]$$

$$= \frac{a}{\sqrt{3}} - \frac{3a}{\pi}\left[\frac{\pi}{6\sqrt{3}}\right] = \frac{a}{\sqrt{3}} + \frac{a}{2\sqrt{3}}$$

$$P_i = \bar{D}_{R.D.} = a.\sqrt{3}/2 \qquad (102)$$

This is the desired result. Stated numerically this is

$$P_i \text{ (rhombic dodecahedron)} = 0.8660a \qquad (103)$$

"a" is the edge of the circumscribed cube.

Frequency of Section Shapes

A detailed investigation of the shapes of sections possible from a rhombic dodecahedron reveals that we may obtain sections having 3, 4, 5, 6, 7, 8, and 9 sides. In any one given orientation not all of these type sections will be possible. The types of sections which are possible as a function of our spherical triangle are shown in Figure 39. It will be noted that we now have three distinct angular regions to consider, and in addition to the angles, $\phi_1 = \text{arccot}(\sin\theta+\cos\theta)$ and $\phi_2 = \text{arccot}(\cos\theta)$, which are the same as for the cube, we now need to know a $\phi_3(\theta)$. This ϕ_3 is the angle at which corners 3 and 9 have the same elevation, and is shown, by the previously described method of analysis, to be:

$$\phi_3 = \text{arccot}\,(3\sin\theta - \cos\theta) \qquad (104)$$

We shall now identify the corners to be considered that determine the shapes of sections we obtain. To do this, we consider one at a time each of the three sub-triangles, labelled I, II, and III on Figure 39. Since the rhombic dodecahedron is symmetrical above and below its mid-point, we need only consider the corners which are above the mid-point for any given orientation. For triangles I, II, and III we obtain the data of Table XIV.

To determine the total possibilities for each type of section, we collect and group those listed in Table XIV by each triangle. Each group is multiplied by two, to account for sections above and below the mid-point, except when we count a range over which the mid-point

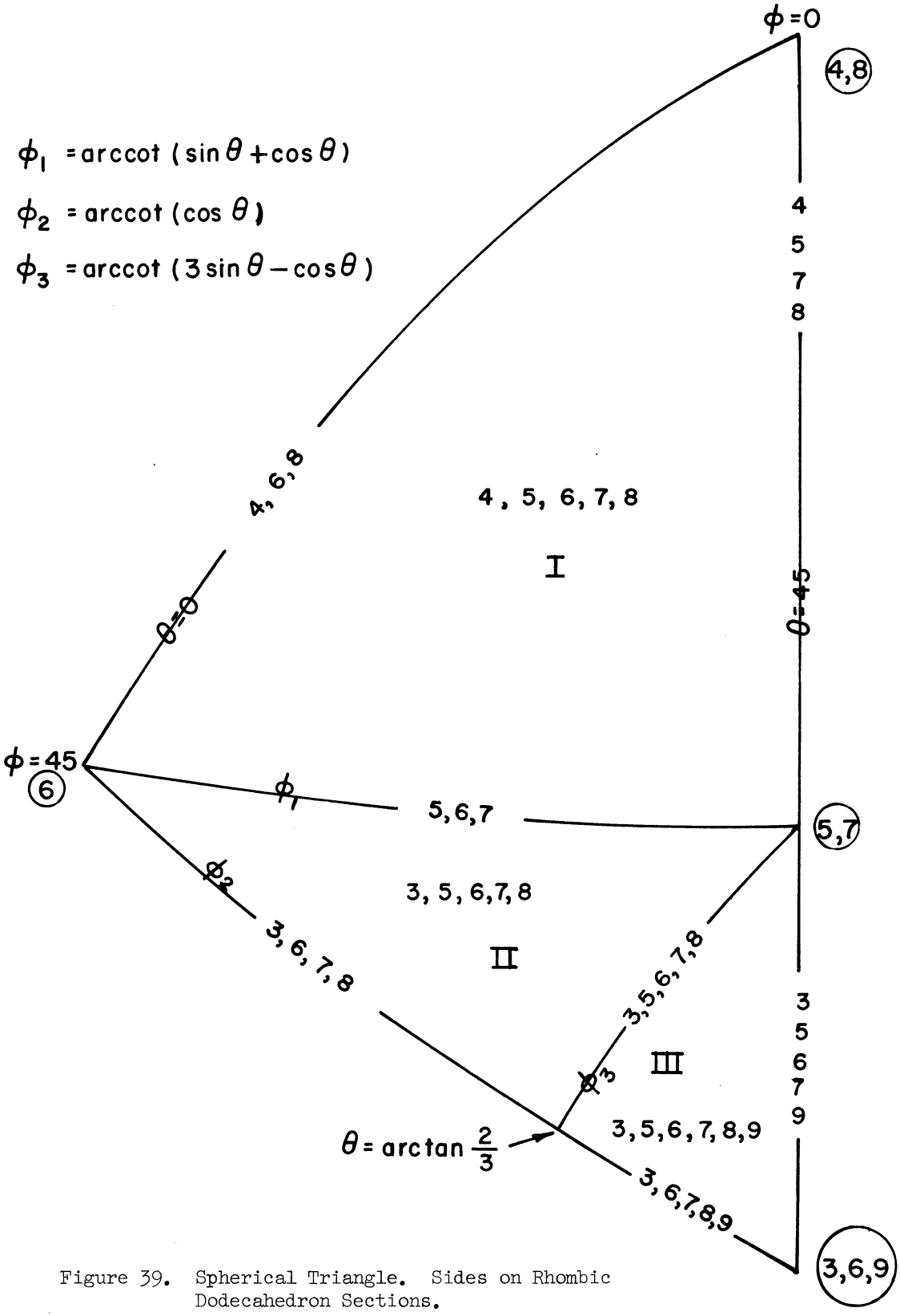

Figure 39. Spherical Triangle. Sides on Rhombic Dodecahedron Sections.

is included. We get then the data of Table XV.

TABLE XIV

SIDES ON RHOMBIC DODECAHEDRON SECTIONS
DEPENDING UPON ADJACENT CORNERS

(Sub-triangles I, II, III, - see Fig. 39)

I		II		III	
Corners	Sides	Corners	Sides	Corners	Sides
1-2	4	2-1	3	2-1	3
2-3	5	1-6	5	1-6	5
3-5	6	6-3	7	6-9	7
5-4	7	3-9	6	9-3	9
4-mid	8	9-5	8	3-5	8
		5-10	7	5-10	7
		10-mid	6	10-mid	6

We can readily compute the D's for the various distances between corners by the previously described technique. We also need the angle at which $\phi_3 = \phi_2$, or $\operatorname{arccot}(3\sin\theta - \cos\theta) = \operatorname{arccot}(\cos\theta)$, and we find this to be $\theta = \arctan \frac{2}{3}$ or $\operatorname{arccot} \frac{3}{2}$. The corners for obtaining various sided sections and the integration ranges listed in Table XV are shown graphically in Figure 40.

We are now in a position to set up and solve the various needed integral equations. It may be noted that for every angular range involving ϕ_1 and ϕ_2 we already have solved in Appendix A all the integral

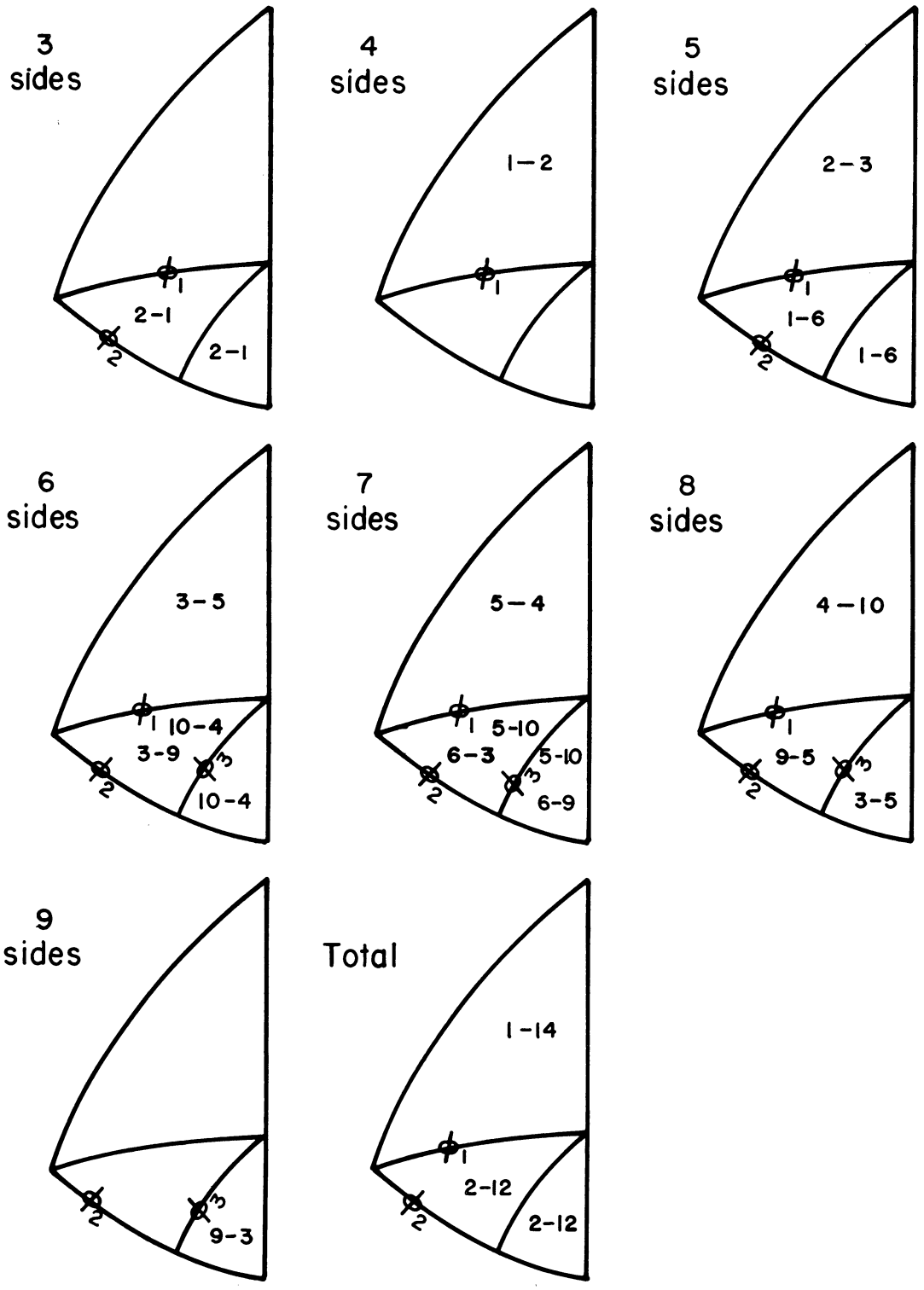

Figure 40. Spherical Triangles. Corners for Obtaining Sections of Rhombic Dodecahedron.

TABLE XV

RHOMBIC DODECAHEDRON. FUNCTIONS NEEDED TO DETERMINE FREQUENCIES OF SECTIONS

Sides	Projected Height	ϕ Range	θ Range
D_3	$2\ h_{2-1}$	ϕ_1 to ϕ_2	0 to $\frac{\pi}{4}$
D_4	$2\ h_{1-2}$	0 to ϕ_1	0 to $\frac{\pi}{4}$
D_5	$2\ h_{2-3}$	0 to ϕ_1	0 to $\frac{\pi}{4}$
	$2\ h_{1-6}$	ϕ_1 to ϕ_2	0 to $\frac{\pi}{4}$
D_6	$2\ h_{3-5}$	0 to ϕ_1	0 to $\frac{\pi}{4}$
	$2\ h_{3-9}$	ϕ_1 to ϕ_2	0 to arccot $\frac{3}{2}$
	$2\ h_{3-9}$	ϕ_1 to ϕ_3	arccot $\frac{3}{2}$ to $\frac{\pi}{4}$
	h_{10-4}	ϕ_1 to ϕ_2	0 to $\frac{\pi}{4}$
D_7	$2\ h_{5-4}$	0 to ϕ_1	0 to $\frac{\pi}{4}$
	$2\ h_{6-3}$	ϕ_1 to ϕ_2	0 to arccot $\frac{3}{2}$
	$2\ h_{6-3}$	ϕ_1 to ϕ_3	arccot $\frac{3}{2}$ to $\frac{\pi}{4}$
	$2\ h_{6-9}$	ϕ_3 to ϕ_2	arccot $\frac{3}{2}$ to $\frac{\pi}{4}$
	$2\ h_{5-10}$	ϕ_1 to ϕ_2	0 to $\frac{\pi}{4}$
D_8	h_{4-10}	0 to ϕ_1	0 to $\frac{\pi}{4}$
	$2\ h_{9-5}$	ϕ_1 to ϕ_2	0 to arccot $\frac{3}{2}$
	$2\ h_{9-5}$	ϕ_1 to ϕ_3	arccot $\frac{3}{2}$ to $\frac{\pi}{4}$
	$2\ h_{3-5}$	ϕ_3 to ϕ_2	arccot $\frac{3}{2}$ to $\frac{\pi}{4}$
D_9	$2\ h_{9-3}$	ϕ_3 to ϕ_2	arccot $\frac{3}{2}$ to $\frac{\pi}{4}$

equations which are necessary for an exact solution. However, when we integrate with one limit being ϕ_3 = arccot (3 sinθ-cosθ) we generate new functions, for which we have not as yet determined the solutions to the integral equations. In the initial solution of these equations a method of approximate integration using the trapezoidal formula, described in any calculus text, was utilized. However, subsequently an IBM 7090 digital computer was utilized to solve the integral equations, and the results obtained were of much better accuracy than the initial results. The description of the digital computer technique is contained in Appendix B. The equations for the rhombic dodecahedron are represented by Equations (16) through (35) on the digital computer print-out sheet in Appendix B.

The probabilities of each of the types of sections of a rhombic dodecahedron, as calculated by the computer, are given in Table XVI. This table also lists the relative frequencies with which the various types of sections are obtained, as calculated directly from the probabilities. It may be noted that the sum of the probabilities of the types of sections, which represents an addition of 18 separately computed integrals, agrees to the fourth decimal place with the previously computed probability of intersection of the rhombic dodecahedron as a whole.

TABLE XVI

RHOMBIC DODECAHEDRON. PROBABILITIES AND RELATIVE FREQUENCIES OF SECTIONS

Sides on Section	Probability	Relative Frequency
3	0.0348 a	4.0 %
4	0.1160 a	13.4 %
5	0.1402 a	16.2 %
6	0.2587 a	29.9 %
7	0.1654 a	19.1 %
8	0.1413 a	16.3 %
9	0.0096 a	1.1 %
	0.8660 a	100.0 %

X. TETRAKAIDECAHEDRON

Probability of Sectioning

The tetrakaidecahedron was sketched in Figure 1 and is shown again in Figure 41, with its corners numbered. The analysis of the probability of intersecting a tetrakaidecahedron by a random sectioning plane is simple and straightforward. Again, only the spherical triangle between 001, 101, and 111 poles is needed. For all orientations represented by this triangle, corners 1 and 24 are always the top and bottom corners. Therefore, we need $h_{1\text{-}24}$ from $0 \leq \phi \leq \phi_2$. We find, in terms of "a", the edge of the circumscribed cube:

$$h_{1\text{-}24} = \frac{a}{2} \cos\theta \sin\phi + a \cos\phi \tag{105}$$

Therefore, the integral which gives probability of sectioning is

$$\bar{D} = \frac{12a}{\pi} \int_0^{\pi/4} \int_0^{\operatorname{arccot}(\cos\theta)} \left[\frac{1}{2} \cos\theta \sin^2\phi + \cos\phi \sin\phi\right] d\phi d\theta$$

$$= \frac{6a}{\pi} \int_0^{\pi/4} \left[\frac{1}{2} \cos\theta \left(\phi - \sin\phi \cos\phi\right) + \sin^2\phi\right]_0^{\operatorname{arccot}(\cos\theta)} d\theta$$

$$= \frac{6a}{\pi} \int_0^{\pi/4} \left[\frac{1}{2} \cos\theta \cdot \operatorname{arccot}(\cos\theta) - \frac{1}{2} \frac{\cos^2\theta}{1+\cos^2\theta} + \frac{1}{1+\cos^2\theta}\right] d\theta$$

Using the integral solutions from Appendix A,

$$P_i = \frac{6a}{\pi} \left[\frac{3}{2\sqrt{2}} \arctan\sqrt{2} + \frac{\pi}{8} - \frac{\pi}{2\sqrt{2}} - \frac{1}{2\sqrt{2}} \arctan\sqrt{2} - \frac{\pi}{8}\right.$$

$$\left. + \frac{\pi}{4\sqrt{2}} + \frac{\pi}{2\sqrt{2}} - \frac{1}{\sqrt{2}} \arctan\sqrt{2}\right]$$

$$= \frac{6a}{\pi} \left[\frac{\pi}{4\sqrt{2}}\right]$$

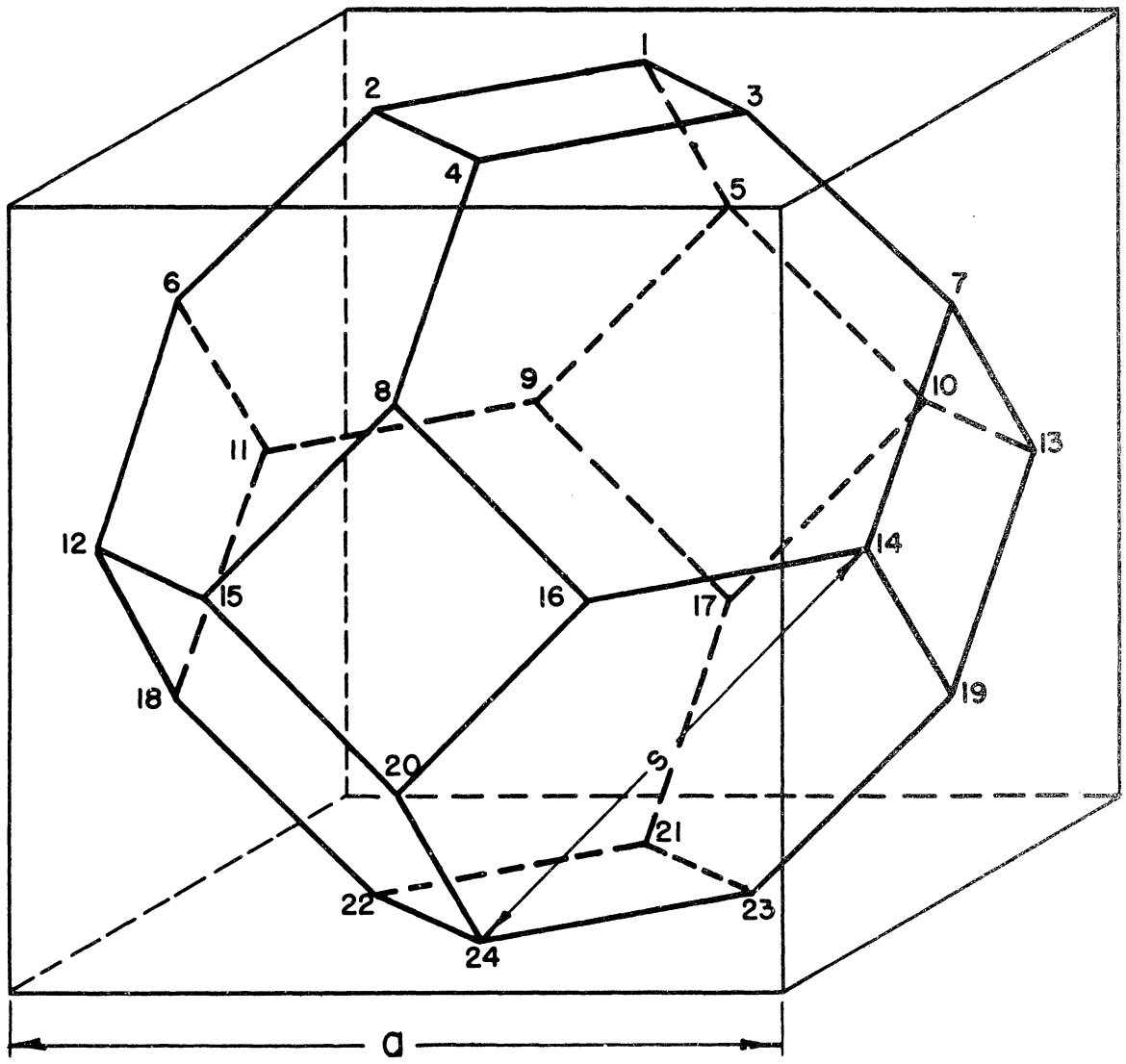

Figure 41. Tetrakaidecahedron

$$P_i(\text{tetrakaidecahedron}) = a \cdot \frac{3}{2\sqrt{2}} \qquad (106)$$

This is the desired result. Numerically, this is

$$P_i(\text{tetrakaidecahedron}) = 1.0607a \qquad (107)$$

"a" is the edge of the circumscribed cube.

Frequency of Section Shapes

It would be nice if the computation for frequencies of sections of the tetrakaidecahedron were as simple as the above, but this turned out to be an exceedingly complex problem. The tetrakaidecahedron has 24 corners, and each time any two corners change their relative positions in elevation as the orientation varies, a new set of possible sections is obtained. It turns out that, over our familiar spherical triangle, 77 separate sub-triangles must be considered and analyzed. The result of this analysis leads to 204 integral equations to be solved, each equation generally requiring an approximate integration technique. Thus, the desire to obtain the frequencies of sections of the tetrakaidecahedron led to the development of the IBM 7090 digital computer solution for our integral equations. This digital computer technique is described in Appendix B.

The method of attack to determine sections of the tetrakaidecahedron is roughly outlined in Section VI of this dissertation entitled, "General Approach to Polyhedron Problem." For the tetrakaidecahedron, this will be described in somewhat more detail now.

As mentioned earlier, some systematic method of preparing sketches representative of different orientations of the polyhedron is essential. The best procedure is to prepare a series of transverse

sketches of the tetrakaidecahedron, showing a vertical projection of the object viewed from the side in a direction normal to the Θ direction. Several of these will usually be required for various values of Θ, depending upon the complexity of the polyhedron and the spatial visual acuity of the investigator.

A typical example of such a sketch is shown in Figure 42 for $\Theta = 28°$. For this choice of Θ, all ϕ's of interest may be investigated by merely placing a transparent protractor at the proper ϕ angle over Figure 42b and then moving a transparent drawing triangle along the protractor to determine elevations. Figure 42a is merely a guide to help draw 42b. It may be seen then that for $\Theta = 28°$, with this figure we can determine for any ϕ the consecutive corners of the tetrakaidecahedron that are passed by parallel sectioning planes from the top to the bottom of the figure. We also can determine the number of sides on the plane section that results between any two consecutive corners. As for example on Figure 42b, for $\Theta = 28°$ and $\phi = 30°$ it may be seen that a 7 sided section is obtained between corners 9 and 11 and a 6 sided section from corner 11 to corner 10. This detailed information is essential, as we need to sum up all 6 sided sections, 7 sided sections, etc., to determine their frequencies. In this instance, a component of the total probability of 7 sided sections would be that contributed by the vertical distance between corners 9 and 11 over the appropriate angular range.

This procedure of finding the corners between which certain types of sections are observed is followed until all orientations within the spherical triangle have been investigated. The result will then be a map of the orientation triangle, which is divided into sub-regions of

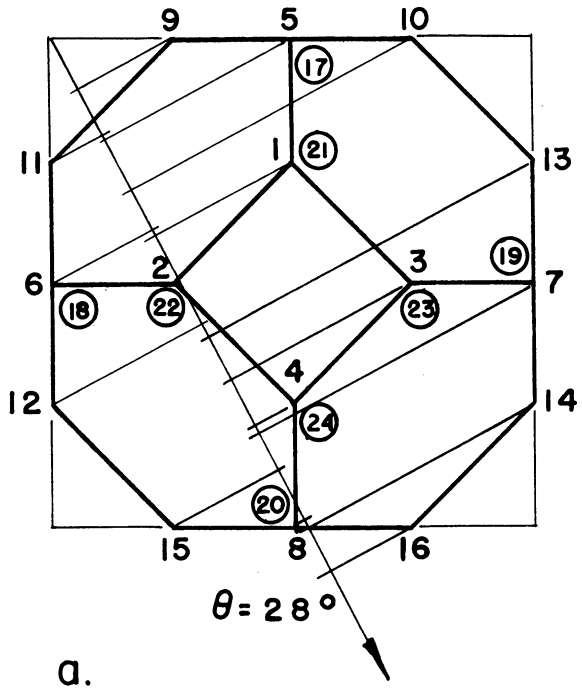

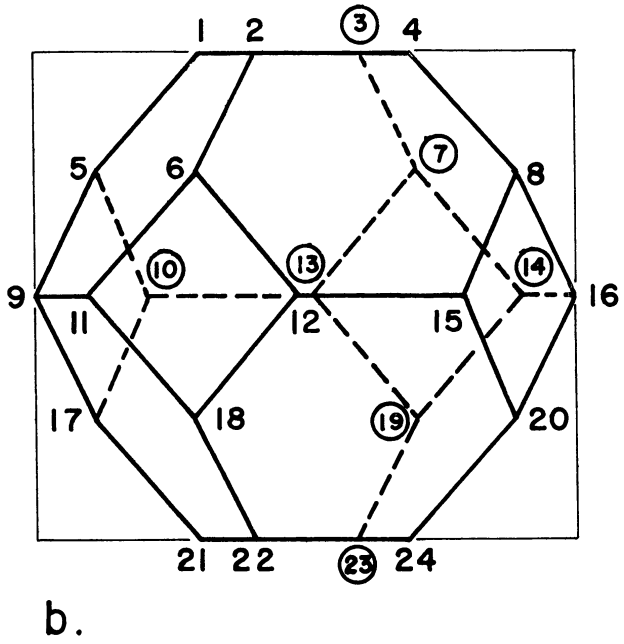

Figure 42. Tetrakaidecahedron at $\theta = 28°$

orientations. For the tetrakaidecahedron there are 77 orientation sub-regions, as shown in Figure 43.

The angles subdividing the sub-regions are expressed as $\phi(\theta)$'s, and are the orientations at which two or more corners have the same elevation. As you cross one of these angles, the types of sections and the corners between which they are observed will usually change discontinuously in the immediate vicinity of these crossing corners. Thus the $\phi(\theta)$ angles represent integration limits for the required equations. By a consideration of the corners that are crossing we may readily compute each $\phi(\theta)$ and we list these in Table XVII, together with two θ angles and all the crossing corners represented. These angles, then, completely subdivide our orientation triangle into the required sub-regions.

We now can map out on an orientation triangle all corner numbers that result in a particular type section by placing these numbers within the applicable orientation range. From the corner numbers we compute the $D(\phi,\theta)$ for these corners, and from the orientation triangle we have the integration limits. We integrate each case, add up all such cases for a particular type of section, and we have the probability of that section.

For instance, for 3 sided sections of a tetrakaidecahedron the orientation plot is shown in Figure 45. It will be noted that, for the top half of the body, 3 sided sections are found between corners 1 and 2 for $0 \leq \phi \leq \phi_6 = \text{arccot}\ (2\cos\theta - \sin\theta)$ and between corners 1 and 5 for $\phi_6 \leq \phi \leq \phi_2 = \text{arccot}\ (\cos\theta)$. We need $h_{1\text{-}2}$ and $h_{1\text{-}5}$; to facilitate finding these and other h's which comprise the D's, we refer to a top

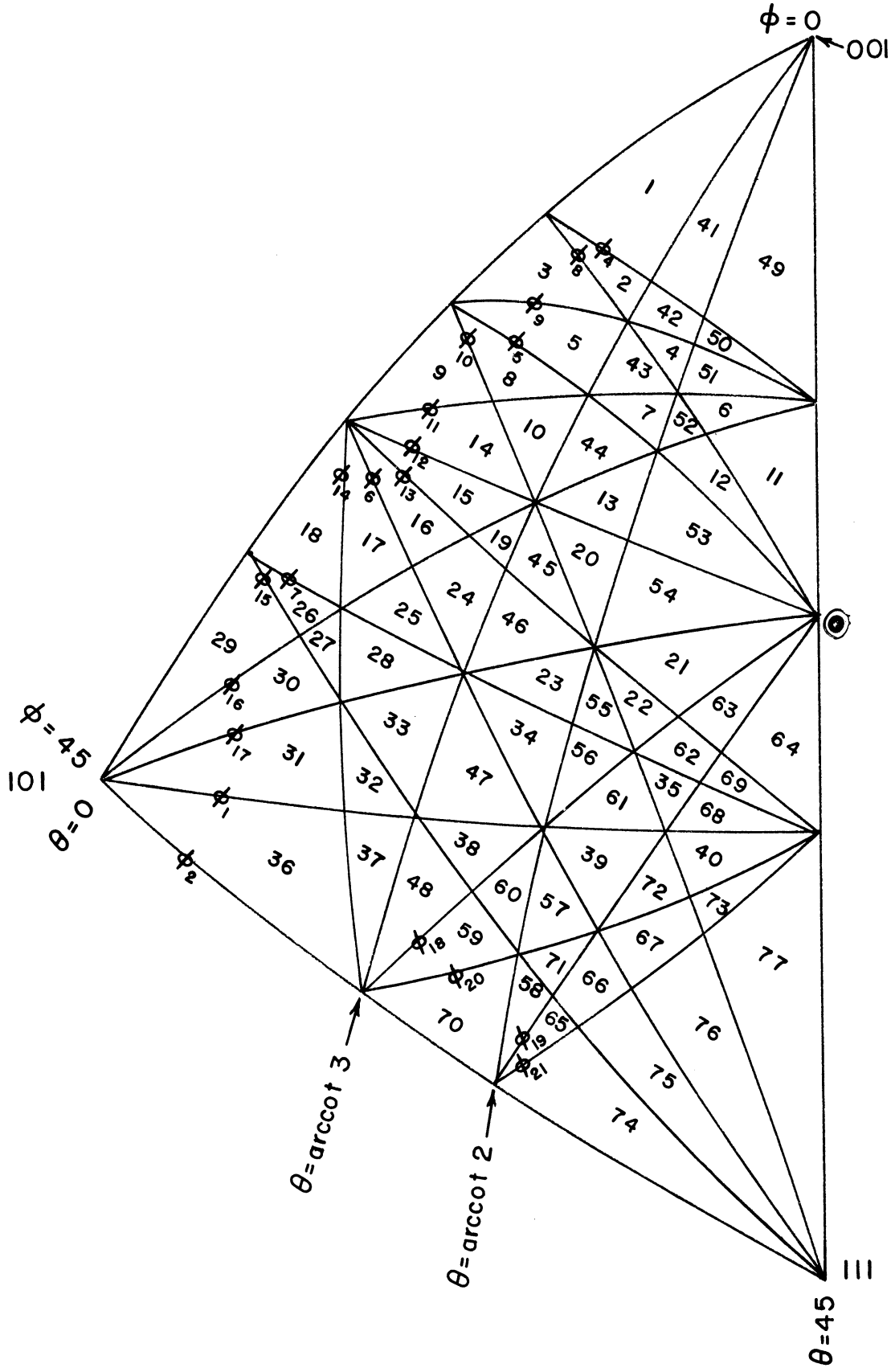

Figure 43. Spherical Triangle. Tetrakaidecahedron Orientation Sub-Regions.

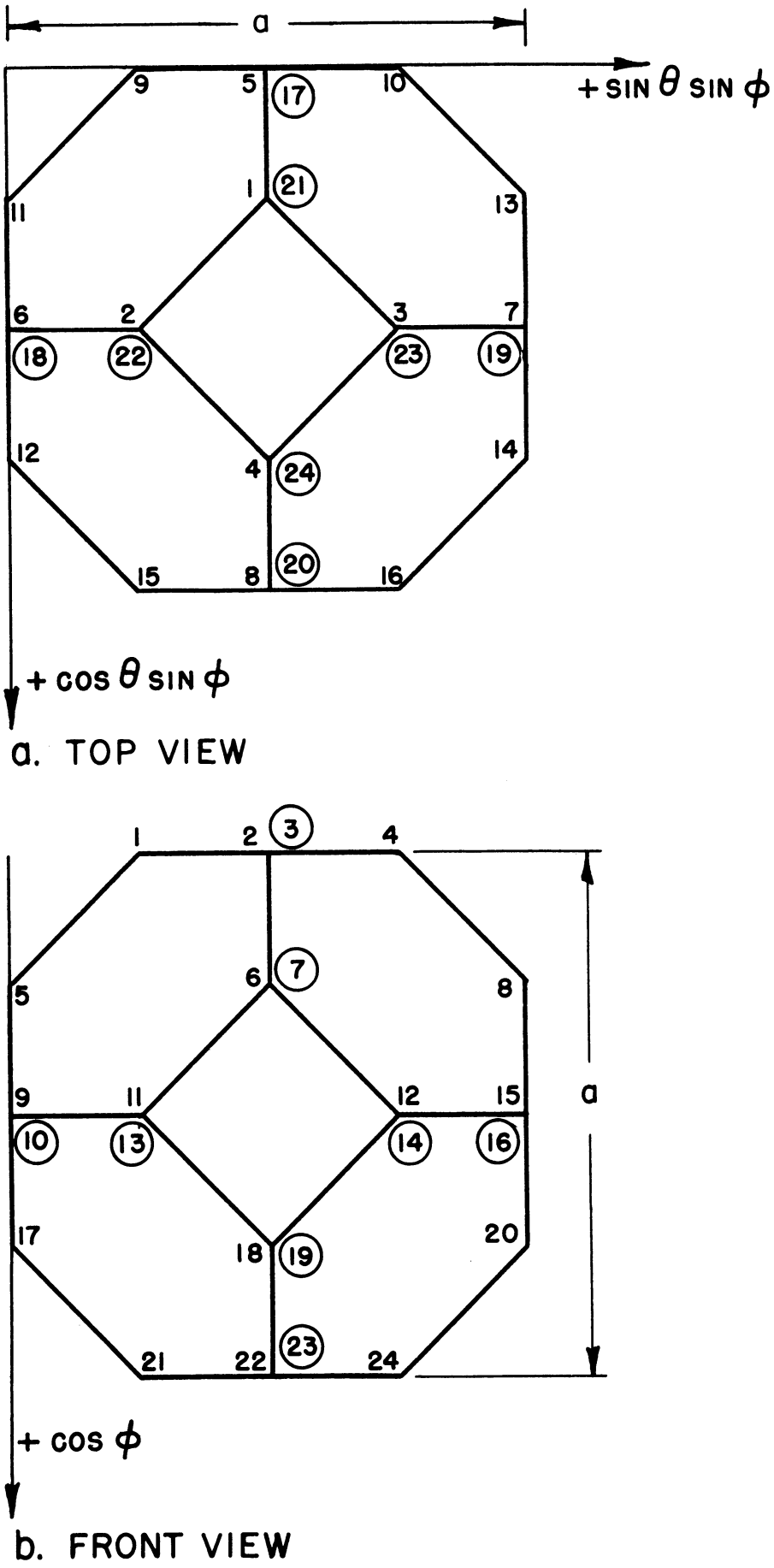

Figure 44. Tetrakaidecahedron. Finding Corner Distances.

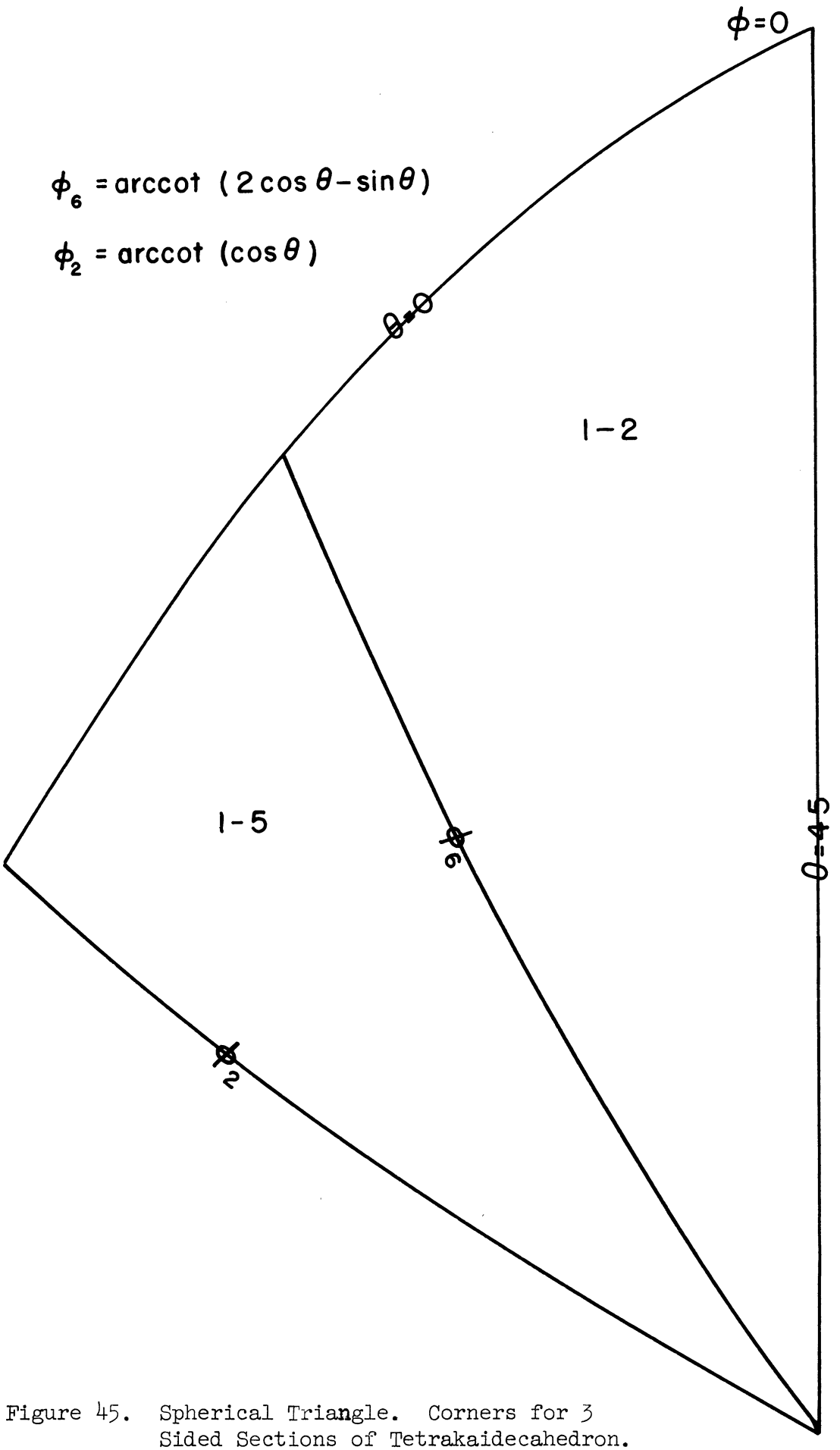

Figure 45. Spherical Triangle. Corners for 3 Sided Sections of Tetrakaidecahedron.

TABLE XVII

TETRAKAIDECAHEDRON. ANGLES DETERMINED BY CORNER ELEVATIONS WHICH SUBDIVIDE THE SPHERICAL TRIANGLE

Angles	Corners
$\phi_1 = \text{arccot}\ (\sin\theta + \cos\theta)$	3=9, 4=11, 8=18, 7=17
$\phi_2 = \text{arccot}\ (\cos\theta)$	1=5, 2=9, 3=10, 6=11, 4=17, 7=13
$\phi_4 = \text{arccot}\ (4\cos\theta + \sin\theta)$	8=9
$\phi_5 = \text{arccot}\ (3\cos\theta)$	4=5
$\phi_6 = \text{arccot}\ (2\cos\theta - \sin\theta)$	2=5, 6=9
$\phi_7 = \text{arccot}\ (\frac{3}{2}\cos\theta + \frac{1}{2}\sin\theta)$	4=9
$\phi_8 = \text{arccot}\ (4\cos\theta - \sin\theta)$	8=10
$\phi_9 = \text{arccot}\ (3\cos\theta + 2\sin\theta)$	8=11
$\phi_{10} = \text{arccot}\ (3\cos\theta - 2\sin\theta)$	8=13
$\phi_{11} = \text{arccot}\ (2\cos\theta + 3\sin\theta)$	7=9
$\phi_{12} = \text{arccot}\ (2\cos\theta + \sin\theta)$	3=5, 7=10
$\phi_{13} = \text{arccot}\ (2\cos\theta)$	8=17
$\phi_{14} = \text{arccot}\ (2\cos\theta - 3\sin\theta)$	6=10
$\phi_{15} = \text{arccot}\ (\frac{3}{2}\cos\theta - \frac{1}{2}\sin\theta)$	4=10
$\phi_{16} = \text{arccot}\ (\cos\theta + 4\sin\theta)$	7=11
$\phi_{17} = \text{arccot}\ (\cos\theta + 2\sin\theta)$	4=6, 13=17, 8=12
$\phi_{18} = \text{arccot}\ (3\sin\theta)$	3=6
$\phi_{19} = \text{arccot}\ (4\sin\theta - \cos\theta)$	7=12, 13=18
$\phi_{20} = \text{arccot}\ (\frac{1}{2}\cos\theta + \frac{3}{2}\sin\theta)$	3=11
$\phi_{21} = \text{arccot}\ (2\sin\theta)$	7=18
$\theta = \text{arccot}\ 3$	10=11
$\theta = \text{arccot}\ 2$	12=13

and front view of the tetrakaidecahedron, as in Figure 44, and read off the difference in coordinates of these points in units of cube edge length, using the convention illustrated by Figure 35. We thus write down

$$h_{1-2} = \frac{a}{4}\left[(\cos\theta-\sin\theta)\sin\phi\right] \tag{108}$$

$$h_{1-5} = \frac{a}{4}\left[-\cos\theta\sin\phi + \cos\phi\right] \tag{109}$$

Now we integrate, using the basic Equation (85) over the appropriate limits, and we have the total probability of 3 sided sections, remembering to consider those sections on the lower half of the body as well.

The integral for P_3 is

$$P_3 = \frac{12a}{\pi}\cdot 2\int_0^{\pi/4}\int_0^{\phi_6}\frac{1}{4}(\cos\theta-\sin\theta)\sin^2\phi\,d\phi\,d\theta + \frac{12a}{\pi}\cdot 2\int_0^{\pi/4}\int_{\phi_6}^{\phi_2}\frac{1}{4}(-\cos\theta\sin\phi+\cos\phi)\sin\phi\,d\phi\,d\theta \tag{110}$$

The angles ϕ_2 and ϕ_6 are

$$\phi_2 = \operatorname{arccot}(\cos\theta) \tag{111}$$

$$\phi_6 = \operatorname{arccot}(2\cos\theta-\sin\theta) \tag{112}$$

Due to the presence of the function ϕ_6 in the above integrals, they have not been solved by exact integration but were calculated with the digital computer. The above integrals are Equations (38) and (39) on the computer print-out in Appendix B.

An identical procedure is followed for 4 sided sections. The orientation map showing corners resulting in 4 sided sections is given in Figure 46. We find h_{2-3}, h_{4-5}, h_{2-5}, and h_{5-2} in an identical manner to that previously described and integrate over the angular regions

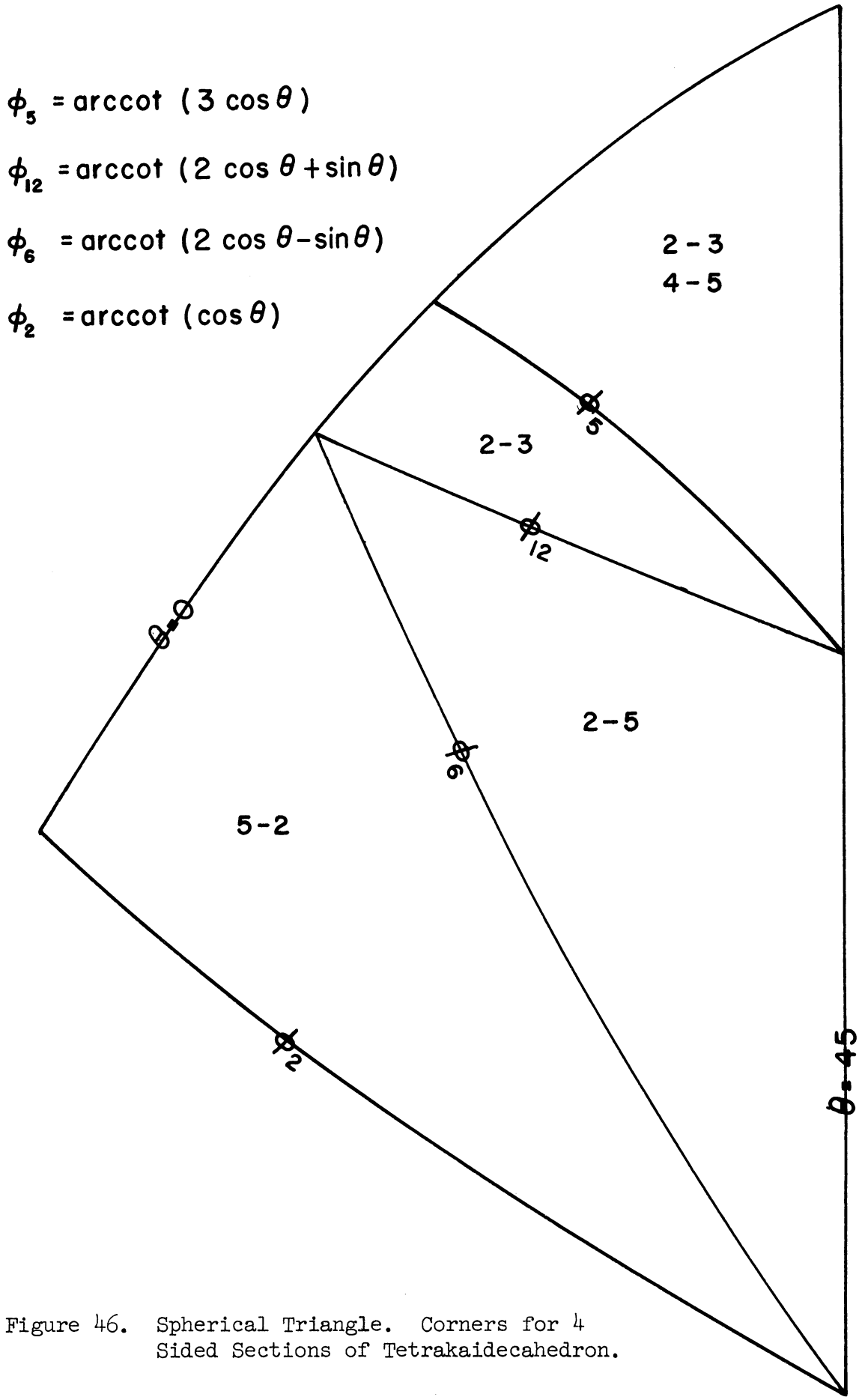

Figure 46. Spherical Triangle. Corners for 4 Sided Sections of Tetrakaidecahedron.

shown in Figure 46. These equations, which when summed give P_4, are those listed on the computer print-out, Appendix B, as Equations (40) through (43).

The orientation map for 5 sided sections is shown in Figure 47. On this map two new factors are apparent for the first time. One is that the second integration over Θ is not always done over the whole range, 0 to 45°, but is limited at times to $\Theta = \text{arccot } 3$ or $\Theta = \text{arccot } 2$. The second factor is that some of the regions indicated in Figure 47 must be further sub-divided for integration where two different upper or lower limits of ϕ are called for. Four such cases appear here. The general procedure is still the same, however, and the equations which give P_5 are listed in the computer print-out, Appendix B, as Equations (44) through (55).

We next show the map for 10 sided sections, Figure 48, which is the maximum number of sides to a plane section of the tetrakaidecahedron. Here it is apparent that 10 sided sections are possible for only a limited portion of the total orientation region. The equations which give P_{10} are Equations (56) through (59) on the computer printout, Appendix B.

For 9 sided sections we show the map, Figure 49. The equations which give P_9 are Equations (60) through (85) on the computer printout.

For 6, 7 and 8 sided sections of the tetrakaidecahedron we do not show corresponding maps of the orientation triangle. Such maps were prepared and are in fact essential to the setting up of the integral equations. However, for pictorial purposes they represent little more than rather impressive worksheets. The 6, 7 and 8 sided sections occur

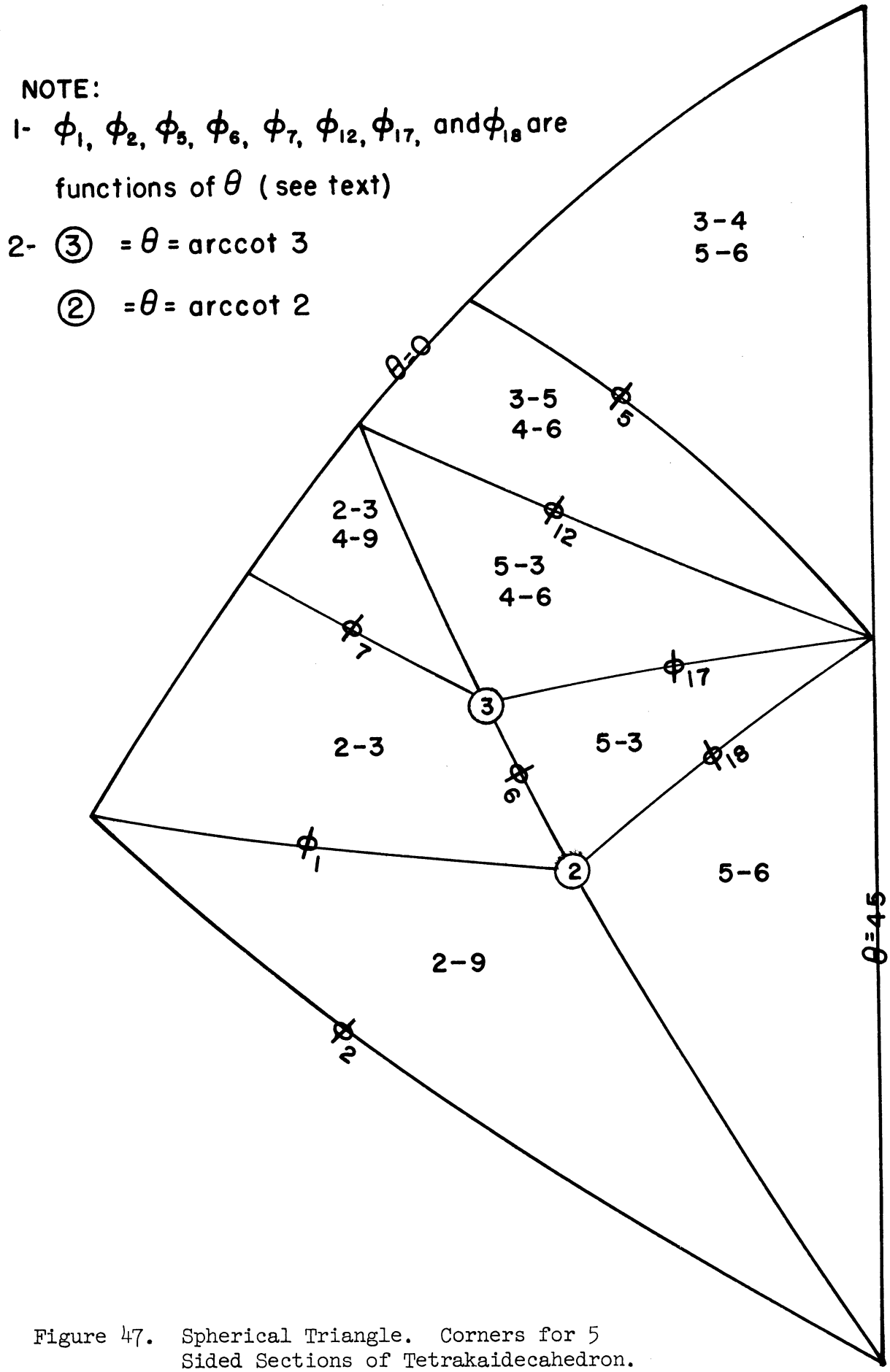

Figure 47. Spherical Triangle. Corners for 5 Sided Sections of Tetrakaidecahedron.

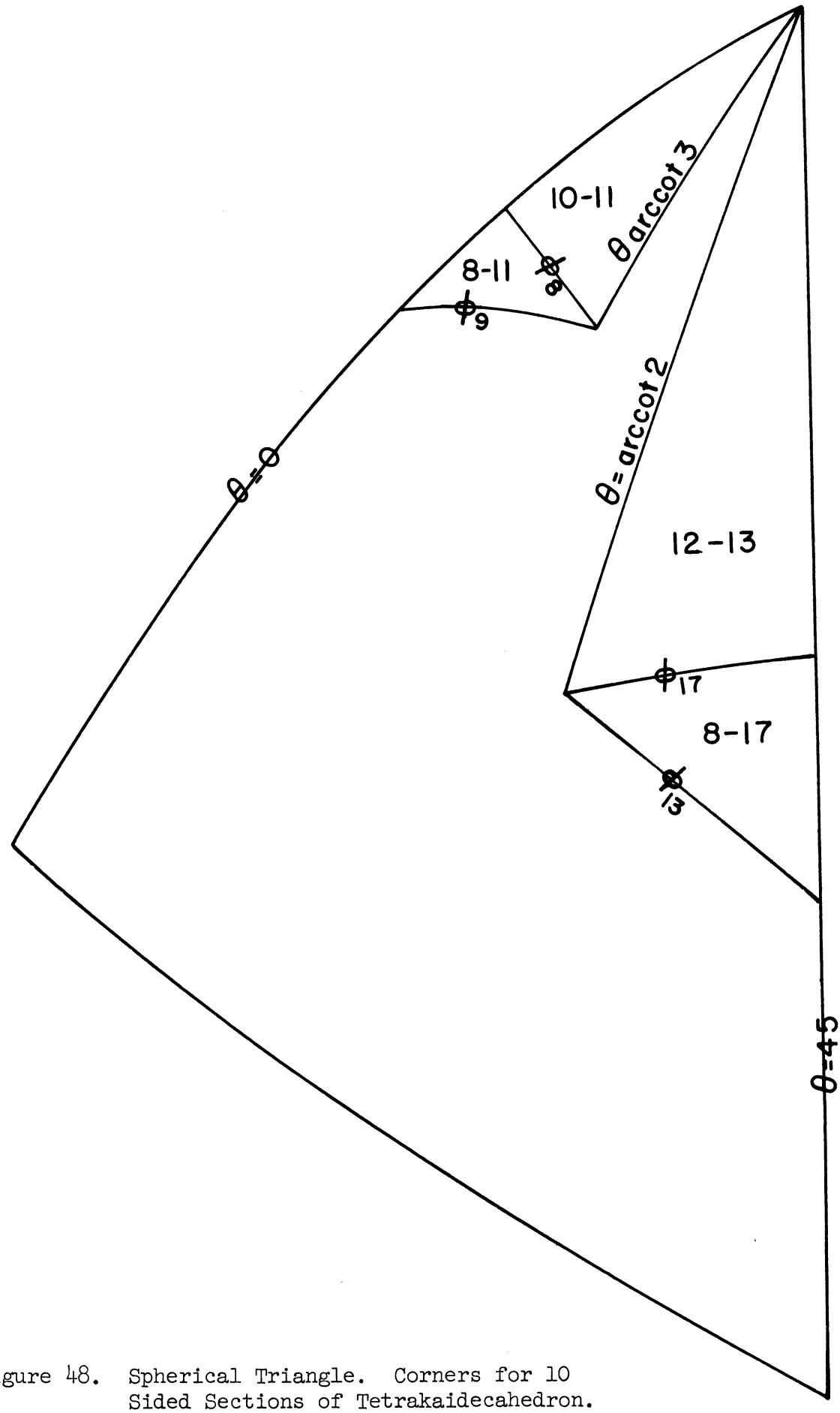

Figure 48. Spherical Triangle. Corners for 10 Sided Sections of Tetrakaidecahedron.

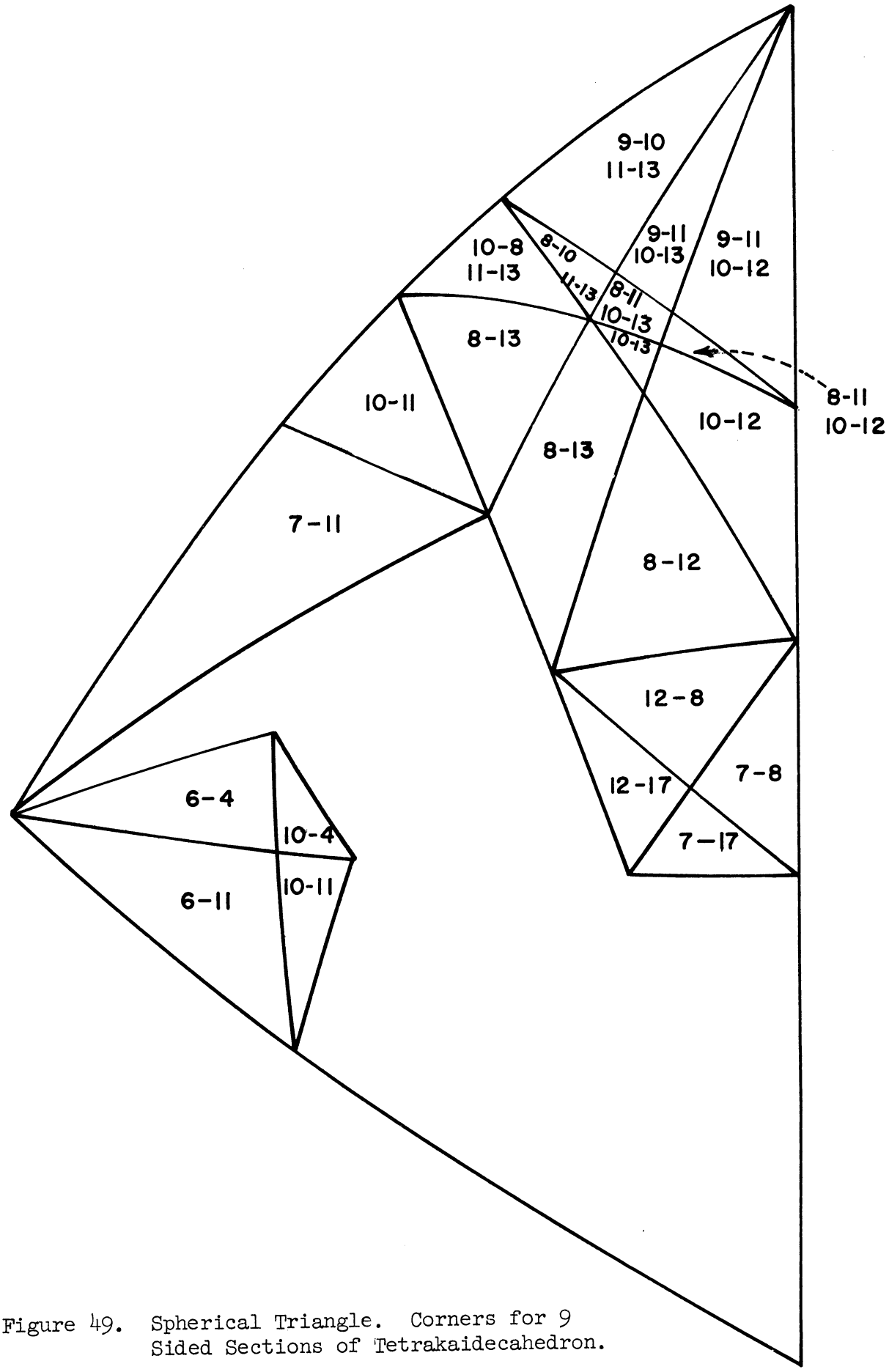

Figure 49. Spherical Triangle. Corners for 9 Sided Sections of Tetrakaidecahedron.

in every one of the 77 sub-triangles of the orientation triangle shown in Figure 43, with multiple frequencies in most such sub-triangles, often for as many as four pairs of points in a given sub-triangle. The equations which give these probabilities may merely be written down, one at a time, by consulting the orientation map. They are listed in the computer printout as follows:

P_6 Equations (138) through (171)

P_7 Equations (172) through (241)

P_8 Equations (86) through (137), plus (242)

The probabilities of each of the types of sections of a tetrakaidecahedron, as calculated by the computer, are listed in Table XVIII. The close agreement between the sum of these separate probabilities, which represents the sum of 204 separate integrations, and the total intersection probability of the tetrakaidecahedron is to be noted. The accuracy to the fourth decimal place gives confidence in the results of the analysis.

The relative frequencies of the various sections of a tetrakaidecahedron are readily computed from the probabilities and are also listed in Table XVIII. Since Hull and Houk[50] also obtained such data for a wire model tetrakaidecahedron, we list their results for comparison. The most obvious comment that can be made relative to the comparison between our result and the previous one by Hull and Houk is the extremely remarkable closeness of the agreement.

TABLE XVIII

TETRAKAIDECAHEDRON. PROBABILITIES AND RELATIVE FREQUENCIES OF SECTIONS

Sides	Probability	Frequency	Hull & Houk[50]
3	0.0770 a	7.3%	7.9%
4	0.1422 a	13.4%	14.5%
5	0.1252 a	11.8%	12.9%
6	0.3313 a	31.2%	29.5%
7	0.1938 a	18.3%	17.9%
8	0.1393 a	13.1%	12.8%
9	0.0403 a	3.8%	4.0%
10	0.0116 a	1.1%	0.5%
	1.0607 a	100.0%	100.0%

XI. HEXAGONAL PRISM

Although a hexagonal prism does not possess cubic symmetry, as have the other polyhedrons considered, the derivation of the probability of its intersection by a randomly oriented plane presents no new difficulties. Computation of relative frequencies of the various possible sections may also be done, but in the present case we restrict ourselves to the body as a whole.

Let us consider such a hexagonal prism, as shown in Figure 50, with corners numbered. Let the diagonal of the base be "a" and the altitude be "c". Due to its symmetry we will be able to represent all possible orientations of the prism by a range of 30° rotation around the vertical axis and a tilt of 90° from the vertical. We therefore consider ϕ from 0 to 90° and θ from 0 to 30°. This is a spherical triangle, 1/24th of a whole sphere. Over this range of orientations our top and bottom corners will always be corners 1 and 10. We then want h_{1-10}. Using the same convention as described previously and illustrated by Figure 35, we write

$$h_{1-10} = \frac{a}{2}\sin\theta\sin\phi + \frac{a\sqrt{3}}{2}\cos\theta\sin\phi + c\cos\phi \qquad (113)$$

Therefore, using Equation (83), we integrate

$$\bar{D} = 24 \cdot \frac{1}{4\pi}\int_0^{\pi/6}\int_0^{\pi/2}\left[\frac{a}{2}\sin\theta\sin\phi + \frac{a\sqrt{3}}{2}\cos\theta\sin\phi - c\cos\phi\right]\sin\phi\, d\phi\, d\theta$$

$$= \frac{6}{\pi}\cdot\frac{1}{2}\int_0^{\pi/6}\left[\frac{a}{2}\sin\theta(\phi-\sin\phi\cos\phi) + \frac{a\sqrt{3}}{2}\cos\theta(\phi-\sin\phi\cos\phi) + c\sin^2\phi\right]_0^{\pi/2} d\theta$$

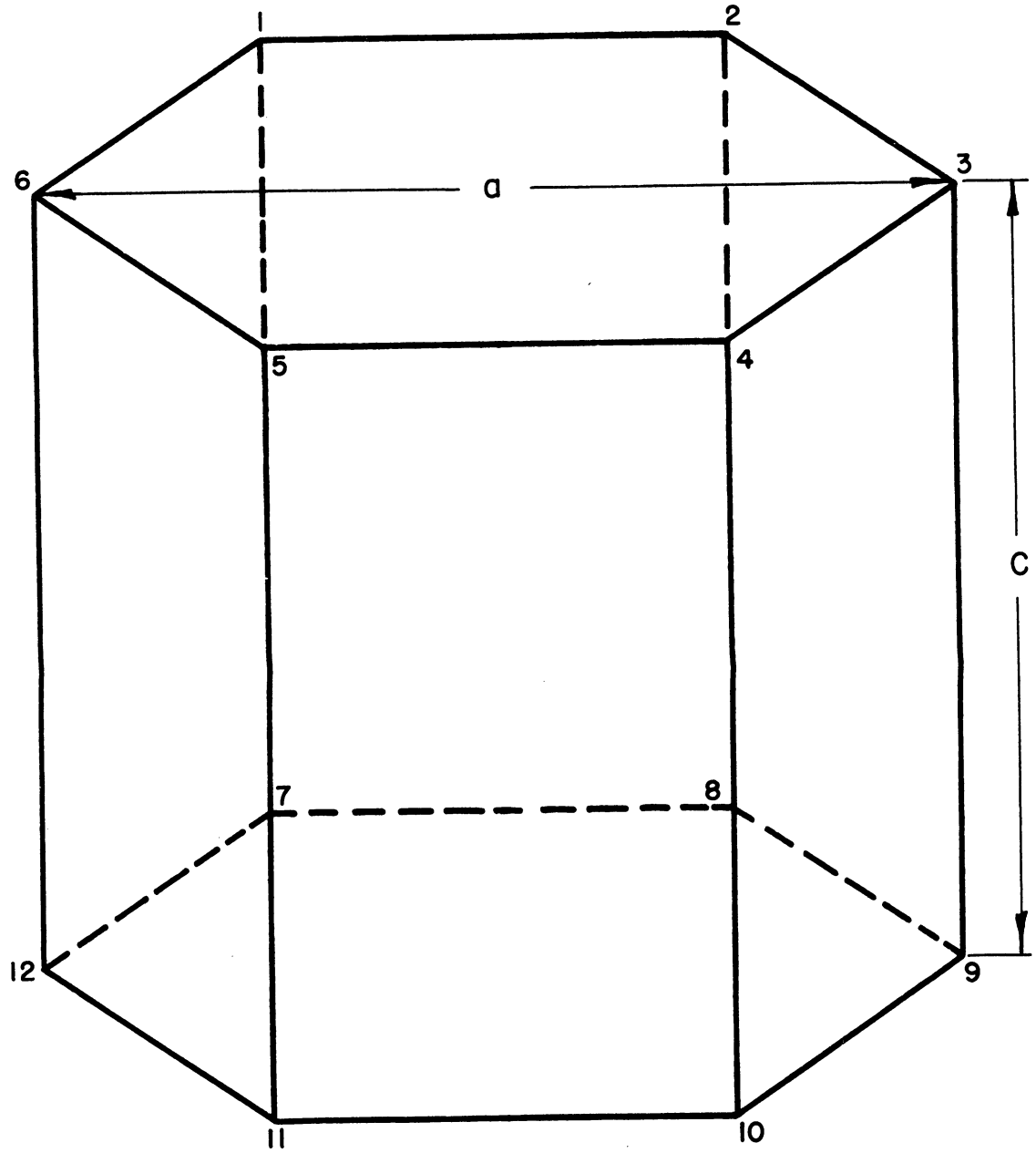

Figure 50. Hexagonal Prism.

$$= \frac{3}{\pi} \int_0^{\pi/6} \left(\frac{a}{2} \sin\theta \cdot \frac{\pi}{2} + \frac{a\sqrt{3}}{2} \cos\theta \cdot \frac{\pi}{2} + c\right) d\theta$$

$$= \frac{3}{\pi} \left[\frac{a\pi}{4} (-\cos\theta) + \frac{a\pi\sqrt{3}}{4} (\sin\theta) + c\theta\right]_0^{\pi/6}$$

$$= \frac{3}{\pi} \left[\frac{a\pi}{4} \left(-\frac{\sqrt{3}}{2} + 1\right) + \frac{a\pi\sqrt{3}}{4} \left(\frac{1}{2}\right) + \frac{c\pi}{6}\right]$$

$$= \frac{3}{\pi} \left[a\left(-\frac{\sqrt{3}\pi}{8} + \frac{\pi}{4} + \frac{\sqrt{3}\pi}{8}\right) + \frac{\pi}{6} c\right]$$

$$P_i(\text{hexagonal prism}) = \frac{3}{4} a + \frac{1}{2} c \qquad (114)$$

With this result we conclude the theoretical derivations for probabilities of intersection of randomly oriented polyhedrons by sectioning planes.

XII. EXPERIMENTAL PROCEDURE

One of the original objectives of this research was to be an attempt to verify experimentally some of the theoretical relations derived connecting particle shape, size, and number in three dimensional opaque bodies with number observed in plane sections and with relative frequencies of the possible plane sections observed. In order to do this it was planned to prepare synthetic samples containing known numbers of particles having known shape and size, to distribute these particles within the body in such a way that their orientations may be considered to vary at random, and then to section the bodies and record the numbers and section shapes observed. The experimental results were then to be compared with the theoretically predicted quantities, and, where possible, a statistical comparison would be made.

The synthetic particles that were prepared consisted of cubes and cylinders having four different ℓ/d ratios. These two general shapes, cubes and cylinders, proved fairly easy to prepare in small particles. Some other shapes, such as rectangular parallelepipeds, would have been equally easy to prepare, but it was felt that little additional information of interest would be gained. More complicated polyhedrons, such as tetrahedrons, octahedrons, rhombic dodecahedrons, and tetrakaidecahedrons, appeared to present greater problems for their preparation in large numbers of small particles, so these were not attempted.

The preparation of the particles, their dispersion in solids, the measurement and results, and the statistical analysis will now be described.

Particle Preparation

Cylinders. Four shapes of cylinders were prepared, varying from flat cylinders, approximating platelets, to long needles. Their dimensions, in inches, are listed in Table XIX.

TABLE XIX

CYLINDRICAL PARTICLES

Shape	Diameter (in.)	Length (in.)	ℓ/d
1. flat cylinder	0.104	0.051	0.49
2. equiaxed cylinder	0.051	0.051	1.0
3. long cylinder	0.060	0.120	2.0
4. round needle	0.020	0.400	20

The flat cylinders and the equiaxed cylinders were prepared by punching them from sheet material. The sheet consisted of aluminum, 0.051 inches thick, which was actually a laminated 1100-H-18 sheet consisting of 13 separate plies glued together. The laminated sheet was available from previous research, and it was felt that cylinders from this material might be analyzed and interpreted in such a way as to obtain information on very thin platelets (one ply) or lamella. While such exhaustive analysis was not conducted, the plies did prove very helpful in interpreting the cylinder section shapes obtained. This was because it proved nearly impossible to obtain punchings without any distortion along the sides and ends, which would have proved confusing in interpreting the observed section shapes without the laminates as a guide. Thus,

if in counting the piles under the microscope you see 13 plies, you may be confident that both ends of the cylinder have been intersected.

The procedure for preparing these punchings consisted of drilling a small hole in a thin steel sheet to use as a die, and then with minimum clearance to use a small steel drill mounted in a drill press, upside down, with flat end as a punch. The aluminum sheet to be punched was inserted between drill and die and then punched out by cranking down on the arm of the drill press. In this way as many punchings could be made as desired. Some of these punched cylinders are shown in Figures 51 and 52.

The long cylinders and the round needles were prepared from wire. The long cylinders were made from 0.060 inch 1100-SO aluminum wire, and the round needles were made from 0.020 inch copper wire. In both cases, many pieces of wire about one half inch or more in length were cut by hand with diagonal wire cutters. The length was a convenient integral multiple of the desired size, allowing for cutting and polishing. These pieces of wire were stacked parallel to each other inside a brass ring one inch in diameter and cut the same length as the wires. When the wires were packed tightly by hand, the space between the wires was filled by a cold-setting liquid plastic and allowed to harden. Two types of cold setting plastic were used, with about equivalent results. One was a liquid epoxy, Shell Epon 828, plus diethylenetriamine hardener, and the other was a dry, powdered self-curing resin known as Koldmount, made by the Vernon-Benshoff Co., to which is also added a liquid hardener. After the plastic had hardened, the wires and brass rings, which were over-length, were cut

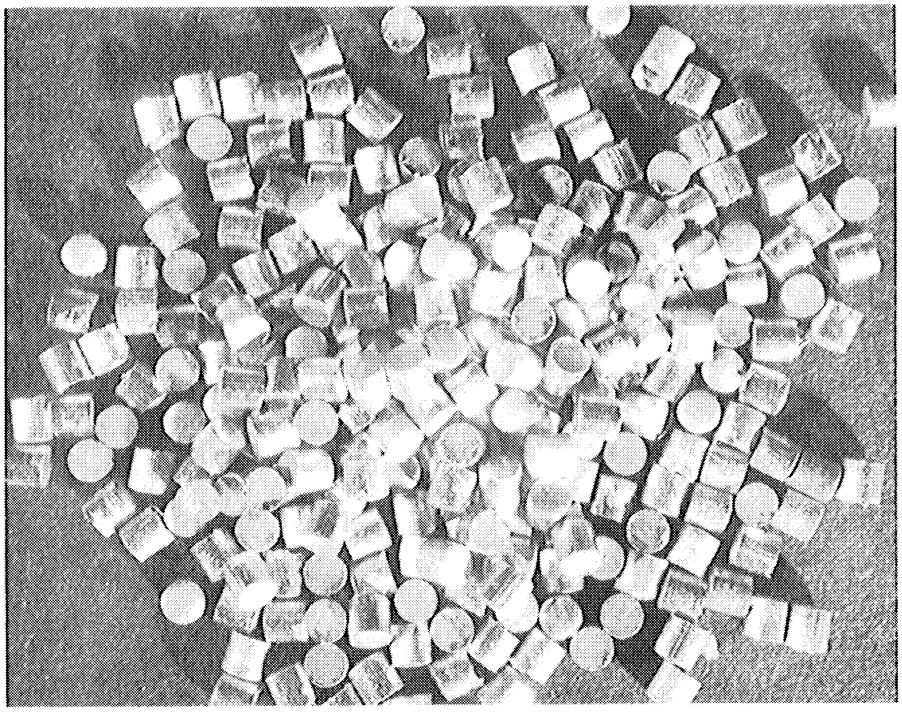

Figure 51. Equiaxed Cylinders. Laminated Aluminum. (mag. approx. 4x)

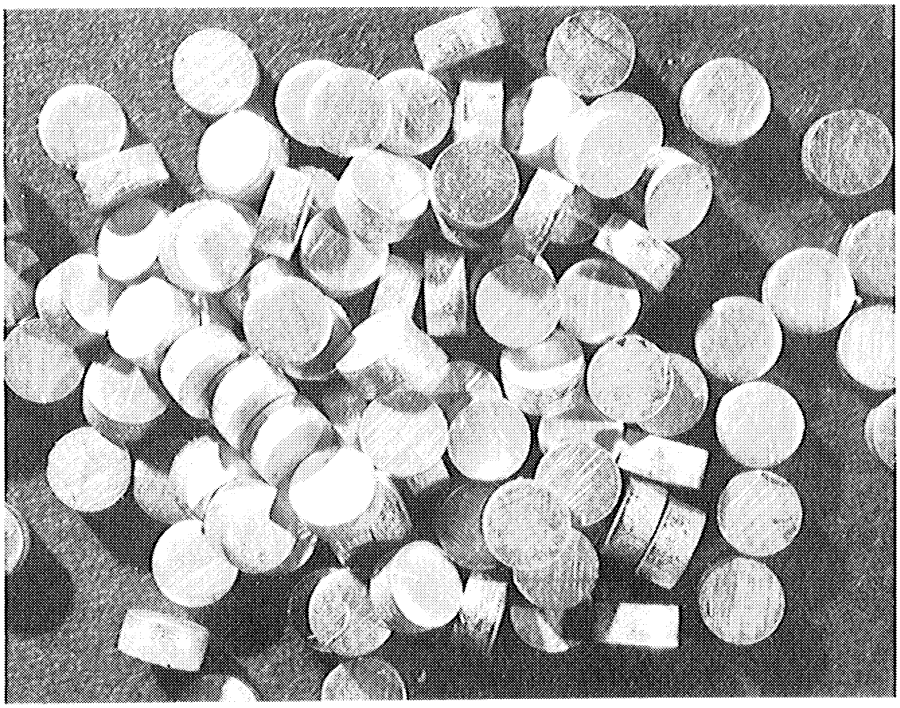

Figure 52. Flat Cylinders. (mag. approx. 4x) Laminated Aluminum.

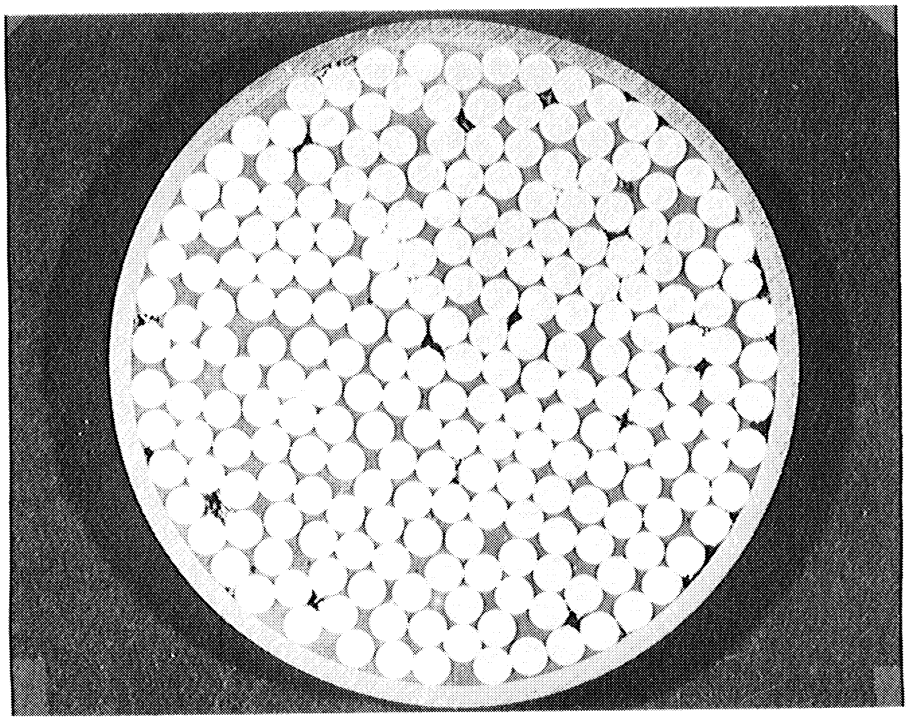

Figure 53. Preparation of Long Aluminum Cylinders. (mag. approx. 3x)

Figure 54. Long Cylinders. Aluminum Wire. (mag. approx. 4x)

to approximate size. In the case of the 0.120 inch long aluminum cylinders, this resulted in four separate sections.

These sections were then ground and polished flat with parallel ends until measurement by micrometer was that desired for cylinder length. Then the wires or cylinders were removed from the brass rings by dissolving the plastic in suitable solvent and separating out the cylinders. As solvent, either butyl cellusolve or ethylene dichloride proved effective, especially if heated slightly.

A photograph of the aluminum cylinders in the brass ring is shown in Figure 53, and some of the aluminum and copper cylinders are shown in Figures 54 and 55.

Cubes. For the production of cubes, one eighth inch square rods of brass and cold-rolled steel were obtained. It was considered that having sharp edges or corners on the rods would be quite important, and the brass was much better as received from this standpoint. The brass rod was sawed into about half inch pieces, mounted parallel lengthwise inside a brass ring, plasticized, cut, ground, polished, and deplasticized in exactly the same fashion as just described for long cylinders. In this way 0.125 inch brass cubes of very good quality were prepared, upon which nearly all the data for cubes were obtained.

The steel rod was converted to cubes by the Air Force Institute of Technology shop, by cutting off the approximate lengths and polishing two opposite faces at a time between magnetic chucks. Many steel cubes were made in this way; however, these were not utilized to as full an extent as the brass cubes for the following reasons. Due to heavy workload in the shops, the hand made brass cubes were ready first. The brass

Figure 55. Needles. Copper Wire.
(mag. approx. $\frac{1}{4}$x)

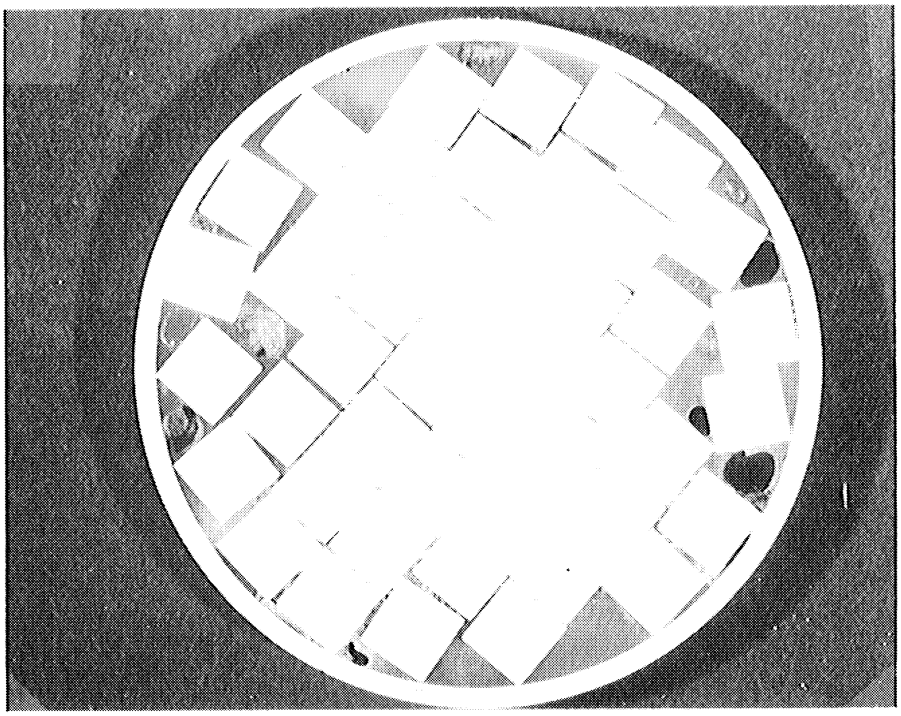

Figure 56. Preparation of Brass Cubes.
(mag. approx. 3x)

cubes when mounted proved easier to section and polish because of less hardness difference between cubes and the rest of the mount. The brass cubes still had sharper edges and corners. This could have been readily corrected for the steel cubes, however, by simply grinding more material from all sides in the magnetic chucks.

A photograph of the brass cubes in the mounting ring is shown in Figure 56, and photos of the brass cubes and steel cubes are in Figures 57 and 58.

Particle Dispersion in Solids

The equiaxed aluminum cylinders were the first ones to be dispersed in a solid. Initial experiments indicated that a metallurgical mounting press would not be suitable for preparing mounts of randomly oriented dispersed particles. Lucite mounts prepared in a press always showed that any particles having a definite shape would tend to line up along the constant pressure surfaces in the mount. Therefore, a cold-setting plastic requiring no pressure was selected. For the initial mounts Shell Epon 828, previously mentioned, was used. This material was most conveniently mixed and allowed to harden in a polyethylene mold, to which it did not adhere, thus allowing easy removal of mount from mold. About 8% by weight liquid catalyst was used, and hardening time was about two hours. The aluminum particles were counted and stirred into the liquid plastic.

Due to density differences, the aluminum particles tended to settle out before the plastic hardened, so a high density powder, lead chloride, $PbCl_2$, was added to thicken and densify the pasty mass. It

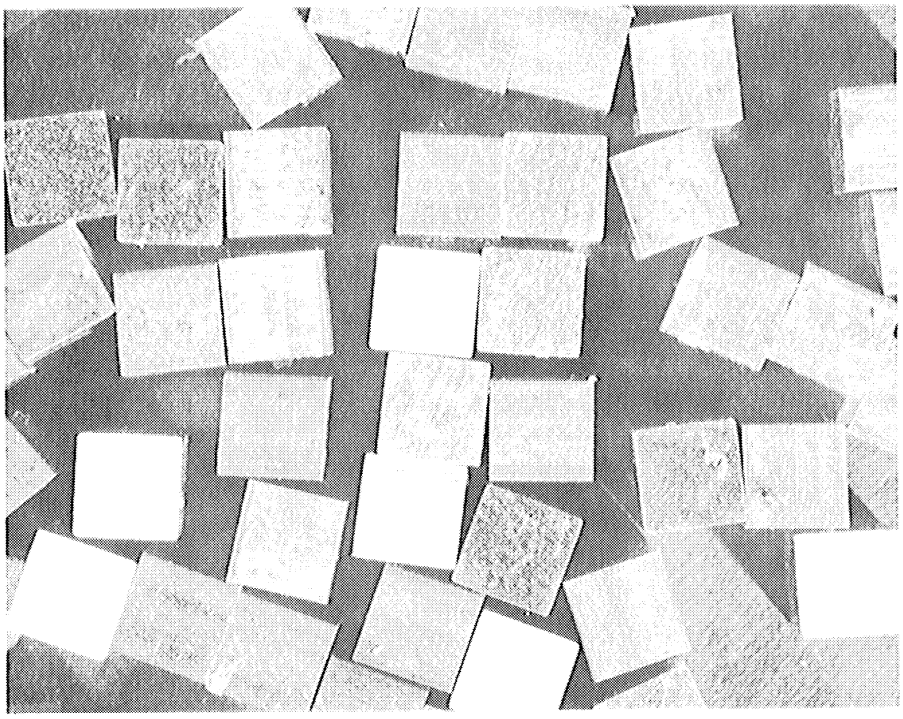

Figure 57. Brass Cubes.
(mag. approx. ½x)

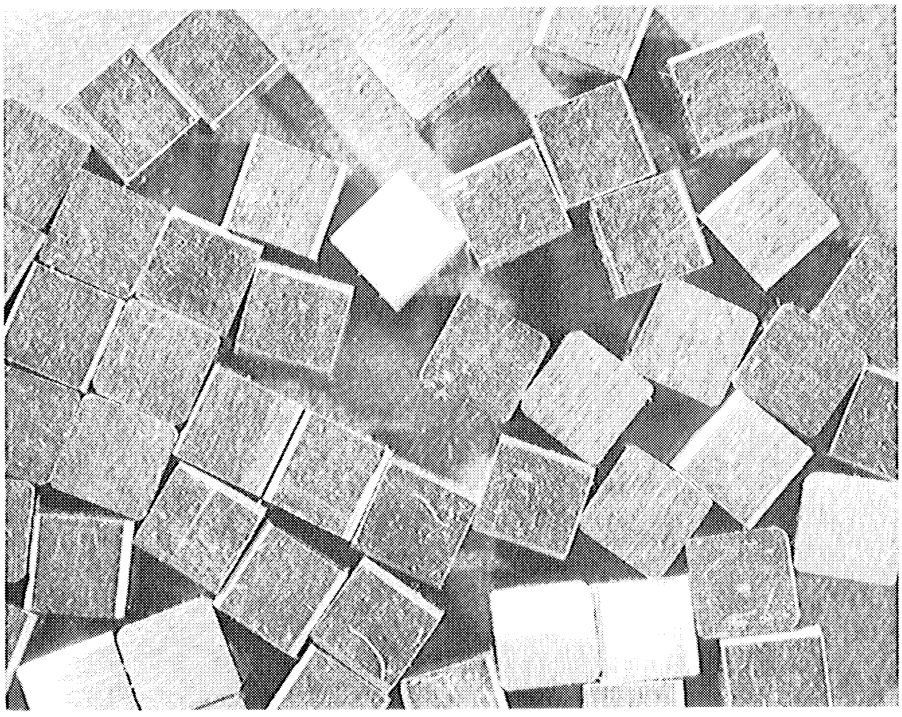

Figure 58. Steel Cubes.
(mag. approx. ½x)

proved satisfactory for this purpose, and several specimens of equiaxed aluminum cylinders were made this way. A photo of such a mount is shown in Figure 59.

The stirring which was necessary apparently did not introduce a detectable degree of preferred orientations or non-randomness. However, for longer or flatter particles, this stirring did tend to destroy randomness of orientation. Furthermore, particles of materials heavier than aluminum, such as brass, copper, or steel, tended to settle out even with the lead chloride densifier. For these reasons, all particles other than the equiaxed cylinders were mounted by a technique developed for cubes, which will now be described.

Since cubes have flat faces, cubes touching each other will tend to align each other and will also tend to align themselves parallel to the walls or bottom of a container. It was thought that if the cubes could be separated by other particles they would not align themselves and if these other particles were spheres they should show no tendency to align the cubes. Lead shot about the same size range as the cubes was tried and proved highly successful.

The cubes were counted out and about four times as many, or more, lead balls were added and mixed with the cubes. This could be dumped into a container and filled with plastic or it could be pre-mixed with plastic and poured into a container. The Vernon-Benshoff Koldmount previously mentioned was used most often, although Shell Epon 828 was equally satisfactory. The Koldmount tended to solidify so rapidly that it proved helpful to cool the ingredients in a refrigerator before mixing to slow down the subsequent hardening process.

No preferred orientations of the cubes separated by lead balls occurred, and data taken agreed well with predictions based upon random orientations. Only cubes in contact with the sides or bottom of the container lined up to conform with the container, and these cubes were not included in the data. As indicated, cylinder shapes other than equiaxed were also mounted using the lead balls as space fillers. Photos of cubes and cylinders mounted in this way are shown in Figures 59 to 63.

In the special case of the long copper needles of ℓ/d ratio equal to twenty, it was felt that preferred orientations would be almost impossible to avoid due to their great length and that contact between neighbors anywhere along the length would tend to line them up. It may be noted, however, that for randomly oriented cylinders having $\ell/d = 20$, the relative frequency for obtaining sections cutting both ends (barrels) is almost zero (actually 0.02%). Therefore, it was felt that only reasonable data for relative frequency of cups versus ellipses would be obtained, and since these did not depend on the needle being straight, that we could bend or twist the needles to reduce their tendency to orient each other. According to Smith and Guttman[5] the average number of intersections of a line by parallel sectioning planes, as in the Buffon needle problem, depends only on the length of the line, not whether it is straight or curved. In spite of going to these extra pains to improve randomness, the twisted needles still proved more difficult than any of the other shapes to obtain reasonably random data. A mount of twisted copper needles is shown in Figure 64.

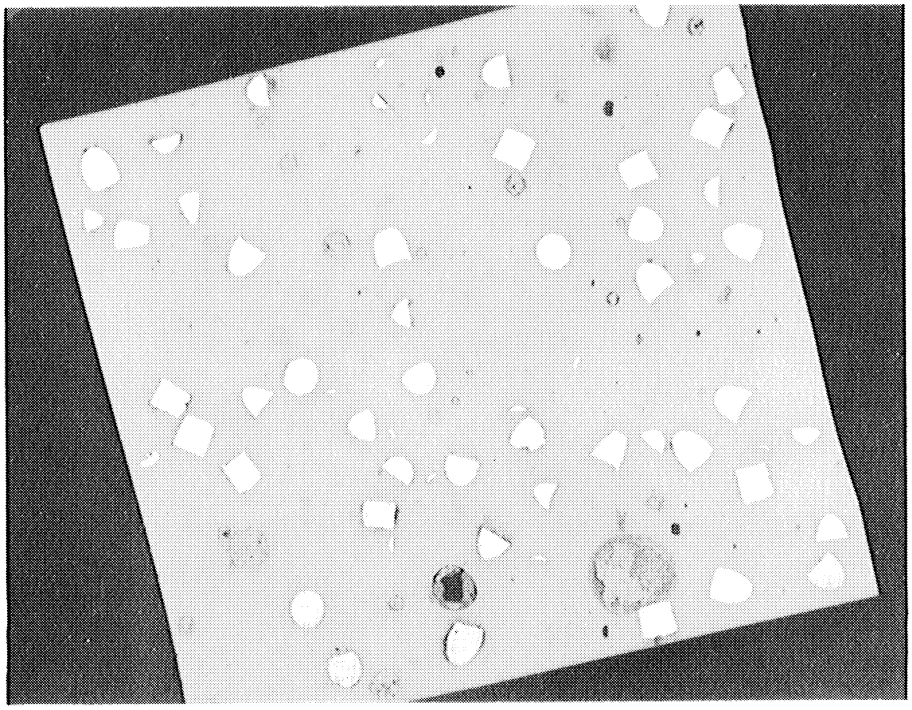

Figure 59. Dispersion of Equiaxed Cylinders.
(mag. approx. 3x)

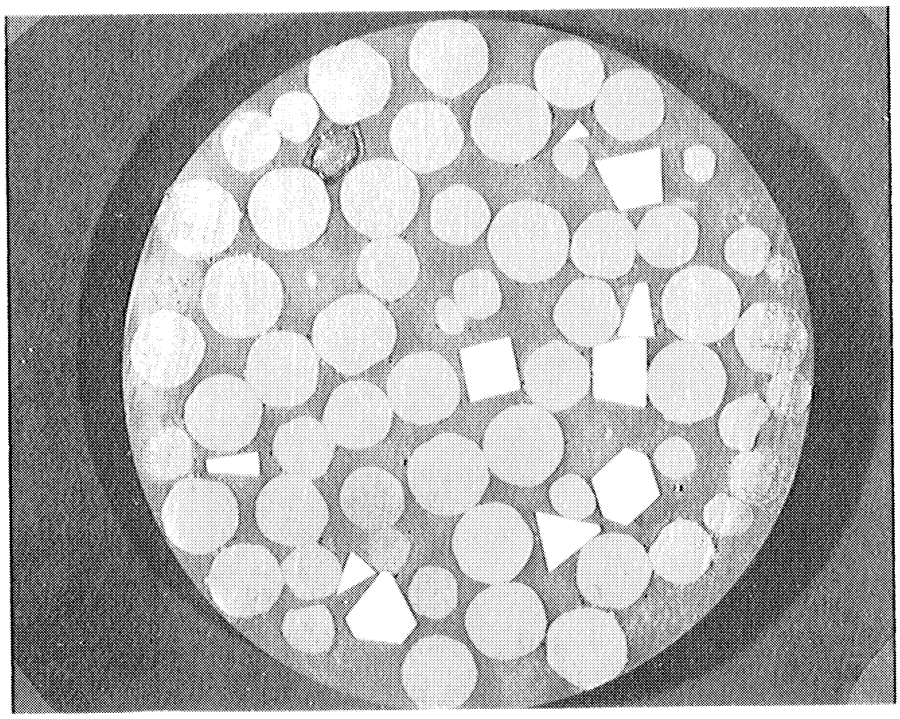

a.

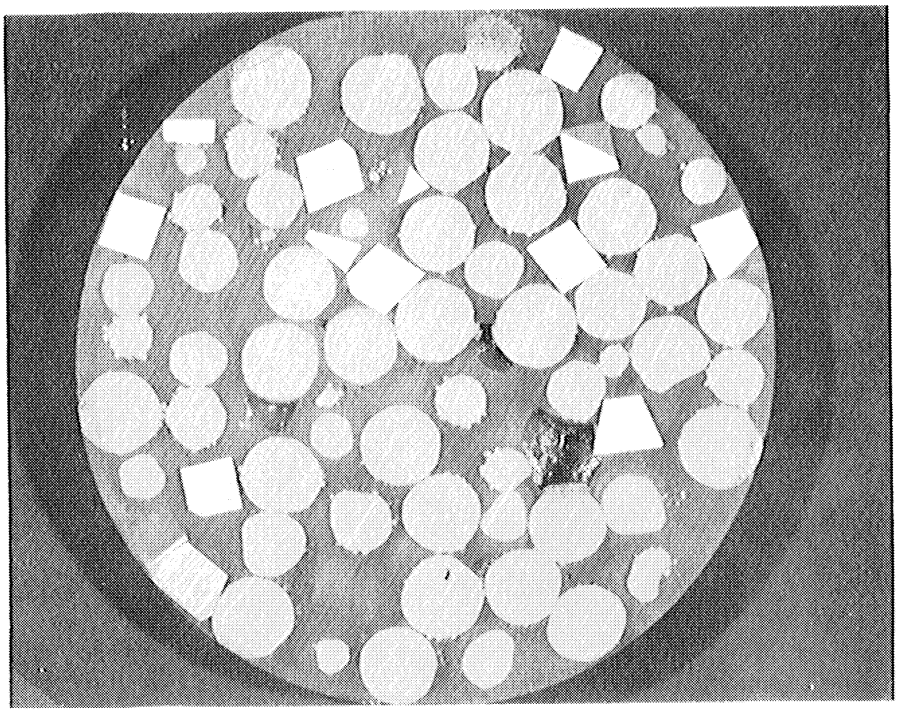

b.

Figure 60. Dispersion of Brass Cubes and Lead Balls. (mag. approx. 2x)

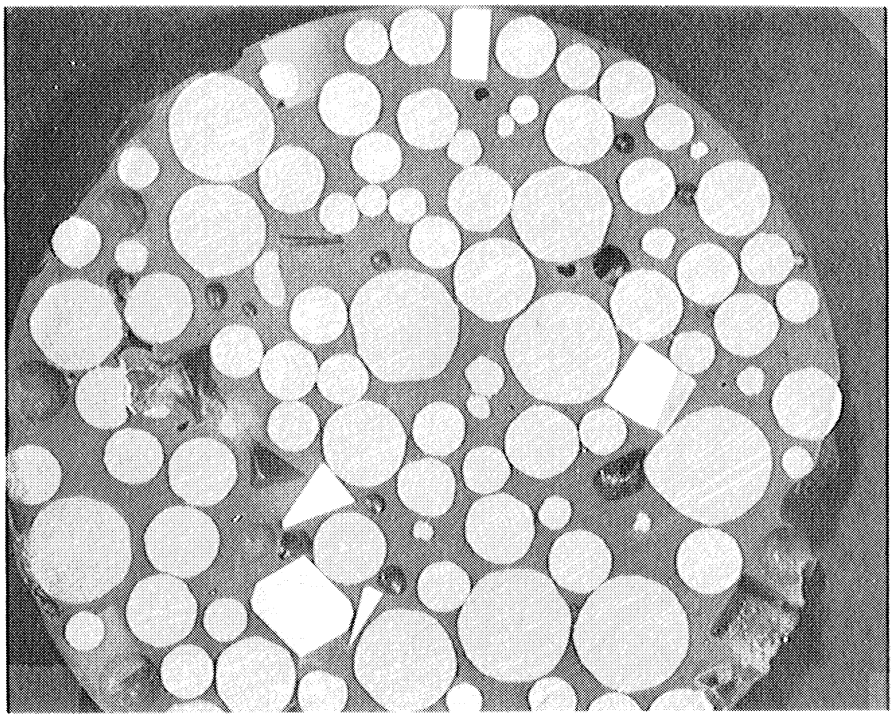

Figure 61. Dispersion of Steel Cubes and Lead Balls. (mag. approx. 2.7x)

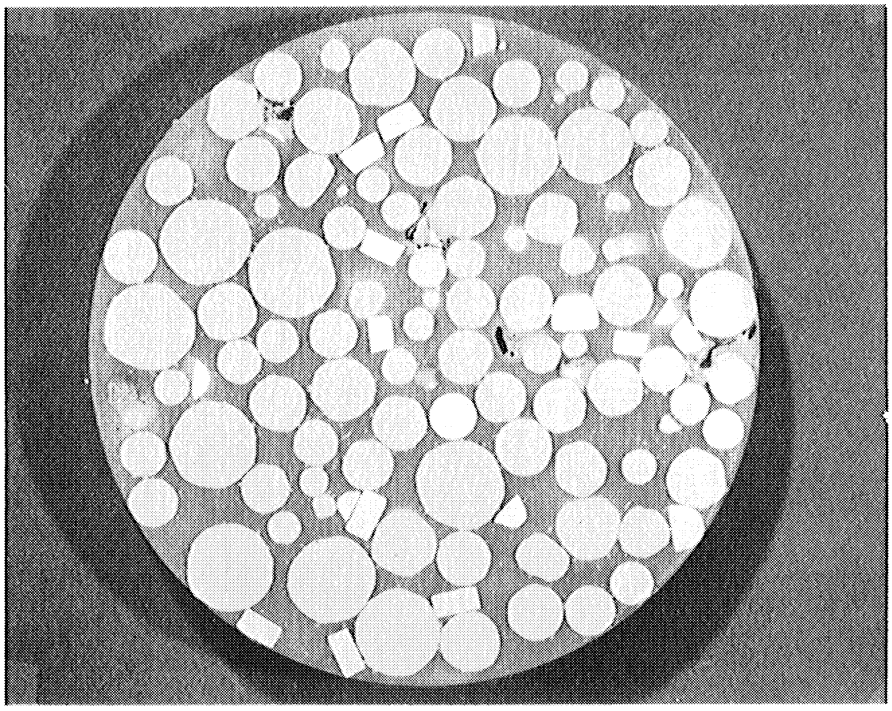

Figure 62. Dispersion of Flat Cylinders and Lead Balls. (mag. approx. 2.1x)

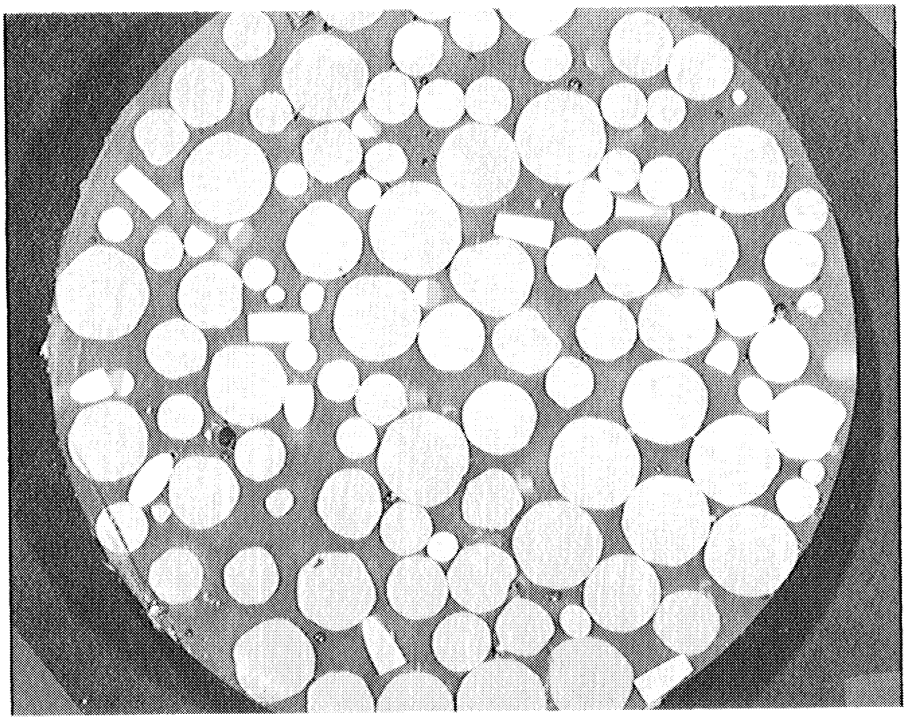

Figure 63. Dispersion of Long Cylinders and Lead Balls. (mag. approx. 2.3x)

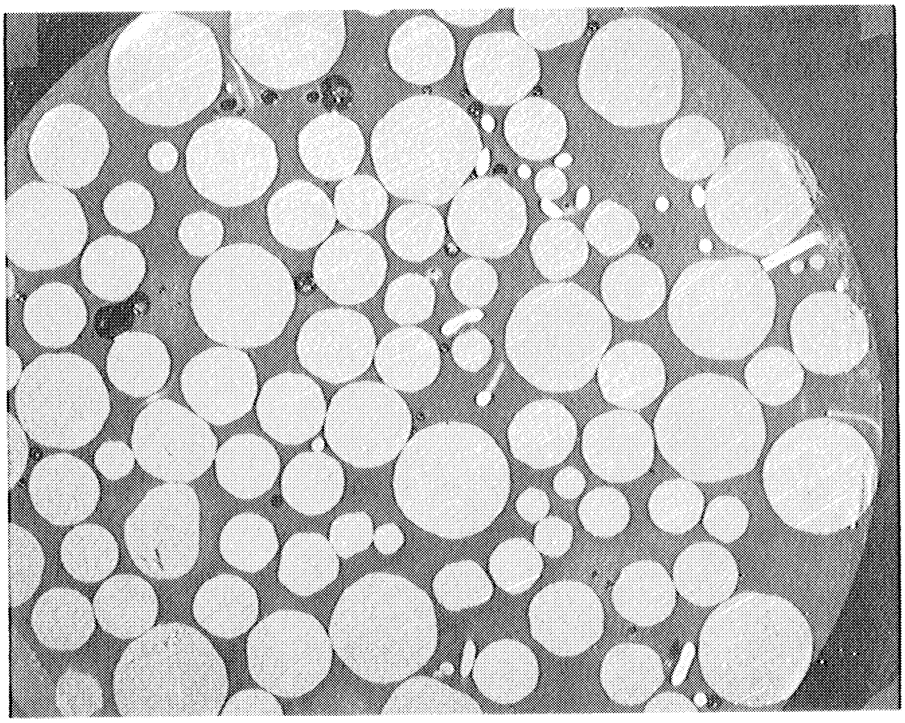

Figure 64. Dispersion of Twisted Needles and Lead Balls. (mag. approx. 3x)

Sectioning and Counting

Initially, sections on mounts of equiaxed cylinders were taken at 0.050 inch intervals by successively grinding and polishing away the mount. This procedure was changed, however, to merely cutting sections at about one quarter inch intervals on a band saw and polishing and examining the faces. The latter procedure had two advantages: one being that it was much less laborious, the other being that it was more suitable for statistical treatment. By sectioning at wider intervals so that a single particle is observed in only one section, randomness of sampling is more closely approximated. Where sections are taken closer together, the same particle is sampled more systematically (and laboriously) and less randomly. This tends usually to give data which are "too good" and not really amenable to statistical analysis. This condition was actually observed in some of the initial cube data.

Polishing was usually carried through by hand polishing to about a 400 grit silicon carbide paper using kerosene as a lubricant. Counting was done under a low power stereoptical microscope, usually at 10 diameter magnification and sometimes up to 45 diameters. Many times during polishing it was unavoidable that small corners of cubes or tiny edges of cylinders would "pull-out", leaving the remainder of their impressions visible under the microscope. It is essential to count these, however, as though they were actually present, and this usually presented no difficulty. As mentioned, cubes or particles in contact with the container wall showed a high degree of preferred orientation and were not counted.

Some observations on the sectioning, counting, and shapes observed are appropriate at this time.

Figure 65 shows sections of the equiaxed cylinders. The three types of cylinder sections, barrels, cups, and ellipses, are readily apparent. The laminations of the material from which the particles were punched are easily seen. The curves in the layers are due to the distortion in punching. These features may also be noted in Figures 59 and 62.

Figure 66 shows sections of brass cubes of all possible types, 3, 4, 5 and 6 sided. In Figure 66f, a 3 sided hole is observed, resulting from a cube corner being dislodged during the cutting or polishing. This, of course, is counted, just as though it were there. Figure 61 of steel cubes shows several such holes due to dislodged particles. Figure 66h shows two cubes on the edge of the mount. Such cubes on the edge showed a strong preference for 4 sided sections, so were eliminated from the statistical analysis.

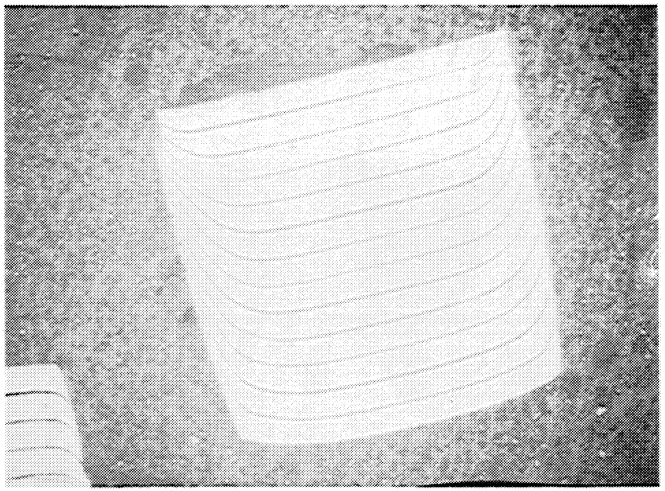

a.

b.

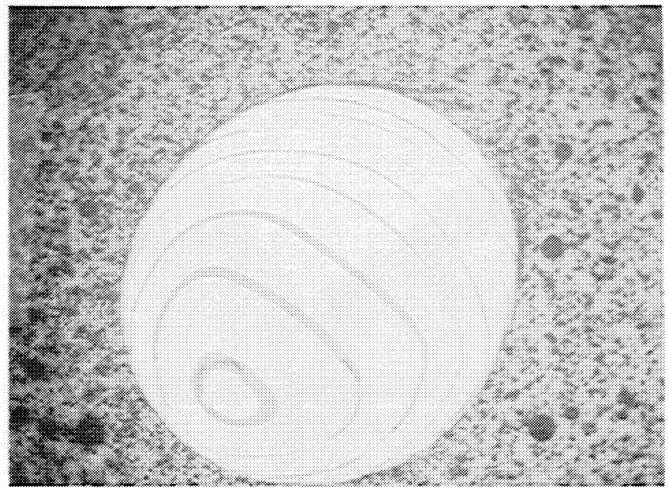

c.

Figure 65. Sections of Equiaxed Cylinders.
(mag. 39.4x)

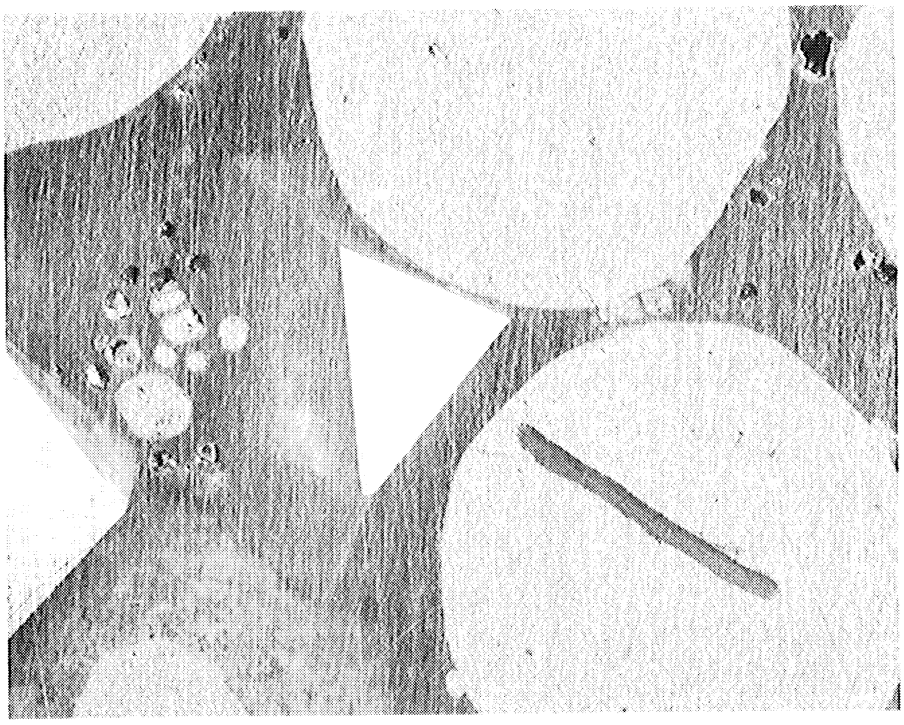

a. 3 Sided.

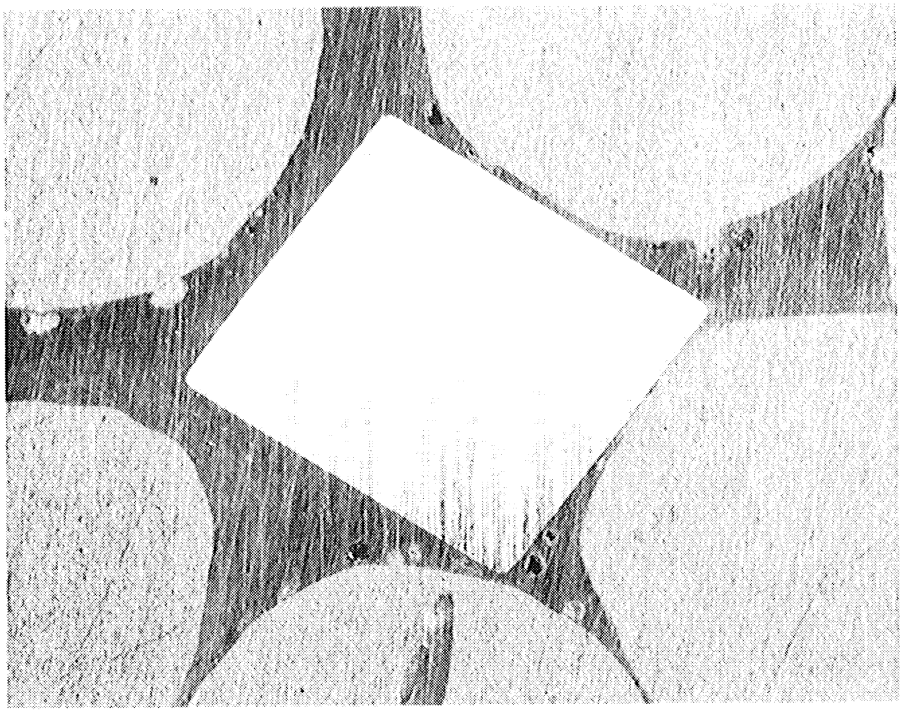

b. 4 Sided.

Figure 66. Sections of Brass Cubes.
(mag. approx. 13x)

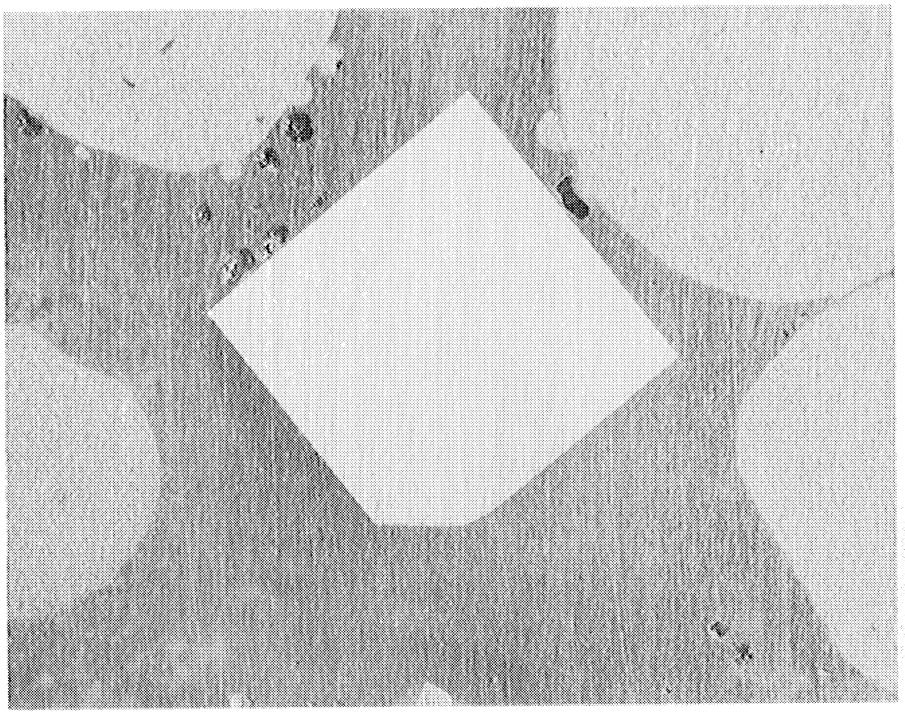

c. 5 Sided.

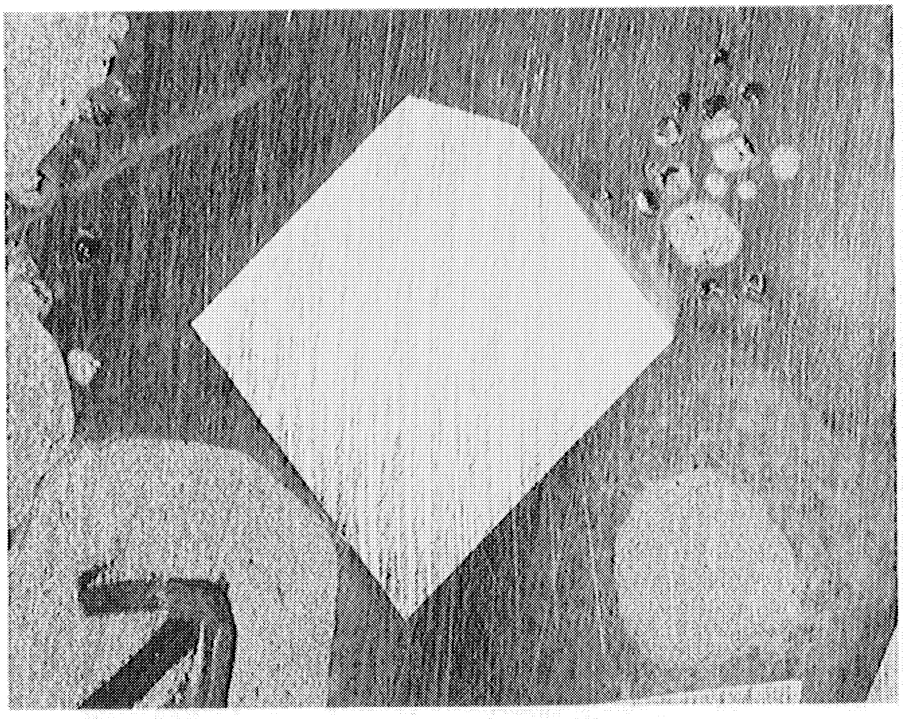

d. 5 Sided.

Figure 66. (Continued)

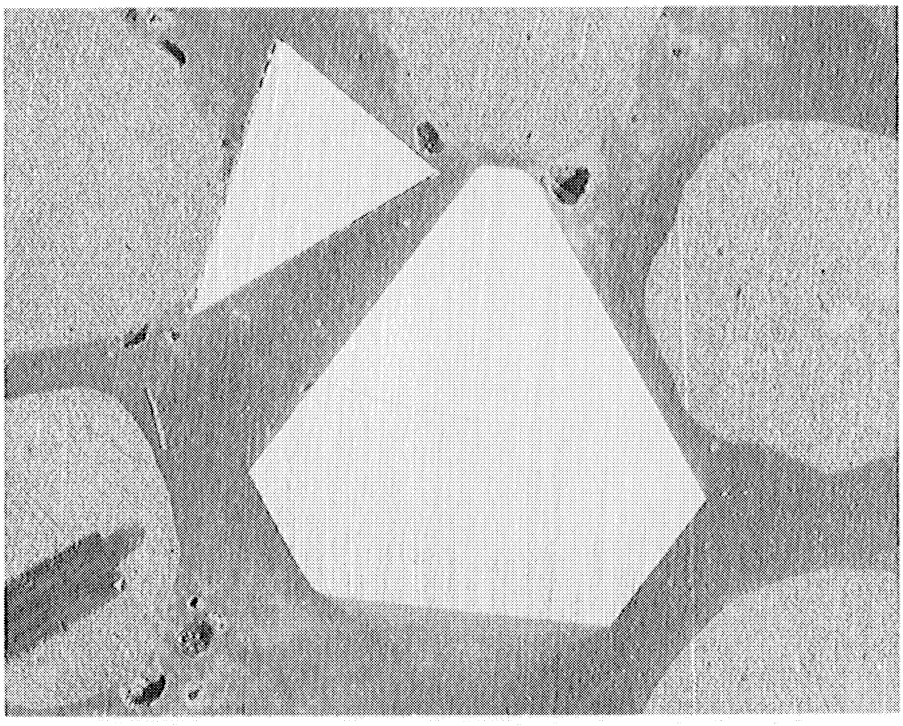

e. 3 and 6 Sided.

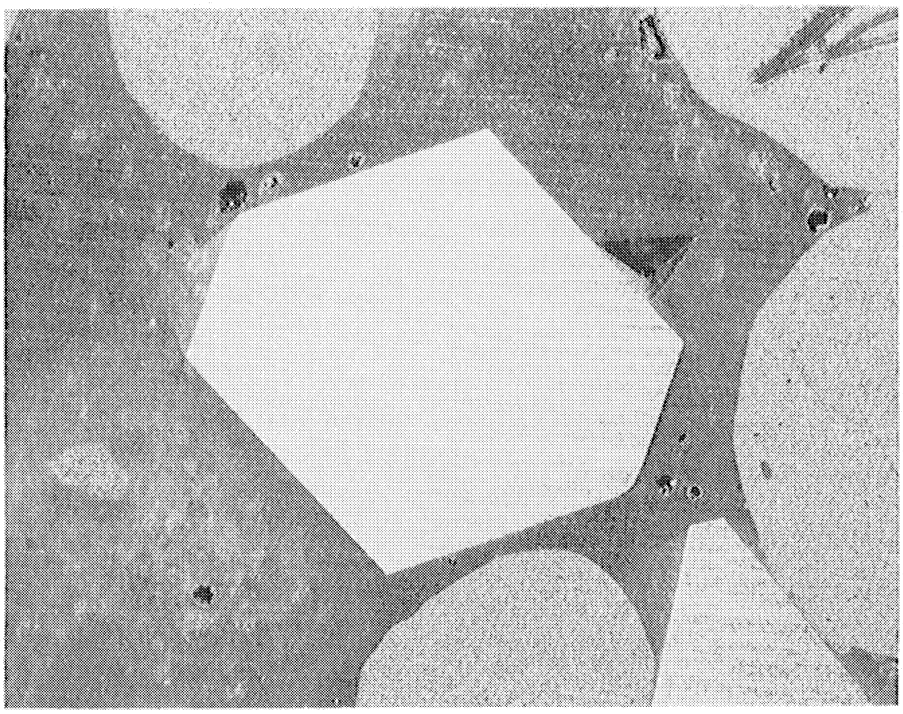

f. 6 Sided and 3 Sided Hole.

Figure 66. (Continued)

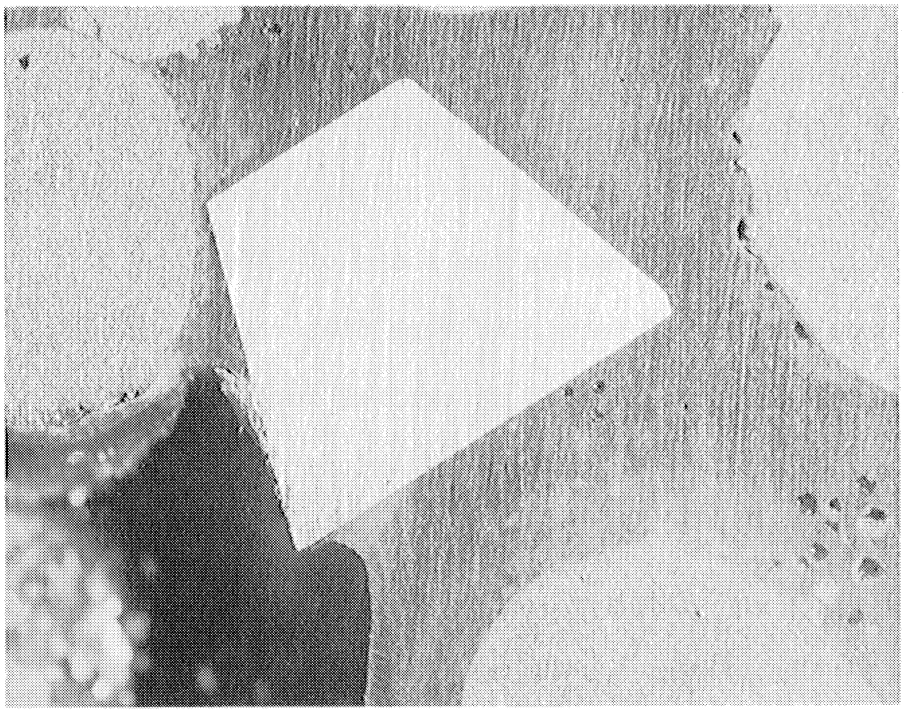

g. 5 Sided.

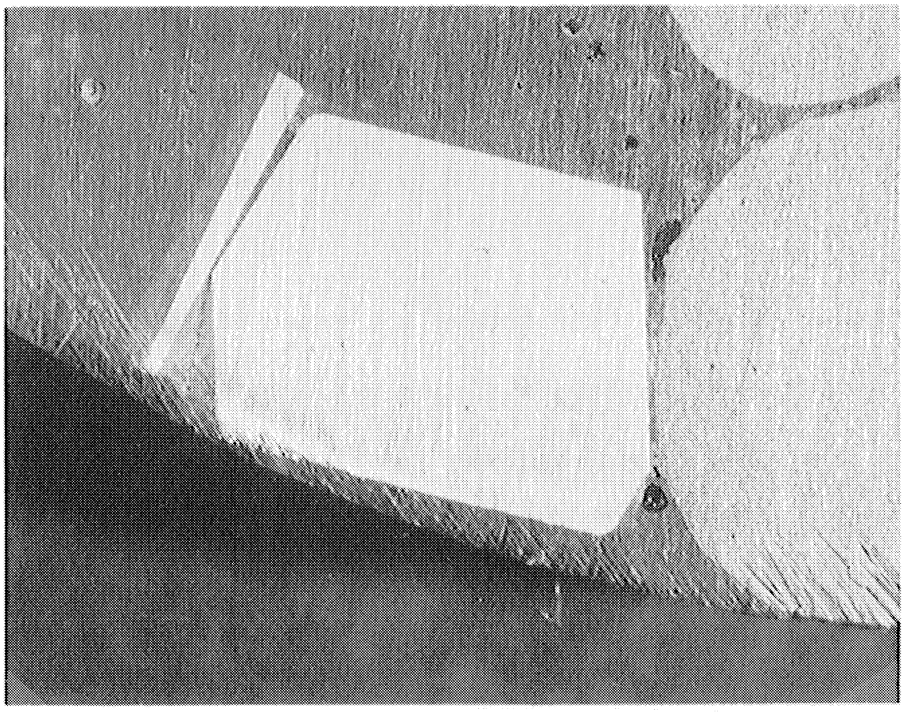

h. 4 and 6 Sided.

Figure 66. (Continued)

XIII. EXPERIMENTAL DATA AND STATISTICAL ANALYSIS

As just described, the synthetic samples prepared to test some of the theoretical relations derived in this work consisted of dispersions of uniformly sized particles having the shape of cubes and four cylindrical shapes. Known numbers of particles were dispersed in as near a random manner as possible in solids of readily determined volume so that number of particles per unit volume is known. From the relations developed connecting size, shape, and probability of intersection by a random plane, the theoretically expected number per unit area of plane section may be calculated. This is done and compared with the average number actually observed on plane sections. The relations to be checked in this case are:

for cylinders

$$N_S = N_V \cdot \left(\frac{\pi d}{4} + \frac{\ell}{2}\right) \tag{9}$$

for cubes

$$N_S = N_V \cdot \frac{3}{2} a \tag{52}$$

For convenience, the actual and expected numbers observed per section were compared instead of number per unit area. This made calculation of the area unnecessary and was justified by the following analysis.

$$N_S = N_V \cdot P_i \tag{13}$$

number per unit area = number per unit volume $\cdot P_i$

$$\frac{\text{number in section}}{\text{area of section}} = \frac{\text{number in volume}}{\text{height x area of section}} \cdot P_i$$

Therefore, we have

$$\text{number in section} = \frac{\text{number in volume}}{\text{height}} \cdot P_i \qquad (115)$$

The height, of course, must be in the same units as P_i, which in this case was in inches.

The experimental results for all four cylindrical shapes agree closely with those predicted by Equation (9), which was first reported by Fullman[48], and the results for the cubes agree well with Equation (52), first derived in this work. The comparisons for numbers experimentally observed per section versus numbers expected from theory will be shown in the following discussion, without an attempt at rigorous statistical analysis.

The major effort in the experimental investigation was that of comparing the observed relative frequencies of section shapes with the expected frequencies developed in this work. For cylinders the expected frequencies of sections having the shapes of ellipses, cups, and barrels were given in Table III. For cubes the expected frequencies of 3, 4, 5 and 6 sided sections were given in Tables V and VI.

The experimentally determined frequencies of the sections of cylinders and cubes are compared with these theoretical predictions, and the frequency distributions are tested for goodness of fit by the widely used Chi-square (χ^2) test, for judging whether or not fit is satisfactory. The Chi-square test is described in most standard texts on statistics, and for this work the application of the test corresponds to that described by Kenney and Keeping[55]. The experimental results will now be presented.

Flat Cylinders

The basic parameters of the flat cylinders prepared are

$$\frac{\ell}{d} = \frac{0.051"}{0.104"} = 0.49$$

$$P_i(\text{cylinder}) = \left(\frac{\pi d}{4} + \frac{\ell}{2}\right) = \left(\frac{0.104\pi}{4} + \frac{0.051}{2}\right) = 0.1071$$

Number per Section. 295 of these cylinders were dispersed in a cylindrical volume having a height of two inches and an approximate diameter of 1 5/8 inches. Their expected number per section were

$$\text{expected number per section} = \frac{\text{number per volume}}{\text{height}} \cdot P_i$$

$$= \frac{295}{2.0}(0.1071) = 15.8$$

Experimentally, 16 plane sections were taken, in which a total of 255 particles were observed.

$$\text{average number observed per section} = \frac{255}{16} = 15.9$$

The close agreement between expected and observed results is apparent. However, it is felt that statistical treatment is not warranted as there is an element of possible judgment or bias on the part of the investigator in measuring the height of the sample in which the particles are dispersed. Since the particles were not uniformly distributed near the top of the sample, an "effective height" had to be estimated. An error as much as 1/8th inch in such estimate is quite possible and would significantly affect the results.

Relative Frequency of Shapes. The shape probabilities for the flat cylinders are

$$P_i(\text{cup}) = d \arctan \frac{\ell}{d} = 0.104 \arctan (0.49) = 0.0484$$

$$P_i(\text{ellipse}) = \frac{\ell}{2} - \frac{d}{2} \arctan \frac{\ell}{d} = \frac{0.051}{2} - \frac{0.0484}{2} = 0.0013$$

$$P_i(\text{barrel}) = \frac{\pi d}{4} - \frac{d}{2} \arctan \frac{\ell}{d} = \frac{0.104\pi}{4} - 0.0242 = 0.0574$$

The expected relative frequencies of these shapes are

$$f_e(\text{cup}) = \frac{0.0484}{0.1071} \times 100 = 45.1\%$$

$$f_e(\text{ellipse}) = \frac{0.0013}{0.1071} \times 100 = 1.2\%$$

$$f_e(\text{barrel}) = \frac{0.0574}{0.1071} \times 100 = 53.6\%$$

After deleting data for cylinders in contact with walls of container, observed types of sections were:

	Number observed	frequency
cups	96	41.2%
ellipses	5	2.1%
barrels	132	57.6%
total	233	

	Number expected
cups	233 x .451 = 105
ellipses	233 x .012 = 2.8
barrels	233 x .536 = 125

Using the Chi-square test for goodness-of-fit, we obtain

Chi-square Test

	obs.	exp.	$\lvert o-e \rvert$	$\frac{(o-e)^2}{e}$
C	96	105	9	.77
E	5	2.8	2.2	1.73
B	132	125	7	.37
	233			2.87

$\chi^2 = 2.87$

For two degrees of freedom, the probability of a deviation greater than $\chi^2 = 2.87$ due to random errors is 0.24. Therefore, 24% of the time the expected deviation would be greater than observed. Since the critical value for significance is usually taken at the 5% level, the hypothesis that the data fit the theory cannot be rejected. This will then be taken as an indication that the data probably do fit the theory. More data would be required to confirm this more positively.

A shortcoming in this application of the Chi-square test may be pointed out. It is usually advisable that no expected frequency be under 5 (in this case, one is 2.8). Any groups expected to be less than 5 are usually combined into larger groups, decreasing the number of groups compared. In this case, since it would have reduced the number to two groups, the calculation was not performed.

Equiaxed Cylinders

The basic parameters of the equiaxed cylinders prepared are

$$\frac{\ell}{d} = \frac{0.051"}{0.051"} = 1.0$$

$$P_i(\text{cylinder}) = (0.051 \times \frac{\pi}{4} + \frac{0.051}{2}) = 0.0655$$

Number per Section. 1600 of these cylinders were dispersed into two cubical volumes, each approximately 1.06 inches high and one inch square. Their expected number per section were

$$\text{expected number per section} = \frac{1600}{2.12} \times 0.0655 = 49.5$$

In 9 sections, a total of 456 particles were observed.

$$\text{average number per section} = \frac{456}{9} = 50.7$$

The very reasonable agreement between theory and experiment is indicated.

Relative Frequencies of Shapes. The shape probabilities for the equiaxed cylinders are

$$P_i(\text{cup}) = 0.051 \arctan 1 = 0.040$$

$$P_i(\text{ellipse}) = \frac{.051}{2} - \frac{.051}{2} \arctan 1 = .0055$$

$$P_i(\text{barrel}) = 0.051 \times \frac{\pi}{4} - \frac{.051}{2} \arctan 1 = 0.020$$

The expected frequencies of sections are

$$f_e(\text{cup}) = \frac{0.040}{0.0655} \times 100 = 61.1\%$$

$$f_e(\text{ellipse}) = \frac{0.0055}{0.0655} \times 100 = 8.4\%$$

$$f_e(\text{barrel}) = \frac{0.020}{0.0655} \times 100 = 30.5\%$$

The observed frequencies of these shapes follow. In this case there was a relatively large number of cylinders in each mount and very few were in actual contact with the sides of the container, so no data are omitted.

	Number observed	frequency
C	271	58.1%
E	36	7.7%
B	159	34.1%
Total	466	

	Number expected
C	466 x .611 = 284
E	466 x .084 = 39
B	466 x .305 = 139

Using the Chi-quare test, we obtain

Chi-square Test

	obs.	exp.	$\lvert o-e \rvert$	$\frac{(o-e)^2}{e}$
C	271	284	13	.59
E	36	39	3	.23
B	159	143	16	1.79
	466			2.61

$\chi^2 = 2.61.$

For two degrees of freedom, the probability of a deviation greater than $\chi^2 = 2.61$ due to random errors is 0.28. Therefore, 28% of the time the expected deviation would be greater than observed. Thus the hypothesis that these data fit the theory may be accepted.

Long Cylinders

The basic parameters of the long cylinders are

$$\frac{\ell}{d} = \frac{0.120"}{0.060"} = 2.0$$

$$P_i(\text{cylinder}) = (0.060 \times \frac{\pi}{4} + \frac{0.120}{2}) = 0.1071$$

Number per Section. 300 of these cylinders were dispersed in a cylindrical body having a height of two inches and an approximate diameter of 1 5/8 inches. Their expected number per section were

$$\text{expected number per section} = \frac{300}{2.0}(0.1071) = 16.1$$

Experimentally, 16 plane sections were taken, in which 274 particles were observed.

$$\text{average number per section} = \frac{274}{16} = 17.1$$

This result agrees reasonably well with the expected value.

Relative Frequencies of Shapes. The shape probabilities for long cylinders are

$$P_i(\text{cup}) = 0.060 \arctan 2 = 0.0664$$

$$P_i(\text{ellipse}) = \frac{0.120}{2} - \frac{0.060}{2} \arctan 2 = 0.0268$$

$$P_i(\text{barrel}) = 0.060 \times \frac{\pi}{4} - \frac{0.060}{2} \arctan 2 = 0.0139$$

The expected relative frequencies are

$$f_e(\text{cup}) = \frac{0.0664}{0.1071} = 61.9\%$$

$$f_e(\text{ellipse}) = \frac{0.0268}{0.1071} = 25.0\%$$

$$f_e(\text{barrel}) = \frac{0.0139}{0.1071} = 13.0\%$$

The observed frequencies were

	Number observed	frequency
C	171	62.4%
E	63	23.0%
B	40	14.6%
	274	

	Number expected
C	274 x .619 = 169
E	274 x .250 = 68.5
B	274 x .130 = 35.6

The statistical analysis follows:

Chi-square Test

	obs.	exp.	$\lvert o-e \rvert$	$\frac{(o-e)^2}{e}$
C	171	169	2	.01
E	63	68.5	5.5	.44
B	40	35.6	4.4	.54
	274			0.99

$\chi^2 = 0.99$.

For two degrees of freedom, the probability of a deviation greater than $\chi^2 = 0.99$ due to random errors is 0.62. Therefore, 62% of the time the expected deviation would be greater than observed, and the data fit the hypothesis very well.

Round Needles

The basic parameters of the round needles are

$$\frac{\ell}{d} = \frac{0.400''}{0.020''} = 20$$

$$P_i(\text{cylinder}) = (0.020 \times \frac{\pi}{4} + \frac{0.400}{2}) = 0.2157$$

Number per Section. 150 of these needles were dispersed in a cylindrical body having a height of 1 3/4 inches and an approximate diameter of 1 5/8 inches. Their expected number per section were

$$\text{expected number per section} = \frac{150}{1.75}\ (0.2157) = 18.5$$

Experimentally, 14 plane sections were taken in which 256 intersections of needles were observed.

$$\text{average number per section} = \frac{256}{14} = 18.3$$

The agreement between theory and experiment is very close.

Relative Frequencies of Shapes. The shape probabilities of these needles are

$$P_i(\text{cup}) = 0.020 \arctan 20 = 0.0304$$

$$P_i(\text{ellipse}) = \frac{0.400}{2} - \frac{0.020}{2} \arctan 20 = 0.1848$$

$$P_i(\text{barrel}) = 0.0020 \times \frac{\pi}{4} - \frac{0.020}{2} \arctan 20 = 0.0005$$

The expected relative frequencies of these shapes are

$$f_e(\text{cup}) = \frac{0.0304}{0.2157} \times 100 = 14.1\%$$

$$f_e(\text{ellipse}) = \frac{0.1848}{0.2157} \times 100 = 85.9\%$$

$$f_e(\text{barrel}) = \frac{0.0005}{0.2157} \times 100 = 0.02\%$$

Since the expected number of barrel sections was so small, one in 5000, to improve randomness of orientations wires were twisted and data for barrel sections were not attempted.

The observed frequencies of shapes were

	Number observed	frequency
C	36	14.0%
E	220	86.0%

A Chi-square test will not be applied to this. It may be seen that agreement between theory and experiment is almost perfect. However, the strong tendency of these long wires to orient themselves was noted, and data obtained from previous specimens not so extensively twisted had to be rejected because of strongly biased orientations.

Cubes

The basic parameters of the cubes prepared are

450 brass cubes 0.125" on edge

100 steel cubes 0.120" on edge

$$P_i(\text{brass cube}) = \frac{3}{2}(0.125) = 0.1875$$

$$P_i(\text{steel cube}) = \frac{3}{2}(0.120) = 0.1800$$

Number per Section. 450 brass cubes were dispersed in five cylindrical bodies approximately 1 1/2 inches in diameter and totalling 8.27 inches in

height. Their expected number per section were

$$\text{expected number per section} = \frac{450}{8.27} \times 0.1875 = 10.2$$

In 56 plane sections, 553 observations of brass cubes were made.

$$\text{average number per section} = \frac{553}{56} = 9.9$$

100 steel cubes were dispersed in two cylindrical bodies about 1 1/2 inches in diameter and totalling 1.73 inches in height. Their expected number per section were

$$\text{expected number per section} = \frac{100}{1.73} \times 0.18 = 10.4$$

In 10 plane sections 96 observations of steel cubes were made.

$$\text{average number per section} = \frac{96}{10} = 9.6$$

The expected and observed results for numbers of cubes per section can be seen to agree quite well for both brass and steel cubes.

To see how this would work in predicting number per unit volume, we shall use the brass cubes as an example.

$$\text{number per section} = \frac{\text{number per volume}}{\text{height}} \times P_i$$

$$\text{number per volume} = \frac{\text{number per section x height}}{P_i}$$

Using our observed number per section, 9.9, we get

$$\text{number per volume} = \frac{9.9 \times 8.27}{0.1875 \; P_i} = 437$$

Therefore, we estimate that there are 437 cubes present in the given volume, compared to a known value of 450. The percentage error is 2.9%, which appears to be a reasonable value. For number per unit volume, we would estimate

$$N_v = \frac{437}{8.27 \times \frac{\pi}{4} \left(\frac{3}{2}\right)^2} = 29.9 \text{ cubes/in.}^3$$

The actual value is about 30.7 cubes/in.^{3}

Relative Frequencies of Shapes. The data for the two kinds of cubes are combined. Data for cubes biased by contact with container walls are excluded. The types of sections observed from cubes were

Sides on Section	Number observed	Frequency
3	185	28.5%
4	321	49.5%
5	112	17.3%
6	31	4.8%
	649	

Comparison with Earlier Data. We compare experimental distribution with theoretical distribution and that of Hull and Houk[50].

Sides	Frequency (%)		
	theoretical	experimental	Hull and Houk[50]
3	28.0	28.5	29.0
4	48.7	49.5	42.9
5	18.7	17.3	18.2
6	4.6	4.8	10.0

The close agreement between our experimental results and our theoretically derived results in contrast to those reported by Hull and Houk is to be noted. We shall test these experimental results statistically for goodness-of-fit against both our theoretical distribution and that of Hull and Houk.

Comparing our experimental data with our theoretical results we obtain

Chi-square Test (Present theory)

sides	obs.	exp.(theory)	$\lvert o-e \rvert$	$\frac{(o-e)^2}{e}$
3	185	181.9	3.1	.07
4	321	316	5	.08
5	112	121.4	9.4	.73
6	31	30.2	0.8	.02
	649			0.90

$\chi^2 = 0.90$

For three degrees of freedom, the probability of a deviation greater than $\chi^2 = 0.90$ due to random errors is 0.82. Therefore, 82% of the time the expected deviation would be greater than observed. The fit is considered excellent, and the hypothesis of agreement between experiment and theory is strongly supported.

Comparing our experimental data with results predicted by Hull and Houk[50] we obtain

Chi-square Test

(our experimental results checked against Hull and Houk's distribution frequency)

Sides	obs.	exp. (H and H)	$\lvert o-e \rvert$	$\frac{(o-e)^2}{e}$
3	185	188	3	.05
4	321	278	43	6.62
5	112	118	6	.30
6	31	64.9	33.9	17.65
	649			24.62

$\chi^2 = 24.62$

For three degrees of freedom, the probability of a deviation greater than $\chi^2 = 24.62$ due to random errors is very much less than 0.01. This result may be considered as highly significant, warranting the rejection of the hypothesis that our experimental frequency distribution may be considered to agree with the distribution by Hull and Houk.

XIV. CONCLUSIONS

1. Relations have been derived which connect the number of particles observed in a plane section with the number and size of particles actually present in the solid for uniformly sized but randomly dispersed and oriented particles of nine different polyhedral shapes. The relations derived are listed as follows:

Shape	Relation
Cubes	$N_S = N_V \cdot 1\ 1/2a$
Rectangular Parallelepipeds	$N_S = N_V \cdot 1/2(a+b+c)$
Thin Rectangular Plates	$N_S = N_V \cdot 1/2(a+b)$
Long Square Rods	$N_S = N_V \cdot 1/2c$
Octahedrons	$N_S = N_V \cdot a \cdot \frac{3\sqrt{2}}{\pi} \operatorname{arccot} \sqrt{2}$
Tetrahedrons	$N_S = N_V \cdot a \cdot \frac{3\sqrt{2}}{\pi} \arctan \sqrt{2}$
Rhombic Dodecahedrons	$N_S = N_V \cdot \frac{\sqrt{3}}{2} a$
Tetrakaidecahedrons	$N_S = N_V \cdot \frac{3}{2\sqrt{2}} a$
Hexagonal Prisms	$N_S = N_V \cdot (\frac{3}{4} a + \frac{1}{2} c)$

In the above table, for octahedrons, tetrahedrons, rhombic dodecahedrons, and tetrakaidecahedrons, "a" is the edge length of the circumscribed cube. For the hexagonal prism, "a" is the length of the base diagonal and "c" is the altitude of the prism.

2. Relations have been derived which determine the relative frequencies of the possible section shapes obtained on random plane sections cutting through a dispersion of randomly oriented particles having the shapes of cylinders, cubes, octahedrons, tetrahedrons, rhombic dodecahedrons, and tetrakaidecahedrons.

3. The relative frequencies of various shaped sections of cylinders depend upon the length to diameter ratio of the cylinders and are proportional to the terms given in the following table.

Cylinder Section	Frequency Relation
Ellipses	$\frac{1}{2}$ (ℓ-d arctan ℓ/d)
Singly Truncated Ellipses	d arctan ℓ/d
Doubly Truncated Ellipses	$\frac{1}{2}$ ($\frac{\pi d}{2}$ - d arctan ℓ/d)

4. The relative frequencies with which sections of polyhedrons having various numbers of sides on a section are observed are presented in the following table.

Relative Frequencies of Sections (%)

Sides on Section	Polyhedron				
	Cube	Octahed.	Tetrahed.	Rh. Dod.	Tetrakai.
3	28.0	--	71.2	4.0	7.3
4	48.7	44.8	28.8	13.4	13.4
5	18.7	--	--	16.2	11.8
6	4.6	55.2	--	29.9	31.2
7	--	--	--	19.1	18.3
8	--	--	--	16.3	13.1
9	--	--	--	1.1	3.8
10	--	--	--	--	1.1

5. To obtain the above relations for polyhedrons, an integration technique has been developed which involves double integration and summation of equations of the form

$$P = A \int_{\theta_a}^{\theta_b} \int_{\phi_a(\theta)}^{\phi_b(\theta)} [(B \sin\theta + C \cos\theta) \sin^2\phi + D \cos\phi \sin\phi] \, d\phi d\theta$$

The integration technique can be extended to the determination of sectioning probabilities for other polyhedral shapes.

6. A digital computer technique has been developed for the solution of some of the integral equations arising from the basic integral equation just listed. The computer program described herein has been used to obtain some of the results reported. It may also prove useful for further development of quantitative metallographic relations for other polyhedral shapes.

7. The above results are exact for dispersed particles having uniform size and shape and random orientations. If particle shape is known, the relations permit analysis of degree of non-randomness of orientation. The relations also permit analysis of non-uniformly sized particles in a more accurate manner than previously possible.

8. Experimental verification of the theoretical relations developed for cubes and cylinders was obtained by preparing synthetic samples containing randomly dispersed cubes and cylinders. Measurements made by sectioning and microscopic examination of synthetic samples of cubes and four different cylindrical shapes support the theoretical predictions. In the case of relative frequency of cube sections, a statistical analysis of the experimental results indicates that previously reported results[50] were in error to a certain extent.

9. The relative frequencies of the various possible section shapes for cylindrical particles and polyhedrons will prove useful in helping to determine shapes of actual dispersed phases or particles observed in a microstructure. For cylindrical particles the frequencies of sections indicate the ℓ/d ratio. For simple polyhedral shapes the observed frequencies of various sided sections will help in indicating whether the phase particles have the shapes of cubes, octahedrons, tetrahedrons, tetrakaidecahedrons, etc. Where the particle shape is known, deviations from the expected frequencies of the various sections will tend to indicate degree of preferred orientation present.

10. Certain measurements made on plane sections cut from polyhedral particles can be expected to be reliable indicators of particle size. For instance, 4 sided sections of cubes can be interpreted to give quite closely the edge length of the cube. Thus a random dispersion of non-uniformly sized cubes could be classed into size groups according to the 4 sided sections observed. Since randomly oriented cubes give 48.7% of 4 sided sections, the total size distribution of cubes in the volume could be estimated from

$$N_{v(i)} = \frac{N_{s(i)} \text{ of 4 sided sections}}{(0.487)\ a_{(i)}\ (1.5)} \qquad (116)$$

APPENDICES

APPENDIX A

Evaluation of Definite Integrals

This appendix contains the detailed steps in the evaluation of 12 definite integrals which occur several times within the text. When an integral is changed into a form which is found in published tables of integrals, such reference is made and used without additional detail. The following integrals are solved, and they are found in this appendix in the order now listed. For convenience, we also list the answers below.

1. $$\int_0^{\frac{\pi}{4}} \frac{\cos\theta\, d\theta}{\sqrt{1+\cos^2\theta}} = \frac{\pi}{6}$$

2. $$\int_0^{\frac{\pi}{4}} \sin\theta \cdot \operatorname{arccot}(\cos\theta)d\theta = \frac{\pi}{4} - \frac{1}{\sqrt{2}} \arctan\sqrt{2} + \ell n \frac{2}{\sqrt{3}}$$

3. $$\int_0^{\frac{\pi}{4}} \frac{\sin\theta\cos\theta\, d\theta}{1+\cos^2\theta} = \ell n \frac{2}{\sqrt{3}}$$

4. $$\int_0^{\frac{\pi}{4}} \frac{\cos^2\theta d\theta}{1+\cos^2\theta} = \frac{\pi}{4} - \frac{\pi}{2\sqrt{2}} + \frac{1}{\sqrt{2}} \arctan\sqrt{2}$$

5. $$\int_0^{\frac{\pi}{4}} \frac{d\theta}{1+\cos^2\theta} = \frac{\pi}{2\sqrt{2}} - \frac{1}{\sqrt{2}} \arctan\sqrt{2}$$

6. $$\int_0^{\frac{\pi}{4}} \cos\theta \cdot \operatorname{arccot}(\cos\theta)d\theta = \frac{\pi}{4} - \frac{\pi}{\sqrt{2}} + \frac{3}{\sqrt{2}} \arctan\sqrt{2}$$

7. $$\int_0^{\frac{\pi}{4}} \frac{d\theta}{2+\sin^2\theta} = \frac{\pi}{6\sqrt{3}}$$

8. $\int_0^{\frac{\pi}{4}} \frac{\sin\theta\cos\theta d\theta}{2+\sin 2\theta} = \frac{\pi}{8} - \frac{\pi}{6\sqrt{3}}$

9. $\int_0^{\frac{\pi}{4}} \frac{\cos^2\theta d\theta}{2+\sin 2\theta} = \frac{\pi}{12\sqrt{3}} + \frac{1}{4}\ln\frac{3}{2}$

10. $\int_0^{\frac{\pi}{4}} \frac{\sin^2\theta\, d\theta}{2+\sin 2\theta} = \frac{\pi}{12\sqrt{3}} - \frac{1}{4}\ln\frac{3}{2}$

11. $\int_0^{\frac{\pi}{4}} \sin\theta\cdot\operatorname{arccot}(\sin\theta+\cos\theta)\, d\theta =$

$$\frac{3\pi}{8} - \frac{\pi}{2\sqrt{2}} - \frac{\pi}{4\sqrt{3}} + \frac{1}{\sqrt{2}}\arctan\sqrt{2} - \frac{1}{4}\ln\frac{3}{2}$$

12. $\int_0^{\frac{\pi}{4}} \cos\theta\cdot\operatorname{arccot}(\sin\theta+\cos\theta)\, d\theta =$

$$\frac{\pi}{8} + \frac{\pi}{2\sqrt{2}} - \frac{\pi}{4\sqrt{3}} - \frac{1}{\sqrt{2}}\arctan\sqrt{2} + \frac{1}{4}\ln\frac{3}{2}$$

1. $\int_0^{\frac{\pi}{4}} \frac{\cos\theta\, d\theta}{\sqrt{1+\cos^2\theta}}$

Let

$$\cos\theta = \sqrt{a^2-1}$$

$$\cos^2\theta = a^2 - 1 = 1 - \sin^2\theta$$

$$1 + \cos^2\theta = a^2$$

$$\sqrt{1+\cos^2\theta} = a$$

$$d(\cos\theta) = d\left(\sqrt{a^2-1}\right)$$

$$-\sin\theta\, d\theta = \frac{1}{2}\,\frac{2a}{\sqrt{a^2-1}}\,da = \frac{a\,da}{\sqrt{a^2-1}}$$

$$\sin^2\theta = 2-a^2$$

$$\sin\theta = \sqrt{2-a^2}$$

$$d\theta = \frac{1}{-\sin\theta}\,\frac{a\,da}{\sqrt{a^2-1}} = -\frac{1}{\sqrt{2-a^2}}\,\frac{a\,da}{\sqrt{a^2-1}}$$

when $\theta = 0$, $\cos\theta = 1$, $a = \sqrt{2}$

when $\theta = \frac{\pi}{4}$, $\cos\theta = \frac{1}{\sqrt{2}}$, $a = \sqrt{3/2}$

$$\int_0^{\frac{\pi}{4}} \frac{\cos\theta\, d\theta}{\sqrt{1+\cos^2\theta}} = \int_{\sqrt{2}}^{\sqrt{3/2}} \frac{\sqrt{a^2-1}}{-\sqrt{2-a^2}} \cdot \frac{a\,da}{\sqrt{a^2-1}\cdot a} = \int_{\sqrt{2}}^{\sqrt{3/2}} \frac{da}{-\sqrt{2-a^2}}$$

$$= \int_{\sqrt{3/2}}^{\sqrt{2}} \frac{da}{\sqrt{2-a^2}}$$

Set $a = \sqrt{2} \sin t$

$da = \sqrt{2} \cos t \, dt$

$a^2 = 2 \sin^2 t$

$2 - a^2 = 2 - 2 \sin^2 t = 2 \cos^2 t$

$\sqrt{2-a^2} = \sqrt{2} \cos t$

when $a = \sqrt{2}$, $t = \frac{\pi}{2}$

when $a = \sqrt{3/2}$ $t = \arcsin \frac{\sqrt{3}}{2} = 60° = \frac{\pi}{3}$

$$\int_{\sqrt{3/2}}^{\sqrt{2}} \frac{da}{\sqrt{2-a^2}} = \int_{\frac{\pi}{3}}^{\frac{\pi}{2}} \frac{\sqrt{2} \cos t \, dt}{\sqrt{2} \cos t} = \frac{\pi}{2} - \frac{\pi}{3} = \frac{\pi}{6}$$

2. $\int_0^{\frac{\pi}{4}} \sin \theta \cdot \operatorname{arccot} (\cos \theta) \, d\theta$

This is of the form, $-\int \operatorname{arccot} u \, du$,

where

$u = \cos \theta$

$du = - \sin \theta \, d\theta$

Therefore,

$$\int_0^{\frac{\pi}{4}} \sin \theta \cdot \operatorname{arccot} (\cos \theta) d\theta = - [u \operatorname{arccot} u + \frac{1}{2} \ell n(1+u^2)]$$

$$= [- \cos \theta \operatorname{arccot} (\cos \theta) - \frac{1}{2} \ell n (1 + \cos^2 \theta)]_0^{\pi/4}$$

$$= -\frac{1}{\sqrt{2}} \arctan\sqrt{2} + \frac{\pi}{4} - \frac{1}{2} \ln\left(\frac{3}{2}\right) + \frac{1}{2} \ln 2$$

$$= \frac{\pi}{4} - \frac{1}{\sqrt{2}} \arctan\sqrt{2} + \ln\frac{2}{\sqrt{3}}$$

3. $$\int_0^{\frac{\pi}{4}} \frac{\sin\theta\cos\theta\, d\theta}{1 + \cos^2\theta}$$

Let $u = \cos^2\theta + 1$

$du = -2 \sin\theta \cos\theta\, d\theta$

Therefore,

$$\int_0^{\frac{\pi}{4}} \frac{\sin\theta\cos\theta\, d\theta}{1 + \cos^2\theta} = -\frac{1}{2}\int \frac{du}{u} = -\frac{1}{2} \ln(1 + \cos^2\theta)\Big|_0^{\frac{\pi}{4}}$$

$$= -\frac{1}{2}\ln\frac{3}{2} + \frac{1}{2}\ln 2 = \ln\frac{2}{\sqrt{3}}$$

4. $$\int_0^{\frac{\pi}{4}} \frac{\cos^2\theta\, d\theta}{1 + \cos^2\theta} = \frac{1}{2}\int_0^{\frac{\pi}{4}} \frac{1/2(1 + \cos 2\theta)d(2\theta)}{1 + 1/2(1 + \cos 2\theta)}$$

$$= \frac{1}{2}\int_0^{\frac{\pi}{4}} \frac{1 + \cos 2\theta}{3 + \cos 2\theta}\, d(2\theta)$$

From Peirce[52], Equations (304) and (300),

$$= \frac{1}{2}\left[\frac{+1\cdot 2\theta}{1}\Big|_0^{\frac{\pi}{4}} + \frac{1\cdot 1 - 3\cdot 1}{1}\int_0^{\frac{\pi}{4}} \frac{d(2\theta)}{3 + \cos 2\theta}\right]$$

$$= \frac{\pi}{4} - \int_0^{\frac{\pi}{4}} \frac{d(2\theta)}{3 + \cos 2\theta} = \frac{\pi}{4} - \frac{2}{\sqrt{8}} \arctan\frac{\sqrt{8}}{4}$$

$$= \frac{\pi}{4} - \frac{1}{\sqrt{2}} \arctan \frac{1}{\sqrt{2}}$$

$$= \frac{\pi}{4} - \frac{1}{\sqrt{2}} \left(\frac{\pi}{2} - \arctan \sqrt{2}\right)$$

$$= \frac{\pi}{4} - \frac{\pi}{2\sqrt{2}} + \frac{1}{\sqrt{2}} \arctan \sqrt{2}$$

$$= \frac{1}{\sqrt{2}} \arctan \sqrt{2} + \frac{(1-\sqrt{2})}{4} \pi$$

5. $$\int_0^{\frac{\pi}{4}} \frac{d\theta}{1 + \cos^2 \theta} = \frac{1}{2} \int_0^{\frac{\pi}{4}} \frac{d(2\theta)}{1 + 1/2(1 + \cos 2\theta)} = \int_0^{\frac{\pi}{4}} \frac{d(2\theta)}{3 + \cos 2\theta}$$

From Peirce[52], Equation (300),

$$= \frac{2}{\sqrt{8}} \arctan \left(\frac{\sqrt{8}}{4} \tan \theta\right) \Bigg|_0^{\frac{\pi}{4}}$$

$$= \frac{1}{\sqrt{2}} \arctan \frac{1}{\sqrt{2}} = \frac{1}{\sqrt{2}} \left(\frac{\pi}{2} - \arctan \sqrt{2}\right)$$

$$= \frac{\pi}{2\sqrt{2}} - \frac{1}{\sqrt{2}} \arctan \sqrt{2}$$

6. $$\int_0^{\frac{\pi}{4}} \cos \theta \cdot \operatorname{arccot} (\cos \theta)\, d\theta$$

Let $u = \operatorname{arccot}(\cos\theta)$

$du = \cos\theta\, d\theta$

$v = \sin\theta$

$$du = \frac{\sin\theta\, d\theta}{1 + \cos^2\theta}$$

$$\int_0^{\frac{\pi}{4}} \cos\theta \cdot \operatorname{arccot}(\cos\theta)d\theta = \sin\theta \cdot \operatorname{arccot}(\cos\theta) \Big|_0^{\frac{\pi}{4}} - \int_0^{\frac{\pi}{4}} \frac{\sin^2\theta\, d\theta}{1 + \cos^2\theta}$$

$$= \frac{1}{\sqrt{2}} \arctan\sqrt{2} - \int_0^{\frac{\pi}{4}} \frac{d\theta}{1 + \cos^2\theta} + \int_0^{\frac{\pi}{4}} \frac{\cos^2\theta d\theta}{1 + \cos^2\theta}$$

From above,

$$= \frac{1}{\sqrt{2}} \arctan\sqrt{2} - \frac{\sqrt{2}\pi}{4} + \frac{1}{\sqrt{2}} \arctan\sqrt{2} + \frac{1}{\sqrt{2}} \arctan\sqrt{2} + \frac{(1-\sqrt{2})}{4}\pi$$

$$= \frac{3}{\sqrt{2}} \arctan\sqrt{2} + \left(\frac{1-2\sqrt{2}}{4}\right)\pi$$

7. $$\int_0^{\frac{\pi}{4}} \frac{d\theta}{2 + \sin 2\theta} = \frac{1}{2} \int_0^{\frac{\pi}{4}} \frac{d(2\theta)}{2 + \sin 2\theta}$$

From Peirce(52), Equation (298)

$$= \frac{1}{2} \cdot \frac{2}{\sqrt{3}} \arctan\left(\frac{2\tan\theta + 1}{\sqrt{3}}\right) \Bigg|_0^{\frac{\pi}{4}}$$

$$= \frac{1}{\sqrt{3}} \left(\arctan\sqrt{3} - \arctan\frac{1}{\sqrt{3}}\right) = \frac{1}{\sqrt{3}} \left(\frac{\pi}{3} - \frac{\pi}{6}\right)$$

$$= \frac{\pi}{6\sqrt{3}}$$

8. $$\int_0^{\frac{\pi}{4}} \frac{\sin\theta\cos\theta\, d\theta}{2+\sin 2\theta} = \frac{1}{4}\int_0^{\frac{\pi}{4}} \frac{\sin 2\theta\, d(2\theta)}{2+\sin 2\theta}$$

From Dwight(54), Equations (436.01) and (436.00)

$$= \frac{1}{4}\left[\frac{2\theta}{1}\Bigg|_0^{\frac{\pi}{4}} - \frac{2}{1}\int_0^{\frac{\pi}{4}} \frac{d(2\theta)}{2+\sin 2\theta}\right]$$

$$= \frac{\pi}{8} - \frac{1}{2}\cdot\frac{\pi}{3\sqrt{3}} = \pi\left(\frac{1}{8} - \frac{1}{6\sqrt{3}}\right)$$

9. $$\int_0^{\frac{\pi}{4}} \frac{\cos^2\theta d\theta}{2+\sin 2\theta} = \frac{1}{4}\int_0^{\frac{\pi}{4}} \frac{(1+\cos 2\theta)d(2\theta)}{2+\sin 2\theta}$$

$$= \frac{1}{4}\int_0^{\frac{\pi}{4}} \frac{d(2\theta)}{2+\sin 2\theta} + \frac{1}{4}\int_0^{\frac{\pi}{4}} \frac{\cos 2\theta\, d(2\theta)}{2+\sin 2\theta}$$

From Dwight(54), Equation (436.00)

$$= \frac{\pi}{12\sqrt{3}} + \frac{1}{4}\ln(2+\sin 2\theta)\Big|_0^{\frac{\pi}{4}}$$

$$= \frac{\pi}{12\sqrt{3}} + \frac{1}{4}[\ln 3 - \ln 2] = \frac{\pi}{12\sqrt{3}} + \frac{1}{4}\ln\frac{3}{2}$$

10. $$\int_0^{\frac{\pi}{4}} \frac{\sin^2\theta d\theta}{2+\sin 2\theta} = \int_0^{\frac{\pi}{4}} \frac{d\theta}{2+\sin 2\theta} - \int_0^{\frac{\pi}{4}} \frac{\cos^2\theta d\theta}{2+\sin 2\theta}$$

$$= \frac{\pi}{6\sqrt{3}} - \frac{\pi}{12\sqrt{3}} - \frac{1}{4}\ln\frac{3}{2} = \frac{\pi}{12\sqrt{3}} - \frac{1}{4}\ln\frac{3}{2}$$

11. $\int_0^{\frac{\pi}{4}} \sin\theta \cdot \operatorname{arccot}(\sin\theta + \cos\theta)d\theta$

Let $u = \operatorname{arccot}(\sin\theta + \cos\theta)$

$dv = \sin\theta\, d\theta$

$du = -\frac{(\cos\theta - \sin\theta)d\theta}{1+1+2\sin\theta\cos\theta} = \frac{(\sin\theta - \cos\theta)d\theta}{2 + \sin 2\theta}$

$v = -\cos\theta$

$$\int_0^{\frac{\pi}{4}} \sin\theta \cdot \operatorname{arccot}(\sin\theta + \cos\theta)d\theta = -\cos\theta \cdot \operatorname{arccot}(\sin\theta + \cos\theta)\Big|_0^{\frac{\pi}{4}}$$

$$+ \int_0^{\frac{\pi}{4}} \frac{\cos\theta(\sin\theta - \cos\theta)d\theta}{2 + \sin 2\theta}$$

$$= -\frac{1}{\sqrt{2}} \operatorname{arccot}\sqrt{2} + \operatorname{arccot} 1 + \int_0^{\frac{\pi}{4}} \frac{\sin\theta\cos\theta\, d\theta}{2 + \sin 2\theta}$$

$$- \int_0^{\frac{\pi}{4}} \frac{\cos^2\theta d\theta}{2 + \sin 2\theta}$$

$$= \frac{\pi}{4} - \frac{1}{\sqrt{2}}\left(\frac{\pi}{2} - \arctan\sqrt{2}\right) + \pi\left(\frac{1}{8} - \frac{1}{6\sqrt{3}}\right) - \frac{\pi}{12\sqrt{3}} - \frac{1}{4}\ln\frac{3}{2}$$

$$= \frac{\pi}{4} - \frac{\pi}{2\sqrt{2}} + \frac{1}{\sqrt{2}}\arctan\sqrt{2} + \frac{\pi}{8} - \frac{\pi}{6\sqrt{3}} - \frac{\pi}{12\sqrt{3}} - \frac{1}{4}\ln\frac{3}{2}$$

$$= \pi\left(\frac{3}{8} - \frac{1}{2\sqrt{2}} - \frac{1}{4\sqrt{3}}\right) + \frac{1}{\sqrt{2}}\arctan\sqrt{2} - \frac{1}{4}\ln\frac{3}{2}$$

12. $\int_0^{\frac{\pi}{4}} \cos\theta \cdot \operatorname{arccot}(\sin\theta + \cos\theta)\,d\theta$

Let $u = \operatorname{arccot}(\sin\theta + \cos\theta)$

$dv = \cos\theta\, d\theta$

$v = \sin\theta$

$du = \dfrac{(\sin\theta - \cos\theta)d\theta}{2 + \sin 2\theta}$

$$\int_0^{\frac{\pi}{4}} \cos\theta \cdot \operatorname{arccot}(\sin\theta + \cos\theta)\,d\theta = \sin\theta \cdot \operatorname{arccot}(\sin\theta + \cos\theta)\Big|_0^{\frac{\pi}{4}}$$

$$- \int_0^{\frac{\pi}{4}} \frac{\sin\theta\,(\sin\theta - \cos\theta)d\theta}{2 + \sin 2\theta}$$

$$= \frac{1}{\sqrt{2}} \operatorname{arccot}\sqrt{2} - \frac{\pi}{12\sqrt{3}} + \frac{1}{4} \ln\frac{3}{2} + \frac{\pi}{8} - \frac{\pi}{6\sqrt{3}}$$

$$= \frac{1}{\sqrt{2}} \left(\frac{\pi}{2} - \arctan\sqrt{2}\right) - \frac{\pi}{4\sqrt{3}} + \frac{\pi}{8} + \frac{1}{4} \ln\frac{3}{2}$$

$$= \frac{\pi}{8} + \frac{\pi}{2\sqrt{2}} - \frac{\pi}{4\sqrt{3}} - \frac{1}{\sqrt{2}} \arctan\sqrt{2} + \frac{1}{4} \ln\frac{3}{2}$$

APPENDIX B

Digital Computer Solution of Trigonometric Integral Equations

The basic integral equation of the general form used to solve all the probability problems for polyhedrons of cubic symmetry is

$$\bar{D} = \frac{12}{\pi} A \int_{\theta_a}^{\theta_b} \int_{\phi_a(\theta)}^{\phi_b(\theta)} [(D \sin\theta + E \cos\theta) \sin^2\phi + H \cos\phi \sin\phi] \, d\phi d\theta \tag{86}$$

This equation gives average distance between top and bottom parallel tangent planes passing through any two points or corners of the polyhedron for all orientations over the spherical triangle represented by the 001, 101, and 111 poles.

The numbers represented by D, E, and H are the coordinate differences between the two points or corners in question. D, E, and H represent distances along the three coordinate axes in units or fractional units of edge length of the cube in which the polyhedron may be inscribed. These directions are taken as positive or negative in line with the convention illustrated by Figure 35.

The number $12/\pi$ is to convert the orientations represented by the spherical triangle between poles 001, 101, and 111 into all possible orientations, represented by the surface of a sphere. The surface area of a sphere of unit radius is 4π, and the spherical triangle described is exactly 1/48th of a sphere so it has surface area of $\pi/12$. This spherical triangle is the smallest range of orientations which represents in correct proportion all possible orientations of a polyhedron of cubic symmetry. While it is

perfectly possible to represent all possible orientations of such a polyhedron by a larger spherical triangle, an octant of a sphere, for example, the smallest such range is usually most convenient. For this reason we integrate only for orientations within this 1/48th triangle and multiply by $12/\pi$ to convert to all orientations.

The number A may be 1 or 2, to take care of those cases where a certain pair of corners on the upper half of a polyhedron resulting in a certain type of section is exactly duplicated by a similar pair of corners on the lower half of the polyhedron. In this situation A = 2 to account for both cases. When the range covered between two corners includes the center of the polyhedron, then A = 1.

The angles $\phi_a(\theta)$, $\phi_b(\theta)$, θ_a, and θ_b, of course, represent the orientation limits for integration. These angles are all within the basic spherical triangle of the 001, 101, and 111 poles. They are used to subdivide the basic triangle into smaller orientation ranges, either spherical triangles or quadrangles, which give the orientation range over which the corners being considered define the property being measured. In the case of the tetrakaidecahedron, it was shown by Figure 43 that 77 such smaller orientation ranges were necessary to adequately consider the shapes of sections of this polyhedron.

The ϕ's are the angles of tilt from the vertical, and the θ's are angles of horizontal rotation, as shown in Figure 9. Since we have chosen to integrate over ϕ first, and since our orientation limits are in general functions of both ϕ and θ, it is necessary to express ϕ as a function of θ.

Then the integration over Θ can be performed between the constant angular values of the Θ range extremities.

Now that the basic double integral equation, Equation (86), has been explained, we shall describe its solution on the digital computer.

For convenience in computer programming, the basic double integral is integrated once to convert it into a single integral. Setting $C = \Theta_a$, $B = \Theta_b$, $G = \phi_a(\Theta)$, and $F = \phi_b(\Theta)$, we have

$$\bar{D} = \frac{12}{\pi} A \int_C^B \int_G^F [(D \sin\Theta + E \cos\Theta) \sin^2\phi + H \cos\phi \sin\phi] \, d\phi d\Theta$$

$$\bar{D} = \frac{12}{\pi} \cdot \frac{A}{2} \int_C^B [D \sin\Theta + E \cos\Theta)(\phi - \sin\phi \cos\phi) + H \sin^2\phi]_G^F \, d\Theta$$

$$\bar{D} = \frac{12}{\pi} \cdot \frac{A}{2} \int_C^B [(D \sin\Theta + E \cos\Theta)(F - G - \sin F \cos F + \sin G \cos G) + H(\sin^2 F - \sin^2 G)] \, d\Theta \qquad (117)$$

This is the basic form of the equation used in programming the digital com-computer.

As previously discussed, several such equations arising from the solutions for simple shaped polyhedrons had been solved exactly by the methods of integral calculus. These equations were included in those to be calculated by the computer as they provided a good check on the work of the computer. Furthermore, the computer result provided a check against the previously calculated results. This double check proved valuable on both counts.

All integral equations, including those already solved and those not yet solved, for probabilities of intersecting whole polyhedrons and for probabilities of various section shapes, were prepared in the form of Equation(117). These were written out as tabular, hand-written data with columns for Equation Number, A, B, C, D, E, F, G, H, Answer, and Description. Initially, 237 such equations were listed, of which answers on the first 37 had already been obtained, and 200 remained to be solved. In the course of obtaining the computer results, errors were found in some of the initial data and this required changes in a few equations and an addition of 5 new equations, making the total 242.

The programming of the trigonometric integral equations was done by the Digital Computation Branch, Aeronautical Systems Division, Wright-Patterson Air Force Base, Ohio. The solution of the equations was performed on an IBM 7090 Digital Computer. The problems were programmed in Fortran language, compiled on an IBM 1401 into binary machine language, written on magnetic tape, and run on the IBM 7090. The out-put tape was placed on an off-line printer to print out the results.

The main program for the solution of these trigonometric integral equations is given in Table XX. The symbol FNX refers to the basic integral equation, Equation (117), to be solved. The expression CALL ISIA refers to an integration sub-routine in the computer's tape library. This integration sub-routine uses Simpson's rule in which the function is evaluated for successively smaller and smaller intervals until two consecutive answers differ by no more than 0.00001. In order to evaluate the function FNX(X)

TABLE XX

MAIN PROGRAM FOR SOLUTION OF
TRIGONOMETRIC INTEGRAL EQUATIONS

SOLUTION OF TRIGONOMETRIC INTEGRAL EQUATIONS

```
F       FNX
        DIMENSION A(241),B(241),C(241),D(241),E(241),F1(241),F2(241),
       1F3(241),G1(241),G2(241),H(241),ANSW(241),DES(241),IC(241),
       2DESB(241)
        COMMON DD,EE,FF1,FF2,FF3,FG1,FG2,HH
        J=1
        K=236
        PI=3.1415926
  600   READ INPUT TAPE 2,100,(A(I),I=J,K),(B(I),I=J,K),(C(I),I=J,K),
       1(D(I),I=J,K),(E(I),I=J,K),(F1(I),I=J,K),(F2(I),I=J,K),
       2(F3(I),I=J,K),(G1(I),I=J,K),(G2(I),I=J,K),(H(I),I=J,K)
  100   FORMAT(6F10.7)
        DO 10 I=J,K
        IF(I-1)7,7,2
    2   IF(I-36)6,7,6
    6   A(I)=A(I)*12./PI
    7   IF(I-88)3,4,4
    3   IC(I)=I
        GO TO 5
    4   IC(I)=I+1
    5   BB=B(I)
        CC=C(I)
        DD=D(I)
        EE=E(I)
        FF1=F1(I)
        FF2=F2(I)
        FF3=F3(I)
        FG1=G1(I)
        FG2=G2(I)
        HH=H(I)
        CALLISIA(BB,CC,5.E-5,T,ANS,FNX)
        ANSW(I)=ANS*(A(I)/2.)
   10   CONTINUE
        IF (K-241) 75,60,60
   75   J=237
        K=241
        GO TO 600
   60   READINPUTTAPE2,101,DES
        READINPUTTAPE2,101,DESB
  101   FORMAT(12A6)
        WRITEOUTPUTTAPE3,200
        WRITEOUTPUTTAPE3,250,(IC(I),A(I),B(I),C(I),D(I),E(I),F1(I),F2(I),
       1F3(I),G1(I),G2(I),H(I),ANSW(I),DES(I),DESB(I),I=1,50)
        WRITEOUTPUTTAPE3,200
        WRITEOUTPUTTAPE3,250,(IC(I),A(I),B(I),C(I),D(I),E(I),F1(I),F2(I),
       1F3(I),G1(I),G2(I),H(I),ANSW(I),DES(I),DESB(I),I=51,100)
        WRITEOUTPUTTAPE3,200
        WRITEOUTPUTTAPE3,250,(IC(I),A(I),B(I),C(I),D(I),E(I),F1(I),F2(I),
       1F3(I),G1(I),G2(I),H(I),ANSW(I),DES(I),DESB(I),I=101,150)
        WRITEOUTPUTTAPE3,200
        WRITEOUTPUTTAPE3,250,(IC(I),A(I),B(I),C(I),D(I),E(I),F1(I),F2(I),
       1F3(I),G1(I),G2(I),H(I),ANSW(I),DES(I),DESB(I),I=151,200)
        WRITEOUTPUTTAPE3,200
        WRITEOUTPUTTAPE3,250,(IC(I),A(I),B(I),C(I),D(I),E(I),F1(I),F2(I),
       1F3(I),G1(I),G2(I),H(I),ANSW(I),DES(I),DESB(I),I=201,241)
        PTRD=ANSW(16)+ANSW(17)
        FSP5=ANSW(20)+ANSW(21)
        FSP6=ANSW(22)+ANSW(23)+ANSW(24)+ANSW(25)
        FSP7=ANSW(26)+ANSW(27)+ANSW(28)+ANSW(29)+ANSW(30)
        FSP8=ANSW(31)+ANSW(32)+ANSW(33)+ANSW(34)
        PTOT=0
        DO 11 I=18,35
   11   PTOT=PTOT+ANSW(I)
        P3=ANSW(38)+ANSW(39)
        P4=ANSW(40)+ANSW(41)+ANSW(42)+ANSW(43)
        SDP5=0
        DO 12 J=44,55
   12   SDP5=SDP5+ANSW(J)
        P10=ANSW(56)+ANSW(57)+ANSW(58)+ANSW(59)
        P9=0
        DO 13 K=60,85
   13   P9=P9+ANSW(K)
        SDP8=0
        DO 14 L=86,136
   14   SDP8=SDP8+ANSW(L)
        SDP6=ANSW(241)
        DO 15 M=137,170
   15   SDP6=SDP6+ANSW(M)
        SDP7=0
        DO 16 N=171,240
   16   SDP7=SDP7+ANSW(N)
        P380N=0
        DO 17 II=38,241
   17   P380N=P380N+ANSW(II)
        WRITE OUTPUT TAPE 3,300
        WRITE OUTPUT TAPE 3,350,PTRD,FSP5,FSP6,FSP7,
       1FSP8,PTOT,P3,P4
        WRITE OUTPUT TAPE 3,400
        WRITE OUTPUT TAPE 3,350,SDP5,P10,P9,SDP8,SDP6,
       1SDP7,P380N,ANSW(37)
  300   FORMAT(1H1,4X,4HPTRD,11X4HFSP5,11X4HFSP6,11X4HFSP7,11X4HFSP8,
       111X4HPTOT,12X2HP3,13X2HP4///)
  400   FORMAT (///5X4HSDP5,12X3HP10,12X2HP9,12X4HSDP8,11X4HSDP6,
       111X4HSDP7,10X5HP380N,9X8HANSW(37)///)
  350   FORMAT(F10.6,7F15.6)
  200   FORMAT(1H1,//4H EQ.,6X,1HA,10X,1HB,10X,1HC,8X,1HD,6X,1HE,6X,
       12HF1,5X,2HF2,5X,2HF3,5X,2HG1,5X,2HG2,5X,1HH,6X,
       220HANSWER   DESCRIPTION//)
  250   FORMAT(1X,I3,3F11.6,8F7.2,F11.6,2X,2A6)
        CALL EXIT
        END(1,0,0,0,0,0,1,0,0,0,0,0,0,0,0)
```

it was necessary to prepare a function sub-routine, which is shown in Table XXI. A Flow Diagram illustrating the entire program is shown in Figure 67.

Some explanation of the change in symbols will be necessary in order to compare the basic equation, Equation (117), with the program. AEE refers to D sinθ. BEE refers to E cosθ. CEE refers to F. DEE refers to G. EEE refers to sinF. EFE refers to cosF. F refers to sin G. FE refers to cos G. HH refers to H, EEE^2 refers to $\sin^2 F$. F^2 refers to $\sin^2 G$. Additional comapplicable to the main program and the function sub-routine will be made in the following description of the flow chart and the print-out sheet.

A clearer picture of the program may be obtained from the flow chart, Figure 67. The dimension block is used when the program is compiled only. It reserves storage cells for the 241 values of A, B, C, D, etc. that will be read in during this program. The common block is also used only in compilation. It is a way to communicate between the main program and the subroutines using the same variables, since Fortran considers each main program and/or subroutine as a separate entity in compiling. The variables IC(I)'s are the equation numbers. The block ISIA is the subroutine that integrates a function using Simpson's Rule. The block FNX is the function subroutine used by the subroutine ISIA to evaluate the function at the increments of integration. Many of the tests indicated are due to "patching-up" the program. If the program were to be run many times, it would be rewritten in a simpler, cleaner fashion. However, since only a single correct solution of the equations was necessary, adding on was much easier than changing the whole program.

TABLE XXI

FUNCTION SUB-ROUTINE FOR EQUATION (116)

```
      FUNCTION FNX(X)

      FUNCTION FNX(X)
      COMMON DD,EE,FF1,FF2,FF3,FG1,FG2,HH
      PI =1.5707963
      AEE=DD*SINF(X)
      DEE=EE*COSF(X)
      IF(FF1+FF2)2,3,2
3     CEE=FF3
      GO TO 50
2     P=FF1*SINF(X)+FF2*COSF(X)
      IF(P)4,5,4
5     CEE=PI
      GO TO 50
4     CEE=ATANF(1./P)+FF3
50    IF(FG1+FG2)6,7,6
7     BEE=0
      GO TO 60
6     Q=FG1*SINF(X)+FG2*COSF(X)
      IF(Q)8,9,8
9     BEE=PI
      GO TO 60
8     BEE=ATANF(1./Q)
60    EEE=SINF(CEE)
      CFE=COSF(CEE)
      F=SINF(DEE)
      FE=COSF(DEE)
      FNX    =(AEE+BEE)*(CEE-DEE-EEE*EFE+F*FE)+HH*
     1(EEE**2-F**2)
      RETURN
      END(1,0,0,0,0,0,1,0,0,0,0,0,0,0,0)
```

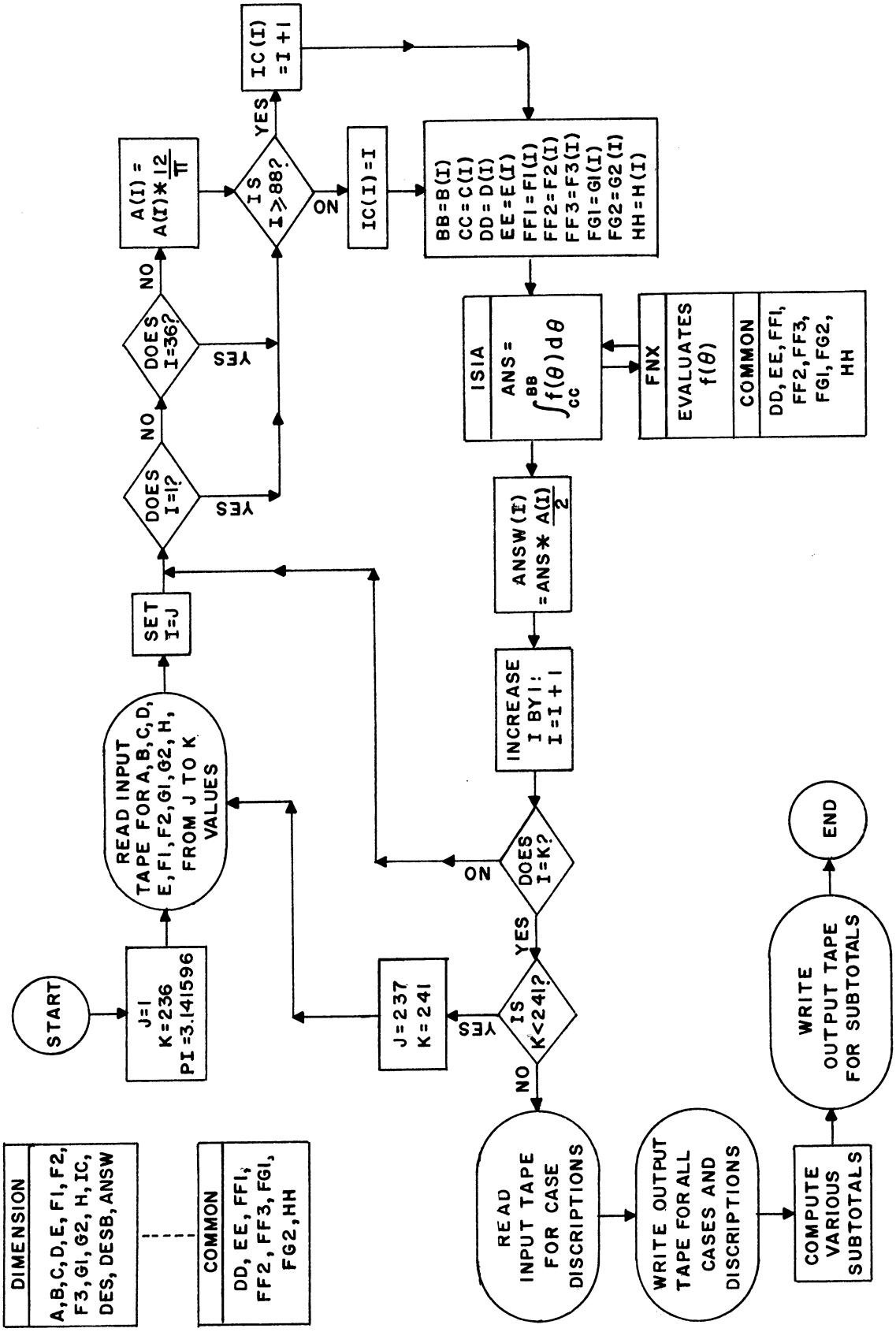

Figure 67. Flow Diagram for IBM 7090 Fortran Program.

The tests for I = 1 and I = 36 were because all equations except these two involved integration within the 001, 101, and 111 triangle and subsequent multiplication by $12/\pi$. Equation (1) was for the cube integrated over one octant so the multiplier was $2/\pi$. Equation (36) was for the hexagonal prism integrated between $\theta = 0°$ to 30° and $\phi = 0°$ to 90°. This is 1/24th of a sphere so the multiplier was $6/\pi$. Initially all other integral equations were read in without the constant factor $12/\pi$ When it was decided to include the factor $12/\pi$, this constituted a change in the program and also required tests for I = 1 and 36. The result was three additional steps shown on the flow diagram.

The test for $I \geq 88$ is because Equation (88) originally written out on the tabulation sheet was later cancelled. Since the equations following (88) were not renumbered, the computer had to be told that, beyond Equation (88), Equation(I) was really Equation (I+1)

The first box showing K = 236 indicates the original number of equations to be solved. Since a later correction added 5 more equations, this resulted in the box "IS K <241?" This meant that data for the last 5 equations were read in after solving the first 236 equations. This was easier than changing the original data input.

The computer print-out data and answer sheet is shown in Table XXII. An explanation of the columns and the equations will now be given.

Column A is the $(12/\pi) \cdot A$ shown in the basic equation, Equation (117), with only two exceptions, these being Equations (1) and (36), which were just discussed. Since A = 1 or 2, also previously discussed, this means that

TABLE XXII

COMPUTER PRINT-OUT OF INPUT DATA AND ANSWERS TO EQUATIONS

EQ.	A	B	C	D	E	F1	F2	F3	G1	G2	H	ANSWER	DESCRIPTION
1	0.636620	1.570796	0.	1.00	1.00	0.	0.	1.57	0.	0.	1.00	1.500000	CUBE
2	3.819719	0.785398	0.	1.00	1.00	0.	1.00	0.	0.	0.	1.00	1.499999	CUBE
3	7.639437	0.785398	0.	1.00	0.	0.	1.00	0.	0.	0.	0.	0.419743	P3
4	7.639437	0.785398	0.	-1.00	1.00	0.	1.00	0.	0.	0.	0.	0.498135	P4
5	3.819719	0.785398	0.	-1.00	-1.00	1.00	1.00	0.	0.	0.	1.00	0.232053	P4
6	3.819719	0.785398	0.	1.00	1.00	0.	1.00	0.	1.00	1.00	-1.00	0.069674	P6
7	7.639437	0.785398	0.	1.00	0.	1.00	1.00	0.	0.	0.	0.	0.182913	P5
8	7.639437	0.785398	0.	0.	-1.00	0.	1.00	0.	1.00	1.00	1.00	0.097481	P5
9	3.819719	0.785398	0.	0.	0.	0.	1.00	0.	0.	0.	1.00	0.831183	OCTAHEDRON
10	7.639437	0.785398	0.	0.	-0.50	0.	1.00	0.	0.	0.	0.50	0.372250	P4
11	3.819719	0.785398	0.	0.	1.00	0.	1.00	0.	0.	0.	0.	0.458939	P6
12	3.819719	0.785398	0.	0.	1.00	0.	1.00	0.	0.	0.	1.00	1.290128	TETRAHEDRON
13	3.819719	0.785398	0.	1.00	1.00	0.	1.00	0.	0.	0.	0.	0.668810	P3
14	3.819719	0.785398	0.	-1.00	1.00	0.	1.00	0.	0.	0.	0.	0.249068	P3
15	3.819719	0.785398	0.	0.	-1.00	0.	1.00	0.	0.	0.	1.00	0.372250	P4
16	3.819719	0.785398	0.	0.	0.	1.00	1.00	0.	0.	0.	1.00	0.577351	RHOMDDDCHDN1
17	3.819719	0.785398	0.	0.50	0.50	0.	1.00	0.	1.00	1.00	0.50	0.288671	RHOMDDDCHDN2
18	7.639437	0.785398	0.	0.25	0.25	0.	1.00	0.	1.00	1.00	-0.25	0.034837	P3
19	7.639437	0.785398	0.	-0.25	-0.25	1.00	1.00	0.	0.	0.	0.25	0.116026	P4
20	7.639437	0.785398	0.	0.50	0.	1.00	1.00	0.	0.	0.	0.	0.091457	P5
21	7.639437	0.785398	0.	0.	-0.50	0.	1.00	0.	1.00	1.00	0.50	0.048741	P5
22	7.639437	0.785398	0.	-0.50	0.50	1.00	1.00	0.	0.	0.	0.	0.162365	P6
23	3.819719	0.785398	0.	0.50	0.50	0.	1.00	0.	1.00	1.00	-0.50	0.034837	P6
24	7.639437	0.588003	0.	-0.75	0.25	0.	1.00	0.	1.00	1.00	0.25	0.058460	P6
25	7.639437	0.785398	0.588003	-0.75	0.25	3.00	-1.00	0.	1.00	1.00	0.25	0.002988	P6
26	7.639437	0.785398	0.	0.50	0.	1.00	1.00	0.	0.	0.	0.	0.091457	P7
27	7.639437	0.785398	0.	0.	-0.50	0.	1.00	0.	1.00	1.00	0.50	0.048741	P7
28	7.639437	0.588003	0.	0.25	0.25	0.	1.00	0.	1.00	1.00	-0.25	0.014230	P7
29	7.639437	0.785398	0.588003	0.25	0.25	3.00	-1.00	0.	1.00	1.00	-0.25	0.003957	P7
30	7.639437	0.785398	0.588003	-0.50	0.50	0.	1.00	0.	3.00	-1.00	0.	0.007060	P7
31	3.819719	0.785398	0.	-0.50	-0.50	1.00	1.00	0.	0.	0.	0.50	0.116026	P8
32	7.639437	0.588003	0.	0.25	0.25	0.	1.00	0.	1.00	1.00	-0.25	0.014230	P8
33	7.639437	0.785398	0.588003	0.25	0.25	3.00	-1.00	0.	1.00	1.00	-0.25	0.003957	P8
34	7.639437	0.785398	0.588003	-0.50	0.50	0.	1.00	0.	3.00	-1.00	0.	0.007060	P8
35	7.639437	0.785398	0.588003	0.75	-0.25	0.	1.00	0.	3.00	-1.00	-0.25	0.009594	P9
36	1.909861	0.523599	0.	0.50	0.87	0.	0.	1.57	0.	0.	1.00	1.250002	HEX PRISM
37	3.819719	0.785398	0.	0.	0.50	0.	1.00	-0.	0.	0.	1.00	1.060659	TETRAHEDRON
38	7.639437	0.785398	0.	-0.25	0.25	-1.00	2.00	0.	0.	0.	0.	0.046569	P3 (1-2)
39	7.639437	0.785398	0.	0.	-0.25	0.	1.00	0.	-1.00	2.00	0.25	0.030388	P3 (1-5)
40	7.639437	0.785398	0.	0.50	0.	1.00	2.00	0.	0.	0.	0.	0.028147	P4 (2-3)
41	7.639437	0.785398	0.	0.	-0.75	0.	3.00	0.	0.	0.	0.25	0.032546	P4 (4-5)
42	7.639437	0.785398	0.	0.25	-0.50	-1.00	2.00	0.	1.00	2.00	0.25	0.033873	P4 (2-5)
43	7.639437	0.785398	0.	-0.25	0.50	0.	1.00	0.	-1.00	2.00	-0.25	0.047593	P4 (3-2)
44	7.639437	0.785398	0.	-0.25	0.25	0.	3.00	0.	0.	0.	0.	0.010170	P5 (3-4)
45	7.639437	0.785398	0.	-0.50	0.50	0.	3.00	0.	0.	0.	0.	0.020367	P5 (5-6)
46	7.639437	0.785398	0.	-0.25	-0.50	1.00	2.00	0.	0.	3.00	0.25	0.004451	P5 (3-5)
47	7.639437	0.463648	0.	0.25	0.50	-1.00	2.00	0.	1.00	2.00	-0.25	0.007674	P5 (3-3)
48	7.639437	0.785398	0.463648	0.25	0.50	3.00	0.	0.	1.00	2.00	-0.25	0.005140	P5 (3-3)
49	7.639437	0.321750	0.	-0.50	-0.25	-1.00	2.00	0.	0.	3.00	0.25	0.016057	P5 (4-6)
50	7.639437	0.785398	0.321750	-0.50	-0.25	2.00	1.00	0.	0.	3.00	0.25	0.005852	P5 (4-6)

TABLE XXII CONT'D

COMPUTER PRINT-OUT OF INPUT DATA AND ANSWERS TO EQUATIONS

EQ.	A	B	C	D	E	F1	F2	F3	G1	G2	H	ANSWER	DESCRIPTION
51	7.639437	0.463648	0.	0.50	0.	1.00	1.00	0.	-1.00	2.00	0.	0.015125	P5 (2-3)
52	7.639437	0.321750	0.	-0.25	-0.75	0.50	1.50	0.	-1.00	2.00	0.50	0.003025	P5 (4-9)
53	7.639437	0.785398	0.463648	-0.50	0.50	-1.00	2.00	0.	3.00	0.	0.	0.016988	P5 (5-6)
54	7.639437	0.463648	0.	0.	-0.50	0.	1.00	0.	1.00	1.00	0.50	0.011183	P5 (2-9)
55	7.639437	0.785398	0.463648	0.	-0.50	0.	1.00	0.	-1.00	2.00	0.50	0.009170	P5 (2-9.
56	7.639437	0.321750	0.	-0.75	0.25	-1.00	4.00	0.	0.	0.	0.	0.001671	P10 (10-11)
57	7.639437	0.321750	0.	-0.50	-0.75	2.00	3.00	0.	-1.00	4.00	0.25	0.000519	P10 (8-11)
58	3.819719	0.785398	0.463648	1.00	-0.50	2.00	1.00	0.	0.	0.	0.	0.006778	P10 (12-13)
59	3.819719	0.785398	0.463648	0.	-1.00	0.	2.00	0.	2.00	1.00	0.50	0.002619	P10 (8-17)
60	7.639437	0.321750	0.	0.50	0.	1.00	4.00	0.	0.	0.	0.	0.000879	P9 (9-10)
61	7.639437	0.785398	0.321750	-0.25	0.25	1.00	4.00	0.	0.	0.	0.	0.001399	P9 (9-11)
62	7.639437	0.463648	0.321750	0.25	0.25	-1.00	4.00	0.	0.	0.	0.	0.002946	P9 (10-13)
63	7.639437	0.785398	0.463648	-0.75	0.75	-1.00	4.00	0.	0.	0.	0.	0.005574	P9 (10-12)
64	7.639437	0.321750	0.	0.25	-1.00	-1.00	4.00	0.	1.00	4.00	0.25	0.000152	P9 (8-10)
65	7.639437	0.321750	0.	-0.25	1.00	2.00	3.00	0.	-1.00	4.00	-0.25	0.000678	P9 (10-8)
66	7.639437	0.321750	0.	1.00	0.	2.00	3.00	0.	0.	0.	0.	0.003161	P9 (11-13)
67	7.639437	0.321750	0.	0.50	-0.75	-2.00	3.00	0.	2.00	3.00	0.25	0.001615	P9 (8-13)
68	7.639437	0.463648	0.321750	0.50	-0.75	-2.00	3.00	0.	-1.00	4.00	0.25	0.003028	P9 (8-13)
69	7.639437	0.321750	0.	-0.75	0.25	1.00	2.00	0.	2.00	3.00	0.	0.005984	P9 (10-11)
70	7.639437	0.785398	0.463648	-0.50	-0.25	2.00	1.00	0.	-1.00	4.00	0.25	0.003552	P9 (8-12)
71	7.639437	0.643501	0.463648	0.50	0.25	0.	2.00	0.	2.00	1.00	-0.25	0.000561	P9 (12-8)
72	7.639437	0.785398	0.643501	0.50	0.25	4.00	-1.00	0.	2.00	1.00	-0.25	0.000388	P9 (12-8)
73	7.639437	0.785398	0.643501	-0.50	0.50	0.	2.00	0.	4.00	-1.00	0.	0.000888	P9 (7-8)
74	7.639437	0.588003	0.463648	0.50	-0.75	-2.00	3.00	0.	0.	2.00	0.25	0.000231	P9 (12-17)
75	7.639437	0.643501	0.588003	0.50	-0.75	4.00	-1.00	0.	0.	2.00	0.25	0.000278	P9 (12-17)
76	7.639437	0.643501	0.588003	-0.50	-0.50	1.00	1.00	0.	4.00	-1.00	0.50	0.000135	P9 (7-17)
77	7.639437	0.785398	0.643501	-0.50	-0.50	1.00	1.00	0.	0.	2.00	0.50	0.000341	P9 (7-17)
78	7.639437	0.321750	0.	-1.00	-0.25	4.00	1.00	0.	1.00	2.00	0.25	0.006120	P9 (7-11)
79	7.639437	0.321750	0.244979	-0.75	0.25	-3.00	2.00	0.	1.00	1.00	0.	0.000343	P9 (10-11)
80	7.639437	0.197396	0.	0.50	0.25	1.00	1.00	0.	2.00	1.00	-0.25	0.000424	P9 (6-4)
81	7.639437	0.244979	0.197396	0.50	0.25	1.00	1.00	0.	-3.00	2.00	-0.25	0.000203	P9 (6-4)
82	7.639437	0.244979	0.197396	-0.25	0.75	-3.00	2.00	0.	-0.50	1.50	-0.50	0.000064	P9 (10-4)
83	7.639437	0.321750	0.244979	-0.25	0.75	1.00	1.00	0.	-0.50	1.50	-0.50	0.000108	P9 (10-4)
84	7.639437	0.244979	0.	0.	-0.25	0.	1.00	0.	1.00	1.00	0.25	0.000945	P9 (6-11)
85	7.639437	0.321750	0.244979	0.	-0.25	0.	1.00	0.	-3.00	2.00	0.25	0.000305	P9 (6-11)
86	7.639437	0.785398	0.	-0.25	-1.00	1.00	4.00	0.	0.	0.	0.25	0.015333	P8 (8-9)
87	3.819719	0.463648	0.	-1.00	0.50	-2.00	3.00	0.	0.	0.	0.	0.007381	P8 (13-12)
89	7.639437	0.785398	0.321750	0.75	-0.25	2.00	3.00	0.	0.	0.	0.	0.004230	P8 (11-10)
90	7.639437	0.321750	0.	0.25	1.00	-1.00	4.00	0.	1.00	4.00	-0.25	0.000178	P8 (9-8)
91	7.639437	0.785398	0.321750	0.25	1.00	2.00	3.00	0.	1.00	4.00	-0.25	0.000281	P8 (9-8)
92	7.639437	0.321750	0.	0.50	0.	3.00	2.00	0.	-1.00	4.00	0.	0.002084	P8 (9-10)
93	7.639437	0.321750	0.	0.50	0.75	-2.00	3.00	0.	2.00	3.00	-0.25	0.002411	P8 (11-8)
94	7.639437	0.785398	0.321750	-0.25	0.25	3.00	2.00	0.	2.00	3.00	0.	0.000869	P8 (9-11)
95	7.639437	0.785398	0.321750	-0.25	1.00	1.00	2.00	0.	-1.00	4.00	-0.25	0.004629	P8 (10-8)
96	7.639437	0.785398	0.321750	0.25	-1.00	-1.00	4.00	0.	2.00	3.00	0.25	0.002523	P8 (8-10)
97	7.639437	0.785398	0.321750	-1.00	-0.25	4.00	1.00	0.	3.00	2.00	0.25	0.000711	P8 (7-11)
98	7.639437	0.321750	0.	1.00	0.	4.00	1.00	0.	-2.00	3.00	0.	0.010235	P8 (11-13)
99	3.819719	0.463648	0.	0.	-1.00	0.	2.00	0.	-2.00	3.00	0.50	0.003183	P8 (8-17)
100	7.639437	0.321750	0.	-0.25	-0.50	1.00	2.00	0.	3.00	2.00	0.25	0.000823	P8 (7-10)
101	7.639437	0.141897	0.	0.25	0.50	-3.00	2.00	0.	1.00	2.00	-0.25	0.000809	P8 (10-7)

TABLE XXII CONT'D

COMPUTER PRINT-OUT OF INPUT DATA AND ANSWERS TO EQUATIONS

EQ.	A	B	C	D	E	F1	F2	F3	G1	G2	H	ANSWER	DESCRIPTION
102	7.639437	0.321750	0.141897	0.25	0.50	4.00	1.00	0.	1.00	2.00	-0.25	0.000945	P8 (10-7)
103	7.639437	0.463648	0.321750	-0.50	0.50	-2.00	3.00	0.	1.00	2.00	0.	0.002191	P8 (7-8)
104	7.639437	0.785398	0.463648	-0.50	0.50	2.00	1.00	0.	1.00	2.00	0.	0.003092	P8 (7-8)
105	7.639437	0.321750	0.	0.	-0.25	2.00	1.00	0.	4.00	1.00	0.25	0.008877	P8 (7-13)
106	7.639437	0.463648	0.321750	0.	-0.25	2.00	1.00	0.	-2.00	3.00	0.25	0.003986	P8 (7-13)
107	7.639437	0.141897	0.	1.00	0.	4.00	1.00	0.	-3.00	2.00	0.	0.002411	P8 (6-7)
108	7.639437	0.197396	0.	-0.25	0.75	2.00	1.00	0.	-0.50	1.50	-0.50	0.005188	P8 (10-4)
109	7.639437	0.197396	0.141897	-0.75	0.25	-3.00	2.00	0.	4.00	1.00	0.	0.000796	P8 (10-11)
110	7.639437	0.321750	0.197396	-0.75	0.25	-0.50	1.50	0.	4.00	1.00	0.	0.002116	P8 (10-11)
111	7.639437	0.141897	0.	0.	-0.25	2.00	1.00	0.	4.00	1.00	0.25	0.001466	P8 (6-11)
112	7.639437	0.197396	0.141897	0.	-0.25	2.00	1.00	0.	-3.00	2.00	0.25	0.000701	P8 (6-11)
113	7.639437	0.197396	0.	-0.75	0.50	0.	1.00	0.	2.00	1.00	-0.25	0.007288	P8 (10-6)
114	7.639437	0.321750	0.197396	-0.75	0.50	0.	1.00	0.	-3.00	2.00	-0.25	0.001338	P8 (10-6)
115	7.639437	0.197396	0.	-0.50	-0.50	1.00	1.00	0.	2.00	1.00	0.50	0.000771	P8 (4-11)
116	7.639437	0.321750	0.197396	-0.50	-0.50	1.00	1.00	0.	-0.50	1.50	0.50	0.000424	P8 (4-11)
117	7.639437	0.463648	0.	-0.50	-0.50	1.00	1.00	0.	2.00	1.00	0.50	0.006001	P8 (7-17)
118	7.639437	0.588003	0.463648	-0.50	-0.50	1.00	1.00	0.	-2.00	3.00	0.50	0.001325	P8 (7-17)
119	7.639437	0.321750	0.	0.50	0.50	0.	1.00	0.	1.00	1.00	-0.50	0.004745	P8 (11-4)
120	7.639437	0.321750	0.197396	0.75	-0.50	-3.00	2.00	0.	-0.50	1.50	0.25	0.000655	P8 (6-10)
121	7.639437	0.321750	0.197396	0.50	0.25	-0.50	1.50	0.	2.00	1.00	-0.25	0.000480	P8 (6-4)
122	7.639437	0.463648	0.321750	0.50	0.25	1.00	1.00	0.	-1.00	2.00	-0.25	0.001313	P8 (6-4)
123	7.639437	0.463648	0.321750	0.	-0.25	3.00	0.	0.	1.00	1.00	0.25	0.001792	P8 (6-11)
124	7.639437	0.785398	0.321750	-0.25	0.75	0.	1.00	0.	-0.50	1.50	-0.50	0.008007	P8 (10-4)
125	7.639437	0.463648	0.321750	-0.75	-0.25	1.50	0.50	0.	3.00	0.	0.50	0.000786	P8 (3-11)
126	7.639437	0.785398	0.463648	-0.75	-0.25	1.50	0.50	0.	1.00	1.00	0.50	0.001404	P8 (3-11)
127	3.819719	0.588003	0.463648	1.00	-0.50	4.00	-1.00	0.	-2.00	3.00	0.	0.001249	P8 (12-13)
128	3.819719	0.588003	0.463648	-1.00	0.	2.00	0.	0.	4.00	-1.00	0.50	0.000527	P8 (7-18)
129	3.819719	0.785398	0.588003	-1.00	0.	2.00	0.	0.	1.00	1.00	0.50	0.000640	P8 (7-18)
130	7.639437	0.785398	0.588003	0.50	-0.75	-2.00	3.00	0.	1.00	1.00	0.25	0.005167	P8 (12-17)
131	7.639437	0.463648	0.321750	0.25	0.75	-1.00	2.00	0.	0.50	1.50	-0.50	0.000465	P8 (9-4)
132	7.639437	0.785398	0.463648	0.25	0.75	1.00	1.00	0.	0.50	1.50	-0.50	0.001131	P8 (9-4)
133	7.639437	0.588003	0.463648	-1.00	0.25	-2.00	3.00	0.	2.00	1.00	0.25	0.001989	P8 (7-12)
134	7.639437	0.785398	0.588003	-1.00	0.25	4.00	-1.00	0.	2.00	1.00	0.25	0.001016	P8 (7-12)
135	7.639437	0.785398	0.588003	1.00	-0.25	1.00	1.00	0.	4.00	-1.00	-0.25	0.002630	P8 (12-7)
136	3.819719	0.588003	0.463648	0.	1.00	-2.00	3.00	0.	0.	2.00	-0.50	0.000263	P8 (17-8)
137	3.819719	0.785398	0.588003	0.	1.00	1.00	1.00	0.	0.	2.00	-0.50	0.000491	P8 (17-8)
138	7.639437	0.785398	0.	1.00	0.	3.00	2.00	0.	0.	0.	0.	0.022358	P6 (6-7)
139	7.639437	0.785398	0.	0.	0.75	1.00	2.00	0.	0.	3.00	-0.25	0.006306	P6 (5-4)
140	7.639437	0.321750	0.	0.25	-0.50	-1.00	2.00	0.	3.00	2.00	0.25	0.004318	P6 (6-9)
141	7.639437	0.785398	0.321750	0.25	-0.50	2.00	1.00	0.	3.00	2.00	0.25	0.028353	P6 (6-9)
142	7.639437	0.785398	0.321750	1.00	0.25	1.00	2.00	0.	4.00	1.00	-0.25	0.005907	P6 (11-7)
143	7.639437	0.321750	0.	-0.25	0.25	0.50	1.50	0.	1.00	2.00	0.	0.015697	P6 (3-4)
144	7.639437	0.785398	0.321750	-0.25	0.25	2.00	1.00	0.	1.00	2.00	0.	0.005159	P6 (3-4)
145	7.639437	0.785398	0.321750	0.75	-0.25	1.00	1.00	0.	1.00	2.00	0.	0.031757	P6 (11-10)
146	3.819719	0.463648	0.	0.	1.00	2.00	1.00	0.	0.	2.00	-0.50	0.016428	P6 (17-8)
147	7.639437	0.141897	0.	-0.25	0.50	-3.00	2.00	0.	-1.00	2.00	-0.25	0.000226	P6 (9-6)
148	7.639437	0.321750	0.141897	-0.25	0.50	0.50	1.50	0.	-1.00	2.00	-0.25	0.000342	P6 (9-6)
149	7.639437	0.141897	0.	0.50	0.	0.50	1.50	0.	-3.00	2.00	0.	0.000464	P6 (9-10)
150	7.639437	0.321750	0.	-0.50	-0.50	1.00	1.00	0.	0.50	1.50	0.50	0.012246	P6 (3-9)
151	7.639437	0.463648	0.321750	-0.50	-0.50	1.00	1.00	0.	-1.00	2.00	0.50	0.000959	P6 (3-9)

TABLE XXII CONT'D

COMPUTER PRINT-OUT OF INPUT DATA AND ANSWERS TO EQUATIONS

EQ.	A	B	C	D	E	F1	F2	F3	G1	G2	H	ANSWER	DESCRIPTION
152	7.639437	0.141897	0.	0.25	-0.75	-0.50	1.50	0.	0.50	1.50	0.50	0.000169	P6 (4-10)
153	7.639437	0.197396	0.141897	0.25	-0.75	-0.50	1.50	0.	-3.00	2.00	0.50	0.000070	P6 (4-10)
154	7.639437	0.197396	0.141897	-0.50	-0.25	-3.00	2.00	0.	0.50	1.50	0.25	0.000153	P6 (4-6)
155	7.639437	0.321750	0.197396	-0.50	-0.25	2.00	1.00	0.	0.50	1.50	0.25	0.000139	P6 (4-6)
156	3.819719	0.463648	0.	-1.00	0.50	0.	1.00	0.	2.00	1.00	0.	0.024698	P6 (13-12)
157	7.639437	0.463648	0.	0.50	0.50	0.	1.00	0.	1.00	1.00	-0.50	0.013952	P6 (17-7)
158	7.639437	0.588003	0.463648	0.50	0.50	4.00	-1.00	0.	1.00	1.00	-0.50	0.003128	P6 (17-7)
159	7.639437	0.321750	0.	0.50	0.50	0.	1.00	0.	1.00	1.00	-0.50	0.004745	P6 (9-3)
160	7.639437	0.463648	0.321750	0.50	0.50	3.00	0.	0.	1.00	1.00	-0.50	0.001779	P6 (9-3)
161	7.639437	0.785398	0.321750	0.25	-0.75	-0.50	1.50	0.	1.00	1.00	0.50	0.025488	P6 (4-10)
162	7.639437	0.463648	0.321750	-0.25	0.50	0.	1.00	0.	3.00	0.	-0.25	0.005226	P6 (9-6)
163	7.639437	0.785398	0.463648	-0.25	0.50	0.	1.00	0.	-1.00	2.00	-0.25	0.005674	P6 (9-6)
164	7.639437	0.785398	0.321750	0.75	0.25	0.	1.00	0.	1.50	0.50	-0.50	0.042472	P6 (11-3)
165	7.639437	0.588003	0.463648	-0.50	0.75	0.	1.00	0.	4.00	-1.00	-0.25	0.008179	P6 (17-12)
166	7.639437	0.785398	0.588003	-0.50	0.75	0.	1.00	0.	-2.00	3.00	-0.25	0.005597	P6 (17-12)
167	7.639437	0.785398	0.463648	0.25	-0.50	-1.00	2.00	0.	1.00	1.00	0.25	0.008572	P6 (6-9)
168	7.639437	0.463648	0.321750	-0.75	0.	-1.00	2.00	0.	2.00	1.00	0.25	0.001756	P6 (3-6)
169	7.639437	0.785398	0.463648	-0.75	0.	3.00	0.	0.	2.00	1.00	0.25	0.001242	P6 (3-6)
170	7.639437	0.785398	0.321750	-0.25	-0.75	0.50	1.50	0.	2.00	1.00	0.50	0.008201	P6 (4-9)
171	7.639437	0.785398	0.463648	0.75	0.	1.00	1.00	0.	3.00	0.	-0.25	0.004363	P6 (6-3)
172	7.639437	0.785398	0.	-0.50	0.50	1.00	4.00	0.	0.	0.	0.	0.007406	P7 (7-8)
173	7.639437	0.785398	0.	-0.75	-0.50	3.00	2.00	0.	1.00	4.00	0.25	0.006634	P7 (7-9)
174	7.639437	0.540419	0.321750	0.50	0.75	-1.00	4.00	0.	2.00	3.00	-0.25	0.000254	P7 (11-8)
175	7.639437	0.785398	0.540419	0.50	0.75	4.00	1.00	0.	2.00	3.00	-0.25	0.000279	P7 (11-8)
176	7.639437	0.540419	0.321750	0.75	-0.25	4.00	1.00	0.	-1.00	4.00	0.	0.000722	P7 (11-10)
177	7.639437	0.463648	0.	-0.50	0.75	0.	2.00	0.	-2.00	3.00	-0.25	0.004489	P7 (13-8)
178	7.639437	0.321750	0.	0.75	0.50	1.00	2.00	0.	3.00	2.00	-0.25	0.001021	P7 (9-7)
179	7.639437	0.785398	0.321750	0.75	0.50	4.00	1.00	0.	3.00	2.00	-0.25	0.000886	P7 (9-7)
180	7.639437	0.785398	0.540419	-0.50	0.50	-1.00	4.00	0.	4.00	1.00	0.	0.000922	P7 (7-8)
181	7.639437	0.540419	0.321750	-0.25	-0.50	1.00	2.00	0.	4.00	1.00	0.25	0.000580	P7 (7-10)
182	7.639437	0.785398	0.540419	-0.25	-0.50	1.00	2.00	0.	-1.00	4.00	0.25	0.000672	P7 (7-10)
183	7.639437	0.785398	0.321750	-0.25	0.25	0.50	1.50	0.	4.00	1.00	0.	0.012311	P7 (9-11)
184	7.639437	0.588003	0.321750	0.25	0.50	1.00	1.00	0.	1.00	2.00	-0.25	0.016481	P7 (10-7)
185	7.639437	0.785398	0.588003	0.25	0.50	4.00	-1.00	0.	1.00	2.00	-0.25	0.002639	P7 (10-7)
186	7.639437	0.463648	0.	-0.50	-0.25	2.00	1.00	0.	0.	2.00	0.25	0.010292	P7 (13-17)
187	7.639437	0.321750	0.	0.50	0.	-1.00	2.00	0.	1.00	2.00	0.	0.003797	P7 (9-10)
188	7.639437	0.321750	0.	1.00	0.25	1.00	1.00	0.	4.00	1.00	-0.25	0.010569	P7 (11-7)
189	7.639437	0.197396	0.	0.75	-0.50	-3.00	2.00	0.	-1.00	2.00	0.25	0.000620	P7 (6-10)
190	7.639437	0.321750	0.197396	0.75	-0.50	2.00	1.00	0.	-1.00	2.00	0.25	0.001282	P7 (6-10)
191	7.639437	0.197396	0.	-0.75	0.50	-0.50	1.50	0.	-3.00	2.00	-0.25	0.001277	P7 (10-6)
192	7.639437	0.197396	0.	0.25	0.75	-0.50	1.50	0.	0.50	1.50	-0.50	0.000499	P7 (9-4)
193	7.639437	0.321750	0.197396	0.25	0.75	2.00	1.00	0.	0.50	1.50	-0.50	0.000303	P7 (9-4)
194	7.639437	0.197396	0.	0.50	0.	1.00	1.00	0.	-0.50	1.50	0.	0.003308	P7 (9-10)
195	7.639437	0.244979	0.197396	0.50	0.	1.00	1.00	0.	-3.00	2.00	0.	0.000573	P7 (9-10)
196	7.639437	0.197396	0.	-0.50	-0.25	2.00	1.00	0.	-0.50	1.50	0.25	0.002029	P7 (4-6)
197	7.639437	0.463648	0.	0.50	0.25	1.00	1.00	0.	2.00	1.00	-0.25	0.003659	P7 (17-13)
198	7.639437	0.244979	0.	0.	-0.50	0.	1.00	0.	1.00	1.00	0.50	0.001890	P7 (3-10)
199	7.639437	0.321750	0.244979	0.	-0.50	0.	1.00	0.	-3.00	2.00	0.50	0.000609	P7 (3-10)
200	7.639437	0.321750	0.	0.	-0.75	0.	1.00	0.	1.00	1.00	0.75	0.006087	P7 (4-17)
201	7.639437	0.785398	0.321750	0.	-0.75	0.	1.00	0.	-0.50	1.50	0.75	0.010315	P7 (4-17)

TABLE XXII CONT'D

COMPUTER PRINT-OUT OF INPUT DATA AND ANSWERS TO EQUATIONS

EQ.	A	B	C	D	E	F1	F2	F3	G1	G2	H	ANSWER	DESCRIPTION
202	7.639437	0.463648	0.	0.	-0.25	0.	1.00	0.	1.00	1.00	0.25	0.005592	P7 (7-13)
203	7.639437	0.244979	0.197396	-0.25	0.50	-3.00	2.00	0.	2.00	1.00	-0.25	0.000529	P7 (9-6)
204	7.639437	0.321750	0.244979	-0.25	0.50	1.00	1.00	0.	2.00	1.00	-0.25	0.001337	P7 (9-6)
205	7.639437	0.463648	0.321750	-0.25	0.50	1.00	1.00	0.	-1.00	2.00	-0.25	0.000556	P7 (9-6)
206	7.639437	0.321750	0.197396	0.25	-0.75	-0.50	1.50	0.	2.00	1.00	0.50	0.000828	P7 (4-10)
207	7.639437	0.321750	0.244979	-0.75	0.	-3.00	2.00	0.	1.00	1.00	0.25	0.001122	P7 (3-6)
208	7.639437	0.463648	0.321750	-0.75	0.	3.00	0.	0.	1.00	1.00	0.25	0.000758	P7 (3-6)
209	7.639437	0.463648	0.321750	0.75	-0.25	1.50	0.50	0.	-0.50	1.50	0.	0.001283	P7 (11-10)
210	7.639437	0.463648	0.321750	0.	-0.50	0.	1.00	0.	1.50	0.50	0.50	0.001089	P7 (3-10)
211	7.639437	0.785398	0.463648	0.	-0.50	0.	1.00	0.	-0.50	1.50	0.50	0.002812	P7 (3-10)
212	7.639437	0.540419	0.321750	0.	-0.25	0.	1.00	0.	1.50	0.50	0.25	0.001862	P7 (6-11)
213	7.639437	0.785398	0.540419	0.	-0.25	0.	1.00	0.	-1.00	2.00	0.25	0.002378	P7 (6-11)
214	7.639437	0.463648	0.321750	0.75	0.	1.50	0.50	0.	3.00	0.	-0.25	0.000438	P7 (6-3)
215	7.639437	0.540419	0.463648	0.75	0.	1.50	0.50	0.	-1.00	2.00	-0.25	0.000514	P7 (6-3)
216	7.639437	0.588003	0.463648	-1.00	0.25	4.00	-1.00	0.	1.00	1.00	0.25	0.001248	P7 (7-12)
217	7.639437	0.588003	0.463648	1.00	-0.25	2.00	0.	0.	4.00	-1.00	-0.25	0.000601	P7 (12-7)
218	7.639437	0.643501	0.588003	1.00	-0.25	2.00	0.	0.	-2.00	3.00	-0.25	0.000544	P7 (12-7)
219	7.639437	0.785398	0.463648	-0.25	0.25	-0.50	1.50	0.	1.50	0.50	0.	0.006964	P7 (3-4)
220	7.639437	0.588003	0.321750	-0.25	0.	-0.50	1.50	0.	1.00	1.00	0.25	0.012680	P7 (10-17)
221	7.639437	0.785398	0.588003	-0.25	0.	-0.50	1.50	0.	-2.00	3.00	0.25	0.007231	P7 (10-17)
222	7.639437	0.785398	0.540419	-0.25	0.25	-1.00	2.00	0.	1.50	0.50	0.	0.003751	P7 (9-11)
223	7.639437	0.643501	0.588003	0.50	0.50	-2.00	3.00	0.	1.00	1.00	-0.50	0.000197	P7 (17-7)
224	7.639437	0.463648	0.321750	0.50	0.50	-0.50	1.50	0.	1.00	1.00	-0.50	0.000745	P7 (11-4)
225	7.639437	0.785398	0.463648	0.50	0.50	1.50	0.50	0.	1.00	1.00	-0.50	0.001569	P7 (11-4)
226	7.639437	0.540419	0.463648	0.50	0.50	-1.00	2.00	0.	1.00	1.00	-0.50	0.000208	P7 (9-3)
227	7.639437	0.785398	0.540419	0.50	0.50	1.50	0.50	0.	1.00	1.00	-0.50	0.000638	P7 (9-3)
228	7.639437	0.785398	0.588003	-0.75	0.75	-2.00	3.00	0.	4.00	-1.00	0.	0.009293	P7 (10-12)
229	7.639437	0.540419	0.463648	-0.50	-0.50	1.00	1.00	0.	3.00	0.	0.50	0.000150	P7 (3-9)
230	7.639437	0.785398	0.540419	-0.50	-0.50	1.00	1.00	0.	0.50	1.50	0.50	0.000460	P7 (3-9)
231	7.639437	0.785398	0.321750	-0.50	-0.50	1.00	1.00	0.	0.50	1.50	0.50	0.002984	P7 (4-11)
232	7.639437	0.463648	0.321750	0.25	-0.50	-1.00	2.00	0.	0.50	1.50	0.25	0.000209	P7 (6-9)
233	7.639437	0.540419	0.463648	0.25	-0.50	3.00	0.	0.	0.50	1.50	0.25	0.000294	P7 (6-9)
234	7.639437	0.540419	0.321750	0.50	0.25	0.50	1.50	0.	2.00	1.00	-0.25	0.000605	P7 (6-4)
235	7.639437	0.785398	0.540419	0.50	0.25	3.00	0.	0.	2.00	1.00	-0.25	0.000542	P7 (6-4)
236	7.639437	0.588003	0.463648	-0.50	0.75	1.00	1.00	0.	-2.00	3.00	-0.25	0.000810	P7 (17-12)
237	7.639437	0.785398	0.540419	-0.25	0.25	0.50	1.50	0.	3.00	0.	0.	0.001381	P7 (3-4)
238	7.639437	0.785398	0.643501	0.50	0.50	2.00	0.	0.	1.00	1.00	-0.50	0.000498	P7 (17-7)
239	7.639437	0.643501	0.463648	0.	-0.25	0.	1.00	0.	2.00	0.	0.25	0.002212	P7 (12-18)
240	7.639437	0.785398	0.643501	0.	-0.25	0.	1.00	0.	-2.00	3.00	0.25	0.001931	P7 (12-18)
241	7.639437	0.785398	0.643501	-0.50	0.50	-2.00	3.00	0.	2.00	0.	0.	0.002534	P7 (17-18)
242	3.819719	0.785398	0.463648	1.00	0.	0.	1.00	0.	2.00	0.	-0.50	0.015154	P6 (18-7)

PTRD	FSP5	FSP6	FSP7	FSP8	PTOT	P3	P4
0.866023	0.140197	0.258670	0.165445	0.141274	0.866044	0.076957	0.142159

SDP5	P10	P9	SDP8	SDP6	SDP7	P38ON	ANSW(37)
0.125203	0.011587	0.040301	0.139349	0.331277	0.193781	1.060614	1.060659

column A in general is either $12/\pi$ or $24/\pi$. These are shown in decimal form as 3.819719 or 7.639437.

Columns B and C are upper and lower limits of Θ. The specific values were tabulated on the data sheet submitted in terms of $\pi/2$, $\pi/4$, $\pi/6$, arccot 3/2, arccot 2, arccot 3, arccot 4/3, arccot 4, arccot 5, arccot 7, arccot 5/3, and 0. These have been converted to decimal radian form and listed in columns B and C.

Columns D, E, and H have values 0, $\pm \frac{1}{4}, \pm \frac{1}{2}, \pm \frac{3}{4}$, and $\pm$ 1, depending upon the relative coordinate differences of the polyhedron corner points in question along the coordinate axes chosen. All corners of the cube, tetrahedron, octahedron, rhombic dodecahedron, and tetrakaidecahedron can be expressed in terms of these numbers. Only the hexagonal prism, Equation (36), is different, and for this $E = \sqrt{3}/2$, which is abbreviated in the print-out as 0.87. It may be mentioned that in other cases as well as this, the data listed on the print-out may be somewhat more abbreviated than the actual data on which the computations were performed.

Column F's represent the upper limits of the $\phi(\Theta)$ integrations. Since the general form of $\phi(\Theta)$ is ϕ = arccot (e sinΘ + g cosΘ), column F1 gives the value for "e", and column F2 gives the value for "g". Column F3 is necessary for the two special cases, Equations(1) and (36), where $F = \pi/2$.

Column G's represent the lower limits of the $\phi(\Theta)$ integrations. Since this has the general form ϕ = arccot (e sinΘ + g cosΘ), column G1 shows "e" and column G2 shows "g".

The answer column gives the integrated average value of the projected height or the probability of each type of intersection within the equation limits and in units of edge length of the circumscribed cube, which we have previously called "a". In the case of the hexagonal prism, Equation (36), the answer given is for a base diagonal "a" equal to the prism height "c". Thus if c = a, then

$$P_i(\text{hex prism}) = \frac{3}{4}a + \frac{1}{2}c \qquad (114)$$

$$= 1.25a$$

It may be noted that the computer answer is 1.250002, an error in the sixth decimal place.

The Description column describes the average projected height or probability sought by each equation. Where a polyhedron is named, it refers to the polyhedron as a whole, except for the rhombic dodecahedron, where this had to be done in two increments. Where a P followed by a number is shown, this indicates a probability computation for a sectional shape having the number of sides indicated by the number following the P. The section belongs to the polyhedron which it follows in the table. Where there is more than one P having the same number after it, these must be added together to get the total probability of a section of that number of sides.

For the tetrakaidecahedron two additional numbers in parentheses follow the P's. The numbers in parentheses indicate the corner numbers which are being integrated between to give that particular shape section. For simpler polyhedrons such corner numbers are either obvious or have been

described in the main text of this dissertation. However, for the tetrakaidecahedron, the print-out sheet is the only place these are listed. For the tetrakaidecahedron, the probabilities for sections were made up from many different sub-probabilities or equations, so a list of the corners for each equation is helpful in any subsequent detailed checking. The P7, for instance, is composed of 70 separate equations.

A discussion of the results now follows. Compare Equations (1) and (2), both for the cube as a whole. Equation (1) gives P_1 = 1.500000 by integrating over one octant, and this result agrees exactly with our previous analytical result. Equation (2) integrates over our 1/48th triangle, with result P_i = 1.499999, which agrees with Equation (1) to within 0.000001. The sum of the P3, P4, P5, and P6 for the cube, Equations (3) to (8), adds exactly to the value given by Equation (2).

For the octahedron, the sum of the probabilities of its sections, Equations (10) and (11), may be seen to agree with its total probability, Equation (9), within 0.000006. For the tetrahedron, the sum of the probabilities of its sections, Equations (13) to (15), agrees exactly with its total probability, Equation (12). For the hexagonal prism, Equation (36), a computer discrepancy of 0.000002 was previously pointed out.

For the rhombic dodecahedron and tetrakaidecahedron the computer has added the sub-totals for computing the various probabilities of sections, and these are listed at the bottom of the print-out sheet. PTRD is the total probability of the rhombic dodecahedron from an addition of Equations (16) and (17). FSP5, FSP6, FSP7, and FSP8 are sub-totals for the sections of the rhombic dodecahedron having the number of sides indicated. These, of

course, are derived from particular sums of Equations (20) to (34). PTOT is the sum of all rhombic dodecahedron sub-probabilities, from Equations (18) to (35). On comparing this total probability with PTRD, we see there is a discrepancy of 0.000021, which is considered to be quite acceptable accuracy.

For the tetrakaidecahedron, sub-totals for probabilities of each type of section are listed at the end of the print-out sheet as P3, P4, SDP5 P10, P9, SDP8, SDP6, and SDP7. (The SDP8 stands for second P8 to distinguish it from FSP8, first P8, previously listed.) It may be seen that P3 is the sum of Equations (38) and (39), P4 sums (40) to (43), SDP5 sums (44) to (55), P10 sums (56) to (59), P9 sums (60) to (85), SDP8 sums (86) to (137), SDP7 sums (172) to (241), and SDP6 sums (138) to (171) plus (242). P380N represents the entire sum from Equations (38) to (242), the total probability for the tetrakaidecahedron. ANSW(37) lists the best value for the probability of intersection a tetrakaidecahedron, obtained by Equation (37). Comparison with P380N shows the discrepancy to be 0.000045, which is considered quite acceptable accuracy.

In conclusion, it may be stated that the basic equation Equation (117), together with the function subroutine FNX(X), permits easy solution on a digital computer of equations arising from probabilities of planar intersections of randomly oriented polyhedrons of cubic symmetry. For simple polyhedrons of non-cubic symmetry, as with the hexagonal prism, Equation (36), necessary modification of the equation is easily accomplished. The principle source of difficulty, which depends upon the complexity of the polyhedron, will be in setting up the integral equations for the computer

to solve. The difficulty of this operation will depend upon the number of corners and faces of the polyhedron and its symmetry or lack thereof.

APPENDIX C

List of Symbols

This appendix contains a listing and explanation of the most frequently used symbols in the test. An effort has been made to minimize duplication of symbol usage, but, as usual, a certain amount of it is difficult to avoid. This is particularly so when it is desired to let a letter stand for a number coefficient in an equation - one soon runs out of different letters, or the deliberate choice of unused letters may itself be awkward. Since these cases are explained in the test, they are not listed here. Neither do we list certain symbols that may appear only once or twice in the text and are adequately explained there.

Thus we list the most frequently used symbols, ones used so often that they may not be explained with every appearance in the text.

Symbol	Meaning
a	length of cube edge, circumscribed cube edge, rectangular parallelepiped edge, or base diagonal of hexagonal prism
c	height
d	diameter
d_o	elliptical minor axis (observed)
f	fraction or frequency
h	projected height, a sub-unit of D
h_{1-2}	projected height between corners 1 and 2
ℓ	length
m	effective radius of revolution or tilt
q_o	elliptical major axis (observed)
r	radius
$\bar{s}$	average cross sectional area
t	thickness
B	barrels, doubly truncated ellipses
C	cups, singly truncated ellipses
D	distance between top and bottom tangent planes
$\bar{D}$	average distance between top and bottom tangent planes
D_3	distance resulting in 3 sided sections
E	ellipses
N_s	number per unit area
N_v	number per unit volume
P	probability
P_i	probability of sectioning a particle
P_3	probability of a 3 sided section

Θ	angle of horizontal rotation
ϕ	angle of tilt from the vertical
ρ	radius vector of orientation sphere
χ^2	statistical measure for "goodness of fit" (chi-square)

BIBLIOGRAPHY

1. Saltykov, S. A. Stereometric Metallography. 2nd Ed., (in Russian), State Scientific - Technical Publishing House of Literature on Ferrous and Nonferrous Metallurgy, Moscow, 1958. (To be available in English translation through Armed Forces Technical Information Agency and Office of Technical Services, Department of Commerce.)

2. Symposium, "Quantitative Metallography." Metallurgical Research Laboratory, University of Florida, Gainesville, February, 1961. (Proceedings to be published by McGraw-Hill.)

3. Smith, Cyril Stanley. "Grain Shapes and Other Metallurgical Applications of Topology." Metal Interfaces, American Society for Metals, Cleveland, (1952) 65.

4. Smith, Cyril Stanley. "Microstructure." Transactions, American Society for Metals, Cleveland, (1953) 533.

5. Smith, Cyril Stanley and Guttman, Lester. "Measurement of Internal Boundaries in Three-Dimensional Structures by Random Sectioning." Transaction, AIME, 197 (1953) 81.

6. Saltykov, S. A. "Author's Certificate No. 72704 for Method of Geometric Quantitative Analysis of Metals, Alloys, and Other Objects, Priority from 28 May 1945." (Russian).

7. Duffin, R. J., Meussner, R. A. and Rhines, F. N. Statistics of Particle Measurement and of Particle Growth. Carnegie Inst. of Tech., Tech. Report No. 32, AF-33(616)-294, April 1953.

8. Delesse, A. "Procede Mechanique Pour Determiner la Composition des Roches." Annales des Mines, 13 (1848) 379.

9. Rosiwal, A. Verhand. der K. K. Geologischen Reichsanstalt, 5-6, (1898) 143.

10. Howard, R. T. and Cohen, M. "Quantitative Metallography by Point-Counting and Lineal Analysis." Transactions, AIME, 172 (1947) 413.

11. Beck, L. H. and Smith, C. S. Journal of Metals, 4, No. 10, 1952.

12. Causely, D. and Young, J. Z. Research, 8 (1955) 430.

13. Hilliard, J. E. and Cahn, J. W. "An Evaluation of Procedures in Quantitative Metallography for Volume - Fraction Analysis." Transactions of the Metallurgical Society of AIME, 221 (April, 1961) 344.

14. Glagolev, A. A. "Authors Certificate No. 38066 for Method and Device for Microscopic Analysis of Rocks, Priority from 19 July 1932." (Russian).

15. Thompson, E. Journal of Geology, 38, No. 3 (1930) 193.

16. Horikawa, E. Tetsu to Hagane, 40, No. 10 (1954) 991.

17. Underwood, E. E. "Quantitative Metallography." Metals Engineering Quarterly, ASM, 1, Nos. 3 and 4 (1961) 70.

18. Chayes, F. The American Mineralogist, 34 (1949) 600.

19. Bain, E. C. and Vilella, J. R. "Austenitic Grain Size in Steel." Metals Handbook, ASM, (1948) 399.

20. ASTM Standards, Part 3 (1958) 498.

21. Grignon, P. C. "Memoires de Physique sur l'art de Fabriquer le fer...." Paris, 1775.

22. Johnson, W. A. "Estimation of Spatial Grain Size." Metal Progress, (January, 1946) 87.

23. Scheil, E. Zeitschrift fur Metallkunde, 27 (1935) 199.

24. Scheil, E. and Wurst, H. Zeitschrift fur Metallkunde, 28 (1936) 340.

25. Scheil, E. and Langeweise, A. Archiv. fur das Eisenhuttenwesen, 11, (1937) 93.

26. Rutherford, J. J. B., Aborn, R. H. and Bain, E. C. Metals and Alloys, (December, 1937) 345.

27. Kaiser, H. F. Metals and Alloys, (January, 1938) 23.

28. Lord Kelvin. "On Homogeneous Division of Space." Proceedings, Royal Society of London, 55 (1894) 1.

29. Williams, W. M. and Smith, C. S. Transactions, AIME, 194 (1952) 755.

30. Thompson, D'Arcy W. On Growth and Form. 2nd Ed., Cambridge, 1942.

31. Harker, D. and Parker, E. R. "Grain Shape and Grain Growth." Transactions, ASM, 34 (1945) 156.

32. Myers, E. J., Unpublished.

33. Courant, R. and Robbins, H. What is Mathematics? Oxford, 1941.

34. Belyayev, N. T. Journal Iron and Steel Institute, 1, 1922.

35. Pelissier, G. E., Hawks, M. F., Johnson, W. A. and Mehl, R. F. Transactions, ASM, 30 (1942) 1040.

36. Gensamer, M., Pearsall, E. B. and Smith, G. Transactions, ASM, 28, No. 2 (1940) 380.

37. Johnson, W. A. and Mehl, R. F. "The Interlamellar Spacing of Pearlite." Transactions, ASM, 30 (1942) 1049.

38. Gensamer, M., Pearsall, E. B., Pellini, W. S. and Low, J. R. Transactions, ASM, 30 (1942) 983.

39. Gregory, B., Hall, H. T. and Bullock, G. "Measurement of Interlamellar Spacing of Pearlite." Transactions Quarterly, ASM, 54, No. 1, (1961) 106.

40. Fullman, R. L. "Measurement of Particle Sizes in Opaque Bodies." Transactions, AIME, (1953) 447.

41. Schwartz, H. A. "The Metallographic Determination of the Size Distribution of Temper Carbon Nodules." Metals and Alloys, (June, 1934) 139.

42. Mirkin, I. L. High Quality Steel. (Russian), No. 5, 1935.

43. Scheil, E. Zeitschrift fur anorganische und allgemeine Chemie, 201, (1931) 259.

44. Hagerman, T. H. Geologiska Foreningens Forhandlingar, Stockholm, 46 (1924) 325.

45. Lord, G. W. and Willis, T. F. "Calculation of Air Bubble Size Distribution from Results of a Rosiwal Traverse of Aerated Concrete." ASTM Bulletin No. 177 (October, 1951) 56.

46. Brophy, J. H. and Sinnott, M. J. "Quantitative Metallographic Analysis of Graphite Size in Ductile Cast Iron." Transactions Quarterly, ASM, 54, No. 1 (1961) 65.

47. Cahn, J. W. and Fullman, R. L. "On the Use of Lineal Analysis for Obtaining Particle Size Distribution Functions in Opaque Samples." Transactions, AIME (May, 1956) 610.

48. Fullman, R. L. "Measurement of Approximately Cylindrical Particles in Opaque Samples." Transactions, AIME, (September, 1953) 1267.

49. DeHoff, R. T. and Rhines, F. N. Transactions of the Metallurgical Society, AIME, 221 (October, 1961) 975

50. Hull, F. C. and Houk, W. J. "Statistical Grain Structures Studies: Plane Distribution Curves of Regular Polyhedrons." Transactions, AIME, (April, 1953) 565.

51. DeHoff, R. T. "Geometric Probabilities," talk given at Symposium on Quantitative Metallography, University of Florida, February, 1961.

52. Pierce, B. O. A Short Table of Integrals. Ginn and Co., Boston, 1929.

53. Barrett, C. S. Structure of Metals. McGraw-Hill, New York, 1952.

54. Dwight, H. B. Tables of Integrals and Other Mathematical Data. 3rd Ed., The Macmillan Company, New York, 1957.

55. Kenney, J. F. and Keeping, E. S. Mathematics of Statistics, Part One, 3rd Ed., Van Nostrand, New York, 1954.